Behavior of Bridge Decks with Precast Panels at Expansion Joints

by

Christin Jennifer Coselli, B.S.

Thesis

Presented to the Faculty of the Graduate School of

The University of Texas at Austin

in Partial Fulfillment

of the Requirements

for the Degree of

Masters of Science in Engineering

The University of Texas at Austin

May 2004

Behavior of Bridge Decks with Precast Panel at Expansion Joints

Committee:

James Jirsa, Supervisor

Oguzhan Bayrak

Dedication

To my parents and my sisters, for always supporting me and making me laugh.

Acknowledgements

Abstract

Behavior of Bridge Decks with Precast Panels at Expansion Joints

Christin Jennifer Coselli, M.S.E.

The University of Texas at Austin, 2004

Supervisor: James Jirsa

The Texas Department of Transportation (TxDOT) currently uses, for most of its bridges, the "IBTS" standard detail for bridge slab edges at expansion joints. That detail has enabled TxDOT to eliminate the use of diaphragms at slab edges by increasing the transverse stiffness at slab edges. Slab edges are stiffened by a 2-in. increase in slab thickness and reduced reinforcement spacing for skewed slabs. The origin of this detail is unknown, but has been used successfully by TxDOT for years. Currently, TxDOT uses a combination of precast prestressed concrete deck panels as stay-in-place formwork and cast-in-place concrete topping for the interior portion of bridge decks. The purpose of this study was to investigate the performance of precast prestressed concrete deck panels and topping slab at the expansion joints. The influence of armor and sealed expansion joint rail on edge performances was also studied.

Comparisons were made between the IBTS, UTSE (an alternate detail with a uniform slab thickness of 8 in.) and PC panel edge details constructed on 0° skew specimens. At design load levels, tensile strains and deflections were small (less than 15% of yield strain and 1/1700). Slab edges were usually did not exhibit flexural cracking until loads higher than design load levels. All edge details failed in punching shear at loads ranging from 5.4 x HS-20 to 7.5 x HS-25.

Table of Contents

List of Tables

xvii

List of Figures

CHAPTER 1

Objectives and Scope

1.1 INTRODUCTION

The Texas Department of Transportation (TxDOT) currently uses, for most of its bridges, the "IBTS" standard detail for bridge slab edges at expansion joints. That detail, shown in Figure 1.1 and 1.2 has enabled TxDOT to eliminate the use of diaphragms at slab edges by increasing the transverse stiffness at slab edges. Slab edges are stiffened by a 2-in. increase in slab thickness and reduced reinforcement spacing for skewed slabs. The origin of this detail is unknown, but has been used successfully by TxDOT for years. Currently, TxDOT uses a combination of prestressed concrete deck panels as stay-in-place formwork and cast in place concrete topping for the interior portion of bridge decks.

1.2 BACKGROUND

All bridges in Texas are designed according to AASHTO provisions. Currently, the AASHTO HS-20 design load is typically used in design of bridges. However concerns from trucks operating beyond their legal weight limits and increased truck traffic as a result of the North American Free Trade Agreement (NAFTA) have led many TxDOT districts to increase their design loads by a factor of 1.25. This increased load has been labeled as the "HS-25" design load.

1

Figure 1.1 IBTS detail, plan view
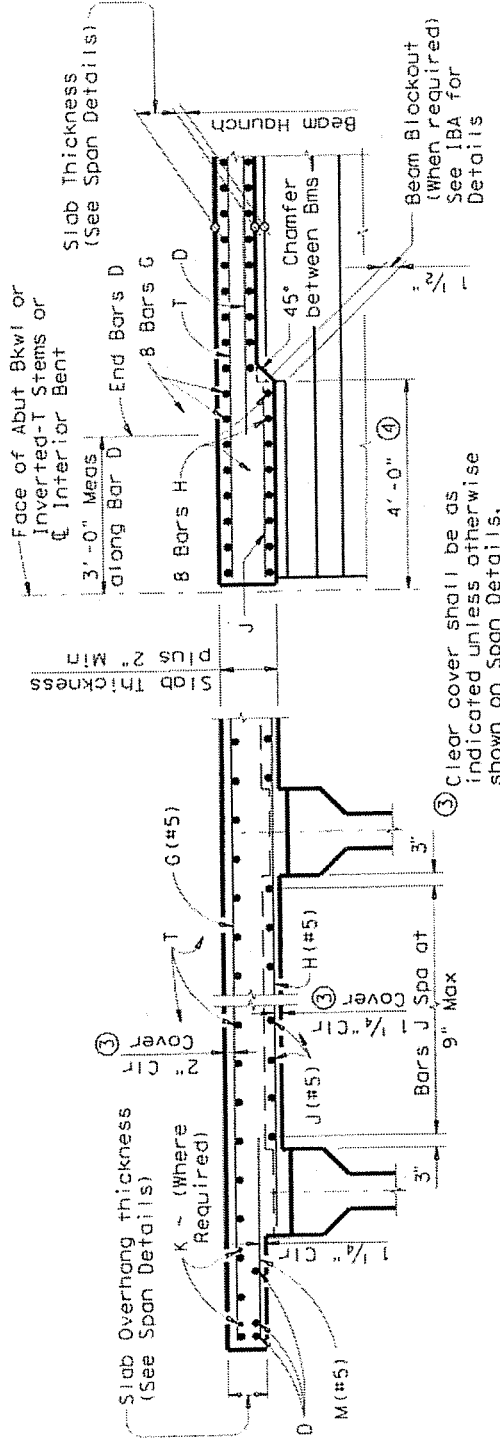
Figure 1.2 IBTS detail, elevation view

3

Prior to this research project, the capacity and behavior of the IBTS slab edge detail under applied AASHTO design loads was unknown. Previous related research had focused on the behavior at interior locations of bridge decks with diaphragms. Tests have indicated that bridge decks fail in punching shear at interior locations at loads that far exceed the design load capacity. This is due to effects of two-way action and arching action that increase flexural capacity. At deck edges, capacity is not expected to increase as much because the slab is less restrained. The effect of different edge details, in particular the IBTS detail and an alternative detail (UTSE detail), were studied in the previous phases of this research project, by Ryan (2003) and Griffith (2003).

An alternative edge detail, shown in Figure 1.3, was developed as an alternate to the IBTS edge detail. The Uniform Thickness Slab Edge Detail (UTSE) has a cast-in-place (CIP) concrete thickness of 8-in. and additional reinforcement to achieve a comparable moment capacity to the IBTS detail. These two details were studied to observe the effect of skew on the behavior of the bridge deck under applied loading. As reported in Ryan (2003) and Griffith (2003), the UTSE and IBTS edge details exhibited similar behavior and capacity, indicating there is no significant advantage to having the increased thickness of the IBTS edge detail with a uniform slab thickness construction is simplified.
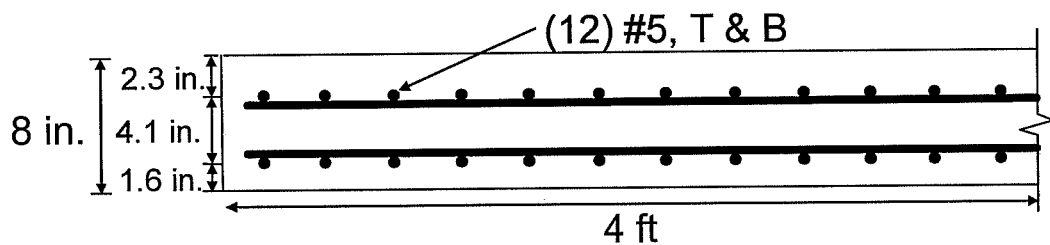
Figure 1.3 Cross-section of UTSE detail (Ryan 2003)

Another alternative to the UTSE detail is the combination of prestressed concrete deck panels and cast in place concrete topping at slab edges, shown in Figure 1.4. Prestressed concrete deck panels were first used in bridge construction to reduce construction time and eliminate the use of formwork in the interior portion of bridge decks. Prior research in prestressed concrete deck panels focused primarily on the composite action between the panels and the cast-in-place concrete topping, and not the behavior and capacity of the section at slab edges (Buth, et al. 1972). The research described here is intended to evaluate the behavior and capacity of an edge detail using prestressed concrete deck panels at slab edges and to help resolve any installation issues concerning expansion joint rails.
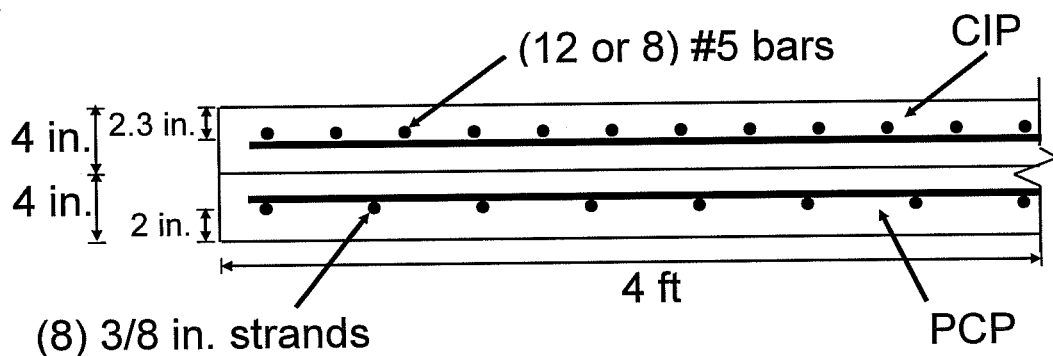
Figure 1.4 Cross-section of Prestressed Concrete (PC) Panel and Cast-in-Place Concrete Topping Section

1.3 OBJECTIVES AND SCOPE

The objectives of the TXDOT research study were as follows:

- To understand and explain the behavior of slab edges at expansion joints, with special emphasis on skew edges.
- To determine the performance of the IBTS detail when loaded with design loads (HS-20 and HS-25) and typical overloads.

5

- To determine the ultimate capacity and failure mechanism of the IBTS detail.

- To test alternate edge details and compare the behavior with the IBTS detail.

- To evaluate the reserve capacity provided by armor and sealed expansion joints.

- To develop guidelines for TxDOT engineers to follow in designing bridge-deck edge details, if current practice is shown to be inadequate.

Three test specimens have been constructed. The first specimen, built with $0°$ skew, had both the IBTS and UTSE edge details and was tested to compare the performance of those details. Results for the tests on the first specimen are given in Ryan (2003). The second specimen, built with $45°$ skew, had both the IBTS and UTSE edge details and was tested to understand the effects of skew on the slab edge behavior. Results for the tests on the second specimen are given in Griffith (2003). The third specimen, the subject of this thesis, was built with $0°$ skew at both edges with stay-in-place prestressed concrete deck (PC) panels and cast-in-place concrete topping. Test results from the PC panel specimen are presented as well as a comparison of results with the CIP $0°$ skew specimen. It is important to note that the purpose of this thesis deviates slightly from the previous theses reported during the progress of this research project. The theses by Ryan (2003) and Griffith (2003) evaluate the behavior of the IBTS and UTSE edge details for slabs. This thesis focuses on the behavior of a simpler detail than the UTSE detail and to resolve construction issues that may impede implementation.

2.4   SITE VISITS

To observe the IBTS detail as constructed in the field, two site visits were made prior to building the first specimen. The first bridge visited, located on IH-35 in San Marcos, TX, crossed the San Marcos River. The second bridge was an overpass on US 290, crossing over US 183. Witnessing the construction of slab edges allowed for observations of differences between the IBTS detail and other slab edges during construction.

As mentioned previously, most TxDOT bridge construction includes prestressed panels as stay in place formwork in the in

terior of the deck, up to the IBTS detail. Prestressed concrete girders were used in both bridges; Figure 1.5 shows the top of a girder with stirrups extending into the deck.
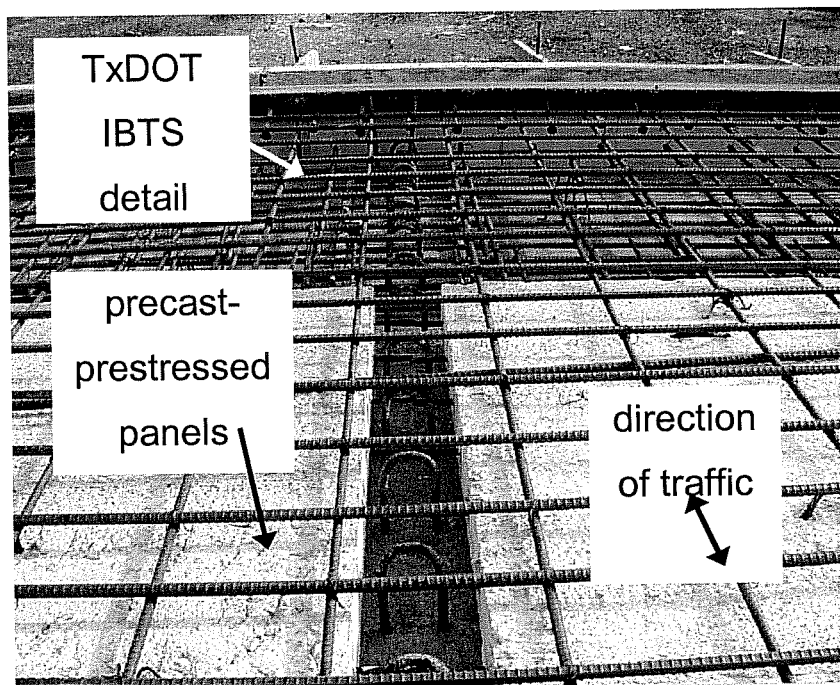
Figure 1.5 Prestressed panels and shear stirrups (Ryan 2003)

Armor joints and sealed expansion joint rails were cast into the top edge of the decks at the expansion joints (Figure 1.6). Although this is a standard detail in TxDOT designs, it was not included in the first and second specimens. The armor and sealed expansion joint rails are assumed not to contribute to the strength of the slab at the joint in design calculations. However, the reserve capacity provided by the armor (AJ) and sealed expansion joint (SEJ) rails was of interest to TxDOT engineers.
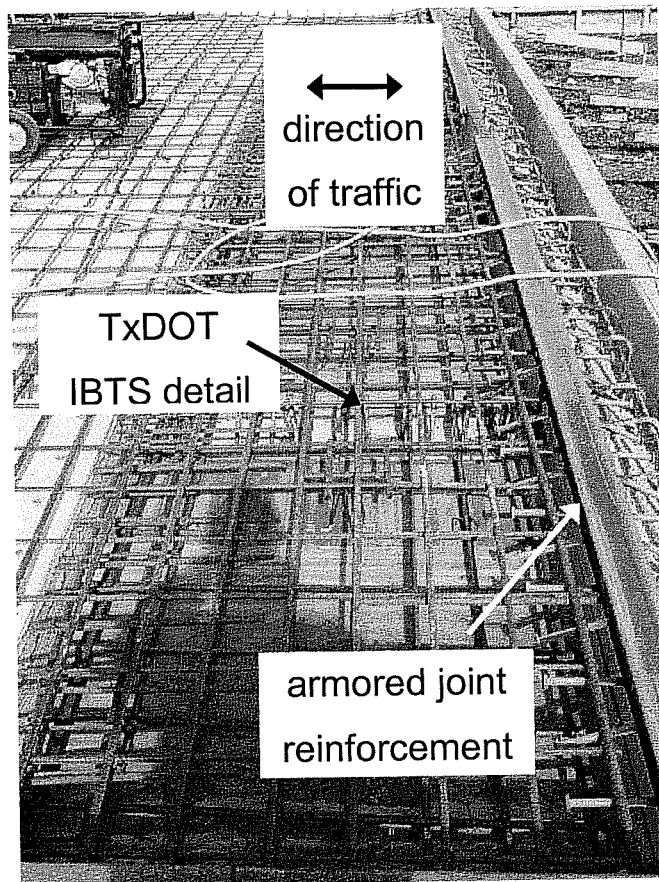
Figure 1.6 IBTS detail prior to concrete placement (Ryan 2003)

In the field, deck concrete was placed using a concrete pump, and was consolidated using mechanical vibrators. The surface was leveled using a vibrating, movable screed on temporary rails (Figure 1.7), and finished with bull floats. Concrete placement was a continuous process, allowing for long lengths of decks to be placed efficiently. These field construction techniques were modified for constructing the laboratory test specimens (Section 4.2).

Figure 1.7 Placing concrete in the field (Ryan 2003)

2.5 OUTLINE OF THIS THESIS

In Chapter 2, previous research in areas related to slab edges at expansion joints and stay in place prestressed concrete panels in bridge decks are

summarized, and their relevance to this research program are discussed. In Chapter 3, the development of the 0° skew and 45° skew specimen with the IBTS and UTSE details are briefly addressed, followed by a detailed discussion of the development of the PC panel specimen. In Chapter 4, test methods and means are discussed. In Chapter 5, results from the PC panel expansion joint edge tests are discussed followed by a comparison of the behavior of the six serviceability and four failure span tests. In Chapter 6, results from tests performed on the overhangs of the PC panel specimen are presented and discussed. In Chapter 7, results from the 0° skew specimen with IBTS and UTSE details and PC panel specimen are compared and discussed. In Chapter 8, the results from the expansion joint edge and the overhang tests in the PC panel specimen are summarized, as well as a discussion of design methodology for slab edges and conclusions based on those results.

CHAPTER 2

Previous Bridge Deck Research

2.1 INTRODUCTION

Research studies pertaining to the understanding of bridge-deck behavior, including punching shear capacity and arching action, are discussed and summarized (Ryan 2003 and Griffith 2003), as part of their theses on the first two specimens tested in this project. However, the purpose of this thesis is to study the behavior of a composite deck made up of prestressed, precast concrete (PC) panels and a cast-in-place (CIP) concrete topping slab. Therefore, research studies that contribute to understanding the behavior of a composite bridge deck sections are summarized in this chapter.

2.2 EARLY RESEARCH-BEFORE 1990

The idea of using a composite bridge section with PC panel and CIP concrete topping began in order to reduce bridge construction cost and time by eliminating the use of formwork. Early research on such composite sections focused on understanding composite action between the PC panel and CIP concrete topping. Experimental research conducted to determine the behavior of PC panels and CIP concrete toppings has varied between full-scale and nearly full-scaled testing.

2.2.1 Buth, Furr and Jones (1972)

To experimentally and theoretically investigate the ability of the composite bridge deck of PC panels and CIP concrete topping to distribute wheel loads and behave as a composite unit, Buth, Furr and Jones (1972) conducted a

11

series of fatigue and static tests on a full-scale specimen and a segment of a full-scale bridge deck. Various locations on the full-scale bridge slab were tested; the emphasis was on the deck performance at the butt joint between two adjacent panels. The specimens were subjected to a series of fatigue loadings and then taken to failure under static loading.

The full-scale bridge slab specimen (Figure 2.1) was constructed using current AASHTO standards. The specimen was 23 ft wide and spanned 50 ft. Four Type B prestressed, precast girders supported the specimen. To better represent then current bridge construction, several diaphragms were installed at the edge and interior of the bridge slab. The deck section consisted of 3-¼ in. thick PC panels and 3-½ in. thick CIP concrete topping. Two types of panels were used: interior panels, which spanned between the girders, and exterior panels, which were supported by two girders and then extended 2 ft, 6 in. past the exterior girder. In addition to the PC panels, various techniques for transfer of forces across the PCP/CIP slab interface were used at various locations on the bridge slab. The three techniques for improving bond were: Z-bars used for shear and tensile bonding (Figure 2.2), portland cement grout used as a bonding agent, and no treatment of the panel or interface (as-delivered) for the remaining sections of the slab. Dowel bars were placed on the surface of the panels over select transverse butt joints to investigate load transfer over those joints (Figure 2.2). The second specimen was a segment of a full-scale bridge deck, 8 ft, 6 in. by 9 ft. The purpose of the slab segment was to evaluate a panel butt joint reinforcing detail of Z-bars and dowel bars across the panel butt joint. The two PC panels were 3-½ in. thick and a 4-½ in. CIP concrete topping was cast atop of the panels. Both specimens were instrumented to measure deflection, deformation, and rotations, especially the deflection between the panel and the girders.

Interior panels
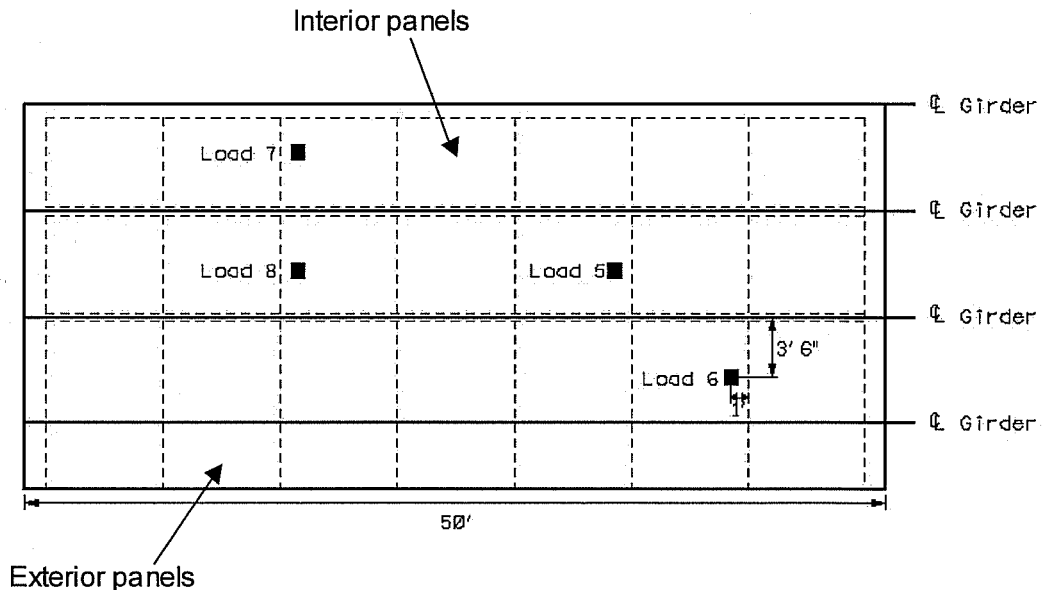
Figure 2.1 Static load locations (Buth, Furr and Jones 1972)
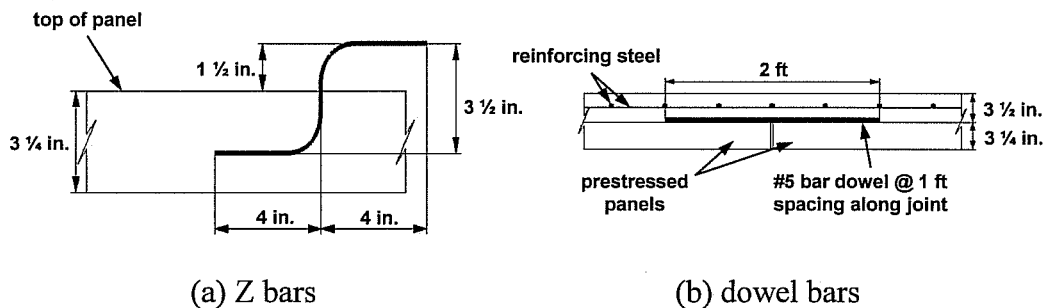
(a) Z bars   (b) dowel bars

Figure 2.2 Techniques for transfer of forces across PC panel and CIP
interface: (a) Z bars; (b) dowel bars (Buth, Furr and Jones 1972)

The specimens were subjected to a series of fatigue loads based on design wheel loads at service loads plus the impact factor. Fatigue loading was applied to the either side of panel butt joint. After the fatigue loading series, the specimens were subjected to static failure loads to determine the magnitude of load at failure, the mode of failure and the influence of the dowel and Z-bars. Static loading locations are shown in Figure 2.1. Fatigue loading locations (Loads

13

1 through 4) are not shown or discussed since behavior due to fatigue loading is not relevant to the scope of this project.

Before testing began, extensive analyses of the structures based on folded-plate theory and Westergaard's theory of plate behavior was conducted. The folded-plate analysis of the composite slab and beam bridge deck consisted of breaking the deck up into a series of plates and beams, and developing relationships between the edge forces and edge displacements, as well as loads, using series expansion. The equations of equilibrium at the juncture between the plates and beams were developed in terms of edge displacements and then solved. Those solutions then could be used to determine moments, stresses, strains, etc. at any point on the beam or plate element. The slab bending moment equations were based on Westergaard's theory of plate behavior and modified to fit the boundaries of the bridge slab. The maximum bending moment equation developed is shown in Equation 2.1, where M_{ox} is the approximate bending moment calculated using Westergaard's theory, P is the applied load, a is the center-to-center spacing of wheel loads, and S is the span length.

$$M_X = M_{OX} + 0.2107P \log_{10} \left(\frac{\cot(\frac{\pi^a}{4S})}{2} \right)$$
Equation 2.1

However, for the analysis the bridge deck, the discontinuity between precast panels was ignored.

The static load results for the full-scale bridge slab indicated cracking developed on the top and bottom surfaces around 80 to 120 kips and 110 to 150 kips, respectively. All test locations failed in punching shear at loads much higher than the design load. For test locations 5, 6 and 8, the failure surface showed no apparent influence of the panel butt joint (Figure 2.3). However, for test location 7, one segment of the surface intersected a panel joint, but did not

develop in the adjacent panel (Figure 2.4). The cracking and failure loads for the full-scale specimen are shown in Table 2.1.
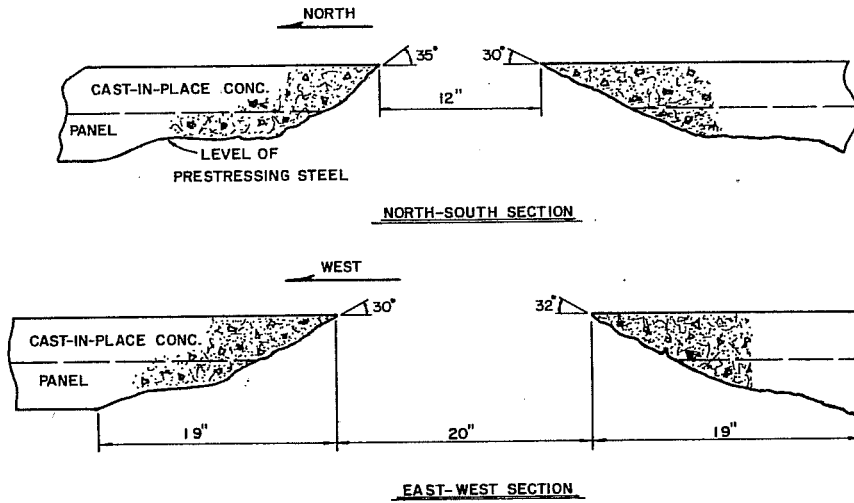
Figure 2.3 Failure surface of loads 5, 6, and 8 (Buth, Furr and Jones 1972)
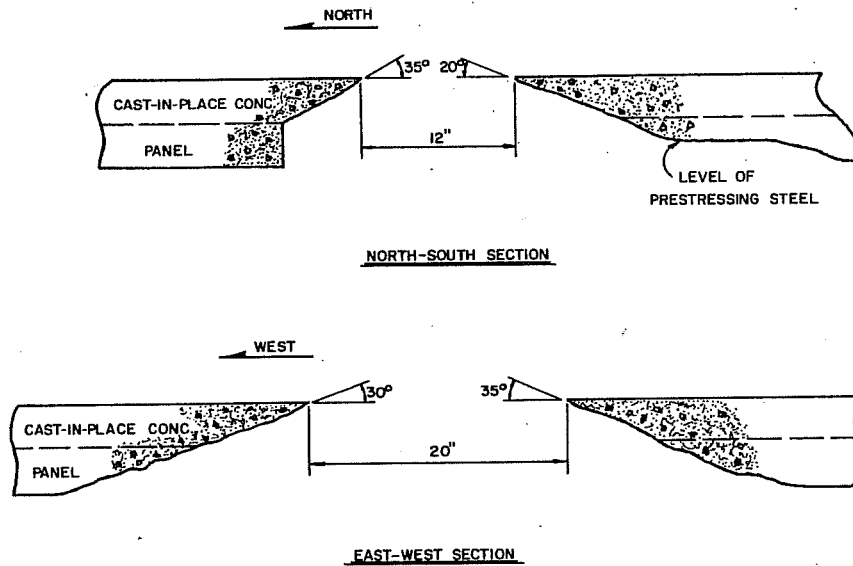
Figure 2.4 Failure surface of load 7 (Buth, Furr and Jones 1972)

15

Table 2.1 Cracking and Failure Loads (Buth, Furr and Jones 1972)

Testing Location	Cracking Load (kips)	Failure Load (kips)
5	90	270
6	110	280
7	120	250
8	80	260

Actual failure loads were compared to failure loads predicted by yield line theory and AASHTO and ACI punching shear theory. ACI assumes a lower bound shear stress not to exceed $4\sqrt{f_c'}$, which gives an ultimate load of 140 kips when the panel butt joint is included and 156 kips when the panel butt joint is not included. However, when the punching shear stress is calculated using Equation 2.2, the loads are 186 kips and 210 kips, with the panel butt joint included or excluded, respectively. The effective depth of the slab is d and r is the side dimension of the loaded area.

$$v_u = 4(\frac{d}{r} + 1)\sqrt{f_c'}$$

Equation 2.2

In any case, the loads predicted using the ACI equations were as much as twice the measured loads at some test locations. The loads predicted by the yield line theory were significantly higher than the actual failure load. Each test showed significant flexural cracking before the test failed in punching shear. The behavior was summarized as follows:

> "With the application of a concentrated load and partial development of the failure mechanism, in-plane extension of the slab occurs in the area of the failure mechanism. This extension is restrained by the surrounding portion of the slab, and compressive in-plane stresses are thereby created in the area of the failure

mechanism. This phenomenon, in a "rigidly" restrained slab, was observed ... to increase the flexural strength of a lightly reinforced slab by 10.9 times. This same phenomenon also enhances the punching shear capacity of a slab" (Buth, Furr and Jones 1972).

For the static failure test of the slab segment model, longitudinal cracking began on top of the slab and extended along the girder before circling around the loading pad. Flexural cracks on the bottom surface of the panel extended the full width of the panel being loaded, but did not extend into the adjacent panel. The failure load was 155 kips, in punching shear.

Transverse cracks were observed in the CIP concrete topping, which was attributed to thermal and shrinkage effects. These cracks did not have any detrimental effect on the performance of the bridge deck. However, when interior diaphragms were used to support the slab, the resulting negative longitudinal bending moment causes cracks near the diaphragms to grow and propagate. In addition, to these observations, the details used for ensuring shear, bond and load transfer did not provide any measurable improvement in performance. Finally, Buth, Furr and Jones (1972) concluded the bond at the interface between the PC panels and CIP concrete topping showed no distress under the fatigue and static loadings.

2.2.2 Kluge and Sawyer (1975)

To determine if the use of stay in place form PC panels without mechanical connectors is possible for concrete bridge decks, Kluge and Sawyer (1975) performed four series of tests to assess the adhesive bond at the interface of the panels and CIP concrete topping, and flexural and shear capacities of the composite section. All specimens were cast with 4 in. of CIP on a 3 in. thick PC panels, with 7/16-in. diameter seven-wire (270 ksi) prestressing strands spaced 9 in. on center placed 1-¼ in. from the bottom surface of the panel.

17

The first series of tests (A) were beam tests in order to assess the dependability of the adhesive bond at the interface between the PC panel and CIP. The specimens were 18 in. wide and 8 ft. long. No special treatments were used to enhance bond between the PC panel and CIP, except that form oil was applied to one specimen to reduce adhesion along the interface. Each beam was subjected to cyclic loading approximately 80 to 95% of the average adjusted ultimate load determined from static load specimens that failed in shear or combined shear and moment. Most beams behaved like a monolithic concrete flexural member in both static and cyclic loading. Flexural cracks and diagonal shear cracks passed through both the PC panel and CIP without deviations of horizontal cracking at the interface. The only exception was the beam with form oil on the interface failed at a lower number of cycles than companion specimens with good adhesion. All the beams reached shear stresses that exceeded $2\sqrt{f_c'}$, the value used by AASHTO standard specifications and ACI for shear strength of concrete beams without flexural reinforcement.

In the second series of tests (B), the shear strength across panel joints was studied. There is an inherent weakness from the transverse joints formed at the abutting edges of the panels, especially in shear. Two types of specimens were built for this series of tests, unjointed and jointed specimens (Figure 2.5). Each specimen was loaded by a 6 in. diameter steel disk on either side of the joint or at the centerline of the specimen. First, a static load of approximately 90% of ultimate capacity was applied with one hydraulic jack. The specimen was then loaded in shear reversal (approximately 77 to 90% of ultimate capacity) by alternately loading hydraulic jacks on either side of the panel butt joint (Figure 2.6), and then tested to failure under static loading. Out of the seven specimens, five failed in punching shear and the other two failed in beam shear. For some of the specimens, there was separation at the interface, but the ultimate capacity was

18

not affected. Separation of the interface occurred at the supports of the jointed specimens. The authors noted this would not likely occur if slab continuity and normal support conditions had existed. For the unjointed specimens, no separation occurred at the interface between the PC panel and CIP. The ultimate punching shear strength was 5% less for the jointed specimens when compared to the unjointed specimens. End slip of the strands was evident at failure for several of the jointed and all of the unjointed specimens.

Cast in place
concrete

7"

3'

Prestressed
concrete panel

3"

1.5'

(a) unjointed specimen
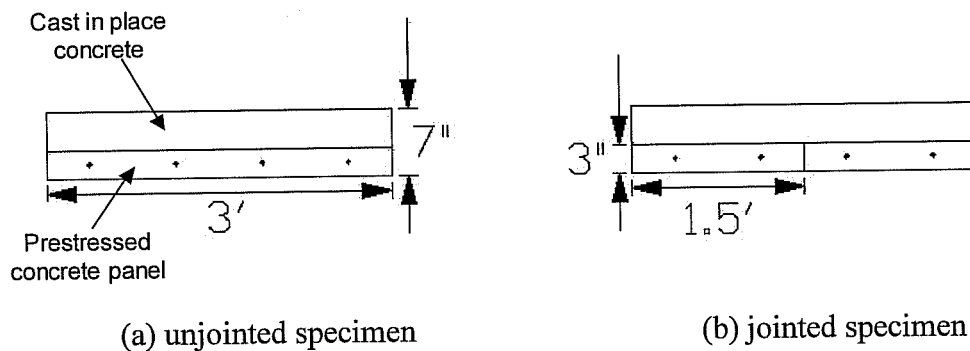
(b) jointed specimen

Figure 2.5 Example of jointed & unjointed specimens (Kluge and Sawyer 1975)

36 in.

transverse joint on jointed
specimens or centerline of
unjointed specimens

30 in.

point support

6 in. diameter
steel load plates
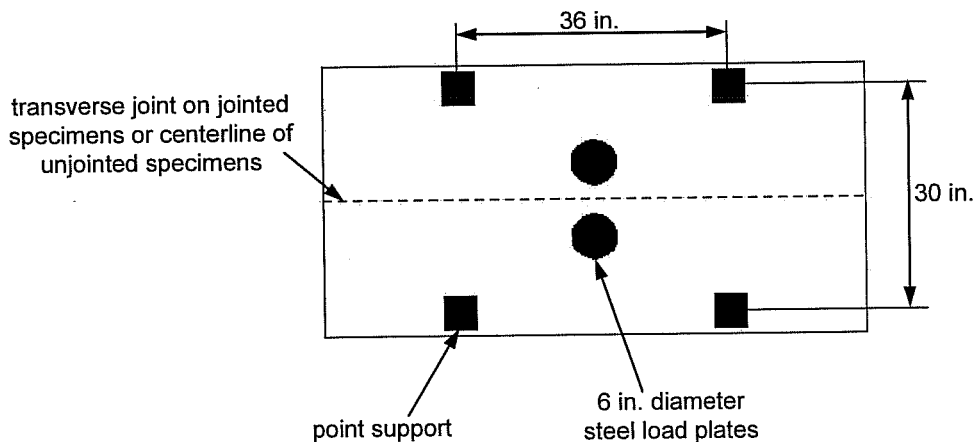
Figure 2.6 Test Series B testing configuration (Kluge and Sawyer 1975)

The next series of tests (C) were conducted to observe the affect of the cracks over the panel butt joints on the flexural strength of the deck. The

19

specimens were subjected to positive moment loading, which included static and cyclic loading. The specimen cross-section was 54 in. by 7 in. with a 50 in. span (Figure 2.7). For all the tests, the ultimate moment capacity agreed well with the calculated ultimate moment capacity.

(a) cross section of specimens   (b) plan view of specimens
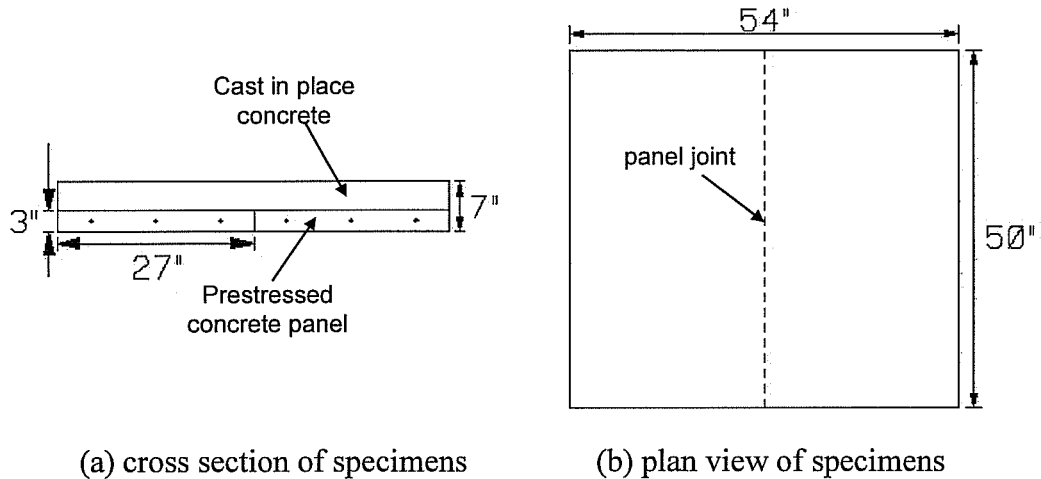
Figure 2.7 Example of specimens, Series C (Kluge and Sawyer 1975)

In the final series of tests (D), the strand development and punching shear strength of the composite section were examined. For these tests, the supports were adjusted to provide indeterminate restraints similar to an actual bridge panel with adjoining bridge girders and decking. Depending on the support location, the strength of flexure and shear effects determined the behavior, but in all specimens, punching shear controlled failure. Ultimate loads generally compared well with the calculated ACI punching shear strength.

Kluge and Sawyer (1975) concluded from all four series of tests that there was excellent interaction between PC panel and CIP concrete topping under flexural conditions. Also, no significant adverse effects of joints between panels on punching shear strength and flexural strength were found. In addition, using grout or concrete that would "flow" to fill the gap under the panel over a support and provide a sound bearing area for the PC panel is suggested instead of relying

on relatively soft materials such as fiberboard. The authors noted that several decks that had panels supported by fiberboard exhibited severe cracking and spalling after a short time in service.

2.2.3 Bieschke and Klingner (1982)

After prestressed precast panels had been in use for some time, construction techniques were developed to provide better quality control of the panels. This included producing more consistent shapes of the panels by having a continuous casting bed. In order to incorporate the continuous casting bed, the strand extensions needed to be eliminated from the panel's transverse edge. Bieschke and Klingner (1982) investigated bridge performance using panels with and without strand extensions under static and fatigue loading. Although, the primary objective of Bieschke and Klingner's (1982) research study is not in the scope of this research project, the other objectives of their research include the response of the bridge deck under concentrated loading and effectiveness of practical construction details, which do pertain to this research study. A full-scale, 50 ft by 18 ft, 9 in., bridge deck was constructed and tested. The bridge deck included two 3 ft, 1-½ in. overhangs and two 6 ft, 3 in. bays. Three TxDOT Type B prestressed precast girders supported the deck. Two types of 4 in. thick PC panels were used, one with strand extensions and one without strand extensions. The U-bars (Figure 2.8) embedded in the surface of the panels for lifting the panels and for shear interaction between the panel and CIP concrete topping, were removed from one-half of the bridge deck. The CIP concrete topping was typical of TxDOT standards, which included a minimum concrete compressive strength of 3600 psi and a 4 in. slump before casting. The total thickness of the bridge deck was 7-¾ in. Typical to current bridge construction at the time, diaphragms were installed at the interior and edges of the specimen.
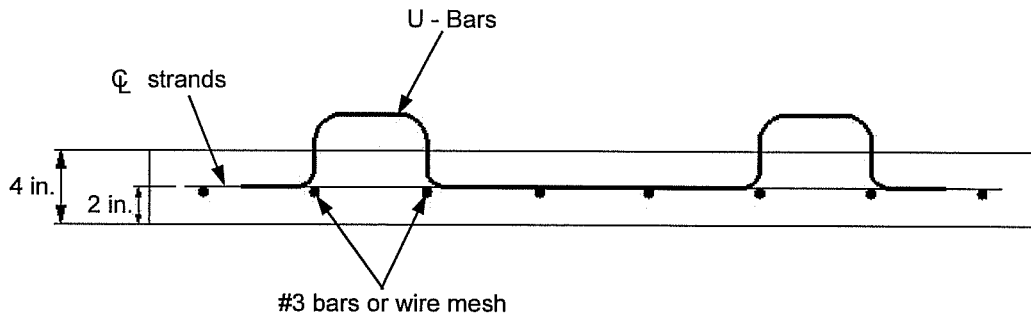
Figure 2.8 U-bars (Bieschke and Klingner 1982)

There were a series of static and fatigue tests to determine the behavior of the bridge deck and girder before and after fatigue testing. After the four static tests and 2 fatigue test series, ten concentrated load tests were conducted at various locations on the bridge deck, including the overhangs (Figure 2.9). Deflection, longitudinal slip between panels and girders, and rotations and separations across panel joints were measured during all tests. For all but one concentrated load test, a 1 in. by 8 in. by 20 in. load plate was used as well as a ¾ in. by 8 in. by 20 in. neoprene pad. For the first concentrated load test, a 1 in. by 12 in. by 12 in. plate was used. All concentrated load tests exhibited either punching shear or combination of flexure and punching shear at failure, as seen in Figure 2.10 and Figure 2.11.
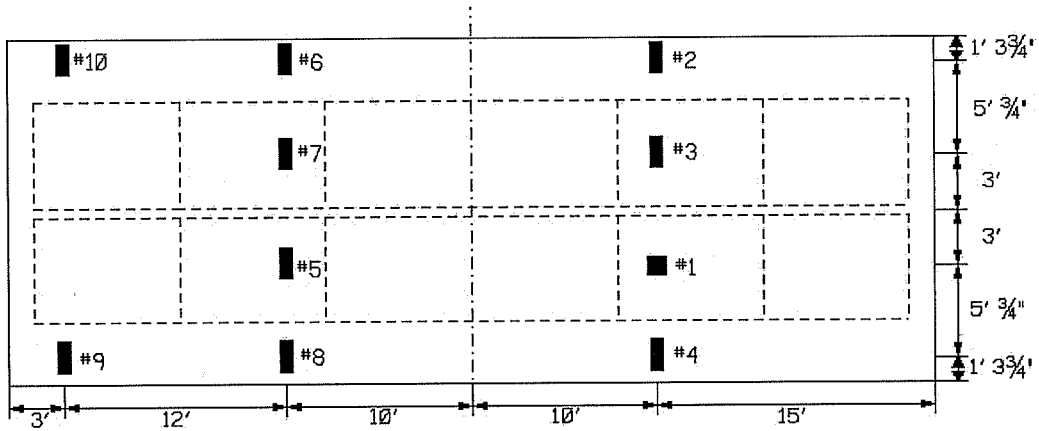
Figure 2.9 Concentrated load test locations (Bieschke and Klingner 1982)

SECTION
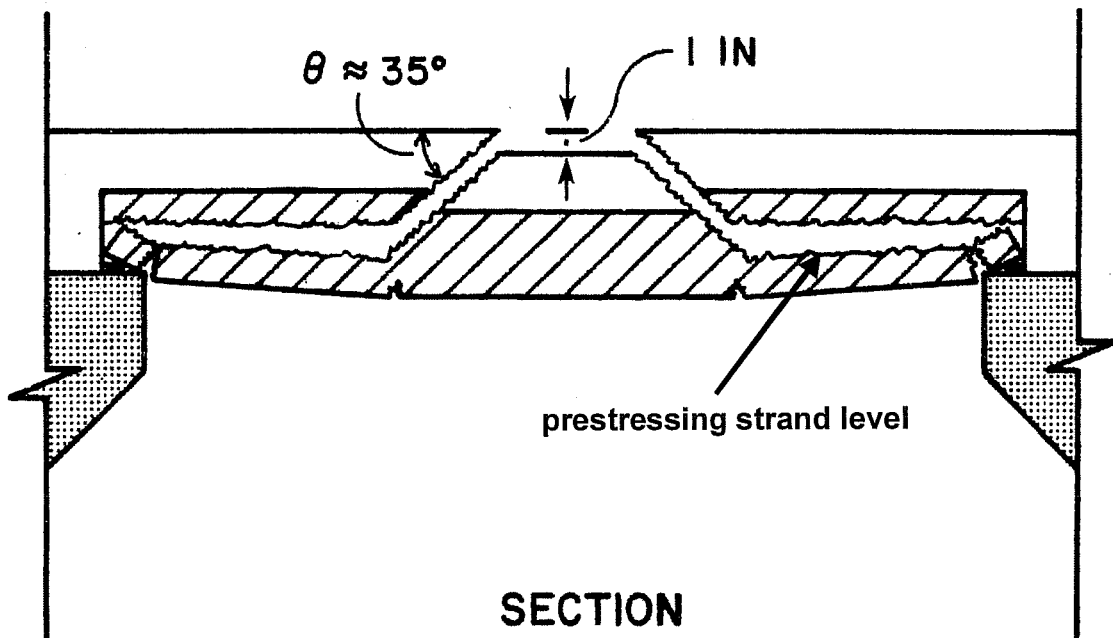
Figure 2.10 Failure surface of interior slab location (Bieschke & Klingner 1982)

23

SECTION
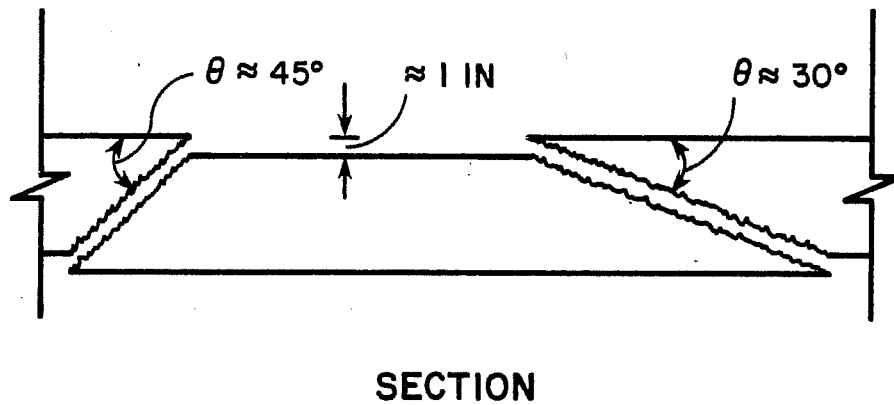
Figure 2.11 Failure surface of overhang location (Bieschke & Klingner 1982)

The failure loads for the concentrated load tests (no moment was induced) were compared to punching shear theory set by the 1977 AASHTO standard specifications and by yield line theory. At failure loads, the panels exhibited significant flexural cracking on the bottom surface of the panel indicating a possible yield line pattern combined with punching shear failure in the upper portion of the panel and the CIP concrete topping. All failure loads exceeded the design loads of the bridge deck. For the test locations at the interior of the bridge deck, a concrete compressive strength of 6000 psi was assumed, to reflect the two different compressive strengths of the panels and the CIP concrete topping. The effective depth of the slab was taken to be the distance from the top of the slab to the centroid of the prestressing strands. The punching shear theoretical calculations were 11 to 19% less than the actual failure loads for the rectangular plate and 36 % less for the square load plate. The loads calculated using yield line theory were comparable to those calculated using punching shear theory. For the punching shear capacity calculations for the test performed on the overhangs, a concrete compressive strength of 4400 psi was assumed, as well as an effective

depth to the centroid of the bottom reinforcement. In addition to these assumptions, one edge of the shear perimeter was considered ineffective due to the loading plate's location near the edge of the slab for the tests performed in the middle of the overhangs. For these tests, the actual failure load was between the load predicted by punching shear and yield line theories, where the calculated yield line load was 8 to 10% higher than the actual failure load. For tests performed at the corners of the overhangs, two sides of the shear perimeter were assumed to be ineffective. The calculated loads based on yield line theory best estimated the actual failure load at the corners of the overhangs.

Bieschke and Klingner (1982) concluded overall bridge deck behavior and local behavior were not different when panels with or without strand extension were used. Yield line and punching shear theories provided conservative estimates of actual failure loads for concentrated loadings. Also, longitudinal reinforcement used in overhangs does increase the capacity of the overhangs. As noted earlier, local continuity between the girders and the panels is dependent on the amount of concrete that fills the space between the end of the panels and the bearing pad (Figure 2.12). Insufficient concrete under the panels creates the situation where the panels bear only on the flexible fiberboard strips, which result in panel settlement and longitudinal cracking along the panel edges at the girders. U-bars were concluded to have no structural contribution, but may improve shear transfer if bonding between the CIP concrete topping and the PC panel is inadequate. The local deformations at transverse joints indicate deformations are associated with decreased local continuity, which is a function of the shape and placement of panels.

Min. ½ in.
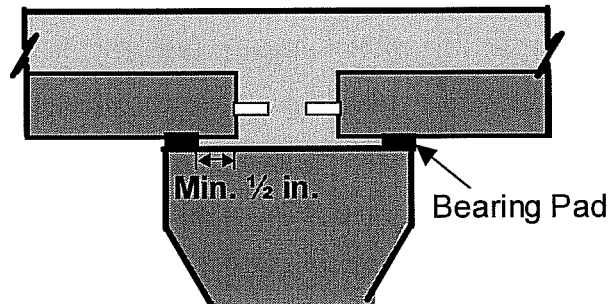
Bearing Pad

Figure 2.12 Minimum amount of concrete fill between panel and bearing pad

2.2.4 Fagundo, Tabatabai, Soongswang, Richardson, and Callis (1985)

Fagundo, et al. (1985) examined a number of issues related to precast stay-in-place bridge deck systems, including the cause of extensive cracking in these systems, structural integrity in the cracked condition, design life, differences in performance between the panel deck system and CIP concrete decks, varying support conditions, and remedial steps for cracked bridge decks. To examine all of these aspects, field testing of panel deck systems and CIP decks in use in Florida was conducted, as well as laboratory testing and finite element modeling.

For field testing, several bridge decks were tested to determine the amount of composite action and structural adequacy provided by three different decking systems: panel decking system supported by fiberboard strips, panel decking system supported on grout, and standard CIP decking system. A fully loaded water tanker was jacked against in order to test the bridge decks to desired loadings. Each bridge was loaded to AASHTO HS-20 wheel load with an impact factor of 0.3. Loads were applied to first maximize bending moment and then to maximize shear near the ends of the panels. Load-deflection behavior indicated a linearly elastic response up to around 1.5 times HS-20. Finite element models were analyzed to compare with the field test data. Moment profiles of the bridge

26

decks indicated moments at the face of the girders for the panel deck systems were essentially zero, but the CIP decks did exhibit significant negative moments at the face of the girders, which were compared with the predictions from the finite element models. The only concern after the field tests were completed was that with the lack of continuity at the ends of the panels, shear would not be effectively transferred across the panel ends. The concern for shear transfer at the panel ends became focus of the laboratory testing.

The laboratory testing focused on the shear behavior at the ends of the stay-in-place panels. Nine slab specimens were tested to failure. Specimens consisted of a full-size 8-ft. by 8-ft., 2-in. thick PC panel, cut in half and then placed side by side to represent a typical transverse joint. The specimens were not supported by fiberboard under the panels. A prefabricated joint along the longitudinal end was made, since previous research showed a separation occurs along the longitudinal end joint in the CIP concrete topping due to differential creep and shrinkage. The edges of the loading plates were placed 4-in. from the transverse panel joint. This configuration was assumed to create the most critical condition for punching shear in the CIP topping. The joints were subjected to static and fatigue loading. In most static tests, cracking began around 60 kips and failure (punching shear) occurred between 90 and 100 kips. Test results showed localized separation or delamination occurred at the interface between the panel and CIP topping at the transverse joint. After failure, field repair methods (no details of the repair procedures were given) were used to repair the specimens, and test results indicated the slabs regained nearly all of the original stiffness after repair and had higher ultimate strengths.

Fagundo, et al. (1985) concluded that panel deck systems behave more like a series of simply supported beams than a continuous span (CIP deck). Similar to Buth, Furr and Jones (1972), the authors stated shear stress

concentrations were reduced when panels were supported by grout or mortar rather than fiberboard or foam. Again, similar to previous research conducted, the performance of the panel deck systems was comparable to CIP decks, especially at AASHTO design loads. Also, delamination occurs in a small area at the interface between the panel and CIP topping under high loading at the panel ends.

2.3 RECENT RESEARCH – 1990 TO PRESENT DAY

Recent studies selected for detailed discussion included those contributing to an understanding of the behavior of the composite section at expansion joint edges. Though no study focused directly on this issue of the behavior of the composite section at the slab ends, many addressed relevant topics.

2.3.1 Fang, Tsui, Burns and Klingner (1990)

Previous research on arching action in cast in place concrete bridge decks have been conducted on scaled specimens, Fang, et al. (1990) investigated the fatigue behavior of panel decks, differences between PC panel deck and CIP concrete decks under fatigue loading and the effects of intermediate diaphragms in a full scale specimen. Although fatigue effects on bridge slabs is beyond the scope of this project, Fang et al. (1990) conducted static tests, which are relevant to this thesis. A full-scale 20 ft. by 50 ft. bridge deck was constructed using TxDOT standard details for Ontario-type decks. One half of the deck consisted of a CIP section and the other half was the composite section of prestressed concrete panels and CIP topping. The bridge deck had a uniform thickness of 7–½ in.

Testing was conducted in two phases: positive moment loading and negative moment loading. For the first phase, a four-point loading representing the AASHTO standard truck axle loading (HS-20) was applied to the specimen. One loading was placed on the CIP half of the deck and another loading on the PC panel half of the deck (Figure 2.13). The specimen was subjected to fatigue and

28

static loading based on AASHTO truck loadings and impact factor. The maximum load during the fatigue testing was 25 percent higher than the service load of 16 kips, and static tests were conducted using multiples of AASHTO design load. The bridge was first loaded statically to approximately three times the AASHTO design load, and then subjected to 5 sets of fatigue loading with 1 million cycles and a maximum and minimum load of 26 and 5 kips, applied in each set. After the fatigue testing cycles, the deck was then loaded statically to approximately 40 kips to observe its service and overload behavior after fatigue loading. A series of dial gauges and strain gauges were used to observe load-deflection and load-deformation of the deck at several locations (midspan, over the girders, slip between girders and concrete). Test results indicated no significant change in stiffness occurred in the CIP and PC panel regions of the deck after fatigue loading. During the first static loading, the cracking load was very close to the load predicted by the analytical model. In addition, cracks formed on the bottom face of the deck under the loading plate and on the top face of the deck over the supports. During the fatigue-loading phase, cracks extended in the CIP deck, but not in the PC panel deck. Crack widths for the CIP and PC panel regions at service loads were 0.008 in. and 0.003 in., respectively. The load-deformation plots indicated fatigue cycling after flexural cracking had developed did not further degrade stiffness. In addition to the pre- and post-fatigue behavior, the effect of intermediate diaphragms was observed. Test results indicated the presence of diaphragms did not significantly change the load-deflection behavior of the deck near the loaded point and the stresses at the girders.

support

10'   10'

3'
3'

Panel (PCP) deck

2 – 7 ft. by 6 ft., 6 in. panel

Cast in place deck

4 – 8 ft. by 6 ft., 6 in. panel
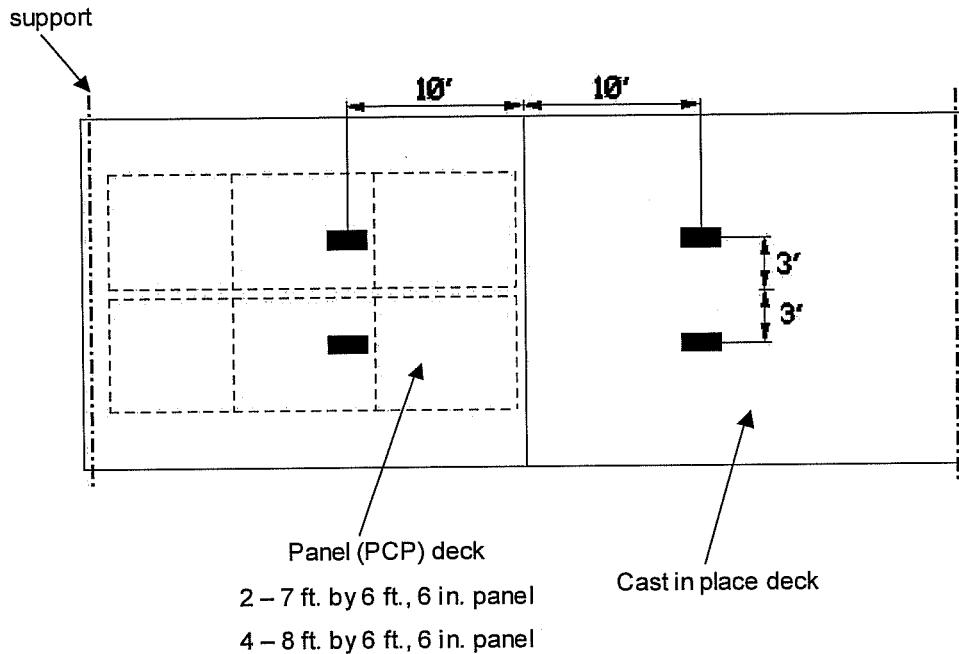
Figure 2.13 Loading pattern for Phase I (Fang et al. 1990)

In the second phase of testing, the loading pattern shown in Figure 2.14 produced maximum moments at the interior support. The testing procedure was similar to the first phase, only the maximum load for the first static loading was 30 kips (1.5 times the service live load). The deck was then subjected to the same number and magnitude of fatigue cycles as in the first phase tests. The maximum static load following the fatigue cycles was 55 kips. Similar to the first phase, deck cracking did not significantly affect the deck's stiffness. Again cracking occurred during the first static loading for both the CIP and the PC panel ends of the deck, and cracking developed in the CIP end of the deck and not the composite end of the deck during fatigue testing. The lack of crack development during fatigue testing indicated the panel deck, with a higher concrete strength and prestressing, has a higher cracking moment than the CIP deck. Test results showed residual strains from fatigue loading did not affect the measured reinforcement strains during static load tests.
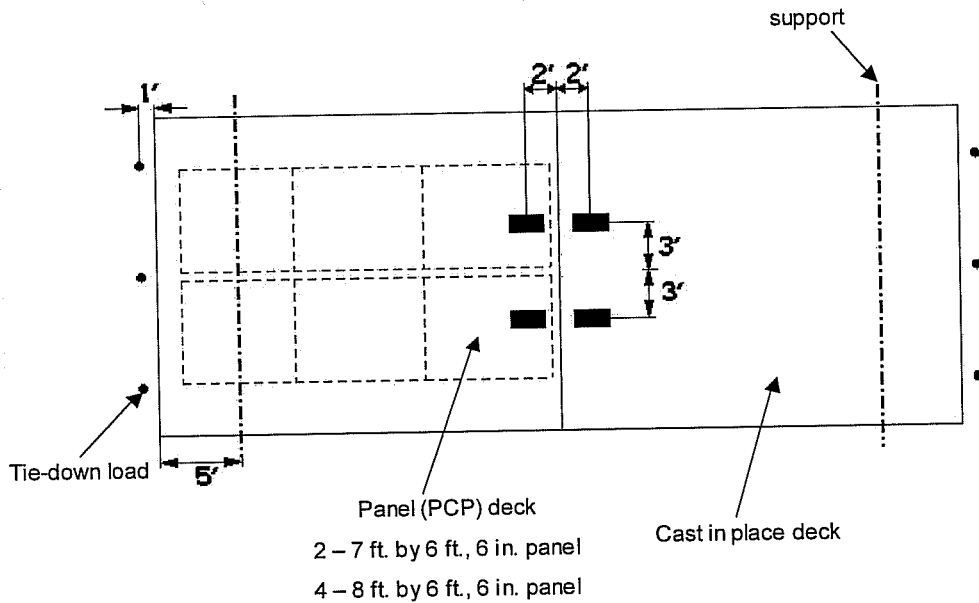
Figure 2.14 Loading pattern for Phase II (Fang et al. 1990)

In summary, Fang, et al. (1990) concluded that panel decks under positive and negative moment loading performed similarly and satisfactorily compared to CIP decks at current AASHTO design loads. Fatigue loading did not significantly change the behavior of the deck under AASHTO service and overload conditions. Intermediate diaphragms had no significant effect on local stiffness, stresses and moment distribution under loading. Panel decks were concluded to be superior to CIP decks in terms of cracking and stiffness of the deck.

2.3.2 Abendroth (1995)

While previous research on precast prestressed concrete panels as subdecks has focused on $0°$ skew specimens, Abendroth (1995) investigated the nominal flexural and shear strength of a composite slab system on $0°$, $15°$, $30°$, and $40°$ full-scale models. He conducted 5 full-scale tests that included static load tests under service level loads and factored service level loads, and eventually

ultimate load tests. Specimens No. 1 and 2 had a 0° skew, and Specimens No. 3, 4, and 5 were 15°, 30°, and 40° skewed, respectively. Specimen No. 1 was to represent a deck at a location away from an abutment and/or pier diaphragm, and Specimens No. 2, 3, 4, and 5 were to represent various skew angles at locations adjacent to an abutment or pier diaphragm that supports the edge of a bridge slab (Figure 2.15). Each specimen consisted of two 2-½ in. thick PC panels and 5-½ in. thick CIP concrete topping. All PC panels had sixteen, 3/8 in. diameter, seven-wire, low-relaxation strands at mid-depth of the panel. All strands were stressed to approximately 17.2 kips (202 ksi) before concrete placement. In addition to the prestressing strands, a layer of welded wire fabric was placed before casting the PC panel. All panels had a raked finish applied to the top surface for bonding to the CIP topping. For the trapezoidal PC panels used in Specimens No. 3, 4, and 5, the two, three and four shortest strands in the 15°, 30°, and 40° skew angle, were sleeved along their entire length. The sleeves were used to prevent breakage of the acute corner of the panel during strand release when constructing the panels using a continuous panel casting bed. The concrete compressive strengths of both the PCP and CIP were a minimum of 5000 psi and 3500 psi, respectively, which was in compliance with the Iowa Department of Transportation standards.

Two 2-½ in. thick prestressed concrete panels

One rectangular and one trapezoidal 2-½ in. thick prestressed concrete panel

8' 8'

8

8' 8'

8

θ, skew angle

Abutment or pier

sleeved strands in skewed end
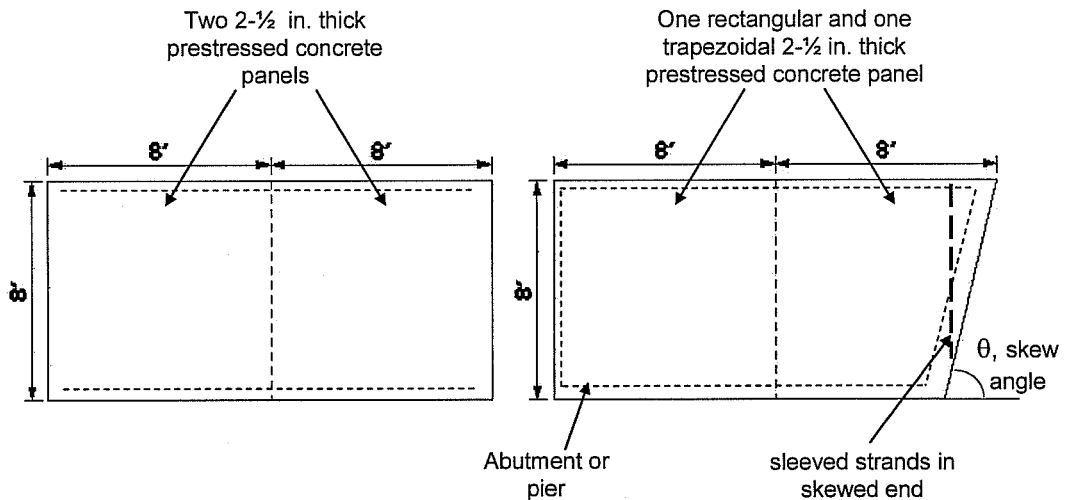
(a) Example of Specimen 1, without abutments and/or piers

(b) Example of Specimens 2, 3, 4, & 5, with abutments and/or piers

Figure 2.15 Example of specimen layouts (Abendroth 1995)

Before ultimate load testing was done, all specimens were subjected to a series of static, service level loads based on AASHTO provisions. These service load tests included a single wheel load or a tandem-loading configuration where wheel loads were 4 ft. apart. The maximum factored service load level for the tandem-loading configuration, was 20.8 kips, which included a 30% impact factor, and the maximum factored service load level for the single wheel load was 48 kips. Based on the recorded strains and displacements, service level loads did not produce noticeable distress in the specimens; however, some hairline cracking formed on the bottom surface of the PC panels. After the service level load tests were completed, a series of ultimate load tests were conducted on all five specimens. All specimens were subjected to two ultimate load tests (two different locations), except for Specimen 1, which was tested at only one location. Specimen 1 had an 8 in. by 20 in. loading plate placed over the joint between the two PC panels. Specimens 2, 3, 4, and 5 were tested to failure with a 9-1/8 in. by

33

18-½ in. plate, where one test was over the PC panel close to the support along the diaphragm, essentially at the geometric centroid of the panel, and the other test was 4 ft. from the free edge. An example of the loading locations for Specimens 1, 2, 3, 4, and 5 are located in Figure 2.16. To fully understand the ultimate capacity of the specimens, yield line models and punching shear strengths were calculated. Yield line models were based on the observed crack patterns, and the punching shear strength was determined using the AASHTO provisions (Equation 2.3).

$$V_{nc} = (2 + \frac{4}{\beta_c})\sqrt{f_c'}b_0 d \leq 4\sqrt{f_c'}b_0 d \qquad \textbf{\textit{Equation 2.3}}$$

(a) Specimen 1   (b) Specimens 2, 3, 4, & 5
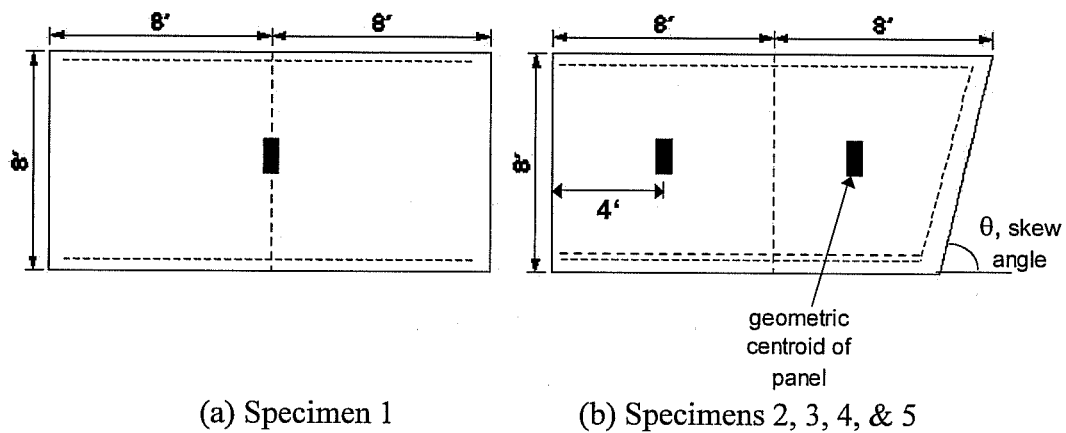
Figure 2.16 Examples of ultimate test loading locations (Abendroth 1995)

Table 2.2 summarizes the experimental ultimate loads, calculated yield line model collapse loads, and calculated punching shear strengths. Based on the tests completed, Abendroth (1995) concluded full composite behavior was observed between the PC panel and CIP and no slippage occurred at the strand ends at initial load levels. A crack always occurred in the CIP topping above the joint between the abutting PC panels, so the flexural resistance was provided by the PC panel section under the load. All specimens had essentially a linear load-

34

displacement behavior beyond the maximum service and factored service load levels. All specimens failed in punching shear, only two tests exhibited significant flexural cracking, but no flexural failure. Failure loads ranged from 6 to 8 times the service level load of 16 kips. Analytical models for punching shear strength were within 20 % of the ultimate load. Skew angles did not affect the nominal strength of the composite section.

Table 2.2 Ultimate Loads (Abendroth 1995)

Specimen	Test No.	P_u, measured (kips)	P_{max}, punching shear (kips)	P_{max}, yield line (kips)
1	U1	145	170	195
2	U1	150	166	189
2	U2	155	174	150
3	U1	175	198	213
3	U2	175	210	242
4	U1	170	224	209
4	U2	165	200	177
5	U1	160	185	201
5	U2	153	193	182

2.3.3 Graddy, Kim, Whitt, Burns and Klingner (2002), (Griffith 2003)

Graddy et al. (2002) studied the punching-shear behavior of bridge decks under fatigue loading, using full scale cast-in-place and precast, prestressed panel specimens.

Using finite-element models, both cast-in-place concrete and precast-prestressed panel specimens were developed to replicate the behavior of complete bridge decks, whose capacity would be governed by punching shear. Cast-in-place (CIP), test specimens were 6 ft (1.83 m) wide, 7 ft (2.13 m) long, and 7.5 in (191 mm) thick. Precast-prestressed (PC) panel specimens, topped with 4 in. (102 mm) of cast-in-place concrete, were 8 ft (2.44 m) long, 6 ft 5 in. (1.96 m) wide, and 7.25 in. (184 mm) thick. Grade 60 reinforcement was used, details of which

35

are shown for a longitudinal section of both types of specimens in Figure 2.17 (a) and (b). Concrete used for the CIP specimens and for the topping of the PCP specimens had an average cylinder strength of 6000 and 5000 psi (41 and 34 MPa), respectively. For static tests, a loading footprint of 14 x 24 in. (610 x 356 mm) was applied to the CIP specimen, and a loading footprint of 10 x 17.5 in. (445 x 254 mm) was applied to the PCP specimens. For both specimens, the longer dimension of the loading footprint was parallel to the transverse direction of the specimen.
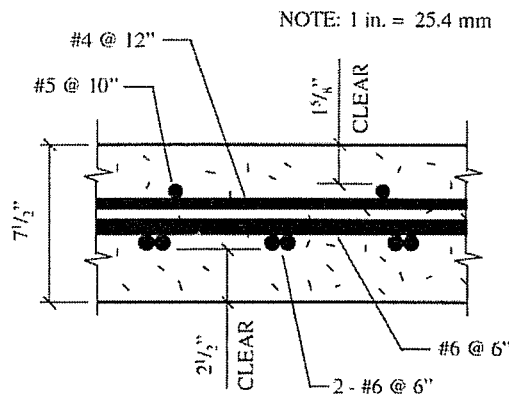
(a) CIP specimens
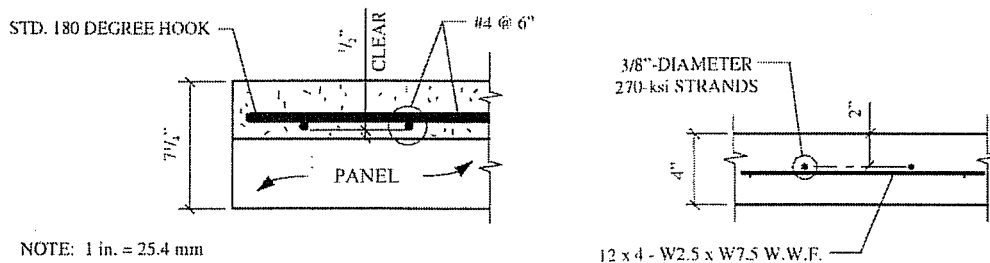
(b) PCP specimens

Figure 2.17 Section of test specimens (Graddy et al. 2002)

Flexural capacities were calculated using yield-line analysis, and compressive membrane forces, estimated using finite-element analysis and the results of previous research, were used in calculations of flexural capacity. In addition, predicted AASHTO LRFD and ACI 318-95 punching-shear capacities were calculated for both the predicted and observed failure mode. Resulting predictions and experimental results are shown in Figure 2.18.

PREDICTED FLEXURAL CAPACITY FROM YIELD-LINE THEORY INCLUDING ARCHING ACTION — 239 kips

PREDICTED FLEXURAL CAPACITY FROM YIELD-LINE THEORY WITHOUT ARCHING ACTION — 232 kips

205 kips   STATIC TEST #2 (PUNCHING SHEAR FAILURE)

PREDICTED PUNCHING SHEAR CAPACITY FROM GENERAL MODEL — 171 kips

173 kips — STATIC TEST #1 (PUNCHING SHEAR FAILURE)

PREDICTED AASHTO AND ACI PUNCHING SHEAR CAPACITIES — 127 kips

ANALYTICAL PREDICTIONS   EXPERIMENTAL RESULTS

0

(a) CIP specimens

Figure 2.18 Predicted versus observed failure loads for static tests: (a) CIP specimens; (b) PCP specimens (Graddy et al. 2002)

PREDICTED FLEXURAL CAPACITY
FROM YIELD-LINE THEORY
INCLUDING ARCHING ACTION

143 kips

PREDICTED FLEXURAL CAPACITY
FROM YIELD-LINE THEORY WITHOUT
ARCHING ACTION

139 kips

115 kips STATIC TEST #2
(COMBINED FAILURE MODE)

112 kips

PREDICTED PUNCHING SHEAR CAPACITY
FROM GENERAL MODEL ADJUSTED FOR
OBSERVED FAILURE MODE

105 kips STATIC TEST #1
(COMBINED FAILURE MODE)

81 kips

PREDICTED AASHTO AND ACI
PUNCHING SHEAR CAPACITIES
ADJUSTED FOR OBSERVED
FAILURE MODE

ANALYTICAL PREDICTIONS   0   **EXPERIMENTAL RESULTS**

(b) PCP specimens

Figure 2.18 cont'd Predicted versus observed failure loads for static tests: (a)
CIP specimens; (b) PCP specimens (Graddy et al. 2002)

Graddy et al. found that AASHTO and ACI punching-shear provisions
were conservative, and could be improved based on the shape of the punching
shear failure surface. Compared to the flexural capacities predicted from yield-
line theory, the beneficial effects of arching action were insignificant in terms of
shear capacity.

2.4   ARMOR AND SEALED EXPANSION JOINT RAILS

In addition to investigating the behavior of a composite section of PC
panel and CIP topping at slab ends, the influence of armor and sealed expansion
joint rails installed at expansion joints on the performance of the deck was studied
in this project. Designers typically do not account for the additional capacity
provided by an installed armor or sealed expansion joint rails when designing a
slab end detail at expansion joints. Current TxDOT practice is to specify a CIP

edge region, where the armor and sealed expansion joint rails are embedded entirely in the CIP concrete. In the use of PC panels, the armor (AJ) and sealed expansion joint (SEJ) rails must be embedded in the 4 in. thick topping slab. In the past ten years, TxDOT has found between ten and fifteen percent of armored bridge deck joint rails installed have failed. The following study completed by Dolan and Frank (1994) summarizes their findings after investigating these failed armored joint rails.

SECTION THRU ARMOR JOINT

(a) Armor Expansion Joint (AJ) rail

(b) Sealed Expansion Joint (SEJ) rail

Figure 2.19 TxDOT armor and sealed expansion joint rail details

2.4.1 Dolan and Frank (1994)

TxDOT experience indicates that ten to fifteen percent of the armored bridge deck joint rails installed have failed while in service. Dolan and Frank (1994) investigated the reasons for these failures. Several failed expansion rails were tested after their removal from the bridge decks. Inspections of the failed expansion rails revealed fractures of the studs along the rails. Often stud failures were located on only one side of the joint unit, which typically is the downstream side of the traffic flow and was on the uphill side of the relevant slab. Examination of the stud failures indicated the failures occurred in the weld region where the stud was welded to the rail. The remaining studs were bent over using a hammer to test the soundness of their welds. However, no additional stud failures occurred when bending over the remaining studs. Inspection of the rails where stud failures occurred showed evidence of lack of concrete consolidation in that area. The lack of concrete consolidation leaves only the aggregate to support the joint rail. One cause for lack of complete concrete consolidation is incorrect placement of reinforcing steel (i.e. too close to the rail). When the reinforcing steel is placed too close to the rail and studs, complete concrete consolidation cannot occur and detrimental voids form. Failures of these types of rails were concluded to be caused by lack of concrete consolidation, which can be avoided by having higher quality control during placement of slab concrete.

2.5 SUMMARY AND RELEVANCE OF PREVIOUS RESEARCH

While studies are reported on the behavior of the bridge decks with stay-in-place prestressed precast concrete panels and cast-in-place concrete topping slab deck, there are no reports of tests at free slab edges of these types of bridge decks. Early research was performed on specimens to determine if the two elements perform as a composite unit and if wheel loads are transferred across the

panel butt joints. All studies emphasized determining the flexural capacity of the composite section using plastic analysis methods. That research is of little relevance to the behavior of bridge slabs constructed with the IBTS and composite section with PC and CIP end details, as no span tested in this research study failed in flexure. Early tests indicated that at interior locations, bridge decks (both full-depth cast-in-place concrete and composite decks failed in punching shear) had reserve strengths greatly exceeding the design punching shear strength. Although this may be true for interior locations of a bridge deck, the reserve capacity at expansion joint edges of decks has not been established. Most research done on full-scale specimens included diaphragms; however, the effects of loads applied at the edge of slabs without diaphragms have not been studied. Slab edges of the composite section must be studied independently for four reasons: the smaller (and unsymmetrical) critical punching-shear perimeter expected for loads applied near an edge; the increase in transverse flexural moments at the slab edge expected due to the lack of two-way action there; the reduction in arching action expected due to decreased in-plane lateral restraint there, and the influence of the edge on composite behavior between the two elements.

CHAPTER 3

Design of Test Specimens

3.1 INTRODUCTION

The goal of the experimental program was to investigate the behavior of slabs at expansion joints, with emphasis on skewed slabs, as well as to develop design guidelines for slab edge details at expansion joints. Three full-scale specimens have been constructed and tested. The test specimens were designed to behave as full-scale bridge slabs while allowing investigation of the effect of different design parameters on the behavior of the slab at the expansion joints.

The first specimen was built with a 0° skew at both edges, with TxDOT's IBTS detail on one edge and the UTSE detail at the other. The purpose of the first specimen was to study the effect of the design parameters other than skew on the behavior at the expansion joints. The design parameters investigated included: slab edge detail, girder spacing, bridge length, and the number of bays. Detailed discussion of the first specimen is presented in Ryan (2003).

The second test specimen was built with a 45° skew at both edges. The purpose of the second specimen was to evaluate the effect of skew on the behavior at the expansion joints. In addition to the four primary span tests in all the specimens, four overhang tests were performed on this specimen. In addition to the design parameters set forth in the first specimen, the skew angle affected the design load placement, how the slab span length between girders affects the response, and how the overhangs should be reinforced. Detailed discussion of the second specimen is presented in Griffith (2003).

42

The third test specimen was built with 0° skew at both edges, similar to the first specimen. The primary purpose of this specimen was an evaluation of the edge detail stay-in-place prestressed concrete (PC) panels instead of a cast-in-place (CIP) segment adjacent to the edge. Top reinforcement spacings were varied. Construction details associated with armor and sealed expansion joint rails were studied. Similar to the second specimen, four overhang tests were conducted on this specimen in addition to the primary tests at the edges between the girders. Two additional span tests at service level loads were conducted to provide sufficient comparison between the two top reinforcement spacings and the two types of expansion joint rails. The objective was to determine how top reinforcement spacing affects the cracking at service levels, how the armor and sealed expansion joint rails contribute to stiffness and capacity of the edge detail, and how the use of panels at the edge detail affect the behavior and capacity of the expansion joints.

3.2   0° SKEW SPECIMEN

The first test specimen was built with a 0° skew at both edges to provide a basic test against which the effects of skewed edges and slab edge details could be compared. Figure 3.1 shows the four primary test areas in the first specimen. Different combinations of slab edge details and girder spacing were tested in each test area.

Test 3
UTSE Detail
10-ft spacing

Test 4
UTSE Detail
8-ft spacing

32 ft

N

18ft

UTSE
detail

IBTS
detail

3 ft   10 ft   8 ft   8 ft   3 ft

Test 2
IBTS Detail
10-ft spacing

Test 1
IBTS Detail
8-ft spacing
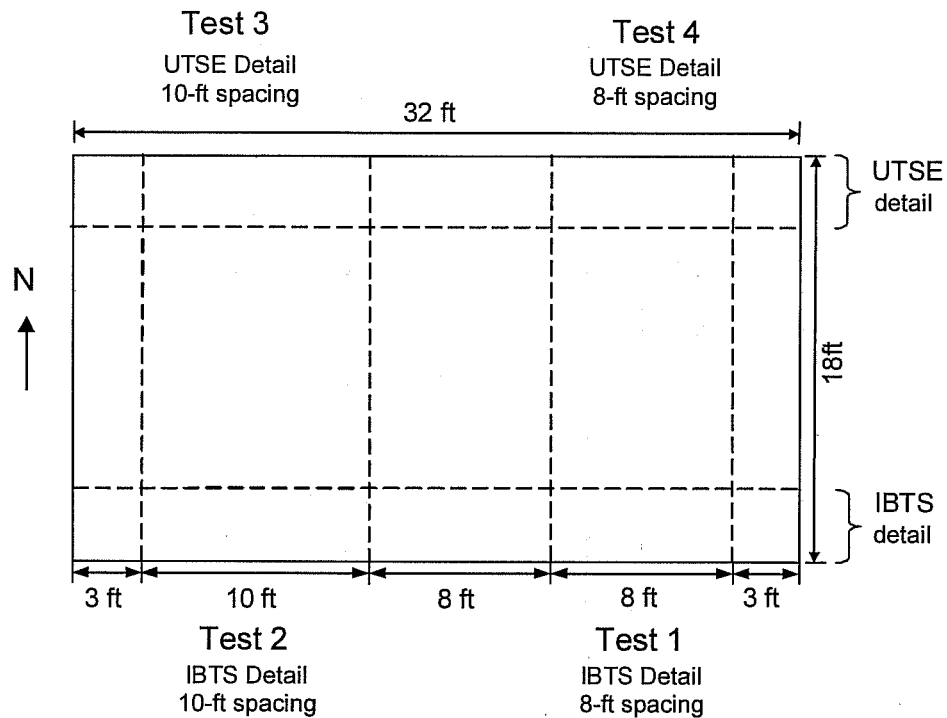
Figure 3.1 0° skew specimen, plan view (Ryan 2003)

3.2.1 Girder Spacing

Although TxDOT bridge standards include bridges with up to six girders, the first 0° skew specimen had only four girders, since six girders would result in a bridge width that could not be tested in the laboratory. Linear-elastic parametric studies done by Ryan (2003) indicated that a four-girder bridge would adequately represent five- or six-girder bridge behavior at slab edges. A detailed discussion of this analysis is given in Ryan (2003).

The girder spacing of the west-exterior bay was 10 ft. The girder spacing of the east-exterior bay and the interior bay was 8 ft. The 8 ft girder spacing was chosen since 8 ft girder spacing is commonly used in TxDOT highway bridges.

The 10 ft girder spacing was used to represent the largest girder spacing used by TxDOT in highway bridges.

3.2.2 Edge Reinforcement Details

Two edge reinforcing details were used, the standard 10 in. thick TxDOT IBTS edge detail and a proposed 8 in. thick alternate edge detail. The IBTS edge detail has a total of 16 No. 5 reinforcing bars, 8 bars on the top and 8 bars on the bottom, placed parallel to the slab edge spaced 6 in. on center. The detail, shown in Figure 3.2, is 4 ft wide, measured perpendicular to the slab edge. As the skew angle increases, the longitudinal length of the edge section increases, as shown in Figure 3.3 for a 45° skew (Griffith 2003). To accommodate for the skewed edge, panels are stair stepped and stopped a given distance away from the expansion joint detail, as seen in Figure 3.4. The use of panels at the edge of a skewed bridge slab includes numerous modifications to the panel and construction techniques, which indicated that panels used at the edge detail are most feasible for a 0° skewed bridge slab.
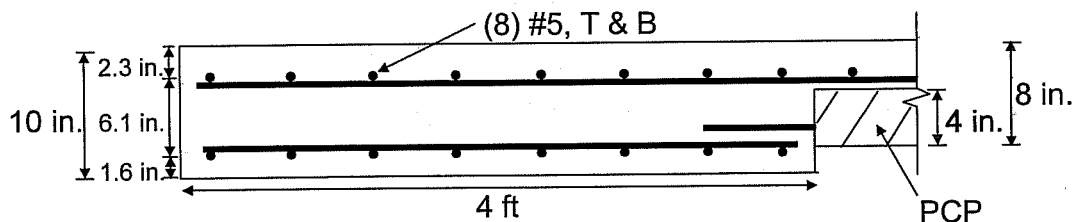
Figure 3.2 Cross-section of IBTS detail (Ryan 2003)
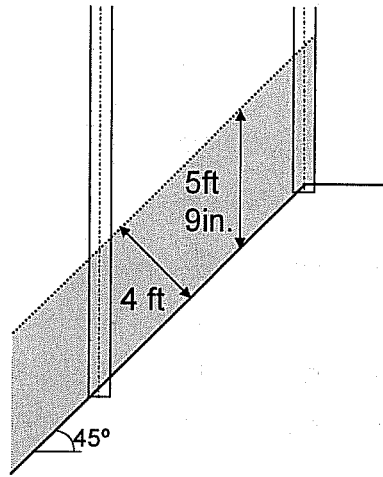
Figure 3.3 Length of edge detail (Griffith 2003)
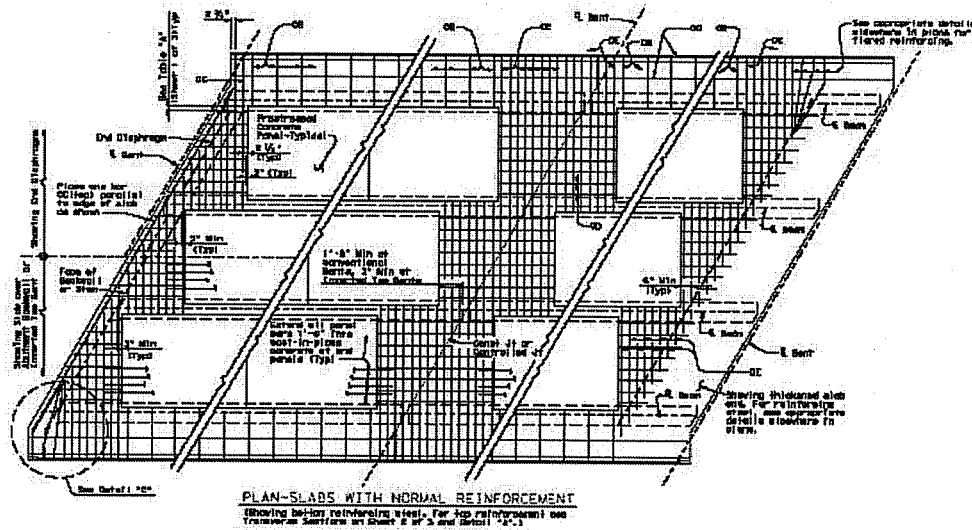
Figure 3.4 Stair-stepped PC panels in bridge slab

To fully utilize the first specimen, an alternative detail was designed for testing the edge opposite the IBTS edge detail. Typically, four-inch thick prestressed concrete panels are topped with 4 in. of cast in place concrete to form

46

the interior of bridge decks, eliminating the need for formwork; then at the slab edges, formwork is constructed in the field to construct the thickened edge. Therefore, an 8 in. thick edge detail would be expected to improve construction efficiency and economy by creating a uniform thickness over the entire length of the bridge deck.

The alternative 8 in. thick slab edge detail, the Uniform Thickness Slab Edge (UTSE) detail, was developed during the first phase of the research study. In order to remain consistent with present construction, the detail contains the same size reinforcement bars (No. 5) as at the interior of the bridge deck, but the reinforcement spacing at the edge detail is reduced from 6 in. to 3-7/8 in., increasing the number of reinforcement bars from 16 to 24 (Figure 3.5).
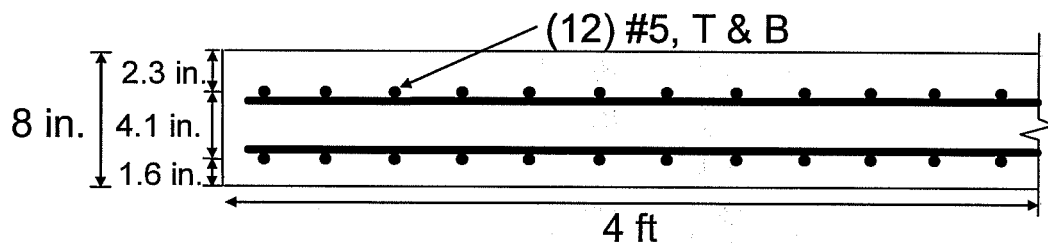
Figure 3.5 Cross-section of UTSE detail (Ryan 2003)

For both details, a 4 ft wide section was analyzed, and the computed moment-curvature response of the two details is shown in Figure 3.6. In Figure 3.7, the initial portion of the curve is expanded to focus on cracking and yielding of the sections. The reinforcing detail in the UTSE detail yielded at about 11% and 6% higher moment than the IBTS detail in positive bending and negative bending respectively (Ryan 2003). The flexural capacity of the UTSE detail is 5% and 3% higher than the IBTS edge detail in positive and negative bending, respectively, due to the increased reinforcement ratio. Due to its reduced depth,

47

the UTSE detail has a lower stiffness before and after cracking. In reality, the continuity of rest of the slab will cause cracking to initiate at the slab edge and penetrate into the slab. The actual cracking moments and stiffnesses for both sections were higher than the analytical values, because the actual slab is restrained along the interior boundary of the edge slab section.
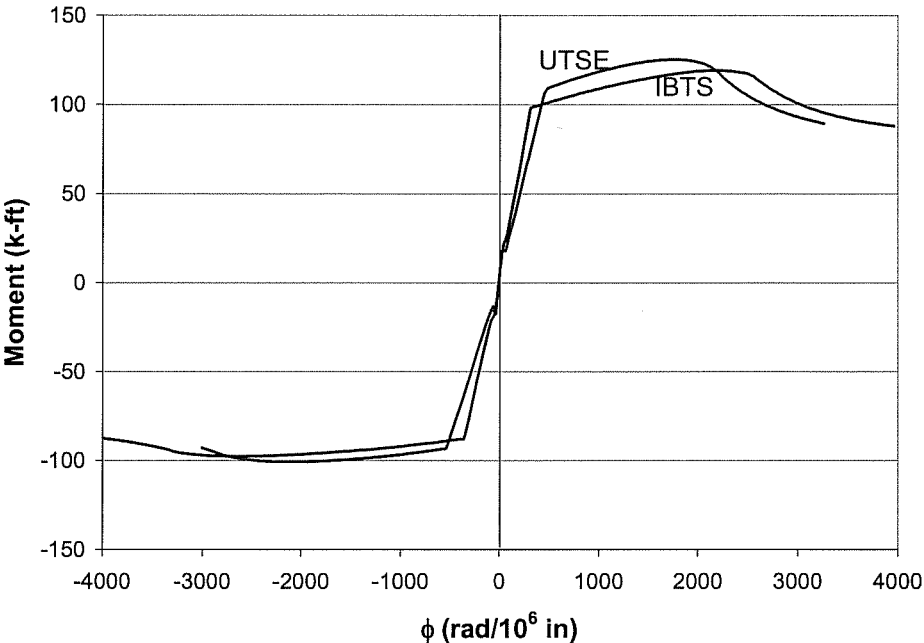
Figure 3.6 Moment-curvature analysis of IBTS and UTSE details (Ryan 2003)
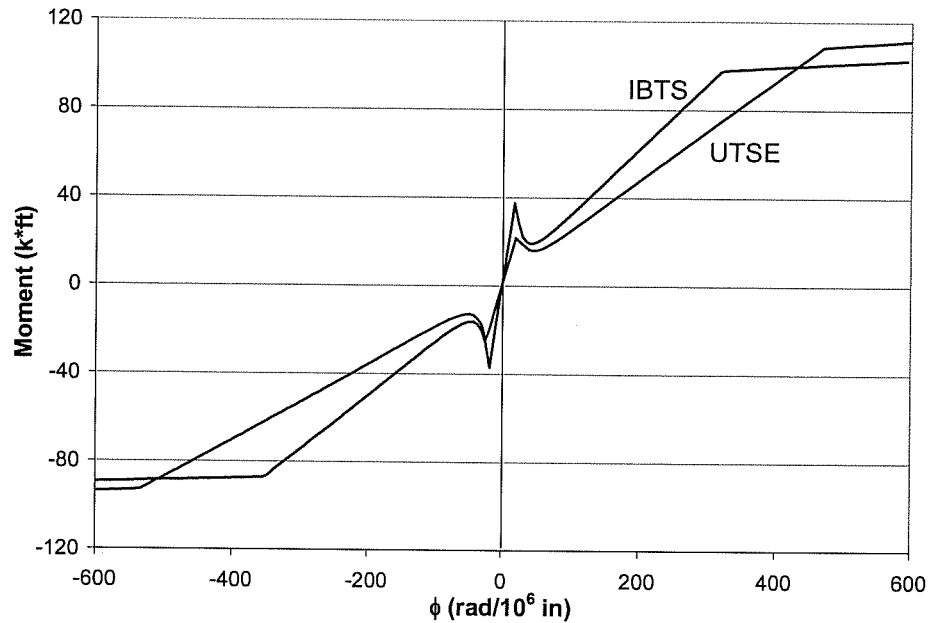
Figure 3.7 Moment-curvature behavior, focused on cracking (Ryan 2003)

3.2.3   AASHTO Design Loads as Applied to These Specimens (Ryan 2003)

One of the main objectives of this research study was to determine the behavior of the TxDOT IBTS and the alternate UTSE edge detail when subjected to AASHTO design loadings, HS-20 and HS-25 (AASHTO LRFD Bridge Design Specifications). Two primary types of vehicle were considered for each design loading (Figure 3.8), similar to the TxDOT Bridge Design Manual (Ryan 2003). Another alternative to the tandem vehicle is the alternate military vehicle with 24-kip axles and the same loading configuration. However, the tandem loading from AASHTO LRFD was applied to all specimens. The HS-25 loading developed utilizes the same vehicle arrangements, but the load magnitudes are increased by 25%. In Figure 3.8, the loadings are axle loads, where half the axle load goes to each set of tires. Each set of tires is spaced 6 feet apart in the transverse direction

as seen in Figure 3.9. A single load plate (20 in. by 10 in.) was used to represent a set of tires in testing.
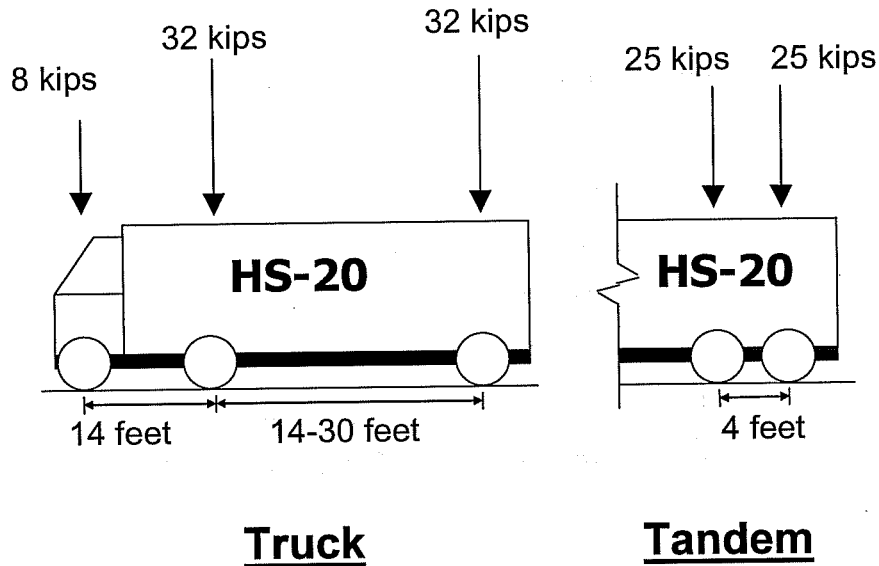
Figure 3.8 AASHTO HS-20 design vehicles (Ryan 2003)
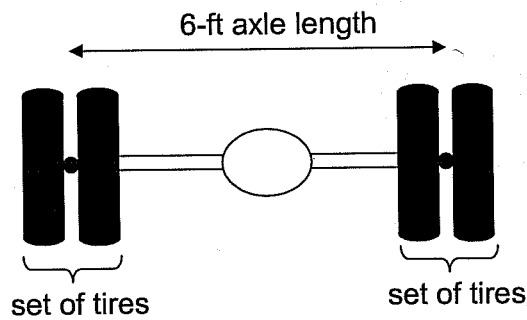
Figure 3.9 AASHTO design vehicle axle (Griffith 2003)

Since the AASHTO truck configuration axles are farther apart than the longitudinal dimension of the edge detail, only one axle would load the bridge test specimen at any one time (Ryan 2003). Therefore, two loading configurations, "truck axle-front" and "truck axle-back", were applied in addition to the tandem axle loading. "Truck axle-front" included one of the axles applied at the edge of

50

the slab, and "Truck axle-back" was the other axle set 4 ft back from the edge. Since the AASHTO tandem vehicle axles are spaced 4 ft apart, both axles affect the edge detail. During testing of the bridge slabs, a loading configuration with four load plates was described as "tandem loading", and a loading configuration with two load plates was labeled as "truck loading".

Section 3.6.2 in the AASHTO LRFD specification establishes a dynamic load allowance, which increases the design vehicle loads by 75% to account for dynamic effects in the bridge at expansion joints (Ryan 2003).

For the first 0° skew specimen, the three loading configurations, truck axle-front, truck axle-back, and tandem, were applied to each of the specimen's test areas. At almost every test area, out of the three loading configurations, the tandem truck loading configuration produced the most critical cracking, strain, and deflection response. Based on this observation, the tandem loading configuration was the only loading configuration used on all test areas for the following two specimens.

3.3 45° SKEW SPECIMEN

The second, 45° specimen, was constructed and tested to observe the effect of skew on slab edge behavior. Skew angle, loading point locations, girder spacing, edge detail, and the inclusion of breakbacks were the test variables considered in this specimen. In addition, four overhang tests were conducted on this specimen. Figure 3.10 shows all test areas for the 45° specimen.
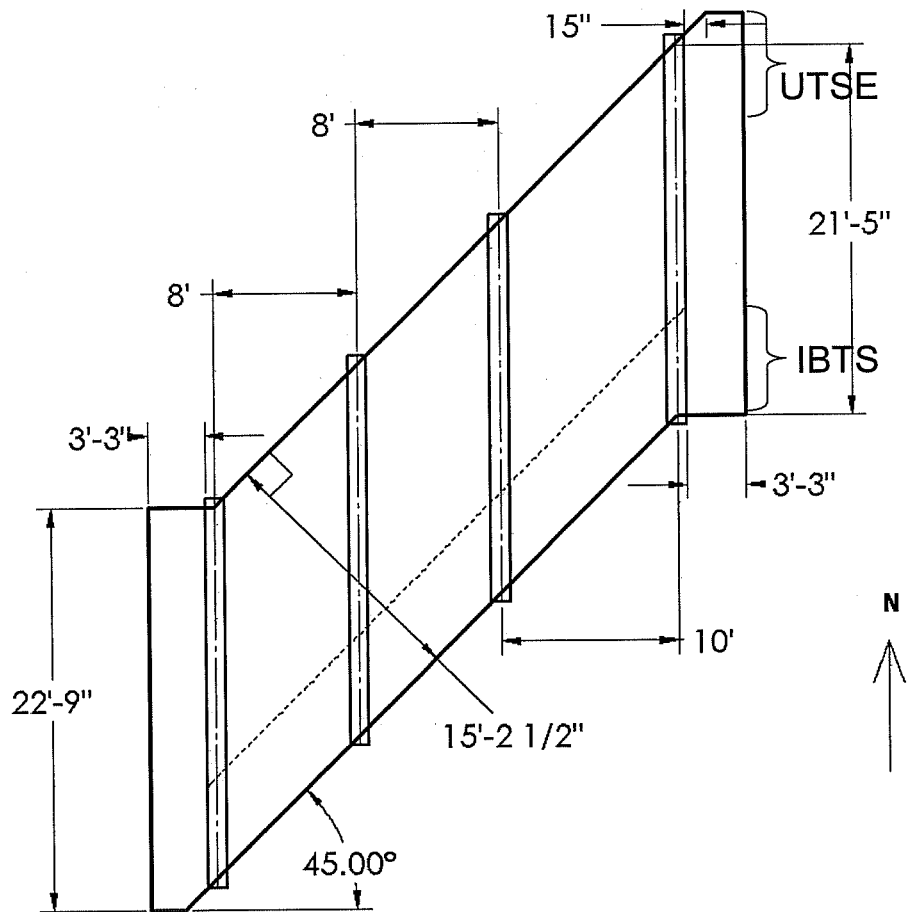
Figure 3.10 45° skew specimen, plan view (Griffith 2003)

3.3.1 Skew Angle and AASHTO Tandem Load Configuration

Since the objective of the second specimen was to observe the effect of skew on slab edges, a skew angle needed to be determined based on loading configuration and size. Because the tandem load configuration produced the most critical results in the 0° specimen, only that load configuration was considered for the second specimen. The next step in determining the skew angle was

establishing load point locations on various skews for maximizing negative and positive moments. These load point locations are shown in Figure 3.11. In order to maximize the number of load points near the edge of the slab, only 3 load plates were used to simulate the AASHTO tandem load configuration, where the fourth tire footprint would be assumed to be off the slab deck. A 45° skew was chosen due to lab space restrictions, as well as the fact that a 45° skew is close to the largest skews used in practice by TxDOT.
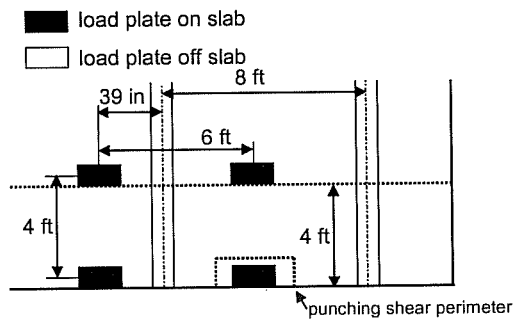
(a) 0° skew, 4 load plates
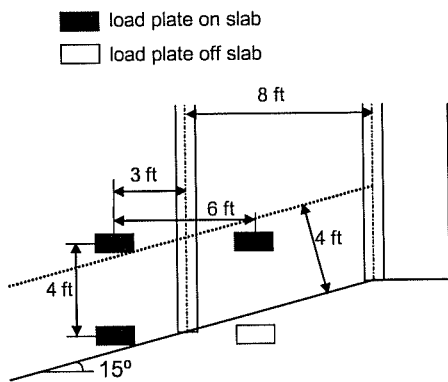
(b) 15° skew, 3 load plates
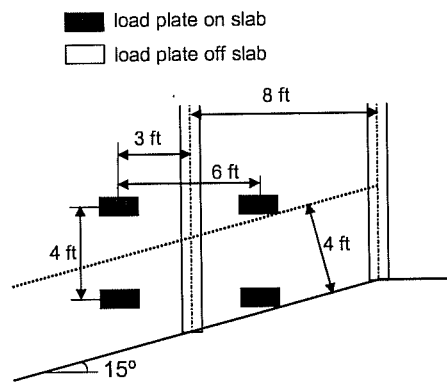
(c) 15° skew, 4 load plates
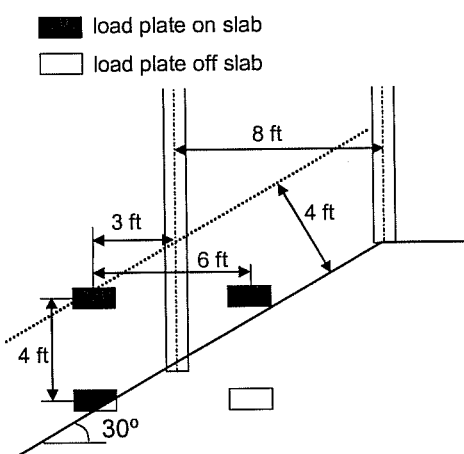
(d) 30° skew, less than 3 load plates
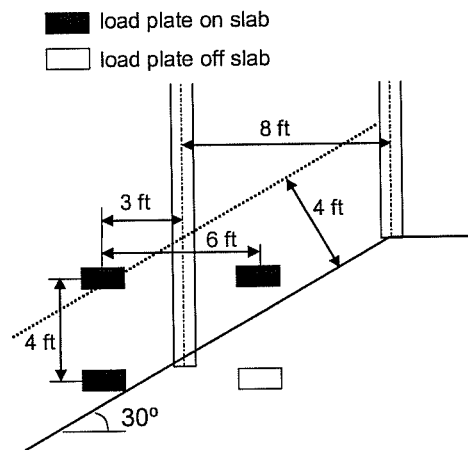
(e) 30° skew, 3 load plates

Figure 3.11 Placement of tandem loading plates, 0°, 15°, 30° skew (Griffith 2003)

54

3.3.2 Specimen Length (Griffith 2003)

The specimen length, which was 18 ft in the first $0°$ specimen, was increased to 21.5 ft in the $45°$ specimen. The increase in length compensated for the decrease in distance between test areas caused by the skew. Two reasons that increasing the skew of the specimen moved test regions closer to one another are as follows:

- With increasing skew, the edge regions increase in length longitudinally. At a $45°$ skew, the length of the edge detail increased to from 4 ft to 5 ft, 9 in along the girder.

- The length of the slab measured perpendicular to both edges is reduced when skew is increased.

For a slab increase from 18 ft to 21.5 ft, the perpendicular length of the slab increased from 12 ft, 9 in. to 15 ft, 2.5 in.

3.3.3 Additional Design Variables

The edge details, girder spacings, and number of bays constructed in the first $0°$ specimen were duplicated in the second ($45°$ skew) specimen. The IBTS and UTSE details were constructed at opposite edges of the specimen. A discussion of these details is given in Section 3.2.2. Girder spacings and the number of bays were also duplicated from the first $0°$ specimen, one 10-ft exterior bay and two 8-ft bays.

3.3.4 Overhang Design

In addition to the tests on the edges between girders, four overhang tests were conducted on the corners of this specimen. For slabs constructed with skews greater than $15°$, TxDOT design standards require breakbacks at bridge slab

55

corners (Griffith 2003). The overhang reinforcement was determined using TxDOT standards.

3.4 PRECAST PRESTRESSED (PC) PANEL SPECIMEN

Following the completion of the test program for the first 0° skew specimen and the 45° skew specimen, a 0° skew specimen was developed, with a composite deck using prestressed concrete (PC) panels and cast in place (CIP) concrete topping throughout the specimen and armor and sealed expansion joint rails on one edge of the slab (Figure 3.12). Its purpose was to explore the possibility of eliminating all formwork by using the PC panels in the edge detail, as well as investigating the effects of varying top reinforcement spacing and the effects of the armor and sealed expansion joint rails in the capacity of the slab edge details. In addition, four overhang tests were conducted on this specimen.

Test 4

6 in. top reinforcement
spacing, SEJ,10-ft spacing,
Serviceability & Failure

Test 5

6 in. top reinforcement
spacing, SEJ, 8-ft spacing,
Serviceability

Test 6

6 in. top reinforcement
spacing, AJ, 8-ft spacing,
Serviceability & Failure
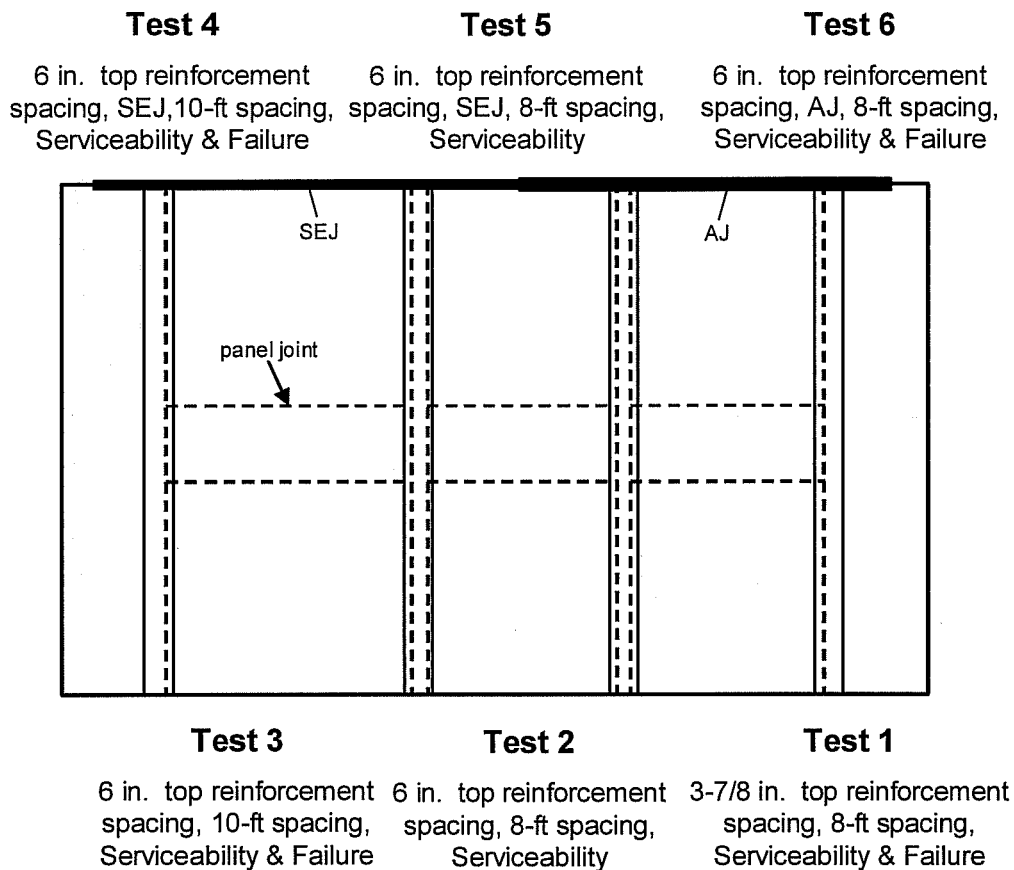
Figure 3.12 PC panel specimen, plan view

Test 3

6 in. top reinforcement
spacing, 10-ft spacing,
Serviceability & Failure

Test 2

6 in. top reinforcement
spacing, 8-ft spacing,
Serviceability

Test 1

3-7/8 in. top reinforcement
spacing, 8-ft spacing,
Serviceability & Failure

3.4.1 AASHTO Tandem Load Configuration

As discussed in Section 3.3.1, the tandem load configuration in the first 0° specimen produced the most critical results. Therefore, similar to the 45° specimen, only the tandem load configuration was considered for the third specimen.

3.4.2 Prestressed Concrete Panels

A major focus of the research project was to understand the behavior of slab edge details at expansion joints under AASHTO LRFD design loading and to

develop an alternative design procedure. After the first two specimens, the UTSE (8 in. thick) detail test results indicated that there was no distinct advantage to the IBTS (10 in. thick) detail. Current TxDOT bridge construction uses a composite section of 4 in. stay-in-place prestressed concrete (PC) panels and 4 in. cast-in-place (CIP) concrete topping in the interior section of bridge decks. Therefore, the natural progression for an alternate detail similar to the UTSE detail would be a detail using a composite section containing the panels and CIP concrete topping as shown in Figure 3.13.

Similar to the development of the UTSE detail, a 4 ft. wide section of the edge detail containing the PCP and CIP concrete topping was analyzed. Following existing TxDOT standards, a panel with eight 3/8-in. diameter, 7-wire prestressing strands, spaced 6 in. on center was needed to develop a moment capacity comparable to the IBTS and UTSE edge details (Figure 3.13). The computed moment curvature behavior of all three details is shown in Figure 3.14. The flexural capacity of the PC and CIP edge detail is 4% and 10% higher than the UTSE and IBTS details in positive bending, respectively. Due to the use of prestressed concrete panels, the PC and CIP edge detail has a higher stiffness before and after cracking. The sectional analysis was intended only to provide a comparison between the three edge details.
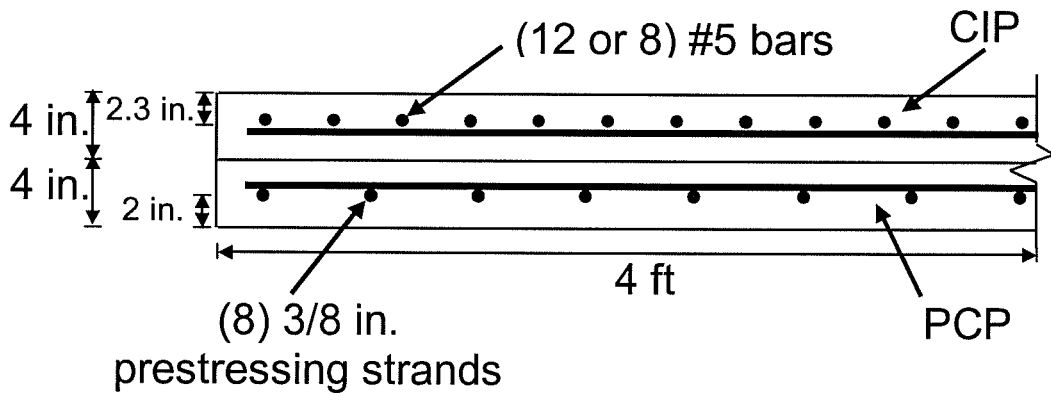
Figure 3.13 Cross-section view of Precast Concrete Panel and Cast-in-Place Concrete Topping
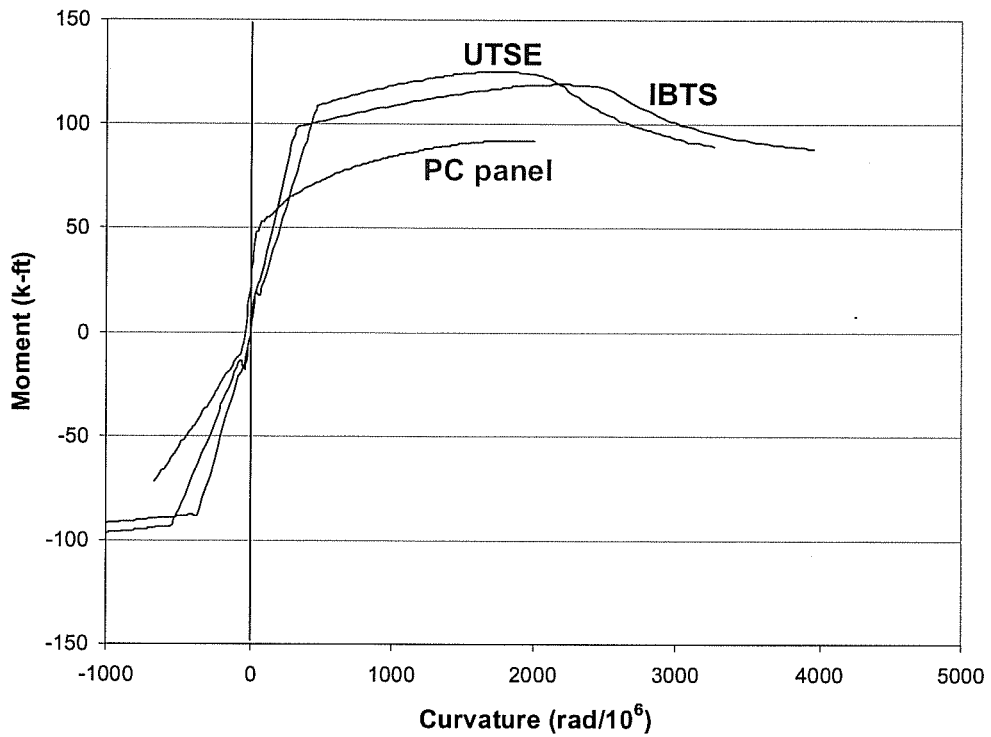
Figure 3.14 Moment-curvature behavior of IBTS, UTSE, and PCP + CIP

3.4.3 Top Reinforcement Spacing

In developing the composite PC panel edge detail, the top reinforcement spacing was assumed to be identical to the UTSE detail (approximately 3-7/8 in.) due to their same concrete depth. Since design procedures were another primary objective of the research study, simplicity of construction was considered when developing the composite PC panel edge detail. In order to be consistent with current bridge construction, the top reinforcement spacing of 6 in. was continued from the interior of the bridge deck to the slab edges. With this, two top reinforcement spacings were tested in the third specimen where both spacings were tested by maximizing negative bending at service load levels.

3.4.4 Armor and Sealed Expansion Joint Rails

As mentioned previously, armor and sealed expansion joint rails (Figure 3.15 and Figure 3.16) are commonly used in construction of bridge decks at expansion joints. Current TxDOT design procedures do not account for any increase in capacity by using these expansion rails. In order to maximize the information gathered from the third specimen, one edge of the specimen included both an armor and a sealed expansion joint rail spliced in the middle 8 ft. bay.
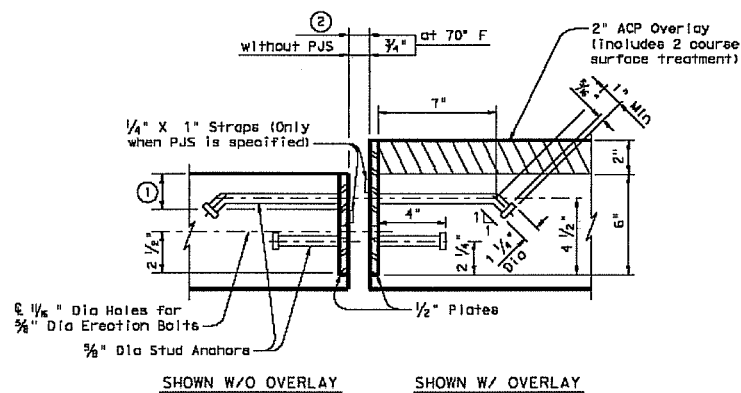
Figure 3.15 TxDOT armor joint rail detail
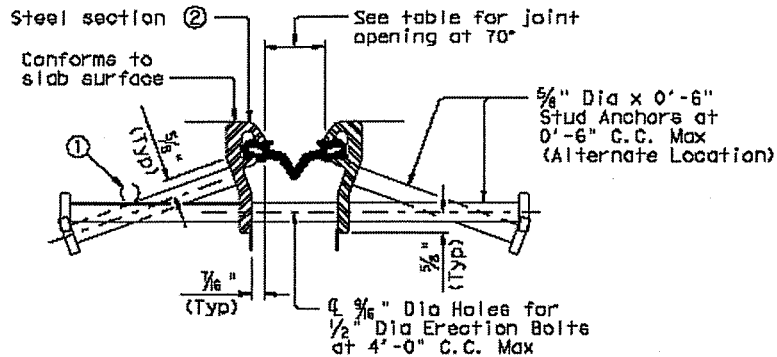
Figure 3.16 TxDOT sealed expansion joint rail

Another issue arose in the use of armor and sealed expansion joint rails concerning the constructability of the two rails when the edge detail includes the 4 in. PC panel. In current TxDOT practice, the armor and sealed expansion joint rails are installed on the bridge deck in the cast-in-place IBTS detail. However, the panel would interfere with the location of the bottom stud anchor in the AJ rail. In order to accommodate the panel depth, the bottom anchors were raised a ¼ of an inch and the plate was installed in the deck by notching the form, so the ½ in. armor plate can be placed (as shown in Figure 3.17) relative to the panel and CIP concrete topping. For the sealed expansion joint rail, the angled anchor bolts were heated and then bent so the anchors fit above the top surface of the PC panel (Figure 3.18).
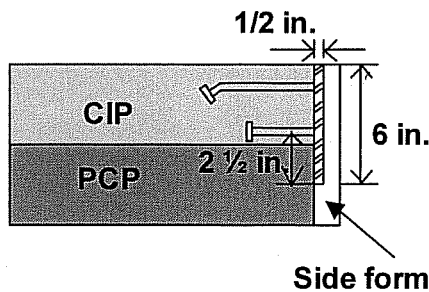
Figure 3.17 Construction modification for armor joint rail
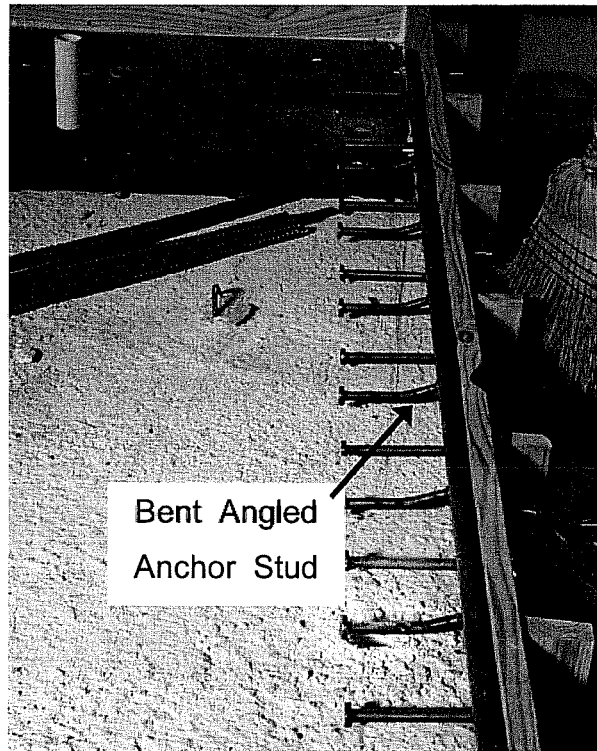
Figure 3.18 Bent angled anchors on sealed expansion joint rail

3.4.5 Specimen Length

For the $0°$ specimen and $45°$ specimen, the specimen lengths were 18 ft and 21.5 ft, respectively. As discussed previously, 18 ft was the minimum length to avoid damage at one edge to influence the performance at the opposite edge of the slab. According to TxDOT standards for the prestressed concrete panels, the maximum length of a panel is 8 ft. For the PC panel specimen, the slab length was increased to 20 ft so that only 3 panels were needed per bay, two 8 ft panels and one 4 ft panel.

3.4.6 Additional Design Variables

As discussed previously, the composite section using PCP and CIP concrete topping were used in the PC panel specimen based on the satisfactory

behavior exhibited by the UTSE detail in the 0° specimen and 45° specimen. Girder spacings and the number of bays were unchanged from the previous two specimens. Three bays were constructed similar to the 0° specimen, one 10 ft exterior bay, and two 8 ft bays. One edge of the slab had the composite PCP edge detail with the only varying top reinforcement spacing between bays, and the other edge of the slab included the installation of the armor and sealed expansion joint rails. The Sealed Expansion Joint (SEJ) rail was installed on the 10 ft bay, since the SEJ rail is the most commonly used in practice by TxDOT.

3.4.7 Overhang Design

In order to compare results from the overhang tests of the 45° specimen, four overhang tests were performed on the corners of the third specimen. All designs of the overhang reinforcements were modeled after TxDOT standards. In addition to the reinforcement details, the overhang length was increased to provide a critical loading pattern for testing the overhang. Typical overhang length is 2 ft from the centerline of the girder. However, after including the size of the load plate and the location and size of the railing (minimum 24 in. from the edge of overhang), the location of the load plate would be over the girder. This location does not create a critical load situation for the overhang. Therefore, the standard overhang length was increased to 45.5 in. to allow testing of the overhang and the minimum 24 in. from the edge of the overhang (Figure 3.). The 45.5 in. results from the geometry of a horizontally curved bridge with a radius of 600 ft, where overhang might be as much as 45.5 in. wide measured from the edge of the centerline of the girder. Detailed discussion of the design of these tests areas, the results of these tests, and comparisons to the overhang test results from the 45° specimen are given in Chapter 8.
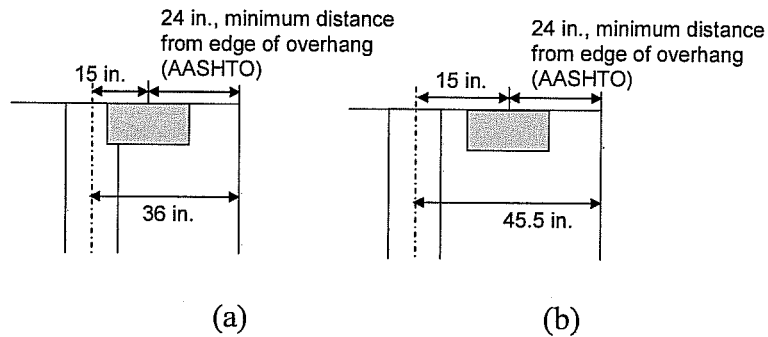
Figure 3.19 Loading plate location: (a) standard 36-in. overhang; (b)
45.5-in. overhang (Griffith 2003)

3.4.8   Slab Reinforcement

The bottom 4 inches of the slab are the PC panels in the 10 ft and two 8 ft bays, and the top 4 in of the slab and 8 in of the overhang are CIP concrete (Figure 3.20). The top mat of slab reinforcement for the PC panel specimen is shown in Figure 3.21. All slab reinforcement and panel sizes were detailed using the TxDOT PC panel and span standards. The 6 in. top reinforcement spacing was based on the TxDOT IBTS Detail (Figure 1.2), and the 3-7/8 in. top reinforcement spacing was modeled from the UTSE edge detail. The TxDOT PC panel standards were used to size panels and position strands in the panels. TxDOT standards were used as a guide for reinforcing the remainder of the slab.
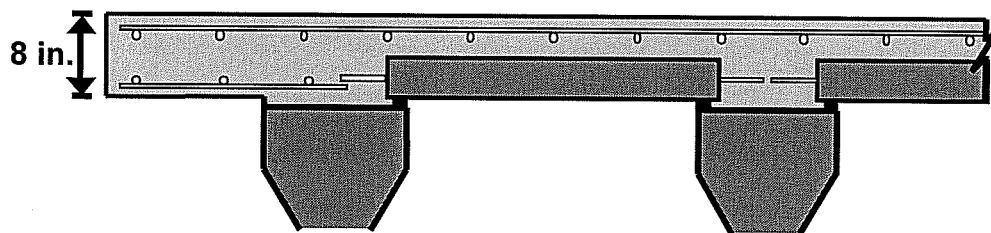
Figure 3.20 Elevation of precast panels and cast-in-place concrete topping
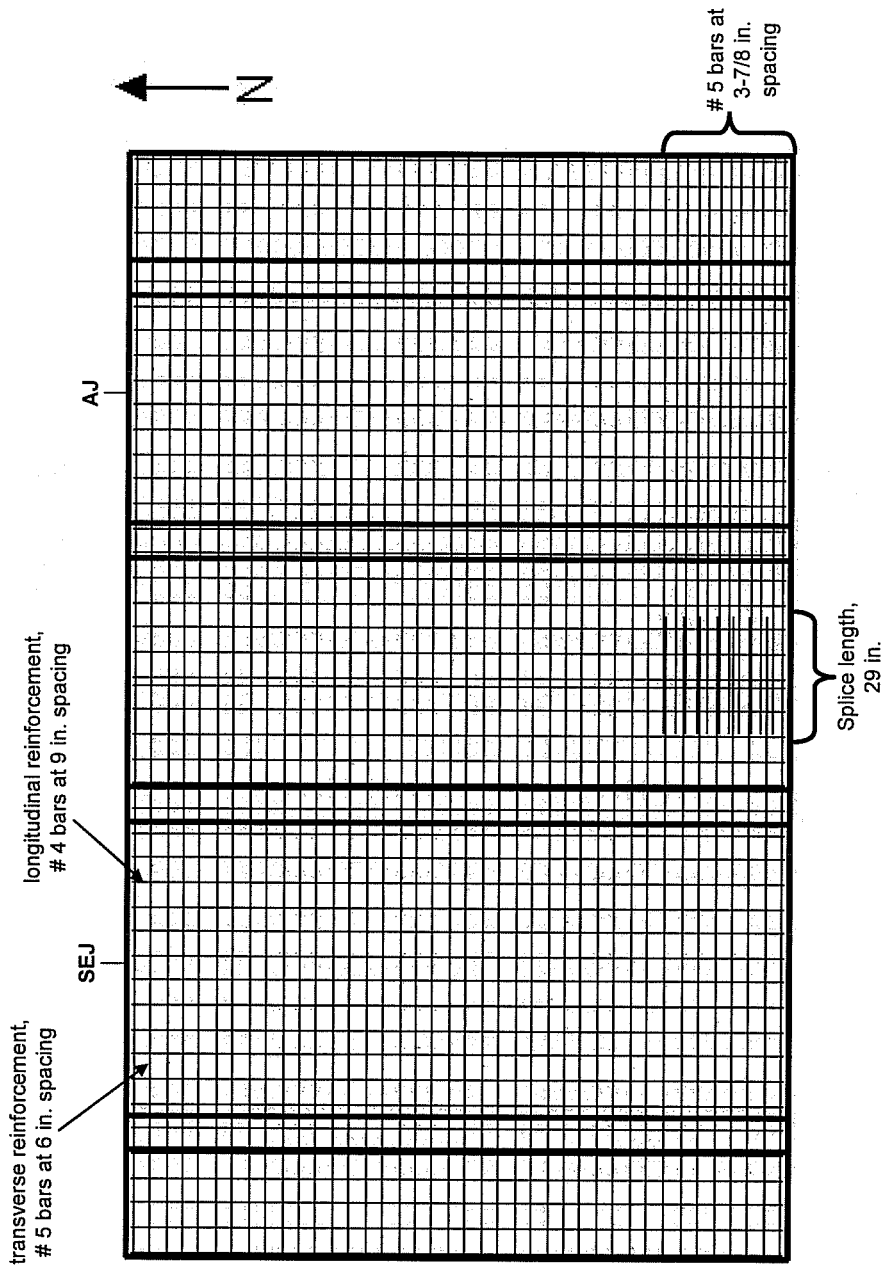
Figure 3.21 PC panel specimen slab reinforcement, top mat

3.4.9 Girders (Ryan 2003)

Bridges in Texas are typically built using precast, prestressed concrete girders. Because the focus of this project was on the behavior of slab edge details, it was not necessary to replicate the longitudinal dimensions of the prestressed concrete girders. Since the girders have little effect on the behavior of the slab along the edge, the same steel girders (W 24 X 104) were used for all three specimens.

3.4.10 Shear Studs (Ryan 2003)

To obtain composite action between the slab and the girders, shear studs were fabricated using double-nutted bolts (Figure 3.22), which allowed the girders to be reused by removing the bottom nut and lifting the slab off the girders. This shear stud detail proved to be a very efficient method to produce composite action. Figure 3.23 shows the method for creating composite action used by TxDOT as well as the equivalent design used in the test specimen. The shear stud diameter and spacing was designed to match the cross-sectional area of the stirrups that are used with precast, prestressed girders (Table 3.1). The locations of the shear studs were adjusted to fulfill the TxDOT requirement of a minimum 1-½ in. of concrete under the edge of the panels at the girders, as seen in Figure 3.24.
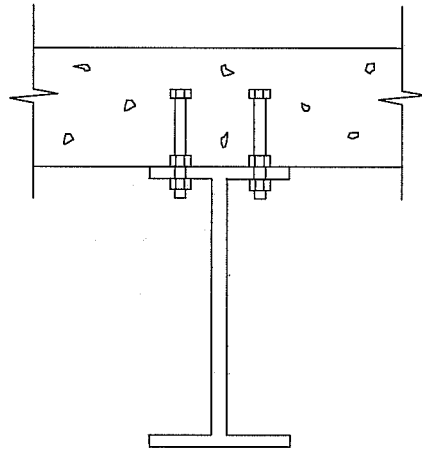
Figure 3.22 Shear stud detail (Ryan 2003)

Prestressed Concrete Girder

#4 HOOPS, TYP

6in   spaced @ 4in   spaced @ 8in

5ft 9in

Test Specimen

3/4Ø BOLTS, TWO ROWS

spaced @ 8in   18in spacing
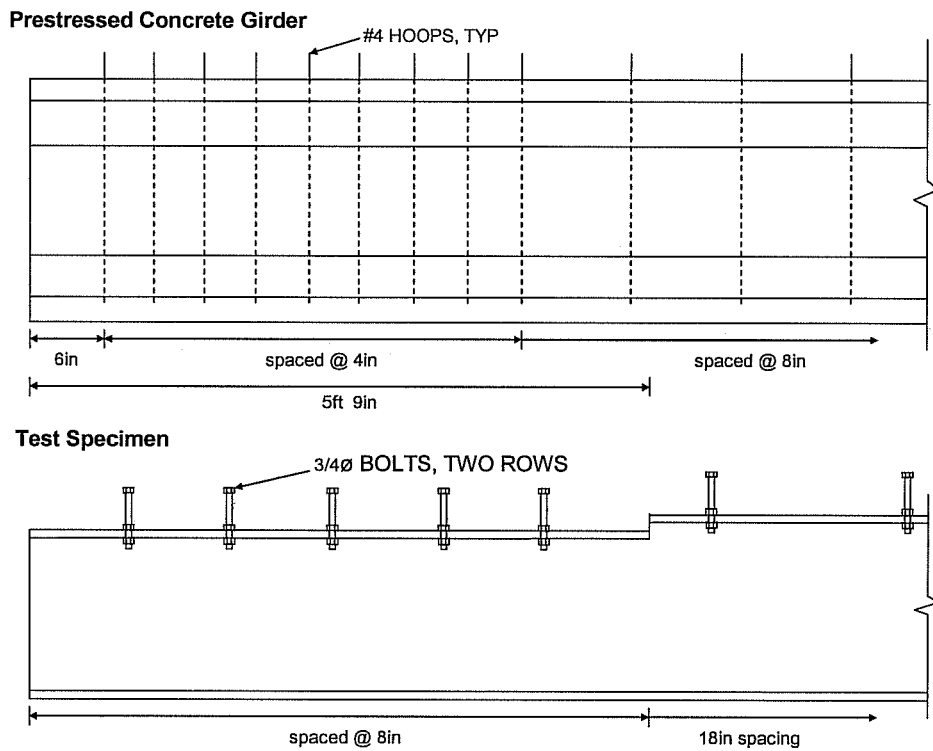
Figure 3.23 Composite shear reinforcement for IBTS edge detail (Ryan 2003)

67

Table 3.1 Comparison of composite shear reinforcement (Ryan 2003)

Girder type	Shear connection method	Area of composite reinforcement (per 4 ft)	
		IBTS Detail	Typical
Prestressed Concrete	CIP No. 4, hoops	4 in.^{2}	0.6 in.^{2}
Steel	CIP 3/4ø bolts, two rows	4.4 in.^{2}	0.59 in.^{2}
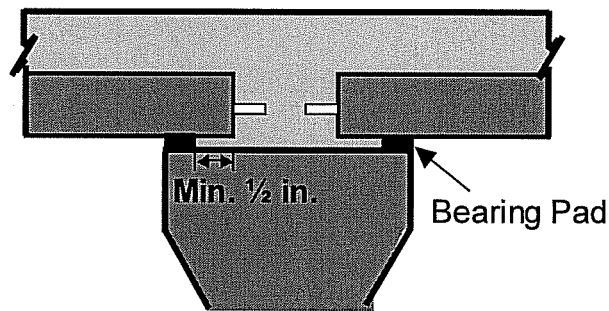
Figure 3.24 Minimum concrete requirement under panels

3.5 SUMMARY

Three specimens were constructed and tested, two 0° specimens and one 45° specimen. Each specimen had three bays with one exterior 10-ft girder spacing and two 8-ft girder spacings. The first 0° specimen and 45° specimen both were constructed with the IBTS and USTE details on either edge of the slab. The full depth of the slab for these two specimens was cast-in-place concrete. For the PC panel specimen, 4 in. PC panels were used in all girder spacings, topped with 4 in. of CIP concrete that was also used for the full depth of the overhangs. This is a typical TxDOT standard design. AASHTO design loads were applied to all slabs. The 0° specimen, 45° specimen, and PC panel specimen lengths were 18

ft, 21.5 ft, and 20 ft, respectively. Details of the specimens and test results from the previous two specimens can be found in Ryan, 2003 and Griffith, 2003.

CHAPTER 4

Experimental Program

4.1 INTRODUCTION

Many of the experimental procedures developed for the 0° and 45° cast-in-place (CIP) skew specimens were repeated for the specimen with prestressed concrete (PC) panels. The girders, forms, and load frame were reused during the construction and testing of the third specimen. While some strain gauge locations were added to account for the inclusion of PC panels, other instrumentation and the testing protocol remained the same.

4.1.1 Terminology

Throughout this thesis, different areas of the slab and PC panel are referenced. To avoid confusion, different areas have been defined as either the edge or end of the slab or panel, as shown in Figure 4.1.
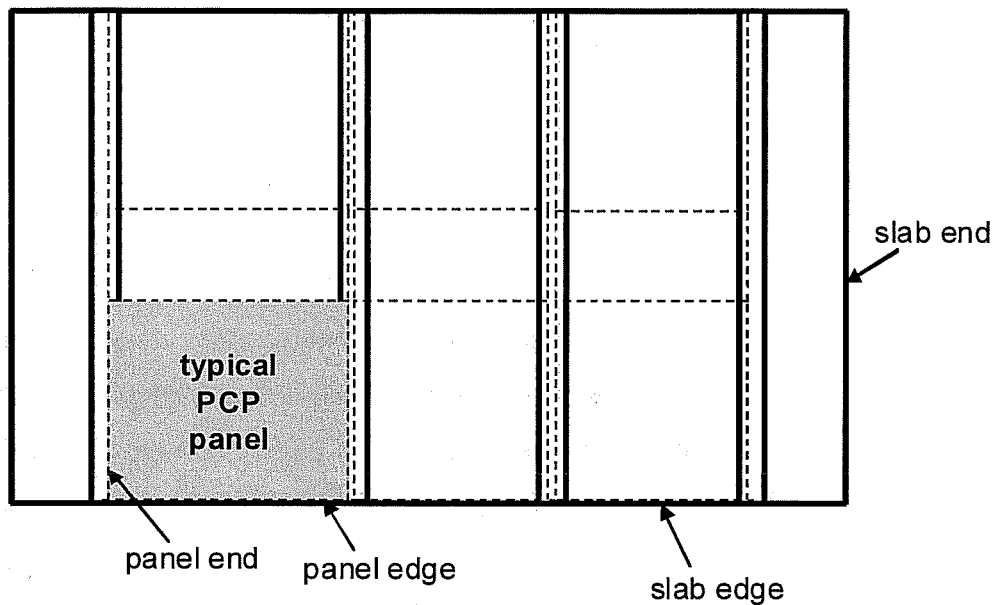
Figure 4.1 Slab and panel terminology

4.2 CONSTRUCTION

The steel W shapes used as girders in the first two specimens were reused for the PC panel specimen. The girders were modified to accommodate the change in slab depth from 8 in. to 10 in. at the IBTS slab edge (Figure 4.2). For the PC panel specimen the bridge deck slab had a uniform thickness of 8 in. The material removed for the drop-down section of the girders was replaced to accommodate the 8-in. thickness on both ends. Two steel channels with a web thickness of approximately ¾ in. were welded to each other and the top flange to make up for the 2 in. drop down, as seen in Figure 4.3.
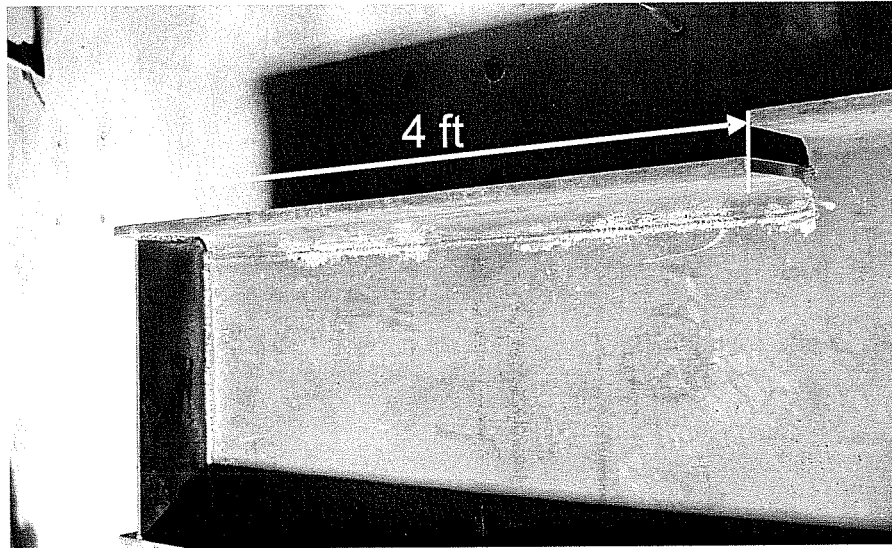
Figure 4.2 Drop-down in top girder flange (Ryan 2003)
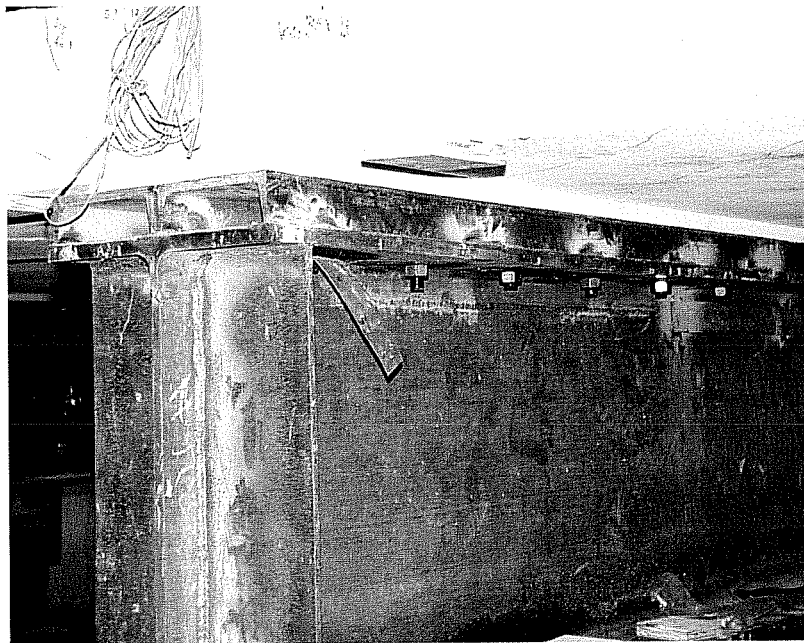
Figure 4.3 Channels welded to drop section of girder

For all three test specimens, the slab and girder assembly was elevated on eight columns, 4 ft tall and 2 ft in diameter. Elevating the slab was necessary to install the loading frame and instrumentation, and to provide access to view

cracking. The columns were positioned on the laboratory floor, and the steel girders were placed on top of them. The girders were placed on 2-in. thick neoprene pads and a load cell that was sandwiched between two steel plates. Load cells were installed under the girders on the side of the slab being tested, and steel plates were used to maintain a constant beam elevation on the opposite side.

Once the girders were erected on the columns, 1-in. wide by 1-in. thick 60-psi foam bedding strips were attached to the top flange along the length of the girders for the PC panels. According to TxDOT standards, the bedding strips were placed to provide space for at least 1-½ in. of mortar to flow under the panels as the slab concrete is placed. After the bedding strips were in place, the panels were placed using the laboratory crane, as seen in Figure 4.4. The crane lifted each panel by the U-shaped bars embedded in the top of the panels. After the panels were in place, a work platform and elevated formwork were built for the overhangs using 4-ft by 8 ft plywood panels, ¾ in. thick (Griffith 2003). Four 2- x 6-in. stringers, spaced 16 in. apart, were attached to each panels. The panels were supported from the ground by 4- x 4-in. posts and from the girder by 2x4's wedged between the bottom girder flange and the 2- x 6-in. stringers. Posts were braced in two directions with 2x4's.
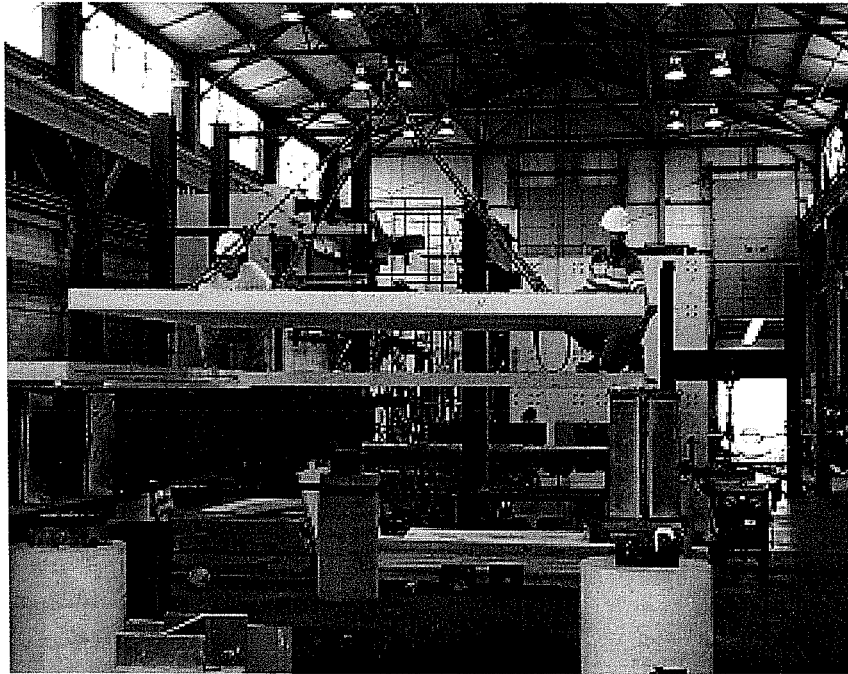
Figure 4.4 Placing precast panels

To provide a redundant connection between the girders and the overhang formwork, fabricated metal clips linked the shear studs to the formwork (Griffith 2003). Edge boards, which formed the sides of the slab, were diagonally braced to the lower formwork. Gaps in the forms were closed with silicone sealant, and the overhang forms were oiled to allow for easier removal of the side forms. Side forms for the CIP topping slab near the panels were not oiled so that bond between the panels and the CIP slab concrete would not be affected.

Before the reinforcing steel was installed, the armor and sealed expansion joint rails were attached to the one edge of the slab side forms. The armor and sealed expansion joints were spliced with 4-in. fillet welds along the top and side of the two joints as seen in Figure 4.5. The two expansion joint rails were

74

temporarily supported by 5/8-in. anchor bolts through the joints and side forms. Reinforcing steel, both instrumented and bare, was then placed on chairs and tied together. After reinforcing steel was in place, the armor and sealed expansion joint were welded to the reinforcing steel for support during concrete placement. Block-outs of PVC pipe were placed in the panels and the bridge slab where loading rods would pass through the slab. Prior to placing the concrete, the locations of strain gauges were recorded and the strain-gauge wires were routed out of the specimen (Figure 4.6).
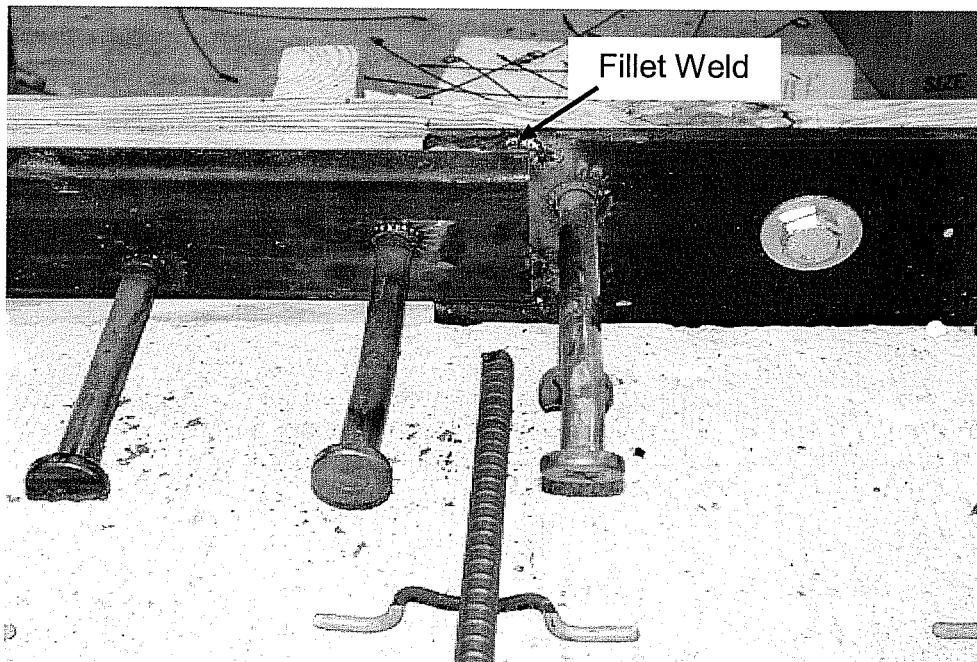
Figure 4.5 Weld splice between sealed expansion and armor joint rails

Concrete was transported and placed with a bottom-drop bucket hoisted by a crane (Figure 4.7). The concrete was consolidated using electric vibrators (Figure 4.8). An aluminum screed was used to level the top surface of the bridge slab. Bull floats and hand trowels were used to create a smooth, flat surface. The

entire surface of the slab was covered in burlap and plastic sheeting to reduce evaporation and then cured for seven days. After seven days, the side forms were stripped and block outs removed; and after 28 days, slab testing began.
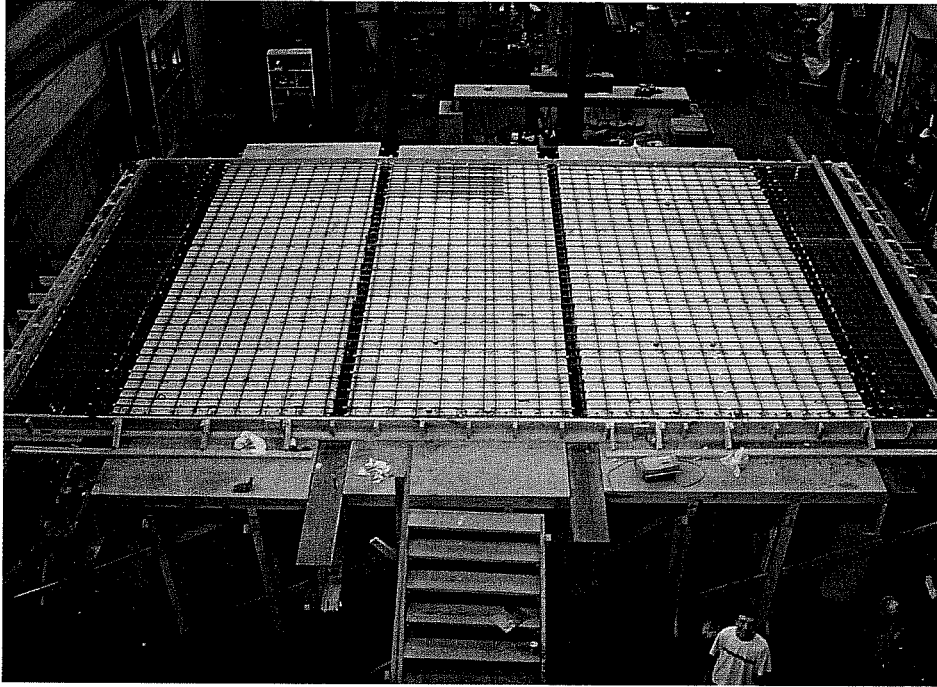
Figure 4.6 Forms before pouring

Figure 4.7 Placing the topping slab

Figure 4.8 Vibrating concrete

77

4.3 LOAD APPLICATION

All three specimens were built and tested on the strong floor of the Ferguson Structural Engineering Laboratory. Since the test specimen was full scale and large simulated truck loads had to be applied at a number of different locations, a compact, reconfigurable load frame was designed and built to fit underneath the bridge slab and be moved using a small forklift (Figure 4.9 and 4.10). This arrangement was much simpler and less costly than a reaction frame constructed over the deck.

Threaded rods were routed through the loading frame on top of the bridge slab and attached to a loading arm, labeled in Figure 4.9 as "upper load arm". The upper loading arm was connected to the two lower loading arms by two, 2-in. diameter threaded rods. The rods connecting the two arms were prestressed to eliminate rotation of the loading arm due to minor misalignments. The upper and lower loading arms were constructed by attaching two C10x20 channels back-to-back with steel plate spacers, to allow loading through their shear center. The lower arm flanges were drilled to match the strong-floor bolt pattern, and were stiffened adjacent to the holes (Figure 4.9, Figure 4.10). Six lower loading arms and four upper loading arms were built, allowing the application of up to four tire loads at any location on the bridge slab.
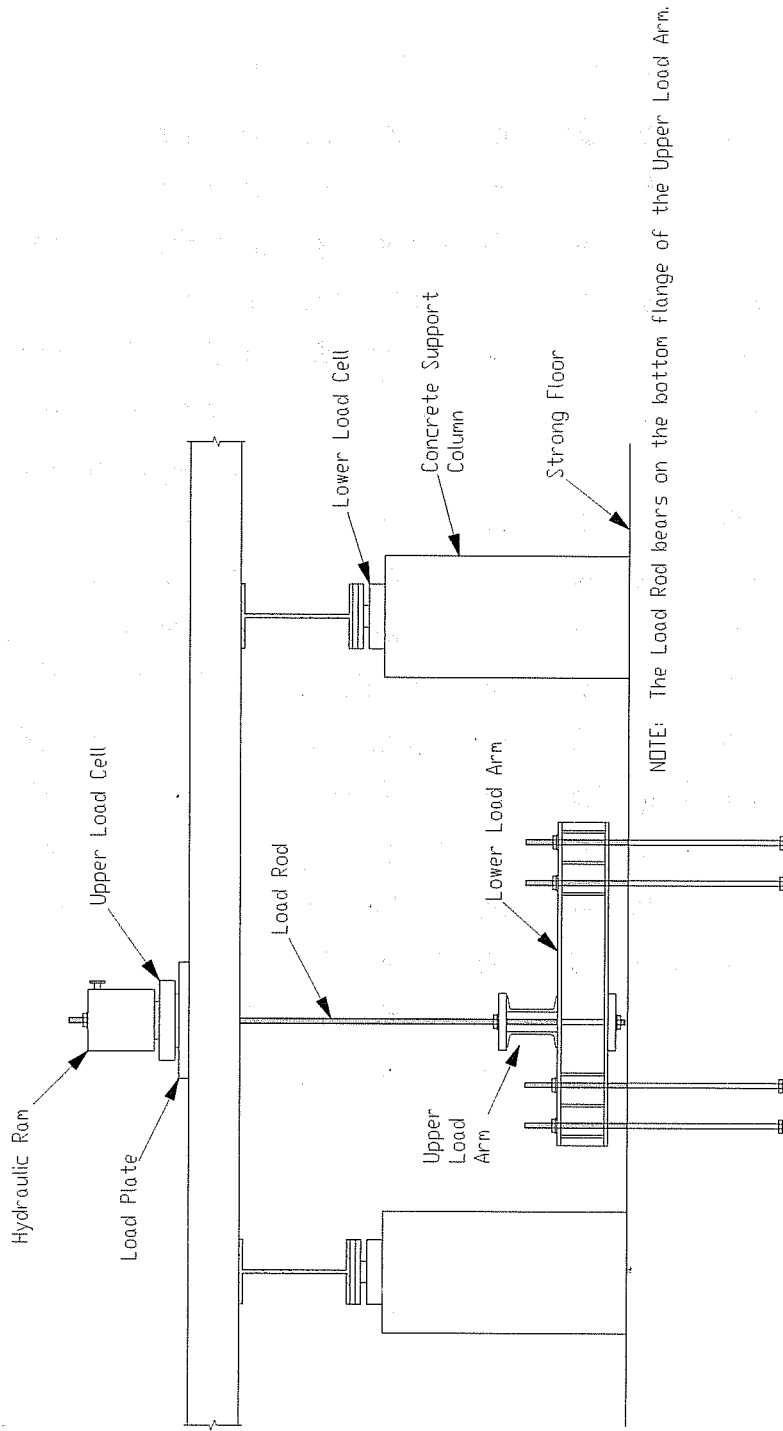
Figure 4.9 Drawing of loading frame (Ryan 2003)

NOTE: The Load Rod bears on the bottom flange of the Upper Load Arm.

Concrete Support Column

Lower Load Cell

Strong Floor

Upper Load Cell

Load Rod

Lower Load Arm

Hydraulic Ram

Load Plate

Upper Load Arm
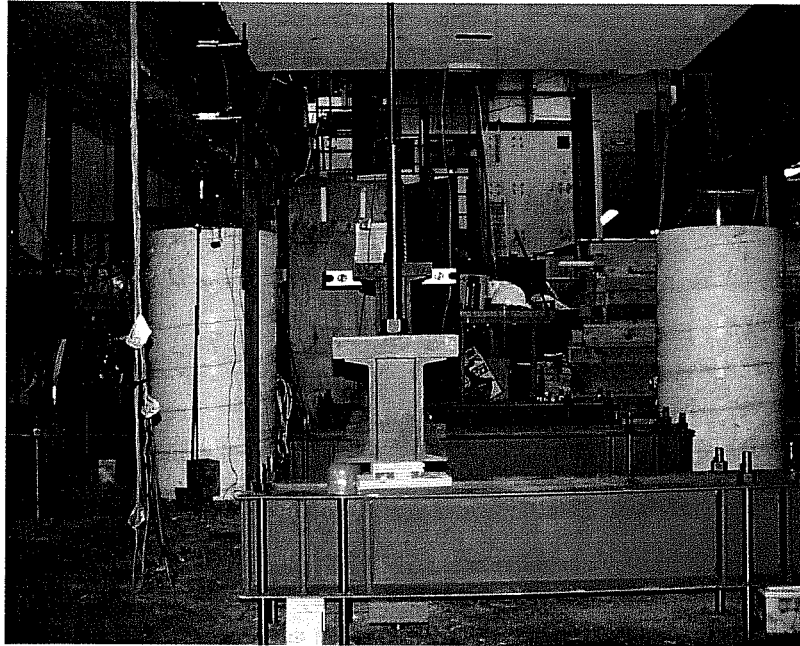
(a)   Facing South (same view as Figure 4.9)
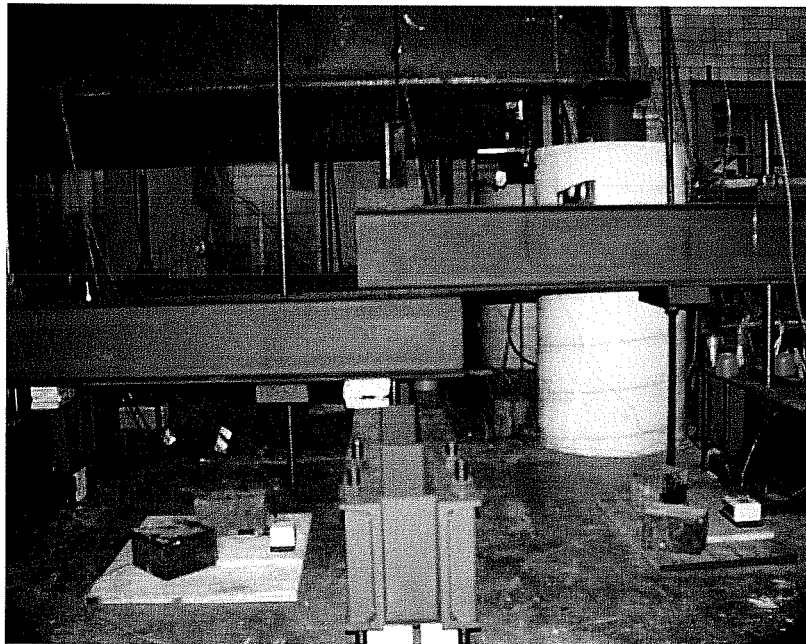
(b) Facing east (perpendicular to view in Figure 4.9)

Figure 4.10 Pictures of loading frame (Ryan 2003)

4.3.1 Tire Loads

Section 3.6.1.2.5 of the AASHTO LRFD Bridge Design Specification, 1999 Supplement specifies that design be carried out using an assumed tire contact of 20-in. wide (transverse direction) and 10-in. long (longitudinal direction). Steel plates measuring 20-in. long, 10-in. wide and 2 ½ -in. thick were used to simulate tire contact areas.

4.4 INSTRUMENTATION

To document the behavior of the test specimen during loading, strain gauges, linear potentiometers, and load cell readings were monitored and recorded during testing. Strain gauges could not be installed on the PC panels during their prefabrication. Instrumentation for the PC panel specimen was adjusted from the previous two test specimens to include a deflection transducer for measuring elongation of the bottom surface of the PC panels.

4.4.1 Strain Measurements

Strain gauges were the primary instrumentation used in the bridge slab of the test specimen (Griffith 2003). Since the strain gauges were placed before the concrete was cast, they were attached carefully and protected to avoid any damage during concrete placement and finishing. In order to measure the strain induced in the panels from testing, a linear potentiometer was mounted to the underside of the panel at midspan of each bay (Figure 4.11). The gage length was about 9-in. These linear potentiometers were added just prior to testing of the bridge slab.
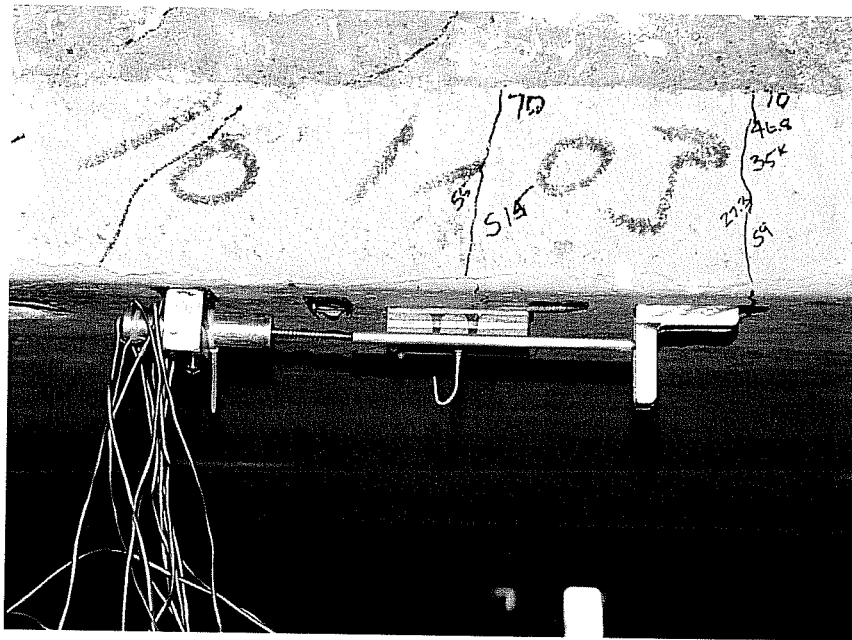
Figure 4.11 Linear potentiometer to measure strain of the panel

4.4.1.1 Locations of Strain Gauges

Strain gauges were used to measure strains in individual reinforcing bars as a function of the applied load. The strain gauges and the linear potentiometers mounted on the under side of the PC panels helped determine the corresponding strain profile within the slab. Strain measurements were used to determine how reinforcing bar stresses are distributed across critical sections of the deck. In the PC panel specimen, the gauges attached to the reinforcing bars on both edges of the slab were situated at critical sections over the girders and at midspan of the 10 ft bay. The gauges were only attached to the top reinforcement mat, since the PC panels were manufactured by Bexar Concrete in San Antonio, TX, and no gauges were attached to the prestressing strands before they were cast. Strain gauges were attached at locations along the armor and sealed expansion joint rails, as seen in Figure 4.15, and on the first two reinforcing bars at the edge of the slab

and then every second reinforcing bar. All strain gauges over the girders were located at the ends of the panels, except for the first flexural reinforcing bar at the slab edge, where a second strain gauge was attached at the face of the girder to compare the stresses with earlier tests (Figure 4.12). Figure 4.13 and Figure 4.14 shows a layout of the locations of the strain gauges in the top mat of reinforcement.
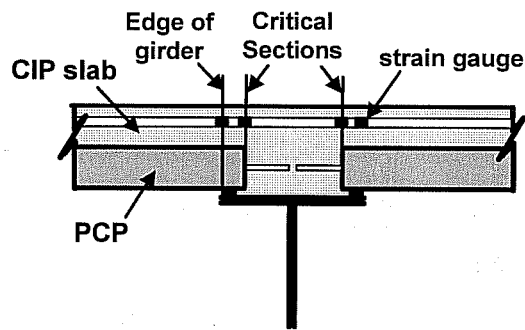
Figure 4.12 Gauge locations over girders

(a) 8-ft girder spacing, 3-7/8 in. top reinforcement spacing

(b) 10-ft girder spacing, 6 in. top reinforcement spacing
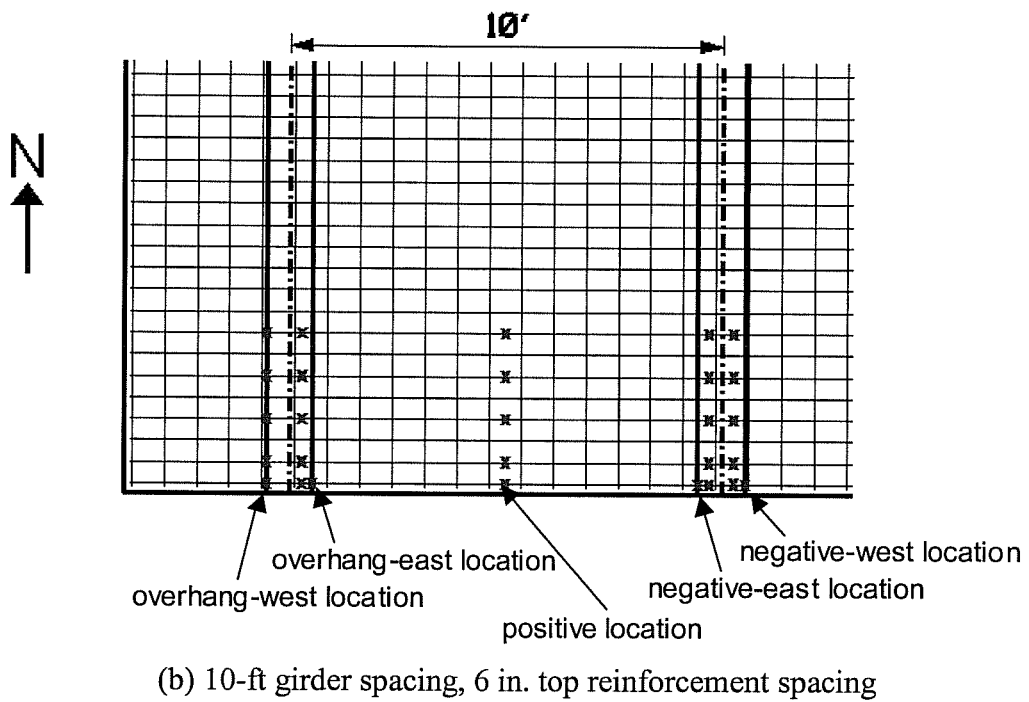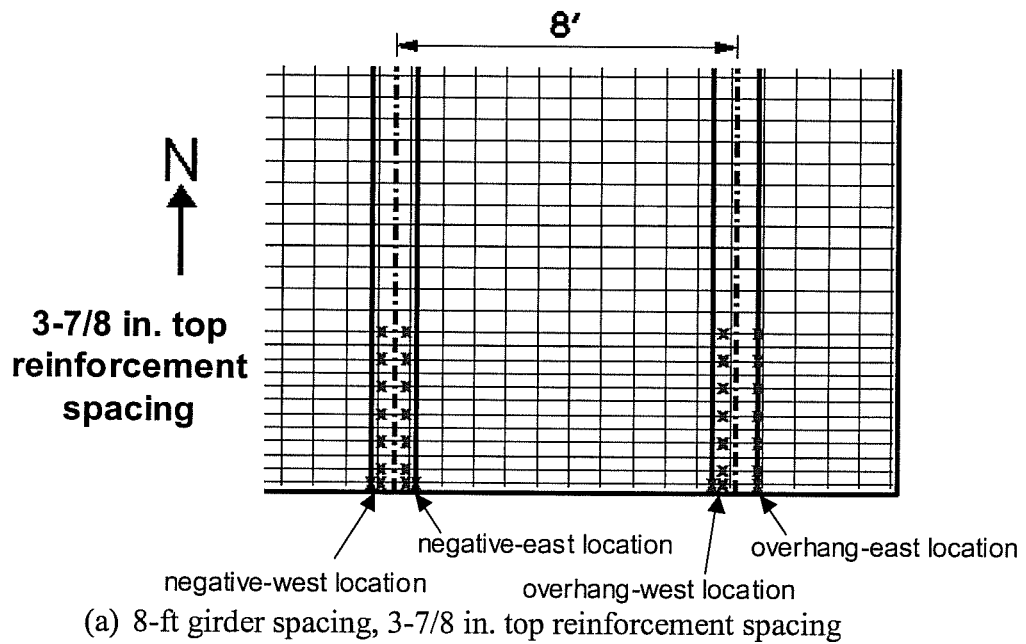
Figure 4.13 Locations of strain gauges, top mat
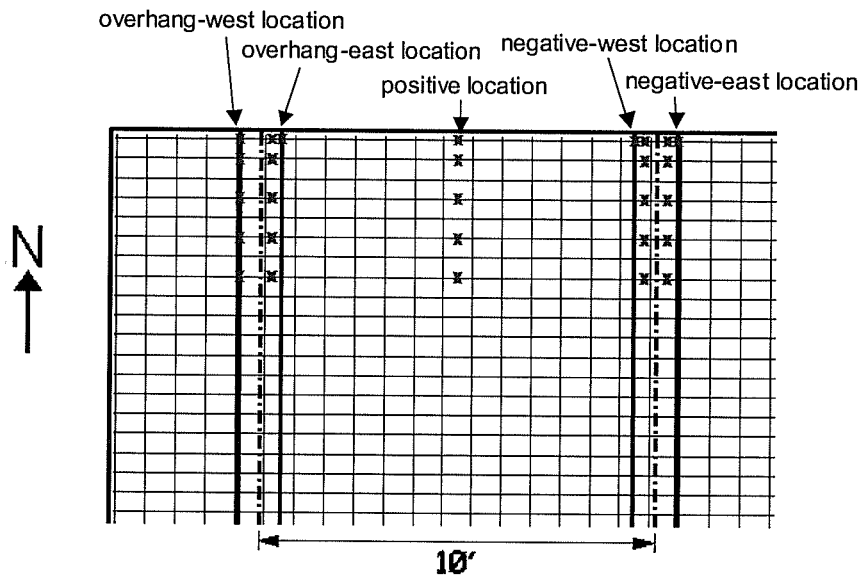
(c) 10-ft girder spacing, Sealed Expansion Joint Rail
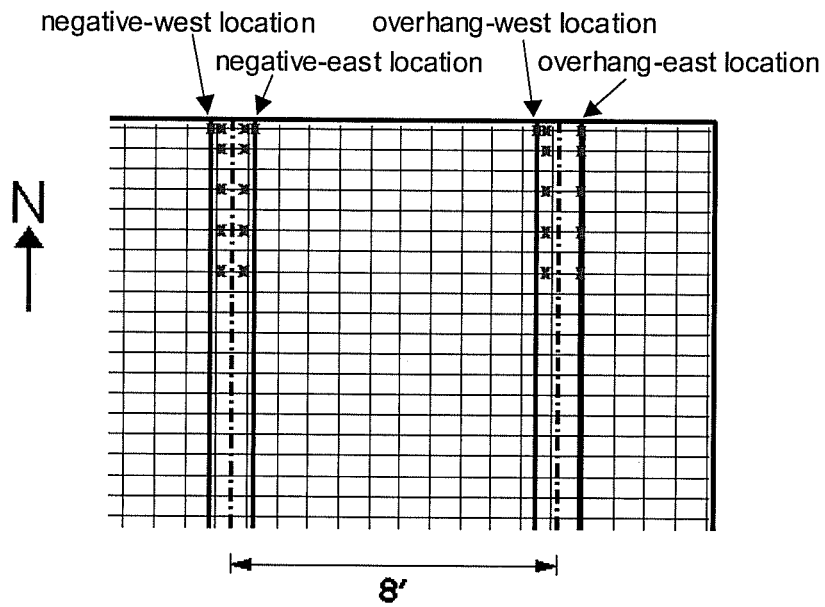
(d) 8-ft girder spacing, Armor Joint Rails

Figure 4.14 Locations of strain gauges, top mat

85
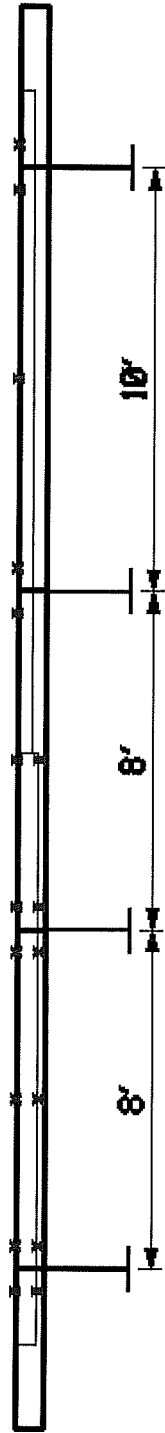
Figure 4.15 Locations of strain gauges, armor and sealed expansion joint rails

4.4.1.2 Installation of Strain Gauges (Ryan 2003)

The strain gauges had a 5-mm gauge length, 3-m pre-attached leads, and were temperature-compensating (3-wire gauges). The reinforcing bars were prepared for strain gauge application by grinding off one rib to create a flat surface (Ryan 2003). The application area was then cleaned with conditioner and neutralizer. Cyanoacrylate (CN) adhesive was used to bond the strain gauges to the reinforcing bar. The gauges were waterproofed with an acrylic coating. Next, a neoprene rubber pad was placed over the gauge for impact protection, and the installation area was covered with foil tape. Finally, the edges of the foil tape were wrapped with electrical tape to seal out concrete and water.

4.4.2 Load Measurements (Ryan 2003)

Load cells, located underneath the girders (lower load cells) and at the hydraulic rams (upper load cells) (Figure 4.9) were used to provide a check on load distribution in the slab. The lower loads cells were only used under the girders at the edge of the bridge slab being tested. The load cells on the loading plates were the primary transducers for measuring the applied load. In addition, a pressure transducer was attached to the hydraulic line at the hydraulic pump to verify load cell readings.

4.4.3 Deflection Measurements (Griffith 2003)

Deflection measurements were made under the girders and midspan, using linear and string potentiometers located as shown in Figure 4.16. Under girders and at midspan, deflections measurements were taken at the edge of the slab, and 4 ft from the edge in the longitudinal direction of the slab. String potentiometers were used in congested locations. Linear potentiometers were placed at the corners of the panels to measure deflections due to compression of the bearing

pads on the girders. In each test, two linear potentiometers were placed 6 in. apart, to measure rotation of the girders. Figure 4.17 shows how the potentiometers were used to measure rotation, and Figure 4.16 shows the locations of the potentiometers.
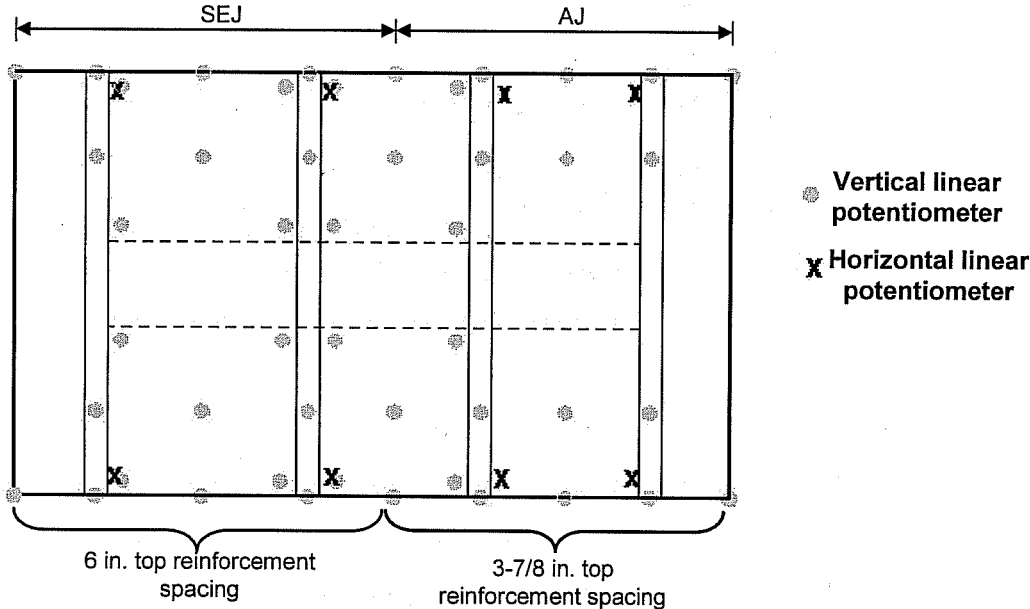
Figure 4.16 Deflection measurement locations, plan view
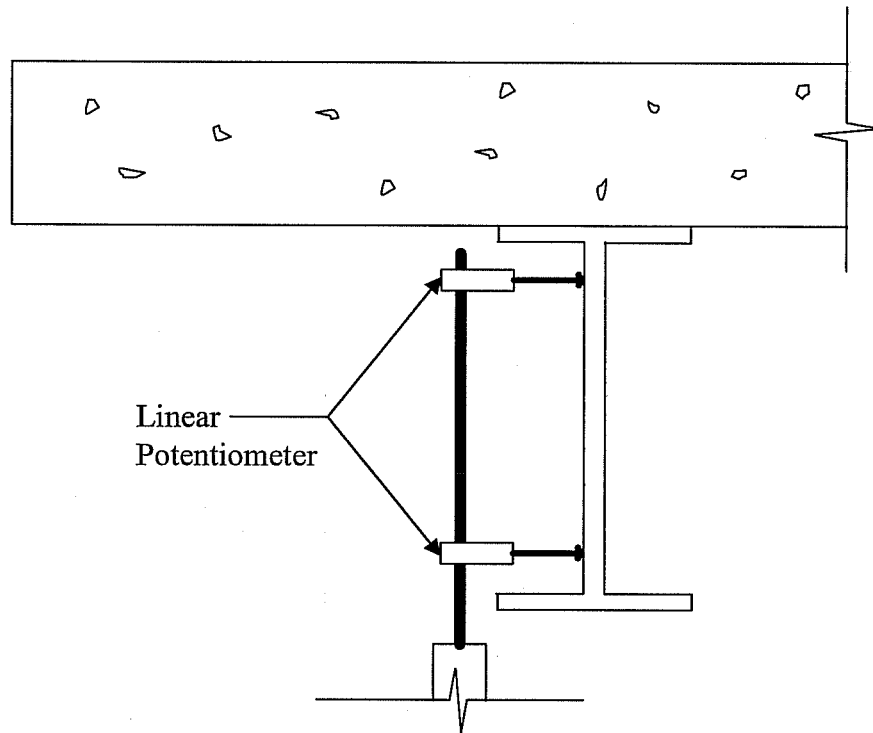
Figure 4.17 Girder rotation measurement (Ryan 2003)

4.4.4   Data Acquisition (Ryan 2003)

Voltage reading (analog signal) from the various sensors was scanned and converted to digital format readable by the data acquisition software installed on a personal computer. Real-time test data could also be plotted to allow monitoring of the behavior during loading.

4.5   MATERIAL PROPERTIES

To better interpret the acquired test data, tests were performed to measure material properties of the reinforcing steel and concrete used in the specimen. Results of material tests were also used to check the strengths reported by the manufacturers.

4.5.1 Reinforcing Steel

All reinforcing steel for the PC panel specimen came from one heat. Two lengths of reinforcing bar were tested in tension. An extensometer and strain gauge were used to determine strains, and load cells in the test machine were used to measure the applied loads (Figure 4.18). Stress-strain plots were created after converting the load measurements to stresses (Figure 4.19).

The PC panels were reinforced with 3/8 in. diameter, low-relaxation prestressing strands with a rupture stress of 270 ksi. Further information on the PC panels is discussed in Section 4.5.3.
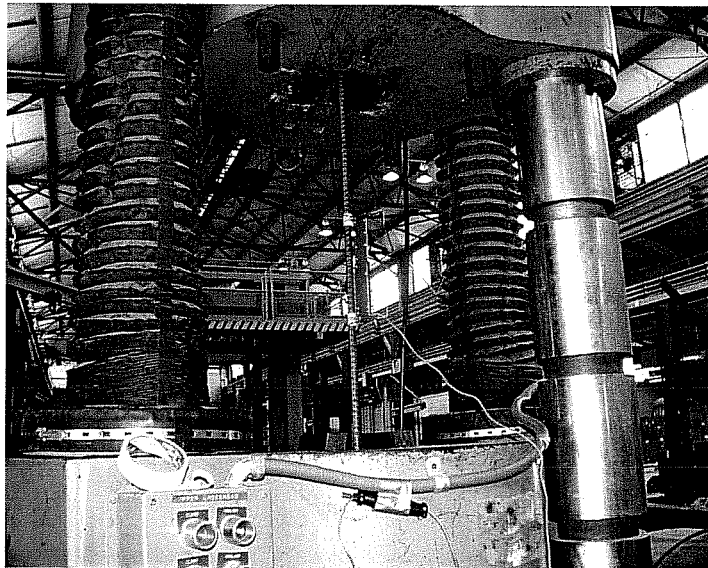
Figure 4.18 Rebar tension test setup (Ryan 2003)
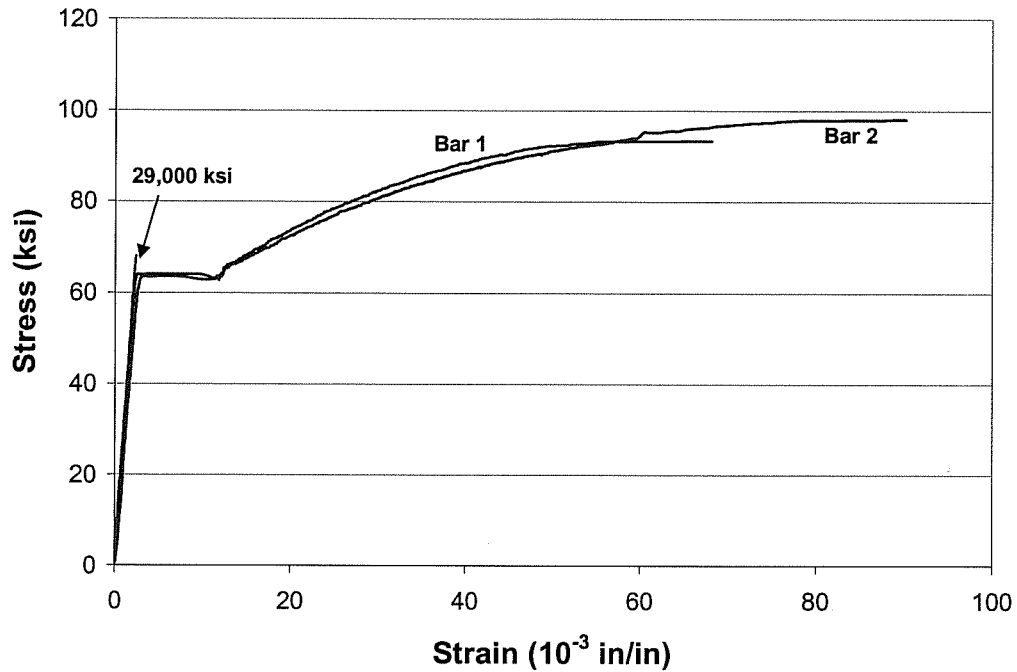
Figure 4.19 Results from rebar tension tests

As seen in Figure 4.19, the reinforcement had a yield stress higher than the specified 60 ksi. The reinforcement yielded at about 63 ksi.

4.5.2 Concrete

The TxDOT Bridge Design Manual currently requires a minimum 28-day compressive strength of 4000 psi for concrete used in bridge slabs. A mix design was ordered with a target compressive strength between 3500 psi and 5000 psi.

Table 4.1 Concrete mixture design for bridge slab (one yard batch) (Griffith 2003)

Mix #	Description	f'$_c$ (psi)	Cement	Fly Ash	Course agg.	Fine agg.	Water	Ad-mixture
225	UT4000A 3/4in	3500 to 5000	470	0	1625	1655	250	20.0

* All quantities are in units of pounds (lbs).

4.5.2.1 Compressive Strength

The 12 yd^3 of concrete used in the slab was delivered in two truckloads; test cylinders were taken from each truck. The concrete in the first truck was placed in the east overhang and the majority of the 4 in. CIP concrete topping in the 10-ft and two 8-ft girder spacing bays. Concrete from the second truck was placed primarily in the west overhang. For each point plotted on the strength versus time curve in Figure 4.20, at least two cylinders were tested. If the two strengths were not close, a third cylinder was tested for verification. The 28-day compressive strength was about 4000 psi.
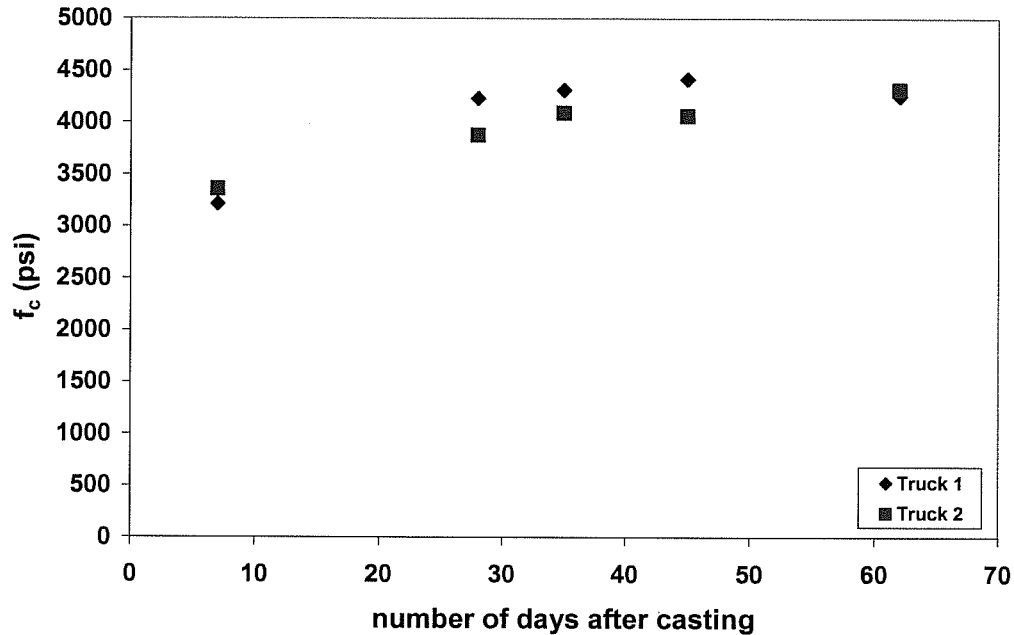
Figure 4.20 History of concrete compressive strength

4.5.2.2 Splitting Tensile Strength

Split cylinder tests were performed two months after casting, on two cylinders from Trucks 1 and 2. The splitting tensile strength, f_{ct}, was determined using Equation 4.1, with P equal to the failure load. The tensile strength of concrete from Trucks 1 and 2 were 380 psi and 350 psi respectively, essentially the same.

$$f_{ct} = \frac{2P}{\pi l d}$$ ***Equation 4.1***

The average of these splitting tensile strengths is about $5.5\sqrt{f_c'}$, slightly lower than $6\sqrt{f_c'}$ often used in design.

4.5.3 Precast Prestressed Concrete Panels

As discussed previously the PC panels were manufactured in accordance with the TxDOT standards that specify a minimum 28-day concrete compressive strength of 5000 psi and a minimum release strength of 4000 psi. PC panels were reinforced with 3/8 in. diameter seven-wire prestressing strands stressed to 16.1 kips per strand.

4.6 TEST PROTOCOL

The specimen was constructed with six test areas, shown in Figure 4.21. Figure 4.21 shows a plan view of the locations of the expansion joint edge test areas and the locations of the load plates in each section. In the 8-ft girder spacing, only negative moment was maximized, and load axles were centered over the girder. Positive moment was maximized in the 10-ft girder spacing, and two load plates were placed at midspan.

All six test areas were tested to service level loads, and then the four test areas similar to those of the 0° skew specimen were tested to failure. Service-level tests were first performed on each area to view cracking behavior in each test section before severe damage occurred anywhere in the slab. For each area, loads were applied until cracking began to extend into neighboring test regions. The area was then unloaded, and the loading frame was moved to the next test area. After all the edge regions were tested, the four overhangs were tested, as discussed in Chapter 6. After all the edge region and overhang tests were completed, two additional punching shear tests were conducted. In one test, the tire load was placed at the joint between two adjacent PC panels, and another test was conducted with the load positioned at the interior of PC panel. These additional tests are discussed in Chapter 5. Expansion joint edge test areas were first loaded to service load levels, and then loaded to failure after all serviceability

tests were completed at all locations. The expansion joint edge tests are listed in the order in which they were performed:

Test 1 - 8-ft girder spacing, no Armor or Sealed Expansion Joint Rail (AJ/SEJ), 3-7/8 in. top reinforcement spacing, negative loading configuration

Test 2 - 8-ft girder spacing, no AJ/SEJ, 6-in. top reinforcement spacing, negative loading configuration

Test 3 - 10-ft girder spacing, no AJ/SEJ, 6-in. top reinforcement spacing, positive loading configuration

Test 4 - 10-ft girder spacing, SEJ, 6-in. top reinforcement spacing, positive loading configuration

Test 5 - 8-ft girder spacing, SEJ, 6-in. top reinforcement spacing, negative loading configuration

Test 6 - 8-ft girder spacing, AJ, 6-in. top reinforcement spacing, negative loading configuration.

Test 4
No. 5 bars at 6 in. o.c.*,
SEJ, 10-ft girder spacing,
Serviceability & Failure

Test 5
No. 5 bars at 6 in. o.c.*,
SEJ, 10-ft girder spacing,
Serviceability

Test 6
No. 5 bars at 6 in. o.c.*,
AJ, 10-ft girder spacing,
Serviceability & Failure

4'

5'   6'   3'   6'

interior
loading plate

N

edge loading
plate

Test 3
No. 5 bars at 6 in. o.c.*,
10-ft girder spacing,
Serviceability & Failure

Test 2
No. 5 bars at 6 in. o.c.*,
10-ft girder spacing,
Serviceability

Test 1
No. 5 bars at 3-7/8 in. o.c.*,
AJ, 10-ft girder spacing,
Serviceability & Failure

* o.c. – on center

(a) Expansion joint edge tests

Overhang Test 2
SEJ

**Interior Punching
Shear Test**

Overhang Test 1
AJ

4'

joint between PCP
panels

3'

Joint Punching
Shear Test

4'

8'

2'

N

Overhang Test 4
No. 5 at 6 in. o.c.

Overhang Test 3
No. 5 at 3-7/8 in. o.c.

(b) Overhang and additional punching shear tests

Figure 4.21 Test areas, PC panel specimen: (a) expansion joint edge tests; (b) overhang and additional punching shear tests

96

Load was applied in increments to the test specimen with 60-ton hydraulic rams connected to a pneumatic hydraulic pump with all rams connected to the same manifold. The scanner required 10 seconds to record readings from 110 channels, so load was increased in small increments to permit generation of continuous force deformation plots. During testing, a load-strain plot of the most critical strain gauge was generated in real time to monitor the response of the slab to applied loads. Intermittently, loading was paused so that cracks could be traced, measured, photographed and recorded.

After all service-level tests had been performed, each test area was loaded to design-level load, overloads as multiples of that design-level, and to failure. Each serviceability test included: load levels HS-20, HS-25, 1.2 HS-25, and 1.75 HS-25. Cracks were marked at the following load levels: HS-20, HS-25, 1.2 HS-25, 1.75 HS-25, 3.0 HS-25, and failure. A factor of 1.2 times HS-25 loading may be considered a typical overload factor to account for overloaded trucks for a typical design load. The factor of 1.75 was chosen because 1.75 is the live-load factor (Section 3.4.1 in AASHTO LRFD). Also, Section 3.6.2 of the same AASHTO Standard requires the design loading to be increased by 1.75 at expansion joints to allow for dynamic loading. An overload level of 3.0 HS-25 was applied because the product of the load factor and the dynamic load allowance is approximately 3.0. When designing the expansion joint of a bridge slab, the required design load is three times the typical load.

CHAPTER 5

Test Results – Expansion Joint Edge Tests

5.1 INTRODUCTION

In this chapter, the results from tests performed on expansion joint edges and interior punching shear tests are presented, including deflections, strains, crack patterns and failure loads. After the results are presented, the expansion joint edge tests are discussed and compared, as are the two interior punching shear tests. In addition, failure modes and capacities are addressed.

Expansion joint edge tests are named by the top reinforcement spacing, highest level of load applied, presence of armor and/or sealed expansion joint rail and whether positive moment or negative moment was maximized by the placement of the AASHTO design truck. If positive moments are maximized, the test is referred to as a "positive moment test", and if negative moments are maximized, as a "negative moment test" (Griffith 2003). For the interior punching shear tests, they are referred by the location of the loading point on the panel. The expansion joint edge tests are listed below in the order in which they were performed:

> **Test Area 1** - 3-7/8 in. top reinforcement spacing, failure, negative
> > moment region
>
> **Test Area 2** - 6 in. top reinforcement spacing, serviceability, negative
> > moment region
>
> **Test Area 3** - 6 in. top reinforcement spacing, failure, positive
> > moment region

Test Area 4 - Sealed expansion joint rail (SEJ), failure, positive

moment region

Test Area 5 - SEJ, serviceability, negative moment region

Test Area 6 - Armor joint rail (AJ), failure, negative moment region

Positive moment at midspan was maximized in the 10 ft bay, and negative moment was maximized over the girder in the 8 ft bays. Although load points may be placed to maximize positive moments, significant negative moments may still develop in other areas of the test region. The same is true for the negative moment tests. In order to better compare test results, the negative moment tests are listed together, as well as the positive moment tests. Loads are reported as multiples of AASHTO design loads as discussed in Section 3.2.3.

Due to restrained shrinkage, significant tensile strains were present in the CIP at the time of testing. As a result at "low transverse" loads, cracking along the edges of PC panels took place. Therefore, each area was first loaded up to 1.75 x HS-25 in order to avoid extensive cracking to the other test areas. After the six initial serviceability tests were performed, the four critical areas were loaded to failure. The load levels in the serviceability tests were limited to avoid extensive damage that could reduce the stiffness in areas tested subsequently. All tests followed the same test procedure. At critical load steps, crack lengths and widths were recorded and pictures were taken.

Figure 5.1 and 5.2 are samples of the graphics used in the chapter to identify the area being tested. Figure 5.1 shows the test region, loading points, linear potentiometer and strain gauge locations. In some tests, the linear potentiometer locations may coincide with the loading point locations; if that is the case the loading point location will be shadowed beneath the linear potentiometer location symbol. The design parameters, usually the girder spacing

and top reinforcement spacing, are identified in the figure. A '+' or '-' sign is shown to designate the maximized moment, negative or positive, in the test region, and the load points are shown to describe the loading of the test region during testing. The strain gauges are located on the flexural reinforcement bars along the axes drawn and are identified as either "negative" or "overhang". The linear potentiometer attached to the bottom face of the panel at midspan to estimate the strain is identified as "positive". Over the interior girders, negative moments are generated, and these locations are referred to as "negative" locations in the figures. The strain gauge locations over the exterior girders are referred to as "overhang" locations. The location of the dashed line on the graphic indicates the orientation of the "negative" and "overhang" gauges relative to the girder.
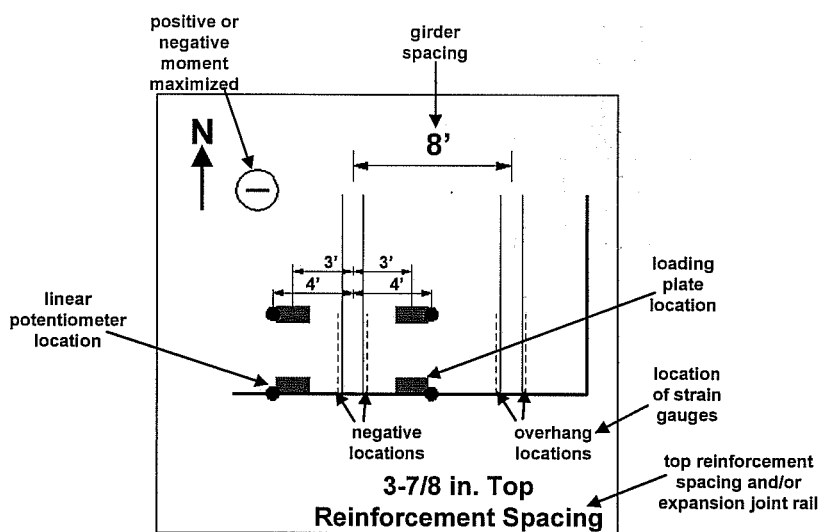
Figure 5.1 Sample test area

100
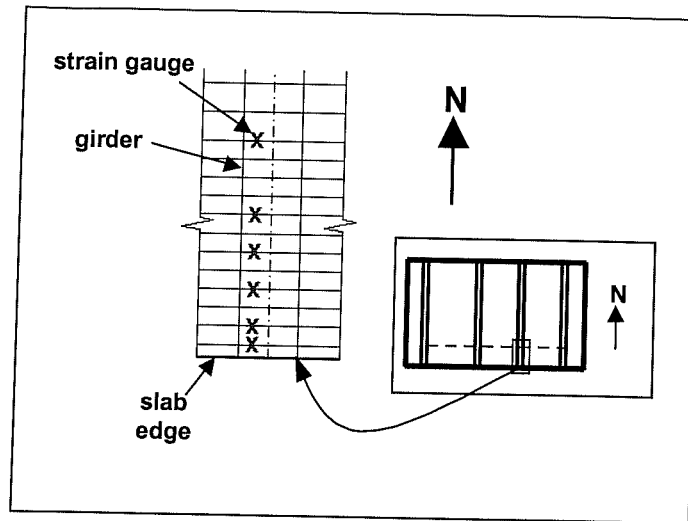
Figure 5.2 Sample strain gauge location

Figure 5.2 shows a more detailed view of the locations of strain gauges in the edge region and will be used to show gauge locations in strain profiles. The slab edge and flexural reinforcement in the edge region are shown, and gauges are shown by an 'x'. The smaller graphic indicates the location of the slab being enlarged. Where gauges are installed on either face of the girder, specifically over the end of the panel, the girder is shown.

To describe the behavior of the test region, individual load points, girders, bays must be identified; naming conventions have been set to aid in this discussion. Figure 5.3 shows the convention used in identifying girders and bays.
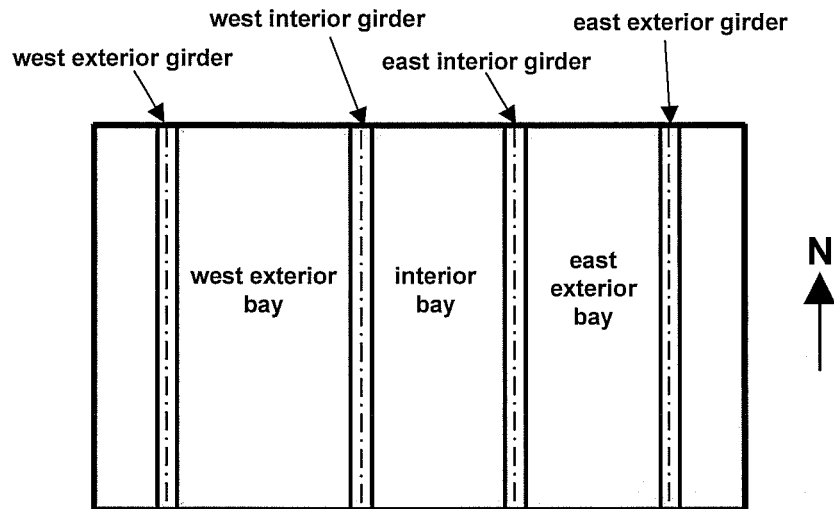
Figure 5.3 Girder and bay notation terminology

Load-deflection plots were created using the readings from the load cells and the linear and string potentiometers measuring vertical deflection of the bridge slab. The relative deflection at the edge was calculated by subtracting the average of the two girder deflection readings made underneath the girders near the supports from the deflection reading at midspan (Figure 5.4). Rigid-body movement of the bridge slab is filtered out this way, so relative deck deformations consistent with recorded stresses and strains could be compared. For each test, the residual deflection is assumed to be the last measured deflection taken after unloading in the previous test.
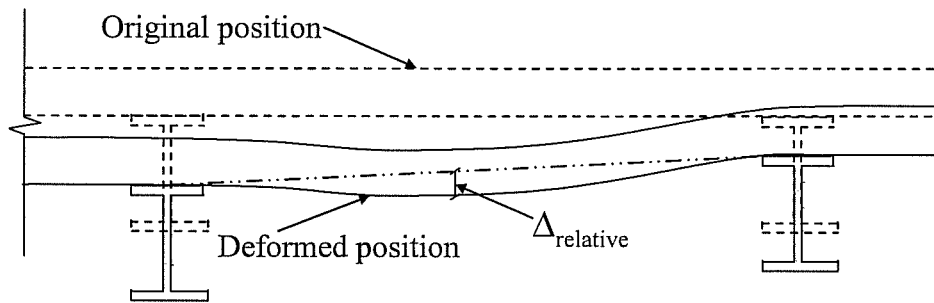
*Deformations are exaggerated.

Figure 5.4 Relative midspan deflection (Ryan 2003)

For the 0° and 45° skew CIP decks, only the relative midspan deflection at the edge of the slab was reported since the deflection measured 4 ft from the edge of the slab was very small and was indistinguishable from noise inherent to the instrumentation. However, with the panels the deflections measured at 4 ft from the slab edge were fairly significant. Therefore, the deflections in the exterior and interior bays, both at the edge of the slab and 4 ft from the slab edge, are reported in this section.

Load-strain plots are shown to analyze cracking and identify loads at which reinforcement yields. Strain gauges were installed on the first and second reinforcing bar and then every other flexural reinforcing bar in the edge detail, for a total of seven gauges on the top mat of reinforcement over the girders. Additional strain gauges were attached to the first reinforcing bar at the midspan of the bays, as well as a linear potentiometer attached to the bottom face of the panel to estimate the strain in the panel over a 9 in. gage length. Only the data from the most critical gauge from each of these locations are shown here. The critical gauge was defined as the gauge measuring the largest strain throughout

most or all of a test. Generally, the critical gauge is located on the reinforcing bar closest to the edge of the slab. Locations of the critical gauges are shown to the right of the plots.

Strain profiles were used to compare strain readings from reinforcement and expansion joint rails in a test area at specific locations and loads. In each strain profile, the figure contains a graphic showing the locations of the strain gauges in the test specimen. A plan view of the strain measurements from reinforcement in the edge detail at selected load stages are shown in the following figures. The strain profiles were used to compare strains in the bridge slab for the two top reinforcement spacings and the contribution of the two types of expansion joint rails. Since the edge deflection was greater than the deflection 4 ft from the edge of the slab, the strains are expected to be greater at the reinforcing bars closest to the edge of the slab. In addition, strains 4 ft from the edge of slab near the interior load point are higher than the strains measured between the two load points, since the panels being loaded are deflecting as a unit due to the inherent separation caused by the adjacent panel joints.

5.1.1 Shrinkage Cracking

In previous research on the composite bridge decks of PC panels and CIP concrete topping, the development of cracking along the slab due to shrinkage and thermal effects is reported. Inspection of many TxDOT bridges that include the PC panels (Figure 5.5) show a pattern of shrinkage cracking in the CIP concrete topping that outlines the locations of the panels in the deck (Brown 2002). Prior to testing, about 27 days after casting, the slab deck was checked visually for any cracking, which no cracks were found. At a very low load (7.5 kips per load point or 0.5 HS-25) when conducting the first test to serviceability loads, the slab was checked for cracking. At this load a great deal of very small (maximum 0.002 in.

104

wide) cracks were found along the girder and the joints between adjacent PC panels (Figure 5.6). Calculations were carried out to determine if a load of 0.5 HS-25 was sufficient to cause such cracking in the CIP concrete topping. Assuming that typical concrete strains due to shrinkage effects are about 300 $\mu\varepsilon$, and adding the effects of the applied loads, it was found that such low applied loads would produce cracking at locations where shrinkage stresses developed. It was decided that although the shrinkage cracking had not developed prior to testing, had the testing begun weeks later, the shrinkage cracking would have been visible prior to testing. Therefore since testing was done before shrinkage cracking had developed, small additional stresses from the first loading and the tensile stresses due to shrinkage and thermal effects caused the CIP concrete topping to crack at such a low load. Later discussions with TxDOT engineers indicated that such cracking is evident in all TxDOT brides using PC panels.
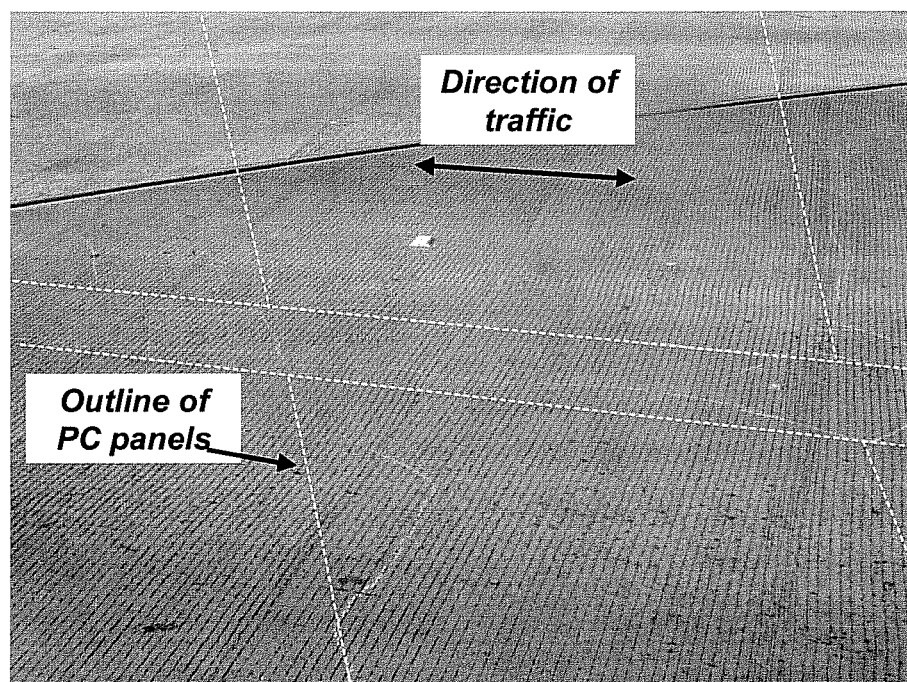
Figure 5.5 Shrinkage cracking in TxDOT bridge (Brown 2002)
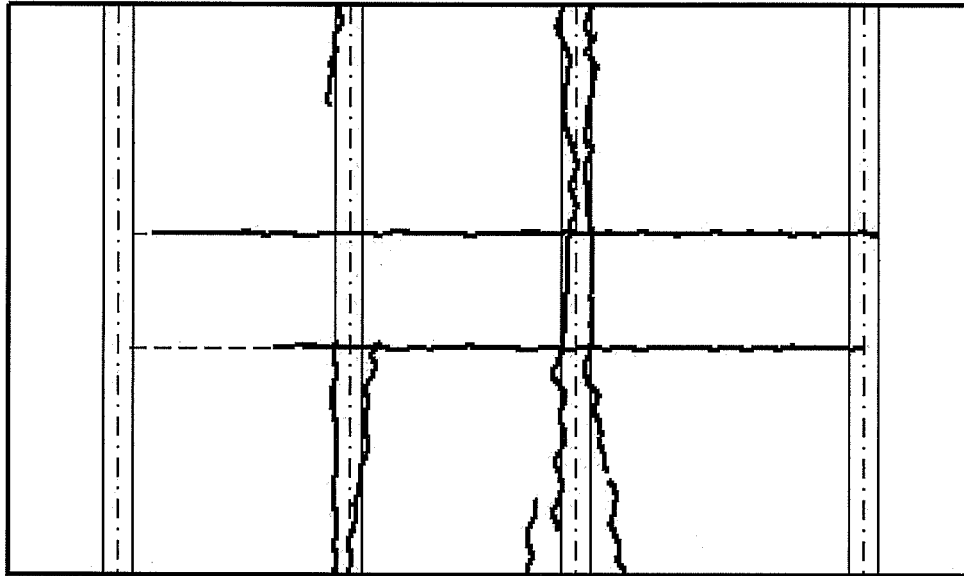
Figure 5.6 Shrinkage cracking, top view of slab

5.2   3-7/8 IN. TOP REINFORCEMENT SPACING, NEGATIVE-MOMENT REGION (TEST AREA 1)

5.2.1   Summary of Response

The 3-7/8 in. top reinforcement spacing test area was loaded to design and overload levels with the AASHTO tandem load configuration placed to maximize negative moments in the edge detail.

Shrinkage cracking developed at a very low load (0.5 x HS-25). However, first flexural cracking was visible at 1.4 x HS-25 on the bottom face of the panel, in addition to the widening of the cracks due to shrinkage effects on the top surface of the slab. Top cracks formed over the ends of the panels, over the girders and propagated parallel to the girder. Developed cracking occurred at approximately 2.9 x HS-25. Even though the first visible cracks (shrinkage effects) were at loads less than the design loads, flexural cracking did not occur

106

until loads higher than design loads. All cracking on the bottom face of the panel was contained within the panels being loaded. Based on the load-deflection and load-deformation responses, the test area performed well at service load levels. At approximately 3.0 x HS-25, elliptical cracks began to form around the load plates, and at 4.8 x HS-25 a punching shear failure initiated at the edge load point in the interior bay. In order to preserve an area for testing the behavior at a load point over a panel butt joint, the exterior bay was not loaded to failure.

The relative midspan edge deflection at failure was 0.31 in. in the interior bay and 0.18 in. in the exterior bay. First reinforcement yield occurred at 3.9 x HS-25 on the west face of the girder at the strain gauge at the face of the girder and not at the end of the panel. The maximum recorded strain was 3.0 ε_y (6650 $\mu\varepsilon$), measured at failure at the same strain gauge location as first reinforcement yield stress.

5.2.2   Detailed Description of Response

5.2.2.1   Loading

Negative moments were maximized over the east-interior girder, between the two 8-ft bays. At the locations shown in Figure 5.7, four 10 in. by 20 in. steel plates were placed in the edge region on a layer of hydrostone. As discussed previously, cracks were first observed in the CIP concrete topping at 7.5 kips per load point, 0.5 x HS-25, during the serviceability test. Cracks at the bottom face of the PC panels in the west-exterior bay were first observed at 22 kips per load point, 1.4 x HS-25. Loading was continued to 1.75 x HS-25 and then the next area was tested.

After all serviceability load tests and tests to failure at the armor joint rail and sealed expansion joint rail tests were completed, Test Area 1 was loaded to

107

failure. At 75 kips per load point, approximately 4.8 x HS-25, a punching shear failure occurred at the edge load point in the interior bay (Figure 5.7).
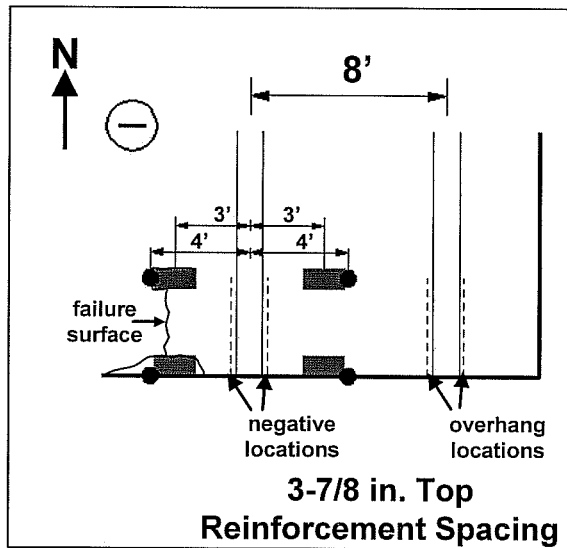
Figure 5.7 3-7/8 in. top reinforcement spacing, negative-moment region (Test Area 1)

5.2.2.2 Load-Deflection Behavior

A complete record of the measured load deflection response is shown in Figure 5.8. The load-deflection envelopes for the edge deflections in the interior and exterior bays are also shown in Figure 5.8. At the interior and exterior bays, the load deflection response for the edge deflection and the deflection measured 4 ft from the slab edge have virtually the same slope to about 1.75 x HS-25. The deflection measured at 4 ft from the slab edge is essentially linear during the entire test program. The load deflection response for the edge deflection of the interior and exterior bays were similar at the low service loads of HS-20, HS-25 and 1.75 x HS-25. At the low service level loads, the deflections were small relative to the girder spacing, so the load-deflection behavior was essentially

linear and elastic at this range. The maximum measured edge deflection was essentially twice the maximum measured deflection 4 ft from the slab edge at failure loads in both the interior and exterior bays. Table 5.1 shows the measured deflections at various load steps for this test area.

Table 5.1 Meausred deflections (inches), Test Area 1

	HS-20	HS-25	1.4 HS-25 first flexural cracking	1.75 HS-25	3 HS-25	4.8 HS-25 Failure
Interior bay, edge	0.01	0.016	0.028	0.04	0.09	0.31
Interior bay, 4 ft from edge	0.01	0.013	0.017	0.02	0.06	0.12
Exterior bay, edge	0.021	0.026	0.035	0.04	0.08	0.18
Exterior bay, 4 ft from edge	0.017	0.024	0.031	0.036	0.06	0.11

5.2.2.2.1 Load-Deflection Envelope

The load deflection envelope indicates three changes in slab stiffness in the interior bay and two changes in stiffness in the exterior bay during all tests in the area. The first change in stiffness, apparent in both bays at approximately 3 x HS-25, was caused by developed cracking in the slab. Throughout this thesis, "developed cracking" refers to the first major change stiffness as interpreted from the load-deflection response. In addition to the change in stiffness evident in the load deflection response, initiation of new cracks and lengthening and widening of existing cracks in the test section are also evident at this load. The load deflection response for the exterior bay shows a slight change in stiffness at this load, but not as apparent as in the interior bay. The slab peak load occurred at approximately 4.8 x HS-25. At failure, deflection in the interior bay is about twice that in the exterior bay. Deflections measured in the interior bay were larger than the deflections measured in the exterior bay. The lap splices between

109

the two top reinforcement spacings, 3-7/8 in. and 6 in., were located in the interior bay. Due to the larger reinforcement spacing over the west-interior girder, crack widths were larger, as seen in Figure 5.12, and as a result deflections were larger in the interior bay than in the exterior bay. Details on the locations and sizes of the cracks are given in Section 5.2.2.5.
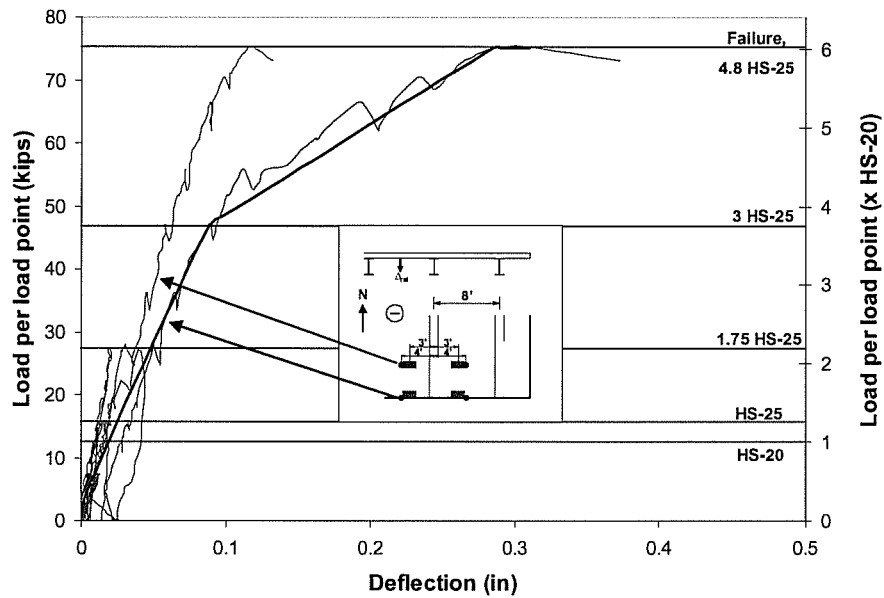
(a) Interior bay

Figure 5.8 Relative midspan deflections and edge deflection envelopes, 3-7/8 in. top reinforcement spacing, negative moment region: (a) interior bay; (b) exterior bay
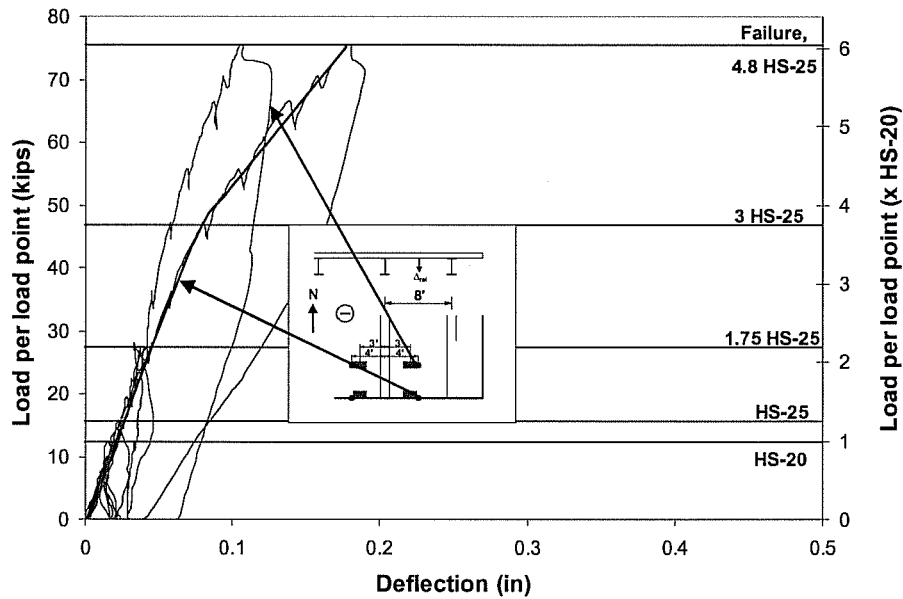
(b) Exterior bay

Figure 5.8 cont'd Relative midspan deflections and edge deflection envelopes,
3-7/8 in. top reinforcement spacing, negative moment region: (a) interior bay;
(b) exterior bay

5.2.2.3 Load-Strain Response

Only gauges located in tension areas are discussed here. For negative moment locations, strains in the top mat of the reinforcement are discussed. For locations where moment is positive, strains estimated at the bottom face of the panel are discussed.

Figure 5.9 shows strain measurements recorded on both faces of the girder and the midspan of the interior bay. At serviceability load levels, strains were small, and maximum strains measured were essentially the same on either side of the girder. At HS-20 and HS-25 load levels measured strains at the girder locations were less than 7% of yield strain (145 $\mu\epsilon$). Maximum strains measured at approximately 1.75 x HS-25 were 9% of yield strain (200 $\mu\epsilon$) on the east face

and 8% of yield strain (165 με) on the west face of the girder between the load points. At 3 x HS-25, the load-strain response was no longer linear at any gauge location. Maximum strains measured at approximately 3 x HS-25 were 30% of yield strain (650 με) on the east and west side of the girder between the load points. First yield of an instrumented reinforcing bar occurred at 3.9 x HS-25 on the first reinforcing bar at the strain gauge located over the west face of the girder (Gauge A). The maximum recorded strain, 3.0 ε_y (6650 με), was on the west face of the girder at the gauge located over the face of the girder and not at the panel end. This strain gauge location was closest to the bay that failed in punching shear. Maximum strain levels on the east face of the girder were 60% (1300 με) of yield strain. At midspan, the average strain on the bottom surface of the panel was estimated to be about 1500 με over a 9 in. gage length (Figure 5.10).
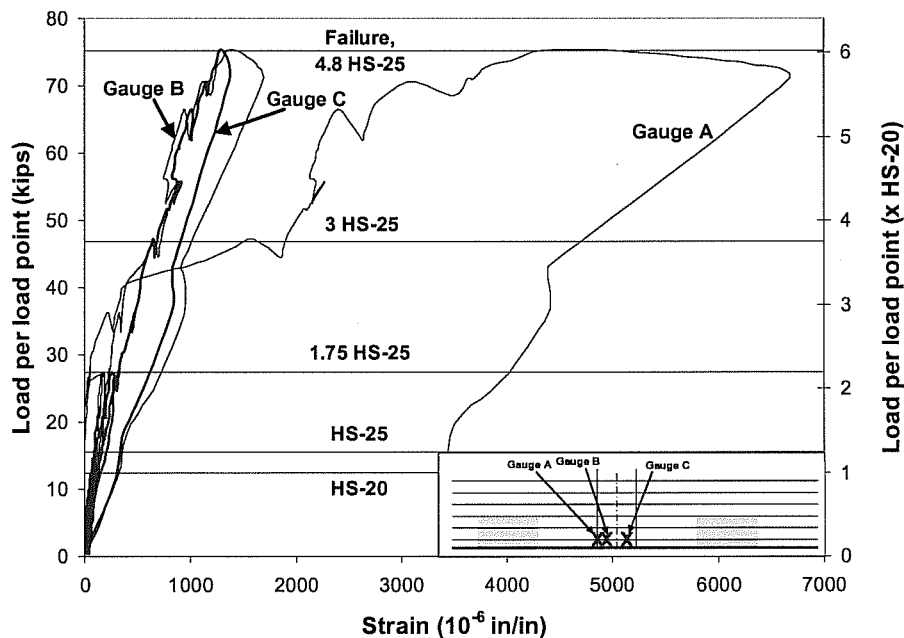
Figure 5.9 Load-strain response, 3-7/8 in. top reinforcement spacing, negative moment region
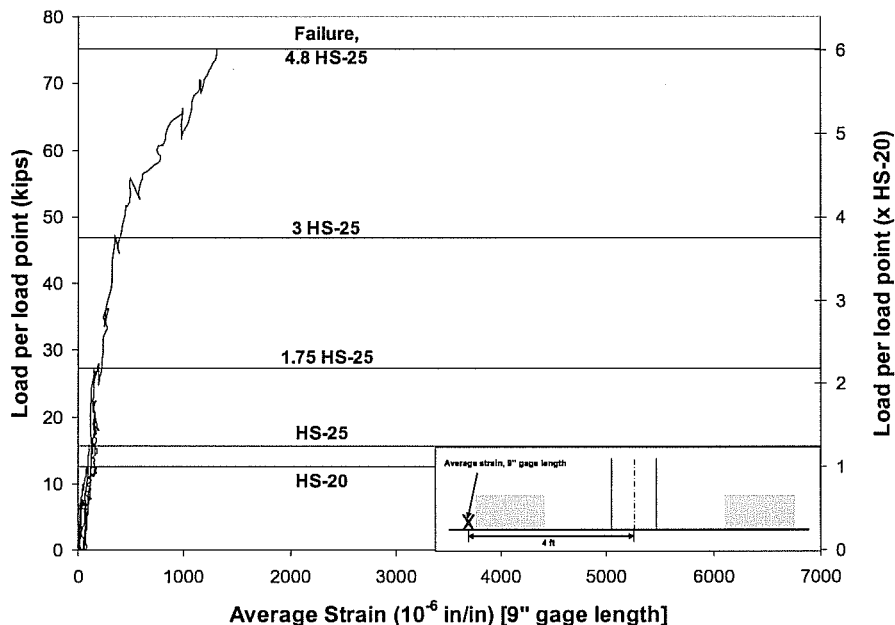
Figure 5.10 Load-average strain response, 3-7/8 in. top reinforcement spacing, negative-moment region, midspan, interior bay, bottom face of panel

5.2.2.4 Strain Profiles

A primary objective was to evaluate the performance of slabs at HS-20 and HS-25 loads. While the strain profiles show strains increasing with increasing load, strains at both HS-20 and HS-25 were relatively small, never exceeding 4% of yield strain (125 $\mu\varepsilon$).

Strain profiles across either face of the girder in the 3-7/8 in. top reinforcement spacing, negative moment test section are shown in Figure 5.11 (a) and (b). In this test area, the largest strains occurred on the west face of the girder. The increase in strain from HS-20 to HS-25 is relatively small, and strains on either face are less than 6% of yield strain (125 $\mu\varepsilon$). At loads HS-20, HS-25 and 1.75 x HS-25, the strain distribution is essentially uniform through the edge region. As loads approached the failure load, strains in the reinforcement near

113

both load points became much larger than the strains measured between the load points.
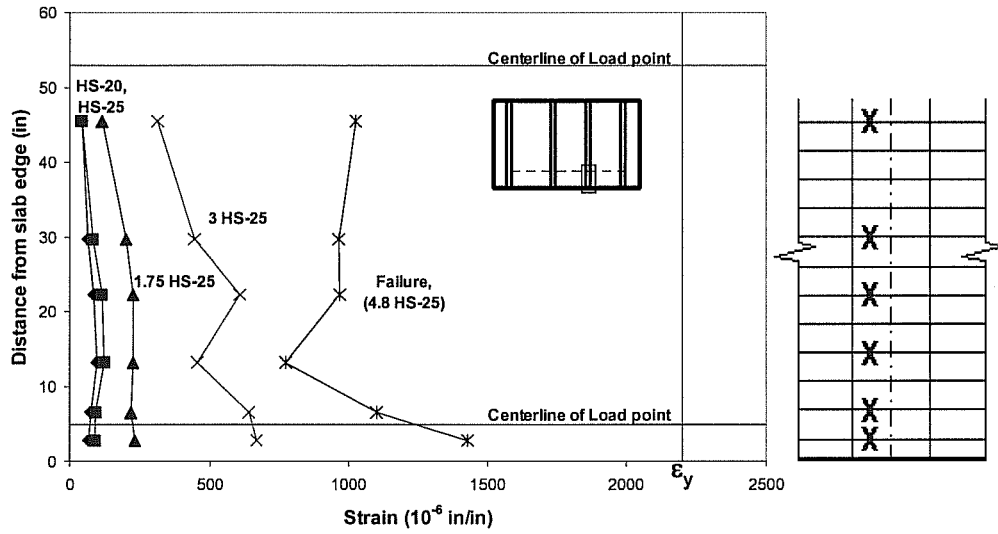
(a) west face of girder, top mat
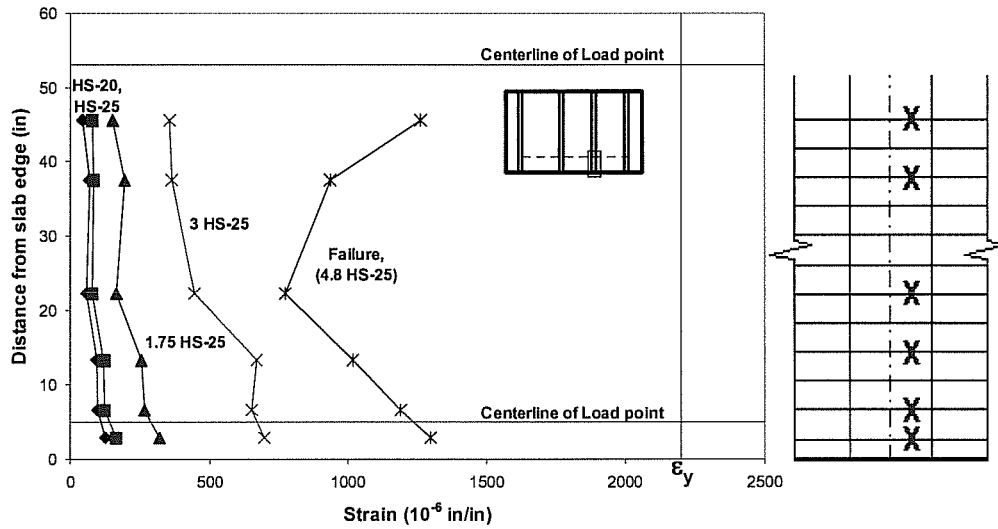
(b) east face of girder, top mat

Figure 5.11 Strain profile, 3-7/8 in. top reinforcement spacing, negative-moment region: (a) west face of girder, top map; (b) east face of girder, top mat

5.2.2.5 Crack Maps

At nearly every load step, the locations, widths and lengths of cracks were photographed, measured and used to produce crack maps that would convey the pattern and extent of cracking at multiple load levels. Crack maps also show the degradation of the test specimen under applied loads and aid in the identification of failure mechanisms. The crack maps were plotted to display the crack propagation from first cracking to ultimate capacity.

The numbering is occasionally non-sequential. The absence of some crack numbers is usually due to two cracks joining and extending as a single crack. When two cracks combine, the two crack records are combined. In addition to propagation of two cracks, crack numbers out of sequential order may be due to previous cracking caused by shrinkage and thermal effects. Original crack numbers, as labeled during testing, are preserved throughout to enable identification of cracks from pictures.

In Figure 5.12, Figure 5.13, and Figure 5.14, crack maps of the top, side and bottom of the test section are drawn illustrating cracks at 1.4 x HS-25 (first visible flexural cracking), 3 x HS-25 (developed cracking), and 4.5 x HS-25 (load step before failure). They are organized by view of the slab to show propagation of crack growth. The side view of the slab is vertically exaggerated to show detail.

The crack map at 1.4 x HS-25 (first cracking) shows the size and shape of the initial flexural cracks occurring in the slab. As discussed in Section 5.1.1, first visible cracking occurred at 0.5 x HS-25 (Figure 5.6). However, the cracks recorded at that load were caused by shrinkage and thermal effects rather than the applied load. Therefore, first cracking is defined as the first visible flexural cracking. Flexural cracking is defined as increased crack widths of existing cracks (those that formed due to shrinkage and thermal effects), and/or newly

developed cracks on top of the slab over the girder or on the bottom face of the panels. The load was applied at 5-kip increments, so first visible flexural cracks could have formed up to 5 kips per load points earlier than 1.4 x HS-25. In this test section, the first flexural cracks in the slab occurred on the bottom face of the panel at midspan of the interior bay and increased crack width of the shrinkage cracks. All cracks on the bottom face of the panel were of hairline width at 1.4 x HS-25. The largest crack widths on top and side of the slab were 0.008 in. and 0.003 in.

The crack map at 3 x HS-25, 55 kips per load point, shows cracks that were observed at the load step where the first major change in stiffness occurred. Though the change in stiffness was determined from the load-deflection plots, the crack map provides further evidence of a change in slab stiffness; multiple cracks developed and existing cracks opened wide at loads greater than 3 x HS-25.

At 3 x HS-25, on the top side of the slab, three flexural cracks were visible over the west-interior girder. These cracks began perpendicular to the slab edge (parallel to the girder) and then began to bend towards the loading plates. The largest measured crack width on the top side of the slab at this load step was 0.013 in. On the bottom face of the panels, the existing cracks running parallel to the girder extended much further at this load step than any previous load step. At 3 x HS-25, the largest measured crack width on the bottom face of the panels was 0.005 in.

The crack map at 4.5 x HS-25 shows cracks that formed during testing and just after failure. At failure, a large shear crack formed between and around the two load points in the interior bay. In addition to the shear cracks, some delamination occurred near the east-interior girder at the interface between the panel and CIP concrete topping. A shear crack developed just prior to reaching 4.5 x HS-25 near the interior-east girder. The crack passed through the CIP

concrete topping and through the panel. The largest measured crack width on the side of the slab was 0.025 in., a shear crack near the east-interior girder on the interior bay. The slippage between the panel and the CIP concrete topping was 0.01 in. at 4.5 x HS-25 and 0.25 in. at failure. Visible on the top of the slab were cracks that circled around the loading plates in both bays at 4.5 x HS-25, indicating that punching shear failure was imminent. These cracks circling the loading plates and a few flexural cracks along the length of the girder widened during the final loading stages. The largest measured crack width before failure was 0.025 in. at one of the cracks circling the edge loading plate in the interior bay. As seen from underneath the slab at failure, a series of flexural cracks formed parallel to the girders in the interior and east-exterior bay, fanning out past the load points. Flexural cracks that formed on the bottom face of the panels in both bays could be seen on the side of the slab. At failure, the widest crack visible from the bottom of the slab in the interior bay was 0.025 in., a crack running parallel to the girder near the panel bearing pad. An additional flexural crack extended the full depth of the panel near the failure surface on the bottom of the panel in the interior bay. Several flexural cracks also formed beneath the location of the loading point 4 ft from the edge of the slab. All cracking was contained within the two panels being loaded; cracks did not propagate into the adjacent panels.
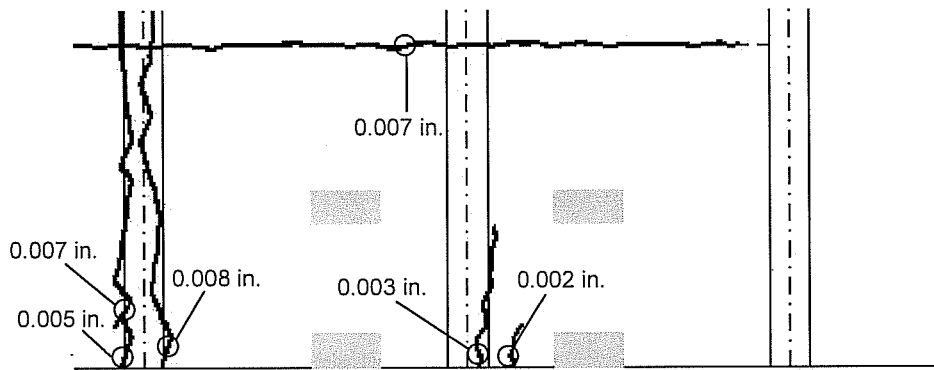
(a) 1.4 x HS-25 (first flexural cracking)
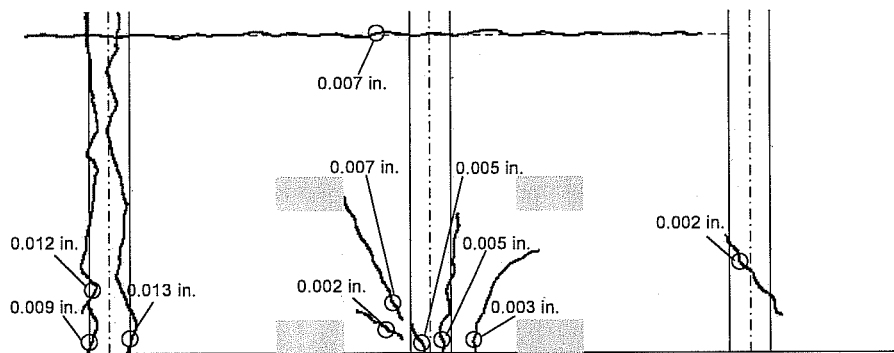
(b) 3 x HS-25 (developed cracking)
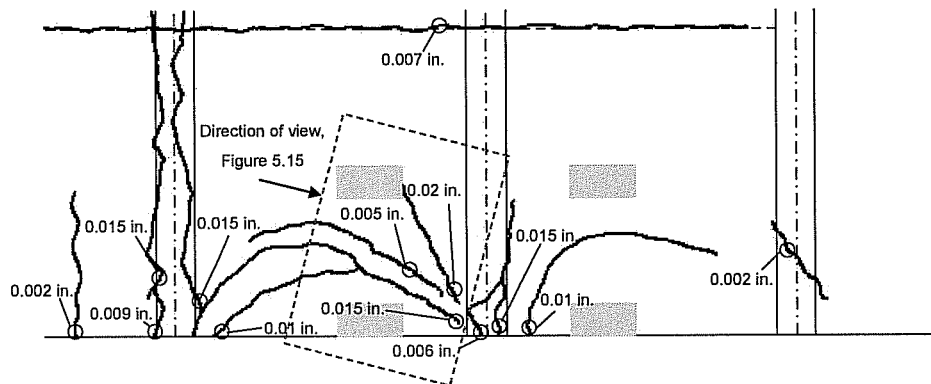
(c) 4.8 x HS-25 (failure)

Figure 5.12 Crack map, 3-7/8 in. top reinforcement spacing, negative moment region; top view of slab

118
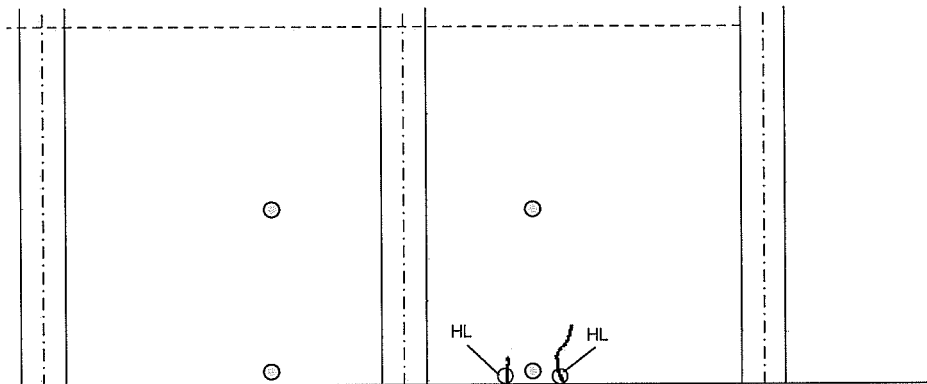
(a) 1.4 x HS-25 (first flexural cracking)
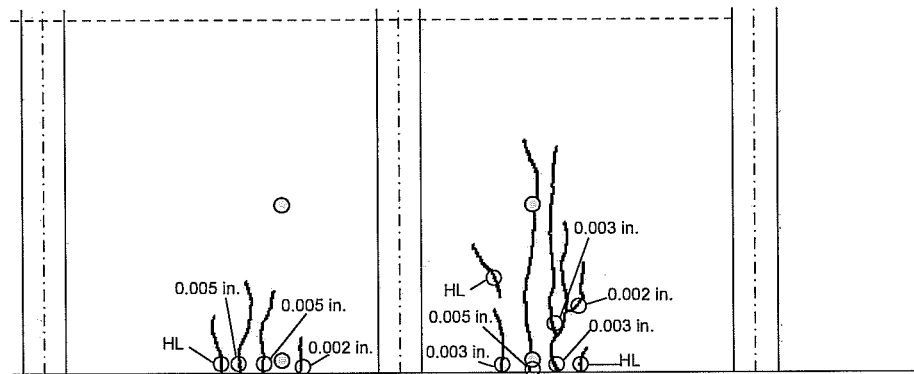
(b) 3.0 x HS-25 (developed cracking)
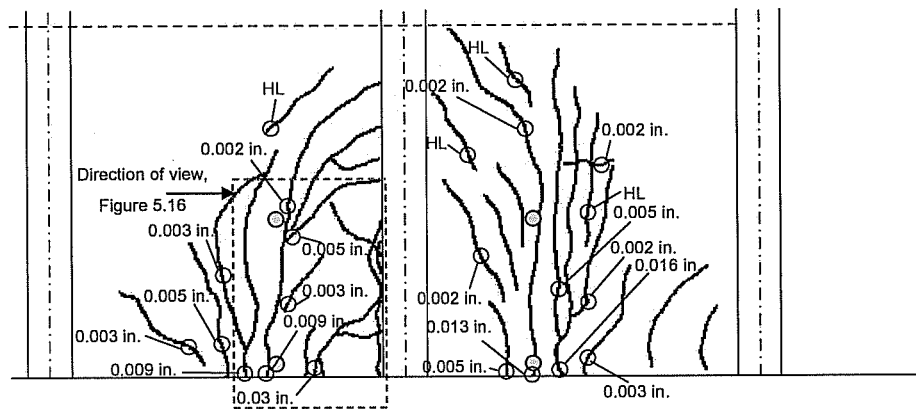
(c) 4.8 x HS-25 (failure)

Figure 5.13 Crack map, 3-7/8 in. top reinforcement spacing, negative moment

region; bottom view of slab

119

(a) 1.4 x HS-25 (first flexural cracking)

(b) 3 x HS-25 (developed cracking)
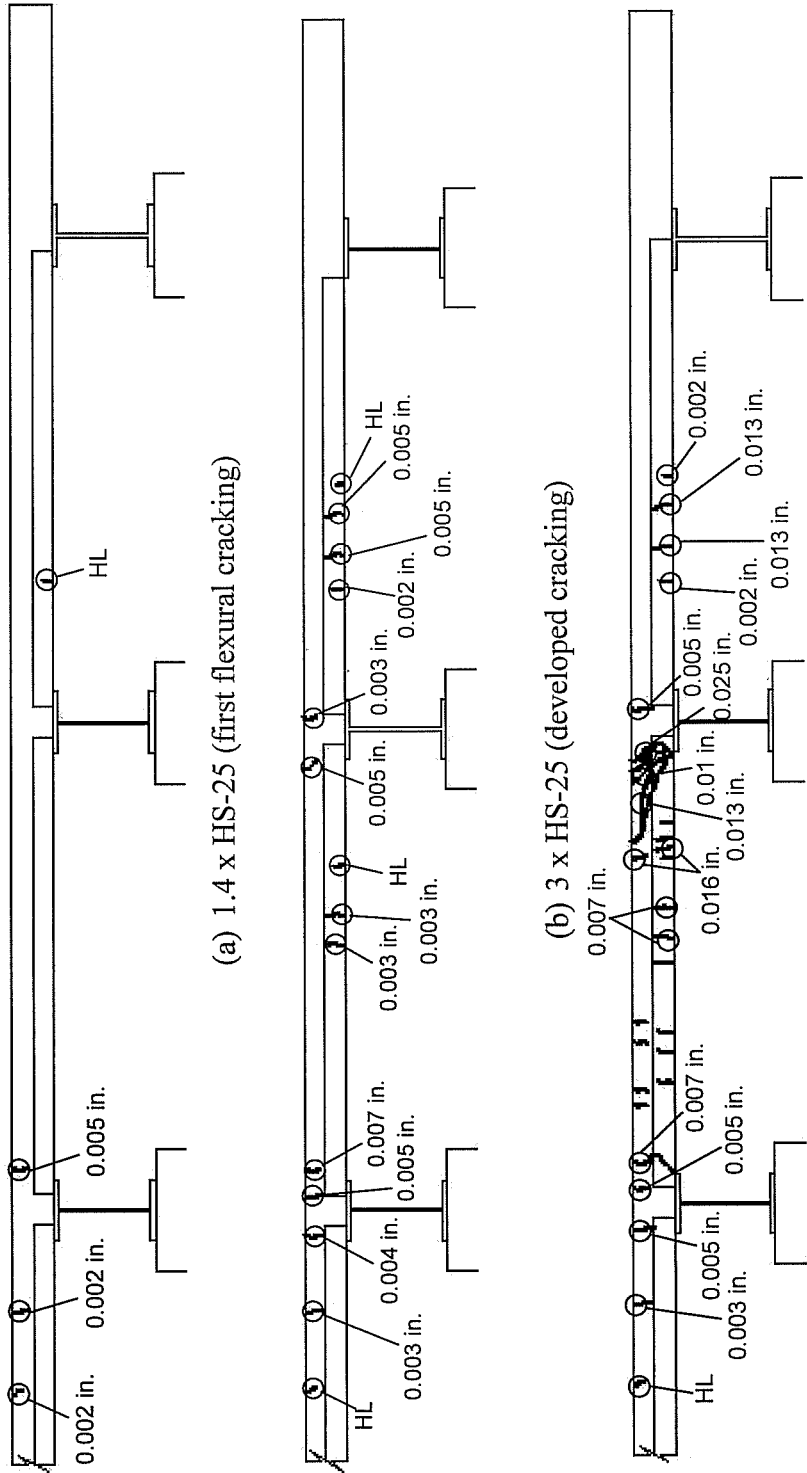
(c) 4.8 x HS-25 (failure)

Figure 5.14 Crack map, 3-7/8 in. top reinforcement spacing, negative moment region; side view of slab

120

5.2.2.6 Appearance after Failure

At 4.8 x HS-25, a punching shear failure occurred at the edge tire in the interior 8 ft bay. Pictures were taken of the failure surface (Figure 5.15, Figure 5.16, Figure 5.17). Cracks formed between the two load points and around the edge load point. Because the area around the edge load point was more extensively damaged than the area around the interior load point, failure was probably initiated by punching shear at the edge load point, where the shear perimeter is significantly less than the interior load point. Cracks wrapping semi-elliptically around the edge load point formed around 3.5 x HS-25 and existing flexural cracks opened on the top surface up to and at failure. Little evidence of failure was visible on the bottom surface of the slab, except for a large crack running parallel to the panel bearing strip. The side surface indicated some delamination (Figure 5.17 b) occurring between the panel and the CIP concrete topping at high loads and failure. Some separation was seen around 4.5 x HS-25.
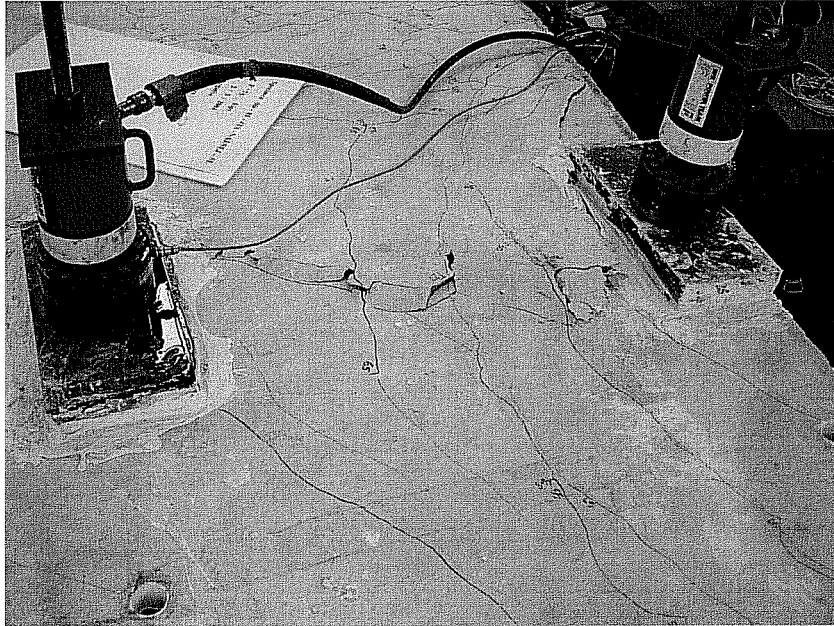
Figure 5.15 Interior bay failure at top of slab, facing southeast
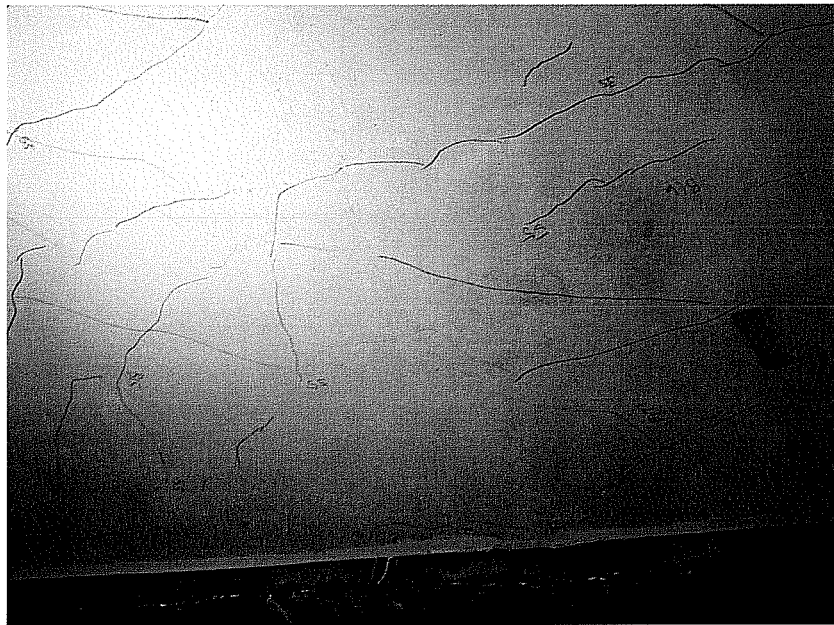
Figure 5.16 Interior bay failure surface at bottom of slab, facing east
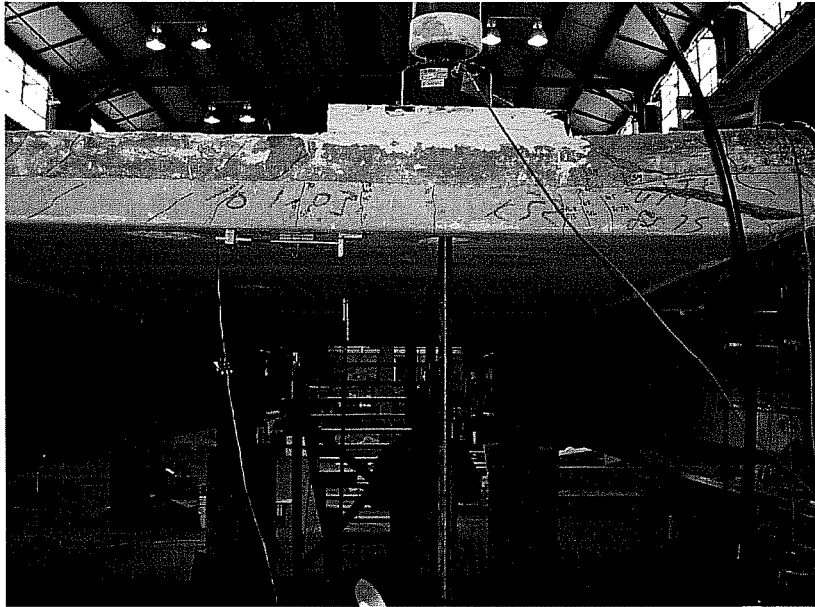
(a) Facing north

(b) Close up of delamination, facing north

Figure 5.17 Interior bay failure surface at side of slab: (a) facing north; (b)
close up of delamination between panel and CIP concrete topping

5.3 6 IN. TOP REINFORCEMENT SPACING, NEGATIVE MOMENT REGION (TEST AREA 2)

5.3.1 Summary of Response

The 6 in. top reinforcement spacing test area was loaded to design and overload levels with the AASHTO tandem load configuration placed to maximize negative moments in the edge detail.

At HS-20, tensile stresses caused by the loading added to existing tensile stresses due to restrained shrinkage and new cracks formed during testing of Test Area 2. No new bottom cracking developed and the existing bottom cracks did not open up during the test. The largest crack widths at 1.75 x HS-25 on the top and side surface of the slab were 0.013 in. and 0.007 in., respectively.

The relative midspan edge deflection at failure was 0.032 in. in the interior 8-ft bay and 0.071 in. in the exterior 10-ft bay. The maximum recorded strain was 40% of yield strain (870 $\mu\varepsilon$), measured at 1.75 x HS-25 at the second reinforcing bar from the slab edge on the west face of the west-interior girder.

5.3.2 Detailed Description of Response

5.3.2.1 Loading

Negative moments were maximized over the west-interior girder, between the interior 8-ft bay and exterior 10-ft bay. Test Area 2 was loaded at the locations shown in Figure 5.18 by four 10- by 20-in. steel plates placed in the AASHTO design load configuration, after the completion of loading Test Area 1 to service level loads. The purpose of this test area was to compare the two top reinforcement spacings at service load levels (1.75 x HS-25).

124
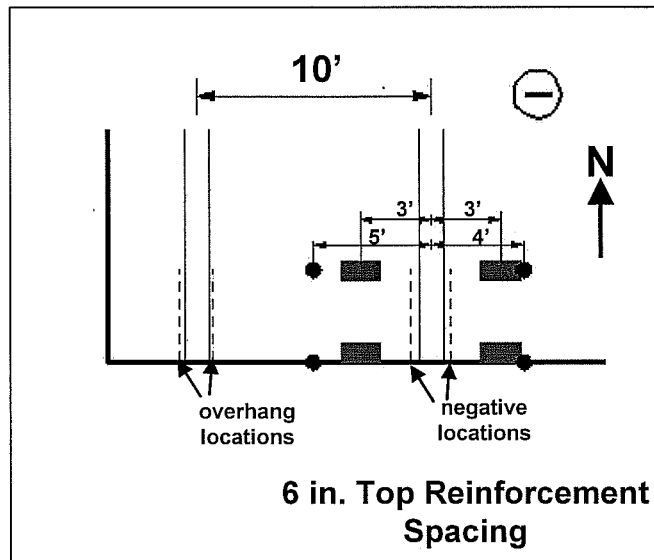
Figure 5.18 6-in. top reinforcement spacing, negative-moment region (Test Area 2)

5.3.2.2 Load-Deflection Behavior

Load-deflection plots show relative midspan deflections measured at the slab edge and 4 ft from the slab edge, corrected to remove rigid-body movement as discussed in Section 5.1 (Figure 5.4). A complete measured load deflection response for the test is shown in Figure 5.19. The load-deflection envelopes for the edge deflections in the 10-ft and 8-ft bays are also shown in Figure 5.19. In the 8-ft bay, the load deflection response for the edge deflection and the deflection measured 4 ft from the slab edge have the same slope until around 0.6 x HS-25. The slope of the load deflection response in the exterior 10-ft bay for the midspan deflection at 4 ft from the slab edge is almost twice the slope of the measured midspan edge deflection. The load deflection response for the edge deflection of the 10-ft bay was twice the measured edge deflection in the 8-ft bay. However, the measured deflections were extremely small compared to the girder spacing at

the service level loads (HS-20, HS-25, and 1.75 x HS-25), so the load-deflection behavior was essentially linear and elastic at this range. Table 5.2 shows the measured deflections at various load steps for this test area.

Table 5.2 Measured deflection (inches), Test Area 2

	HS-20	HS-25	1.5 HS-25
Interior 8' bay, edge	0.012	0.016	0.032
Interior 8' bay, 4 ft from edge	0.0076	0.0096	0.017
Exterior 10' bay, edge	0.028	0.039	0.071
EXterior 10' bay, 4 ft from edge	0.023	0.026	0.053

5.3.2.2.1 Load-Deflection Envelope

Both the 8-ft and 10-ft bays exhibited a relatively linear elastic response up to 1.75 x HS-25. The 8-ft bay exhibited a slightly higher stiffness than the 10-ft bay (Figure 5.19). The load deflection envelope indicates one change in slab stiffness in the 8-ft bay, occurring around 0.6 x HS-25. This change in stiffness is most likely caused by cracking due to shrinkage effects. Although cracking occurred due to shrinkage effects, it does influence the overall response of the test specimen.
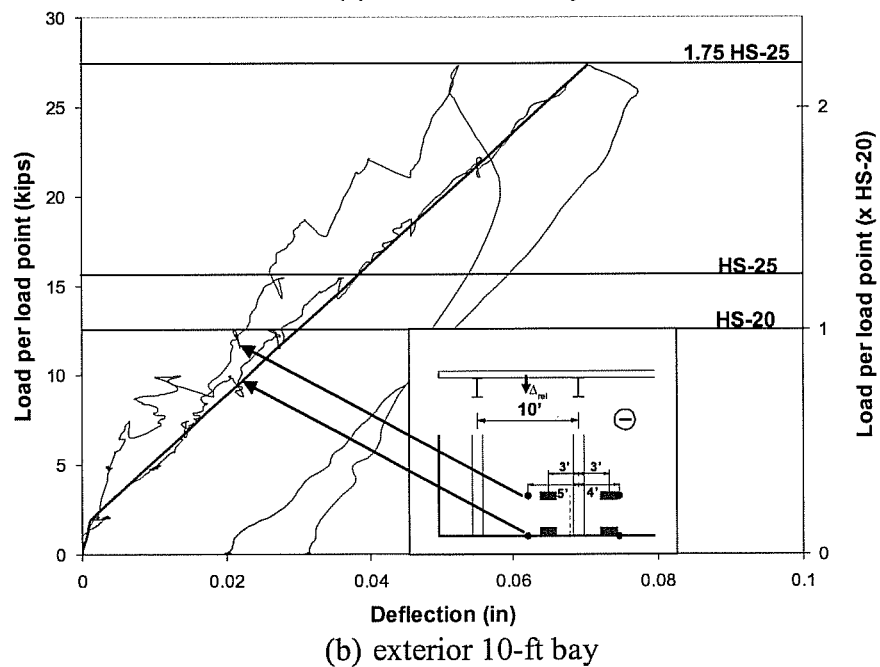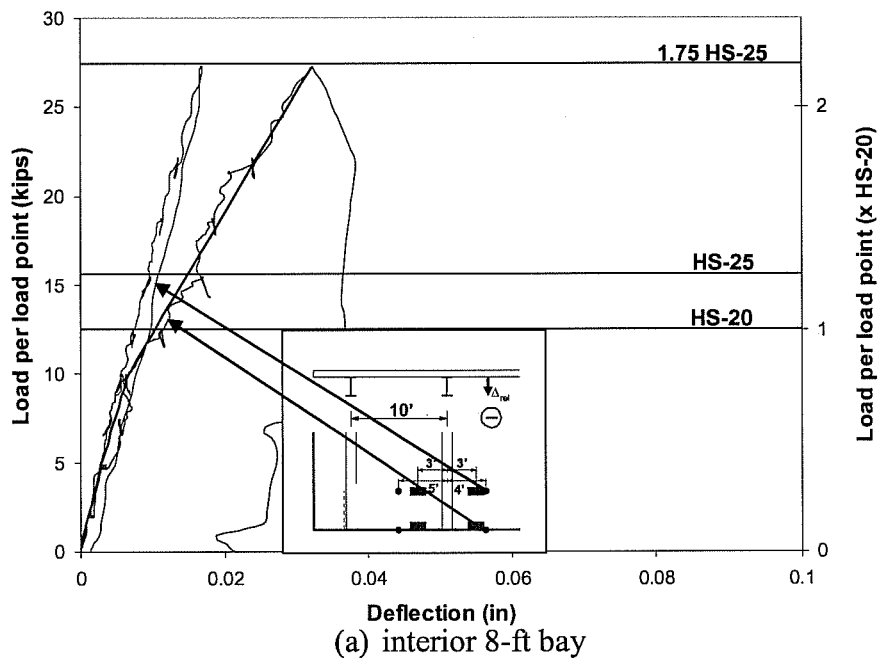
Figure 5.19 Relative midspan deflections and edge deflection envelopes, 6-in. top reinforcement spacing, negative-moment region: (a) interior 8-ft bay; (b) exterior 10-ft bay

127

5.3.2.3 Load-Strain Response

Figure 5.20 shows strain measurements recorded on both faces of the girder and the midspan of the interior 8-ft bay. At serviceability load levels, strains were small, and strains measured were essentially the same on either side of the girder.

At HS-20 load level measured strains at the girder locations were less than 15% of yield strain (290 $\mu\epsilon$). At HS-25 load level measured strains at the girder locations were less than 20% of yield strain (440 $\mu\epsilon$). Maximum strains measured at 1.75 x HS-25 were 40% of yield strain (870 $\mu\epsilon$) on the east face and 34% of yield strain (760 $\mu\epsilon$) on the west face of the girder between the load points. At midspan, the average strain on the bottom surface of the panel in the interior 8-ft bay was estimated to be about 180 $\mu\epsilon$ over a 9 in. gage length at 1.75 x HS-25 (Figure 5.21).
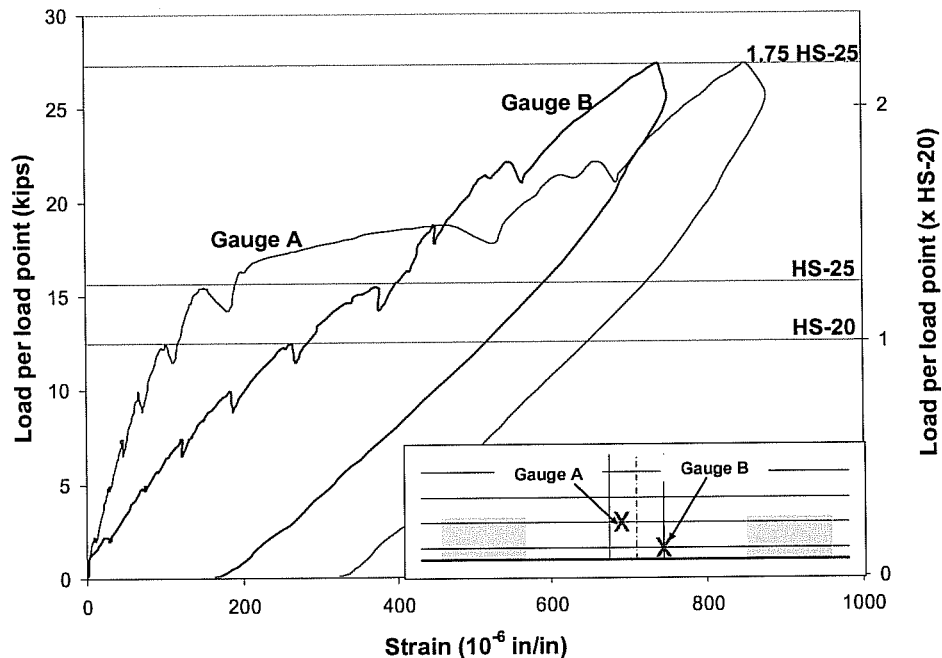
Figure 5.20 Load-strain response, 6-in. top reinforcement spacing negative-moment region

128
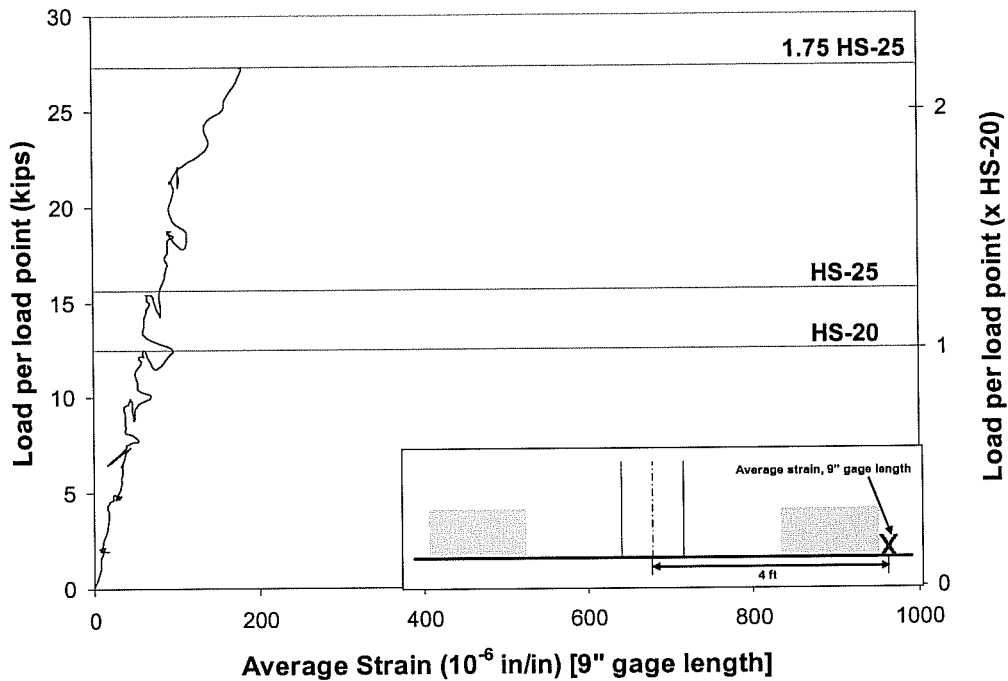
Figure 5.21 Load-average strain response, 6 in. top reinforcement spacing, negative-moment, midspan, interior 8-ft bay, bottom face of panel

5.3.2.4 Strain Profiles

A primary objective was to evaluate the performance of slabs at HS-20 and HS-25 loads. While the strain profiles show strains increasing with increasing load, strains at HS-20 were relatively small, never exceeding 15% of yield strain (290 µε). Strains at HS-25 never exceeded 20% of yield strain (440 µε).

Strain profiles from either face of the girder in the 6 in. top reinforcement spacing, negative moment test section are shown in Figure 5.22 (a) and (b). In this test area, the largest strains occurred on the east face of the girder. The increase in strain from HS-20 to HS-25 is relatively small, where neither strain

exceeds 20% of yield strain (440 µε). The largest measured strain was at the east face of the girder at the second reinforcing bar from the slab edge.
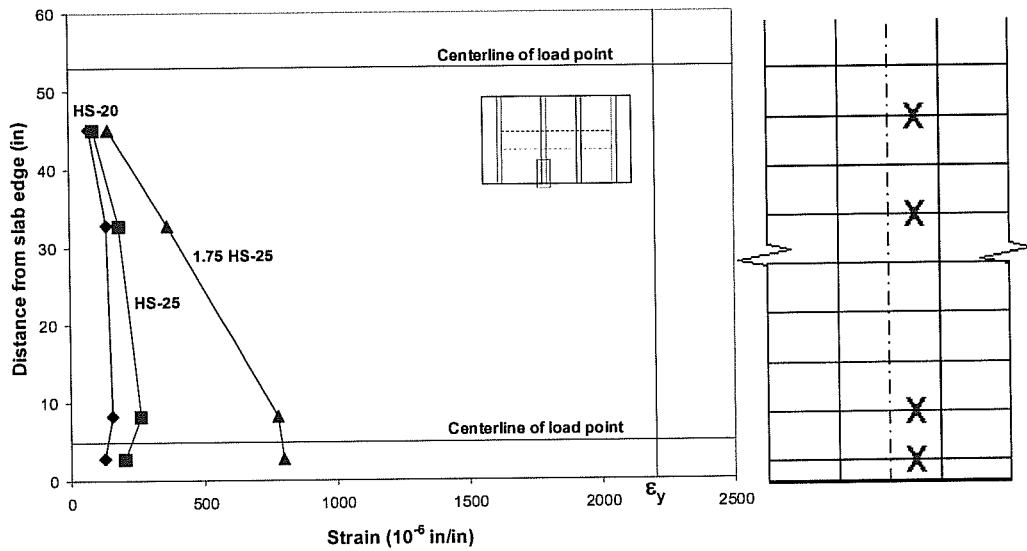
(a) east face of girder
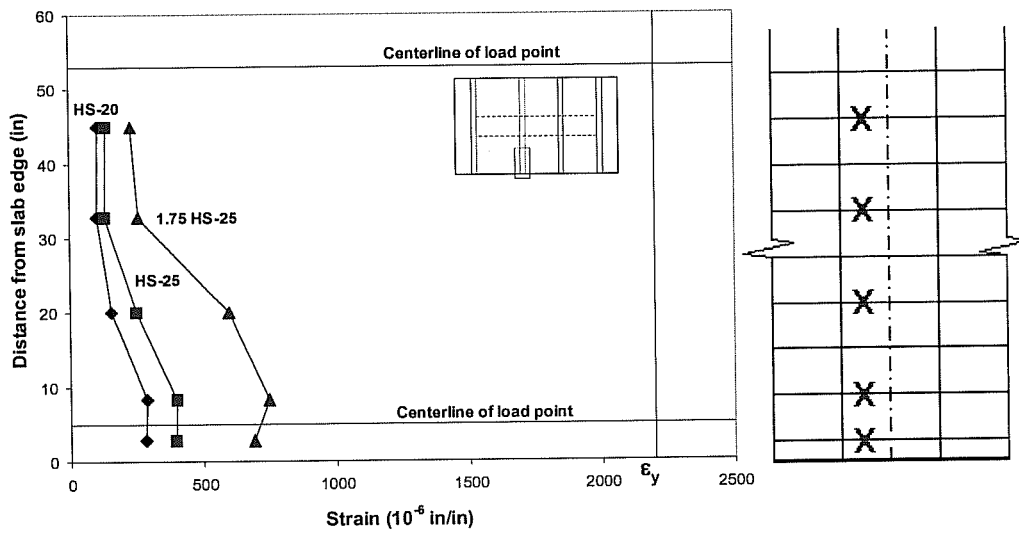
(b) west face of girder

Figure 5.22 Strain profile, 6-in. top reinforcement spacing, negative-moment region: (a) east face of girder, top mat; (b) west face of girder top mat

130

5.3.2.5 Crack Maps

In Figure 5.23 and Figure 5.24, crack maps of the top and side of the test section are drawn illustrating cracks at HS-20, HS-25, and 1.75 x HS-25. To create crack maps, the locations, widths, and lengths of cracks were measured at every load step during testing. Additional discussion of crack maps is given in Section 5.1.

Only two new cracks formed at HS-20 on the top surface of the slab during testing of Test Area 2. These new cracks and previous cracks from Test Area 1 on the top and side surface of the slab widened during loading of Test Area 2. No new cracks developed on the bottom surface of the slab during the test, and the bottom cracks from Test Area 1 did not open up during testing of Test Area 2. The crack map at HS-20 shows the size and shape of the initial cracks occurring in the slab. The largest crack widths on top and side of the slab were both 0.005 in. The crack map at HS-25, 15.625 kips per load point, shows cracks at TxDOT design load level. At HS-25, the largest measured crack widths on the top face and the side of the slab were 0.007 in. and 0.005 in. The crack map at 1.75 x HS-25 shows crack formed during testing. The largest measured crack width on the side of the slab was 0.007 in. The largest measured crack width on the top surface of the slab at 1.75 x HS-25 was 0.013 in.

131
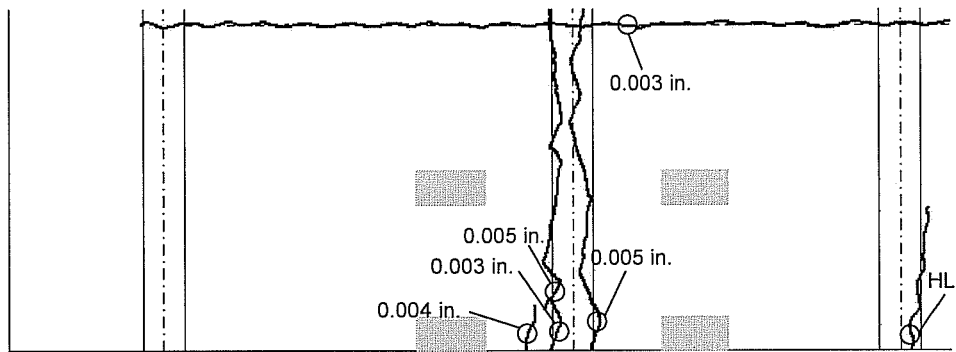
(a)   HS-20
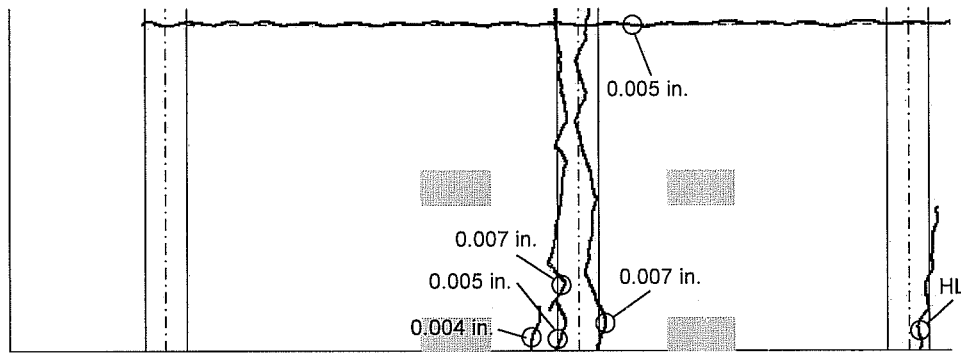
(b) HS-25
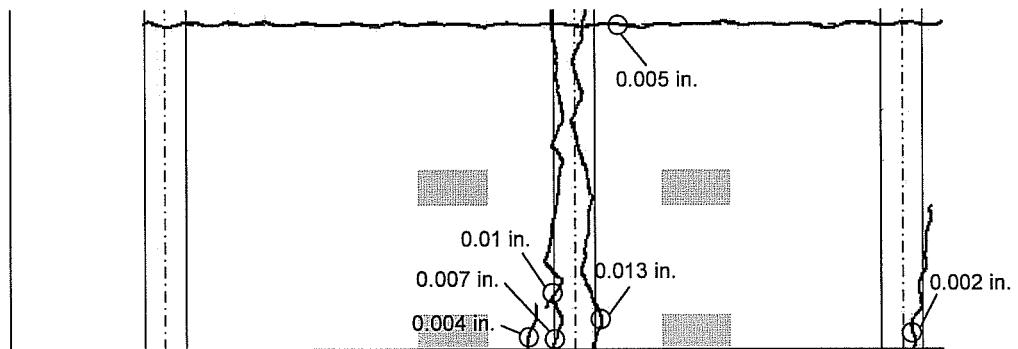
(c) 1.75 x HS-25

Figure 5.23 Crack map, 6 in. top reinforcement spacing, negative-moment region, top view of slab

(a) HS-20

(b) HS-25

(c) 1.75 x HS-25
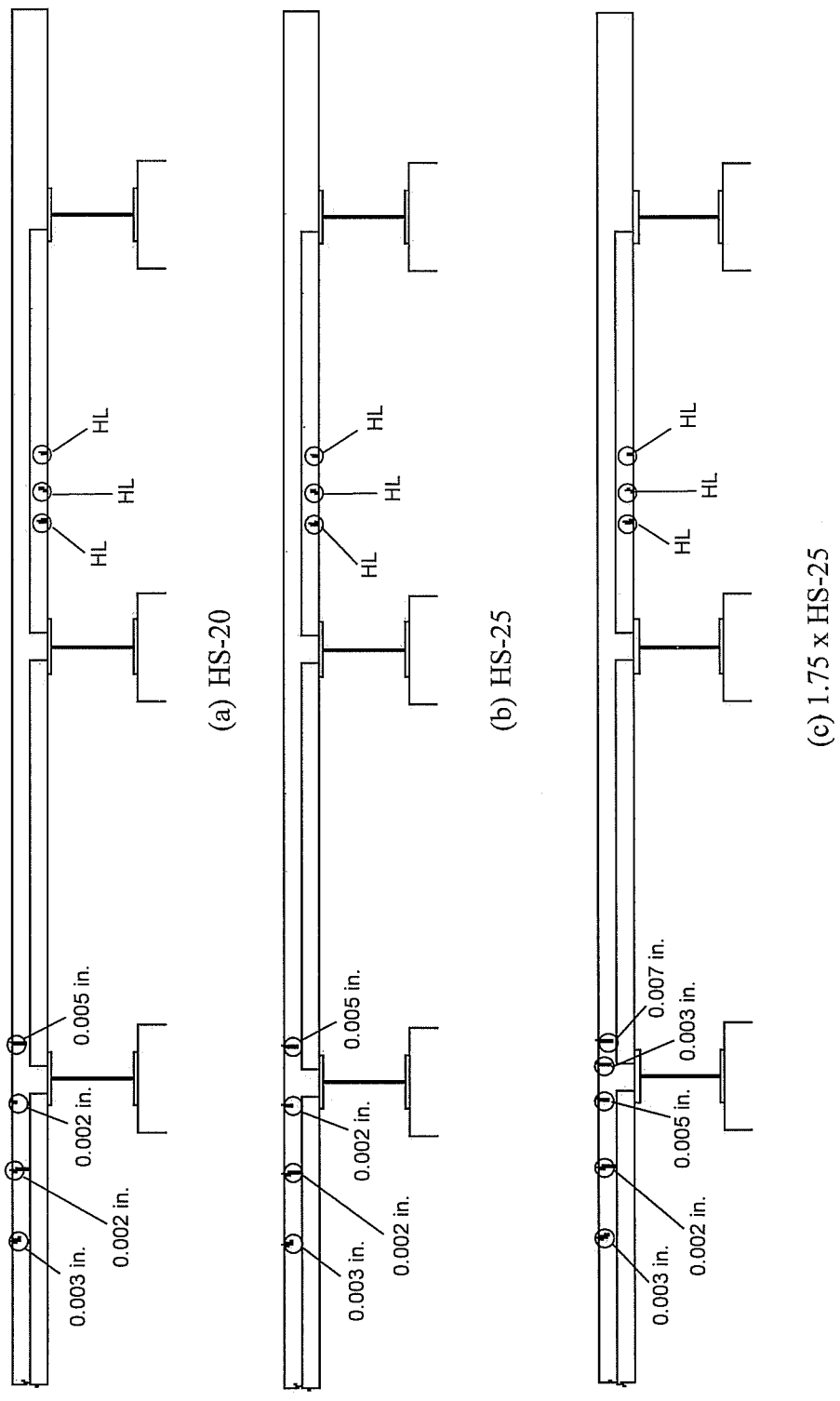
Figure 5.24 Crack map, 6 in. top reinforcement spacing, negative-moment region, side view of slab

133

5.4 SEALED EXPANSION JOINT RAIL (SEJ), 6-IN. TOP REINFORCEMENT SPACING, NEGATIVE MOMENT REGION (TEST AREA 5)

5.4.1 Summary of Response

The SEJ test area was loaded to design and overload levels with the AASHTO tandem load configuration placed to maximize negative moments in the edge detail.

One new crack on both the top and side surface of the slab formed during the testing of Test Area 5. These cracks formed at HS-25 and 1.75 x HS-25, respectively, and were believed to be additional cracking due to shrinkage and not from loading. No new bottom cracking developed and the existing bottom cracks from loading to service loads in Test Area 4 were barely visible at 1.75 x HS-25. The largest crack widths at 1.75 x HS-25 on the top and side surface of the slab were 0.009 in. and hairline, respectively.

The relative midspan edge deflection at failure was 0.029 in. in the interior 8-ft bay and 0.056 in. in the exterior 10-ft bay. The maximum recorded strain was 20% of yield strain (370 $\mu\varepsilon$), measured at 1.75 x HS-25 at the first reinforcing bar from the slab edge on the east face of the west-interior girder over the end of the panel.

5.4.2 Detailed Description of Response

5.4.2.1 Loading

Negative moments were maximized over the west-interior girder, between the interior 8-ft bay and exterior 10-ft bay. Test Area 5 was loaded at the locations shown in Figure 5.25 by four 10- by 20-in. steel plates placed in the AASHTO design load configuration, after the completion of loading Test Areas 1,

2, 3 and 4 to service level loads. The purpose of this test area was to compare the two expansion joint rails when maximizing negative moment at service load levels (1.75 x HS-25).
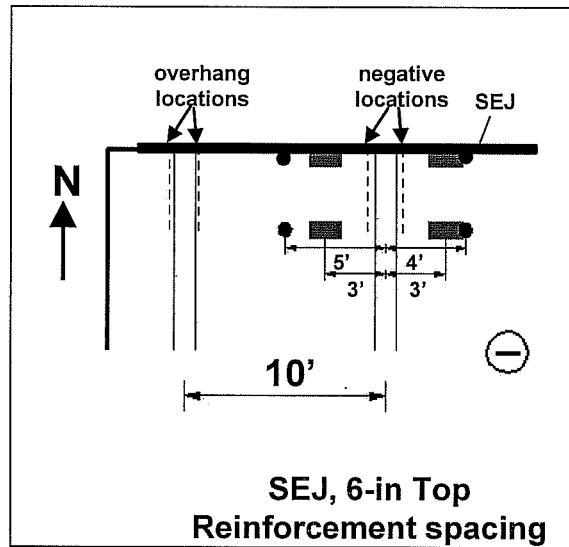
Figure 5.25 SEJ, 6-in. top reinforcement spacing, negative-moment region (Test Area 5)

5.4.2.2 Load-Deflection Behavior

Load-deflection plots show relative midspan deflections measured at the slab edge and 4 ft from the slab edge, corrected to remove rigid-body movement as discussed in Section 5.1 (Figure 5.4). A complete measured load deflection response for the test is shown in Figure 5.26. The load-deflection envelopes for the edge deflections in the 10-ft and 8-ft bays are also shown in Figure 5.26. In the 8-ft bay, the load deflection response for the edge deflection and the deflection measured 4 ft from the slab edge have the same slope until around 0.8 x HS-25. The slope of the load deflection response in the 10-ft bay for the midspan deflection at 4 ft from the slab edge is almost twice the slope of the measured

midspan edge deflection. The load deflection response for the edge deflection of the 10-ft bay was twice the measured edge deflection in the 8-ft bay. However, the measured deflections were extremely small compared to the girder spacing at the service level loads (HS-20, HS-25, and 1.75 x HS-25), so the load-deflection behavior was essentially linear and elastic at this range. Table 5.3 shows the measured deflections at various load steps for this test area.

Table 5.3 Measured deflection (inches), Test Area 5

	HS-20	HS-25	1.75 HS-25
Interior 8' bay, edge	0.012	0.015	0.029
Interior 8' bay, 4 ft from edge	0.008	0.012	0.020
Exterior 10' bay, edge	0.026	0.033	0.056
Exterior 10' bay, 4 ft from edge	0.014	0.017	0.030

5.4.2.2.1 Load-Deflection Envelope

Both the 8-ft and 10-ft bays exhibit a relatively linear elastic response up to 1.75 x HS-25. The 8-ft bay exhibits a slightly higher stiffness than the 10-ft bay (Figure 5.26).

136
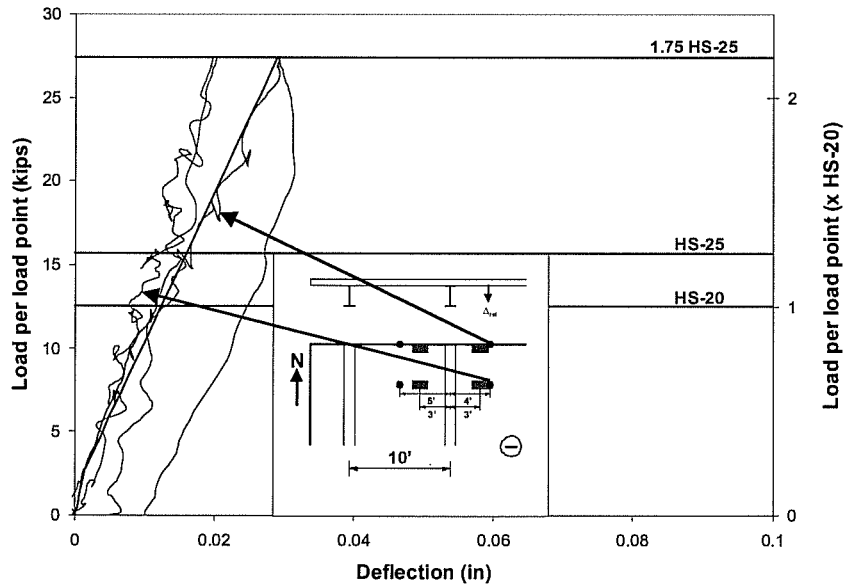
(a) interior 8-ft bay
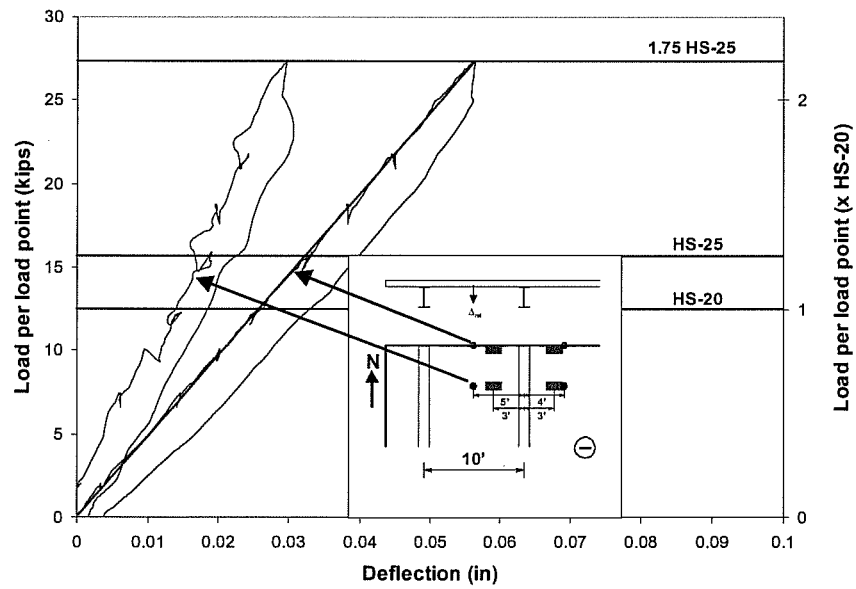
(b)   exterior 10-ft bay

Figure 5.26 Relative midspan deflections and edge deflection envelopes, SEJ, 6-in. top reinforcement spacing, negative-moment region: (a) interior 8-ft bay; (b) exterior 10-ft bay

137

5.4.2.3 Load-Strain Response

Figure 5.27 shows strain measurements recorded on both faces of the girder and the midspan of the interior 8-ft bay. At serviceability load levels, strains were small, and strains measured were essentially the same on either side of the girder.

At HS-20 load level measured strains at the girder locations were less than 7% of yield strain (150 $\mu\varepsilon$). The maximum strain measured at SEJ was 90 $\mu\varepsilon$ on the east face of the girder. At HS-25 load level measured strains at the girder locations were less than 10% of yield strain (210 $\mu\varepsilon$). The maximum measured strain on the SEJ was 120 $\mu\varepsilon$ on the east face of the girder. Maximum strains measured at 1.75 x HS-25 were 17% of yield strain (370 $\mu\varepsilon$) on the east face and 12% of yield strain (260 $\mu\varepsilon$) on the west face of the girder between the load points. The maximum measured strain on the SEJ was 220 $\mu\varepsilon$ on the east face of the girder. At midspan, the average strain on the bottom surface of the panel in the interior 8-ft bay was estimated to be about 300 $\mu\varepsilon$ over a 9 in. gage length at 1.75 x HS-25 (Figure 5.28).

Figure 5.27 Load-strain response, SEJ, 6 in. top reinforcement spacing, negative-moment region

Figure 5.28 Load-average strain response, SEJ, 6-in. top reinforcement spacing, negative-moment region, midspan, interior 8-ft bay, bottom face of panel

139

5.4.2.4 Strain Profiles

A primary objective was to evaluate the performance of slabs at HS-20 and HS-25 loads. While the strain profiles show strains increasing with increasing load, strains at HS-20 were relatively small, never exceeding 7% of yield strain (150 $\mu\varepsilon$). Strains at HS-25 never exceeded 10% of yield strain (210 $\mu\varepsilon$).

Strain profiles from either face of the girder in the 6 in. top reinforcement spacing, SEJ, negative moment test section are shown in Figure 5.29 (a) and (b). In this test area, the largest strains occurred on the east face of the girder. The increase in strain from HS-20 to HS-25 is relatively small, where neither strain exceeds 10% of yield strain (210 $\mu\varepsilon$). The largest measured strain was at the east face of the girder at the first reinforcing bar from the slab edge at the strain gauge over the end of the panel. At loads HS-20, HS-25 and 1.75 x HS-25, the strain distribution is essentially linear.
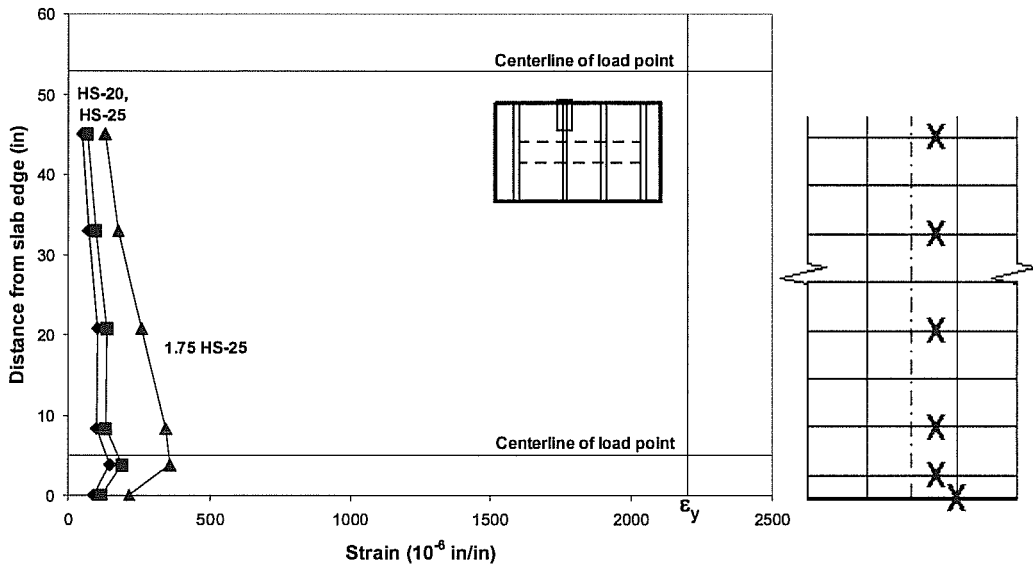
(a) east face of girder, top mat
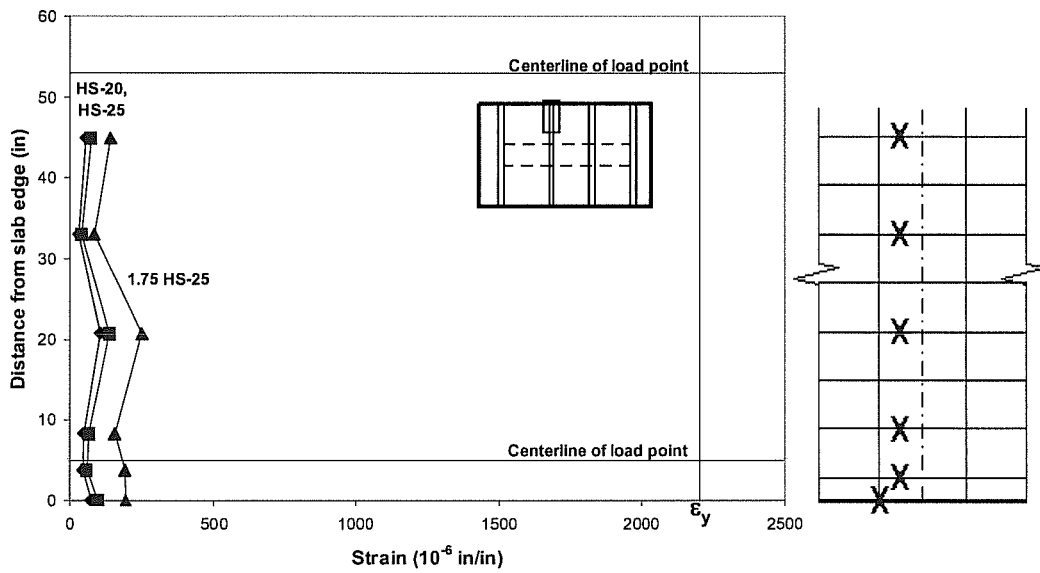
(b) west face of girder, top mat

Figure 5.29 Strain profile, SEJ, 6-in. top reinforcement spacing, negative-moment region: (a) east face of girder, top mat; (b) west face of girder top mat

141

5.4.2.5 Crack Maps

In Figure 5.30, Figure 5.31, and Figure 5.32, crack maps of the top, side and bottom of the test section are drawn illustrating cracks at HS-20, HS-25, and 1.75 x HS-25. To create crack maps, the locations, widths, and lengths of cracks were measured at every load step during testing. Additional discussion of crack maps is given in Section 5.1.

One new crack due to shrinkage effects formed on the top surface of the slab during testing of Test Area 5 at HS-20. These new cracks and previous cracks from Test Area 4 on the top and side surface of the slab widened during loading of Test Area 5. No new cracks developed on the bottom surface of the slab during the test, and the bottom cracks from the serviceability test of Test Area 4 (Figure 5.60 a) were barely visible at 1.75 x HS-25 during testing. The crack map at HS-20 shows the size and shape of the initial cracks occurring in the slab. The largest crack width on top of the slab was 0.007 in. The crack map at HS-25, 15.625 kips per load point, shows cracks at TxDOT design load. At HS-25, the largest measured crack width on the top face was 0.007 in. The crack map at 1.75 x HS-25 shows crack formed during testing. The largest measured crack width on the top and side of the slab were 0.009 in. and hairline. The largest measured crack width on the bottom surface of the panels at 1.75 x HS-25 was hairline.
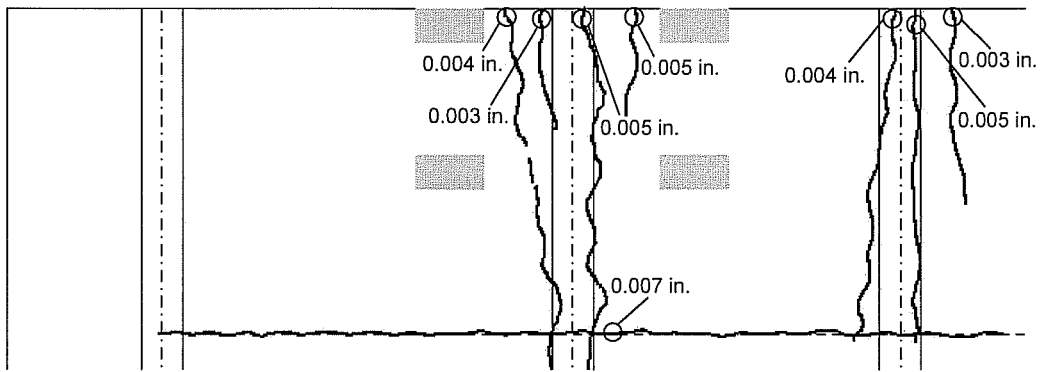
(a) HS-20
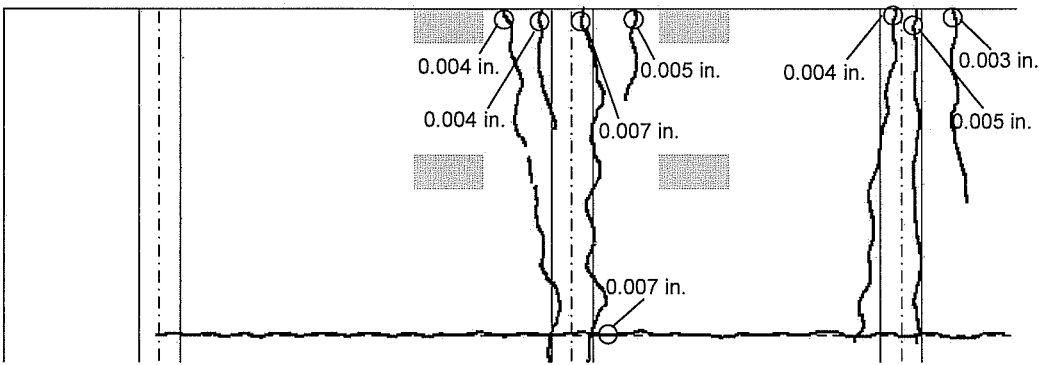
(b) HS-25
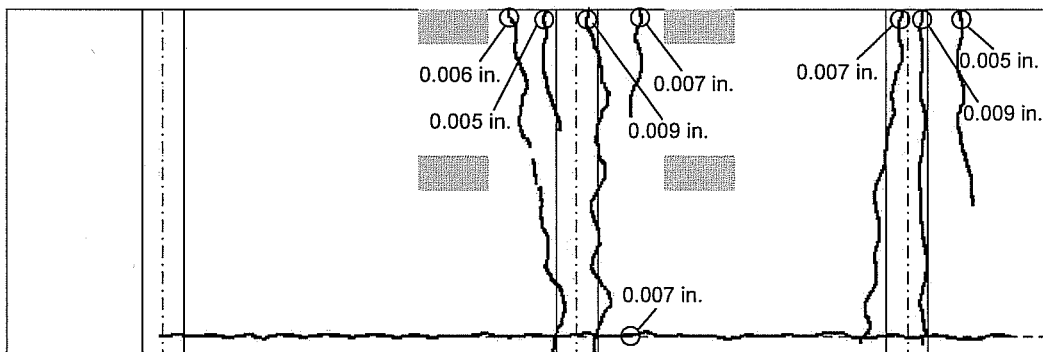
(c) 1.75 x HS-25

Figure 5.30 Crack map, SEJ, 6 in. top reinforcement spacing, negative-moment region, top view of slab

143
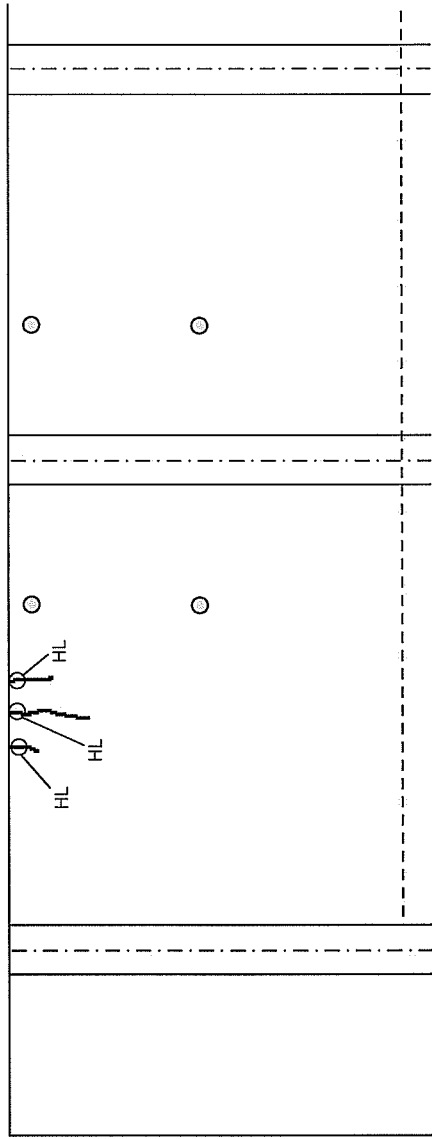
Figure 5.31 Crack map, SEJ, 6 in. top reinforcement spacing, negative-moment region, bottom view of slab,

1.75 x HS-25
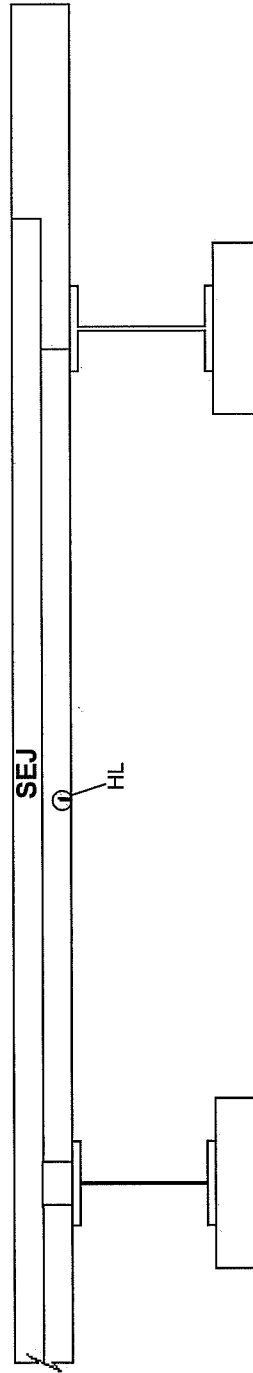
Figure 5.32 Crack map, SEJ, 6 in. top reinforcement spacing, negative-moment region, side view of slab,

1.75 x HS-25

144

5.5 ARMOR JOINT RAIL (AJ), 6-IN. TOP REINFORCEMENT SPACING, NEGATIVE MOMENT REGION (TEST AREA 6)

5.5.1 Summary of Response

The AJ, 6-in. top reinforcement spacing test area was loaded to design and overload levels with the AASHTO tandem load configuration placed to maximize negative moments in the edge detail.

First flexural cracking and developed cracking was visible at 2.2 x HS-25 on the bottom face of the panel, in addition to the widening of the cracks due to shrinkage effects on the top surface of the slab. Top cracks formed over the ends of the panels over the girders and propagated parallel to the girder. A second change in stiffness occurred at approximately 5.2 x HS-25. Even though the first visible cracks (shrinkage effects) were at loads less than the design loads, flexural cracking did not occur until loads higher than design loads. All cracking on the bottom face of the panel was contained within the panels being loaded. Based on the load deflection and load deformation responses, the test area performed well at service load levels. At approximately 4.8 x HS-25, elliptical cracks began to form around the load plates, and at 5.8 x HS-25 a punching shear failure initiated at the interior load point in the exterior bay. The failure mechanism indicates the AJ contributes to the capacity of the edge region, by making the interior load point the critical section and not the edge location. In order to preserve an area for testing the behavior at a load point in an interior location of a panel, the interior bay was not loaded to failure.

The relative midspan edge deflection at failure was 0.18 in. in the interior bay and 0.24 in. in the exterior bay. None of the measured reinforcing bars reached yield strains. The maximum recorded strain was 63% of yield (1400 με) at the second reinforcing bar from the slab edge.

145

5.5.2 Detailed Description of Response

5.5.2.1 Loading

Negative moments were maximized over the east-interior girder, between the two 8-ft bays. At the locations shown in Figure 5.33, four 10 in. by 20 in. steel plates were placed in the edge region on a layer of hydrostone. Cracks at the bottom face of the PC panels in the interior bay were first observed at 35 kips per load point, 2.2 x HS-25. At 91 kips per load point, approximately 5.8 x HS-25, a punching shear failure occurred at the interior load point in the exterior bay.
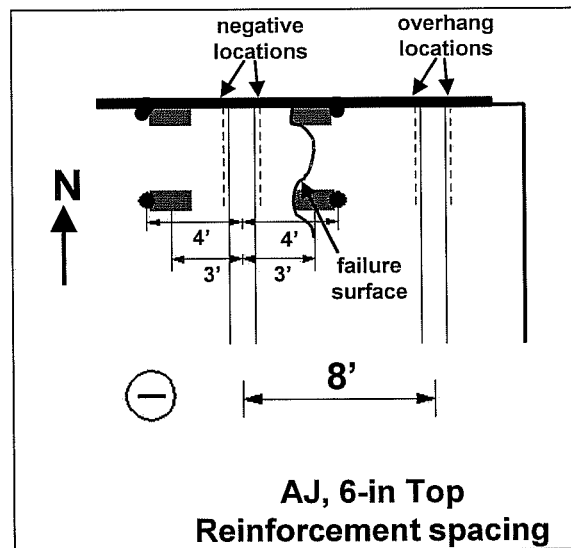
Figure 5.33 AJ, 6 in. top reinforcement spacing, negative-moment region (Test Area 6)

5.5.2.2 Load-Deflection Behavior

A complete record of the measured load deflection response is shown in Figure 5.34. The load-deflection envelopes for the edge deflections in the interior and exterior bays are also shown in Figure 5.34. At the interior bay, the load

146

deflection response for the edge deflection and the deflection measured 4 ft from the slab edge have virtually the same slope to about HS-20. The deflection measured at 4 ft from the slab edge in the interior bay is essentially linear during the entire test program. The maximum measured edge deflection was almost twice the maximum measured deflection 4 ft from the slab edge at failure loads in the interior bay. The load deflection response for the edge deflection of the interior and exterior bays were similar at the low service loads of HS-20, HS-25 and 1.75 x HS-25. At the low service level loads, the deflections were small relative to the girder spacing, so the load-deflection behavior was essentially linear and elastic at this range. Table 5.4 shows the measured deflections at various load steps for this test area.

Table 5.4 Meausred deflections (inches), Test Area 6

	HS-20	HS-25	1.75 HS-25	2.2 HS-25, first flexural cracking	3 HS-25	5.2 HS-25, developed cracking	5.8 HS-25, Failure
Interior bay, edge	0.017	0.021	0.038	0.053	0.075	0.15	0.18
Exterior bay, edge	0.015	0.017	0.035	0.047	0.064	0.15	0.24
Exterior bay, 4 ft from edge	0.010	0.011	0.023	0.031	0.040	0.085	0.10

5.5.2.2.1 Load-Deflection Envelope

The load deflection envelope indicate four changes in slab stiffness in the interior bay and three changes in stiffness in the exterior bay during testing of the area. A slight change in stiffness was seen in both bays at approximately 2.2 x HS-25, was caused by the first flexural cracking. Developed cracking or a major change in stiffness occurred at approximately 5.1 x HS-25. In addition to the change in stiffness, initiation of new cracks and lengthening and widening of existing cracks in the test section are also evident at this load. The slab stiffness

approaches zero at approximately 5.8 x HS-25 in the exterior bay. The edge deflection practically doubles in the exterior bay compared to the deflection in the interior bay. Details on the locations and sizes of the cracks are given in Section 5.5.2.5.
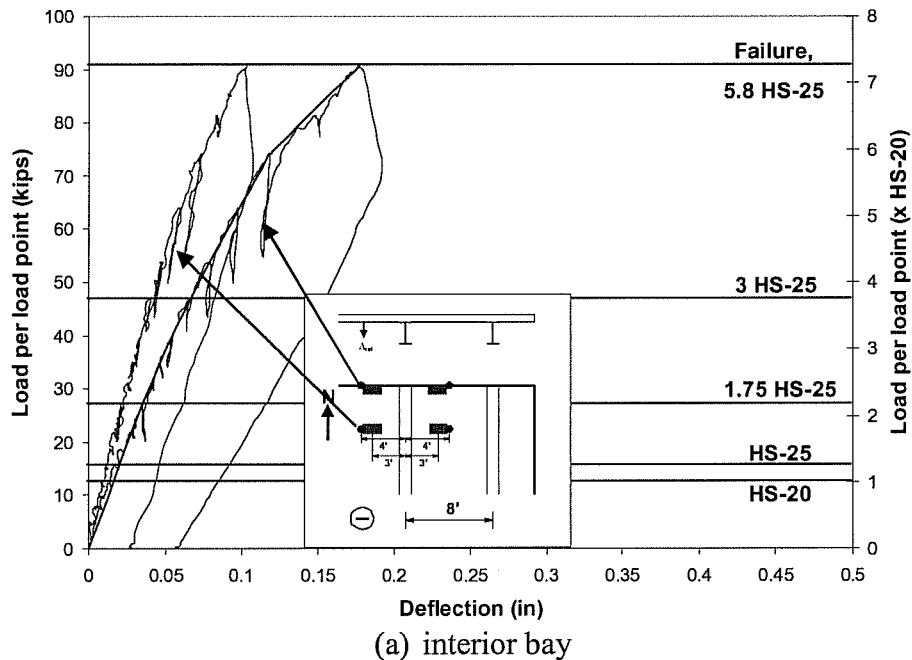
(a) interior bay

Figure 5.34 Relative midspan deflections and edge deflection envelopes, AJ, 6-in. top reinforcement spacing, negative-moment region: (a) interior bay; (b) exterior bay
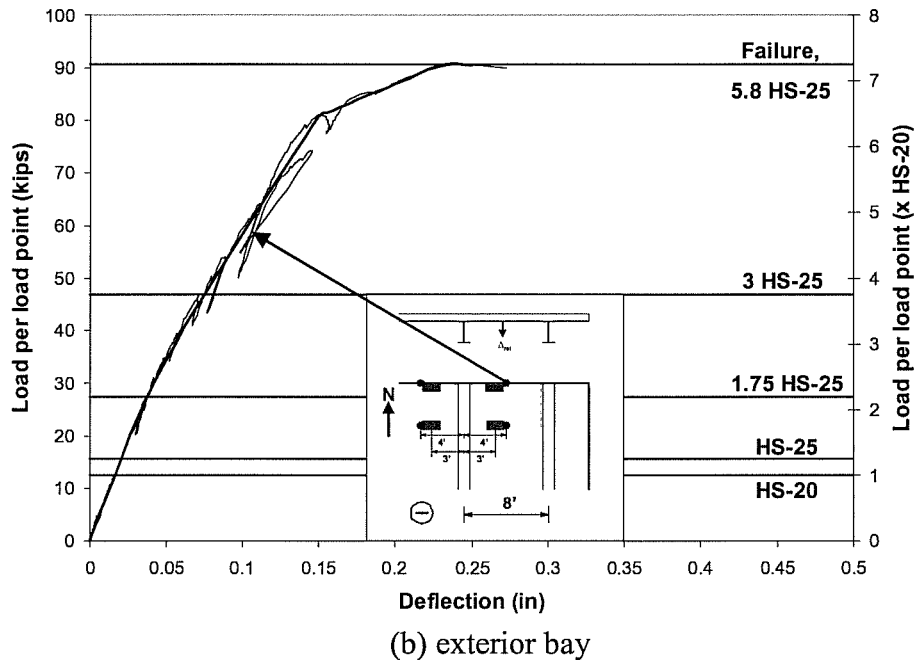
(b) exterior bay

*Figure 5.34 cont'd Relative midspan deflections and edge deflection envelopes,
AJ, 6-in. top reinforcement spacing, negative-moment region: (a) interior bay;
(b) exterior bay*

5.5.2.3 Load-Strain Response

Figure 5.35 shows strain measurements recorded on both faces of the girder and the midspan of the interior bay. At serviceability load levels, strains were small, and maximum strains measured were essentially the same on either side of the girder.

At HS-20 and HS-25 load levels measured strains at the girder locations were less than 8% of yield strain (180 με). Maximum strains measured at approximately 1.75 x HS-25 were 21% of yield strain (470 με) on the east face and 12% of yield strain (260 με) on the west face of the girder between the load points. The maximum strain measured on the AJ was 25 με on the west face of

149

the girder. At 3 x HS-25, the load-strain response was no longer linear at any gauge location. Maximum strains measured at approximately 3 x HS-25 were 30% of yield strain (650 με) on the east side and 28% of yield strain (610 με) on the west side of the girder between the load points. The maximum recorded strain on the AJ was 110 με on the west face of the girder. None of the instrumented reinforcing bars reached yield strain. The maximum recorded strain, 63 % of yield strain (1400 με), was recorded on the west face of the girder at the second reinforcing bar from the slab edge. Maximum strain levels on the east face of the girder at the second reinforcing bar from the slab edge were 59% (1300 με) of yield strain. The maximum recorded strain on the AJ was 360 με on the west face of the girder. At midspan, the average strain in the exterior bay on the bottom surface of the panel was estimated to be about 2700 με over a 9 in. gage length (Figure 5.36).
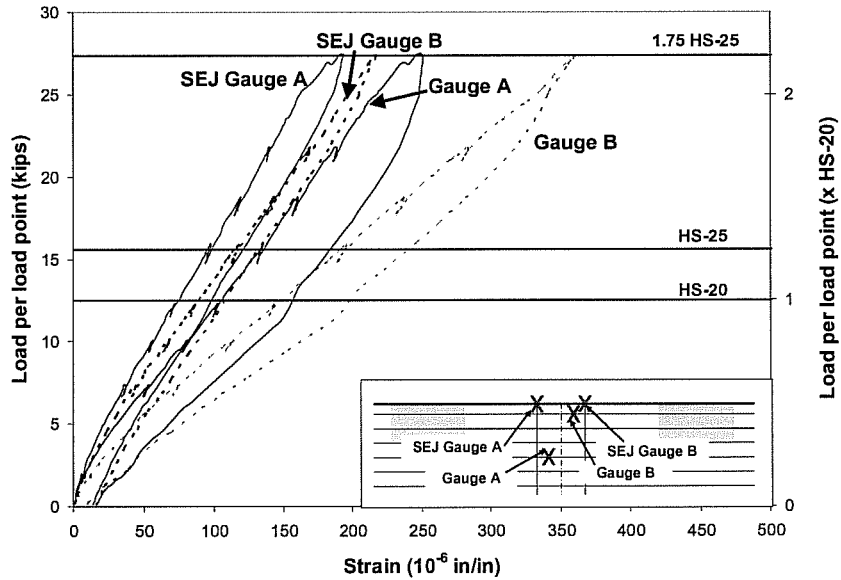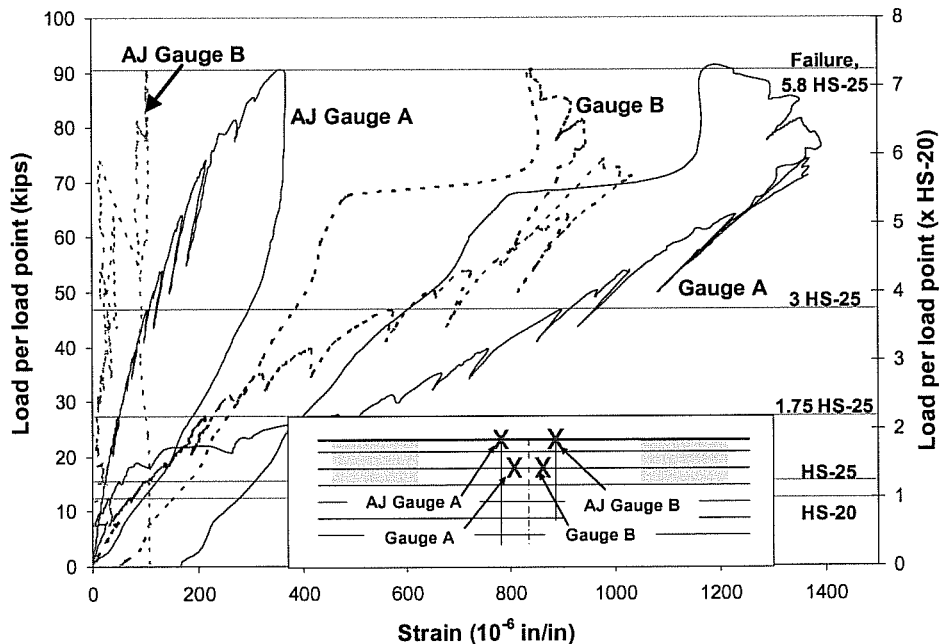

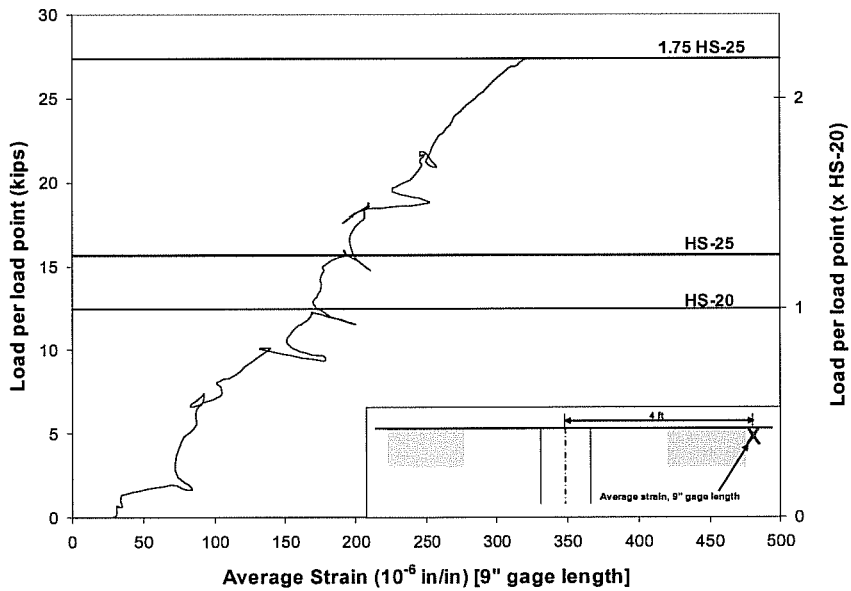*Figure 5.35 Load-strain response, AJ, 6 in. top reinforcement spacing, negative-moment region*
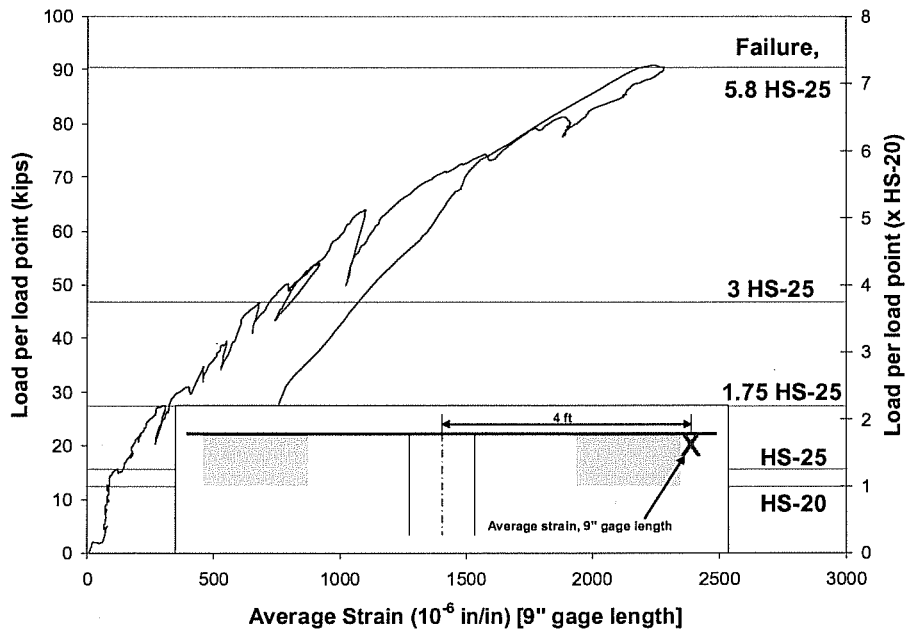
Figure 5.36 Load-average strain response, AJ, 6-in. top reinforcement spacing, negative-moment region, midspan, exterior bay, bottom face of panel

5.5.2.4 Strain Profiles

A primary objective was to evaluate the performance of slabs at HS-20 and HS-25 loads. While the strain profiles show strains increasing with increasing load, strains at both HS-20 and HS-25 were relatively small, never exceeding 8% of yield strain (180 $\mu\varepsilon$).

Strain profiles from either face of the girder in the AJ, 6 in. top reinforcement spacing, negative moment test section are shown in Figure 5.37 (a) and (b). In this test area, the largest strains occurred on the east face of the girder. The increase in strain from HS-20 to HS-25 is relatively small, where neither strain exceeds 8% of yield strain (180 $\mu\varepsilon$). At loads HS-20, HS-25 and 1.75 x HS-25, the strain distribution is essentially uniform through the edge region. As

151

loads approached the failure load, strains in the reinforcement near both load points became much larger than the strains measured between the load points. As seen in the profiles, the second reinforcing bar measures the most critical strain due to the addition of the AJ.

(a) east face of girder, top mat
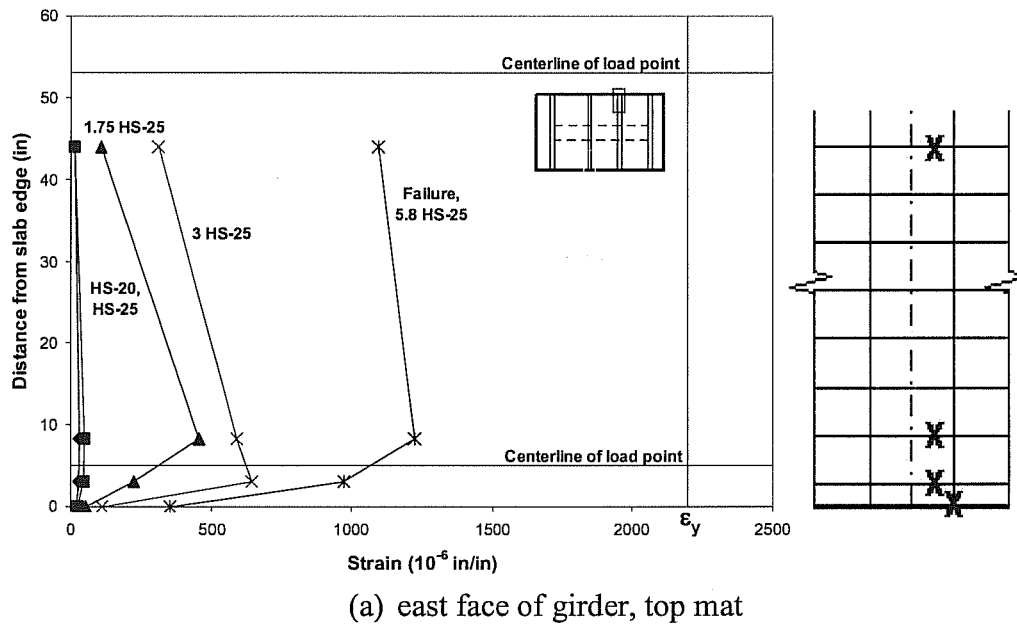
Figure 5.37 Strain profile, AJ, 6 in. top reinforcement spacing, negative-moment region: (a) east face of girder, top mat; (b) west face of girder, top mat
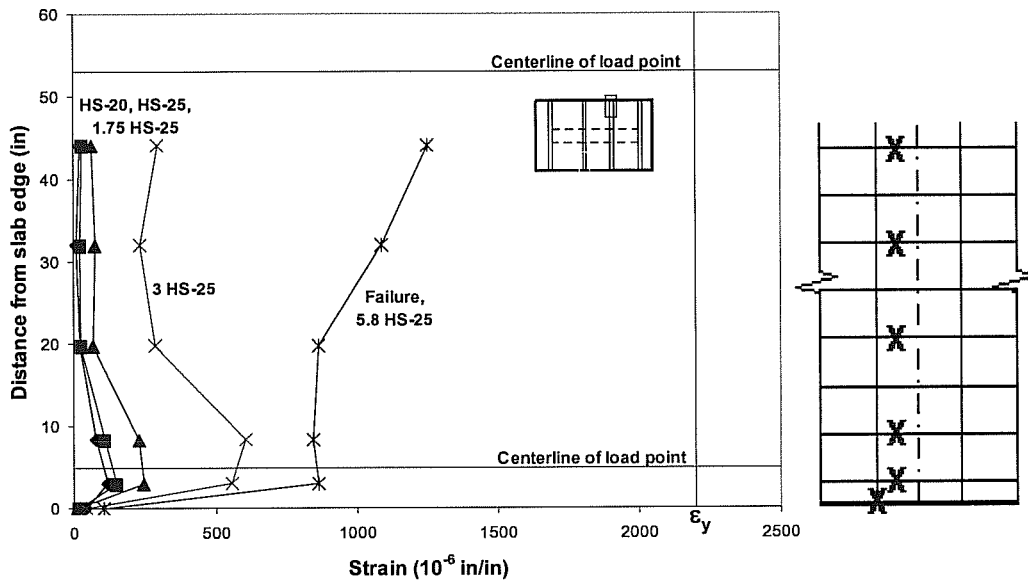
(b) west face of girder, top mat

*Figure 5.37 cont'd Strain profile, AJ, 6 in. top reinforcement spacing, negative-moment region: (a) east face of girder, top mat; (b) west face of girder, top mat*

5.5.2.5 Crack Maps

In Figure 5.38, Figure 5.39, and Figure 5.40, crack maps of the top, side and bottom of the test section are drawn illustrating cracks at 2.2 x HS-25 (first visible flexural cracking) and 4.8 x HS-25 (load step before failure and developed cracking).

The crack map at 2.2 x HS-25 shows the size and shape of the initial flexural cracks occurring in the slab and a slight change in stiffness. The load was applied at 5-kip increments, so first visible flexural cracks could have formed up to 5 kips per load points earlier than 2.2 x HS-25. In this test section, the first flexural cracks in the slab occurred on the bottom face of the panel at midspan of the exterior bay, in addition to increased crack widths of the shrinkage cracks.

153

The largest crack width on the bottom face of the panel at 2.2 x HS-25 was 0.002 in. The largest crack width on top of the slab was 0.007 in.

The crack map at 4.8 x HS-25, 55 kips per load point, shows cracks observed at the load step prior to the major change in stiffness, developed cracking, and before failure. At 4.8 x HS-25, on the top side of the slab, three flexural cracks were visible over the west-interior girder. These cracks began perpendicular to the slab edge (parallel to the girder) and then began to bend towards the loading plates. The largest measured crack width on the top side of the slab at this load step was 0.013 in. On the bottom face of the panels, the existing cracks running parallel to the girder extended much further at this load step than any previous load step. At 4.8 x HS-25, the largest measured crack width on the bottom face of the panels was 0.005 in. At failure, a large shear crack formed between and around the two load points in the exterior bay. A shear crack developed at just prior to reaching 4.8 x HS-25 near the interior-east girder in the exterior bay. The crack is assumed to have passed through both CIP concrete topping and the panel since most of the crack was hidden behind the AJ. The largest measured crack width on the side of the slab was 0.005 in. at a shear crack near the east-interior girder on the exterior bay. Visible on the top of the slab were cracks that circled around the loading plates in both bays at 4.8 x HS-25, indicating a punching shear failure. These cracks circling the loading plates and a few flexural cracks along the length of the girder widened during the final loading stages. The largest measured crack width before failure was 0.013 in. at one of the cracks circling the edge loading plate in the exterior bay. As seen from underneath the slab at failure, a series of flexural cracks formed parallel to the girders in the interior and east-exterior bay, fanning out past the load points. Flexural cracks formed on the bottom face of the panels in both bays could be seen on the side of the slab. At failure, the widest crack visible from the bottom

of the slab in the exterior bay was 0.25 in. at a crack running parallel to the girder near the panel bearing pad. Several flexural cracks formed beneath the location of the loading point 4 ft from the edge of the slab. All cracking was contained within the two panels being loaded; cracks did not propagate into the adjacent panels.
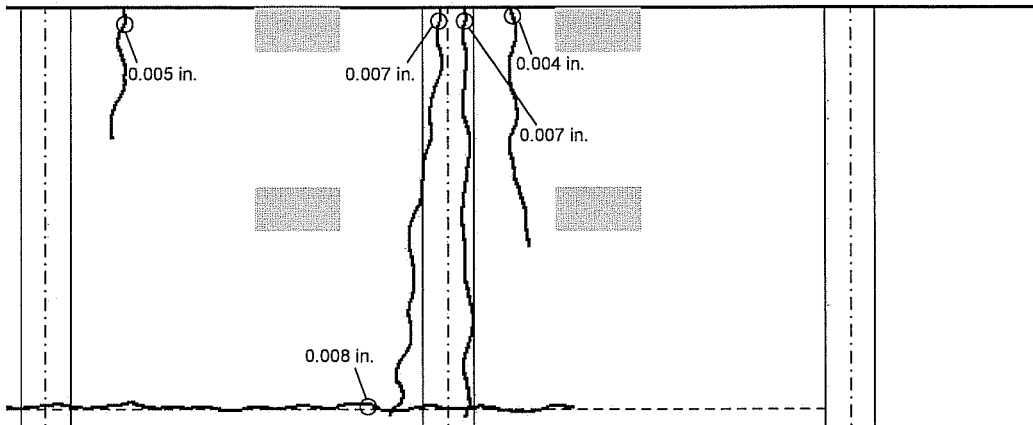
(a) 2.2 x HS-25 (first flexural cracking)
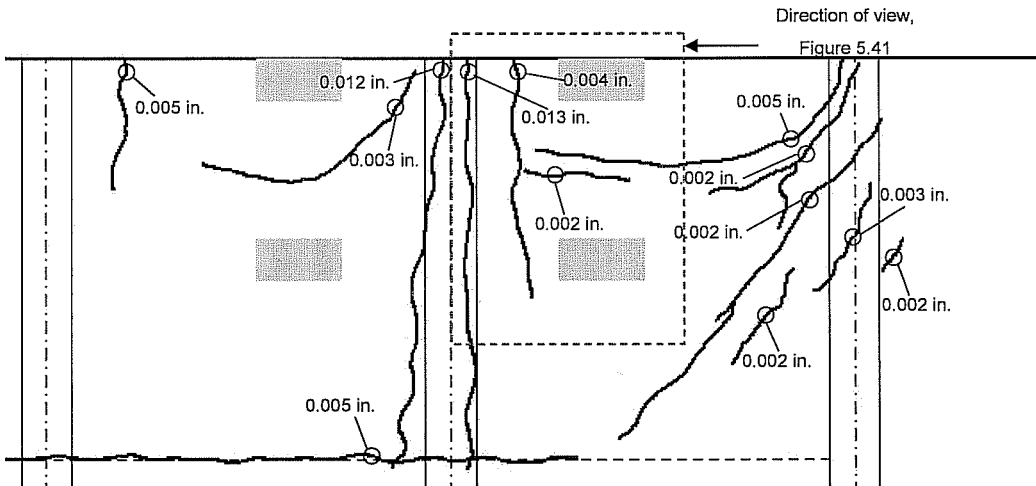
(b) 4.8 x HS-25 (developed cracking and failure)

Figure 5.38 Crack map, AJ, 6 in. top reinforcement spacing, negative-moment region, top view of slab

156
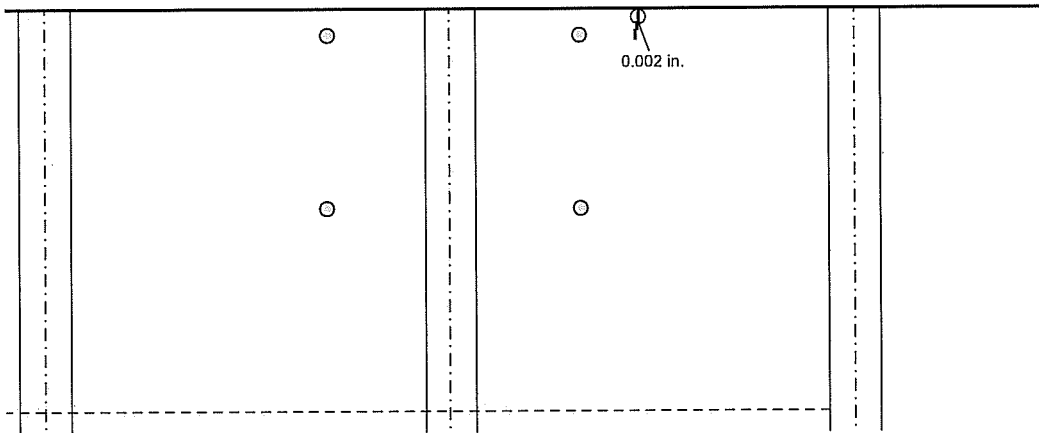
(c) 2.2 x HS-25 (first flexural cracking)
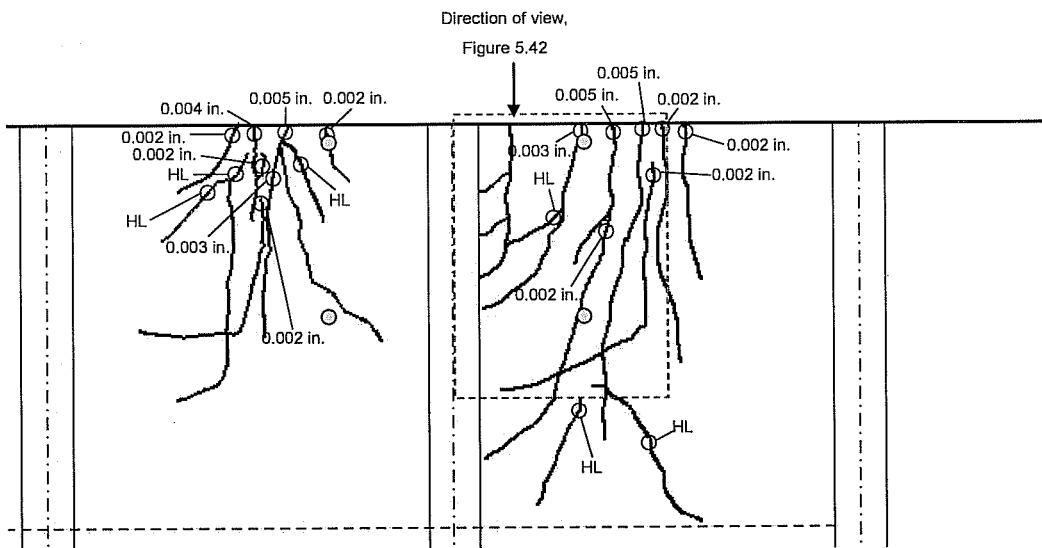
(d) 4.8 x HS-25 (developed cracking and failure)

Figure 5.39 Crack map, AJ, 6 in. top reinforcement spacing negative-moment

region, bottom view of slab
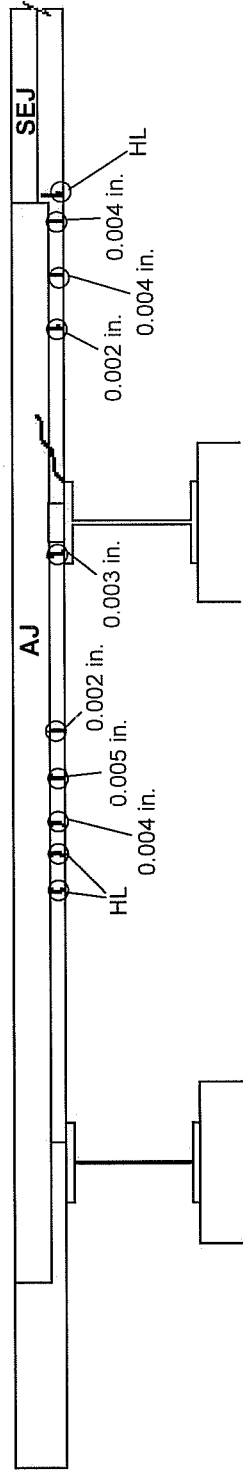
Figure 5.40 Crack map, AJ, 6 in. top reinforcement spacing, negative-moment, side view of slab, 4.8 x HS-25 (developed cracking and failure)

5.5.2.6 *Appearance after Failure*

At 5.8 x HS-25, a punching shear failure occurred at the loading plate 4 ft from the slab edge in the exterior 8 ft bay. Pictures were taken of the failure surface (Figure 5.41, Figure 5.42, Figure 5.43). Crack formed between the two load points and around the interior load point. Because the area around the interior load point was more extensively damaged than the area around the edge load point, failure was probably initiated by punching shear at the interior load point. The failure surface indicates the AJ contributes to the capacity of the edge region by making the interior loading point, not the edge loading point, the critical section. Cracks wrapping semi-circularly around the edge load point formed around 4.8 x HS-25 and existing flexural cracks opened on the top surface up to and at failure. Little evidence of failure was visible on the bottom surface of the slab, except for a large crack running parallel to the panel bearing strip. The side surface of the slab was not visible due to the AJ.
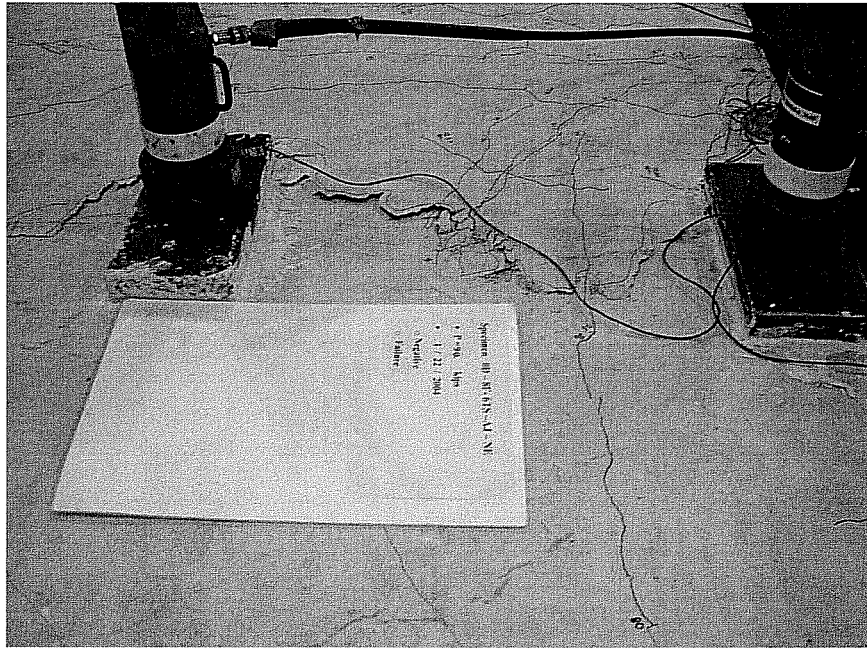
Figure 5.41 East exterior 8-ft bay failure at top of slab, facing west
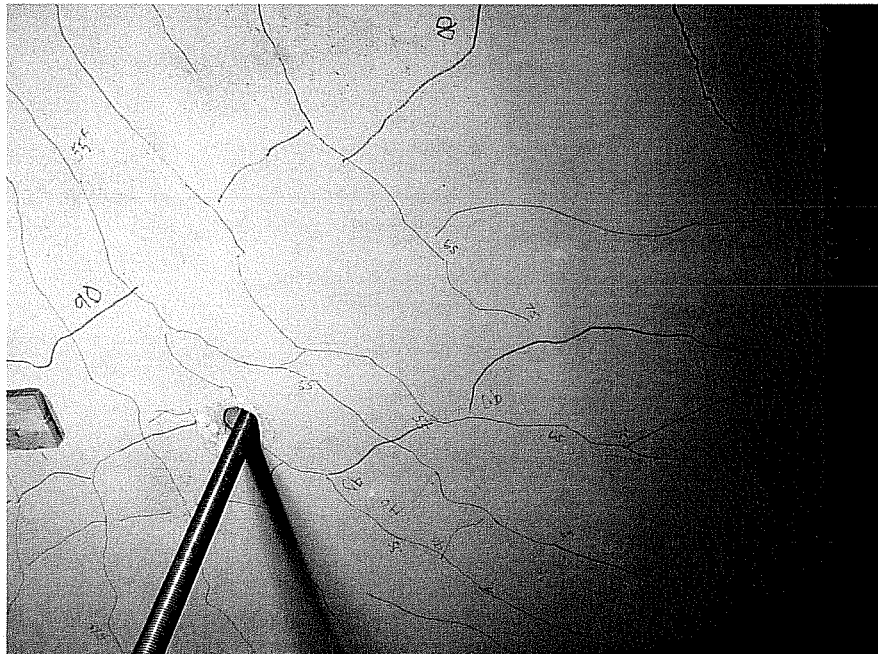
Figure 5.42 East exterior 8-ft bay failure at bottom of slab, facing west

160
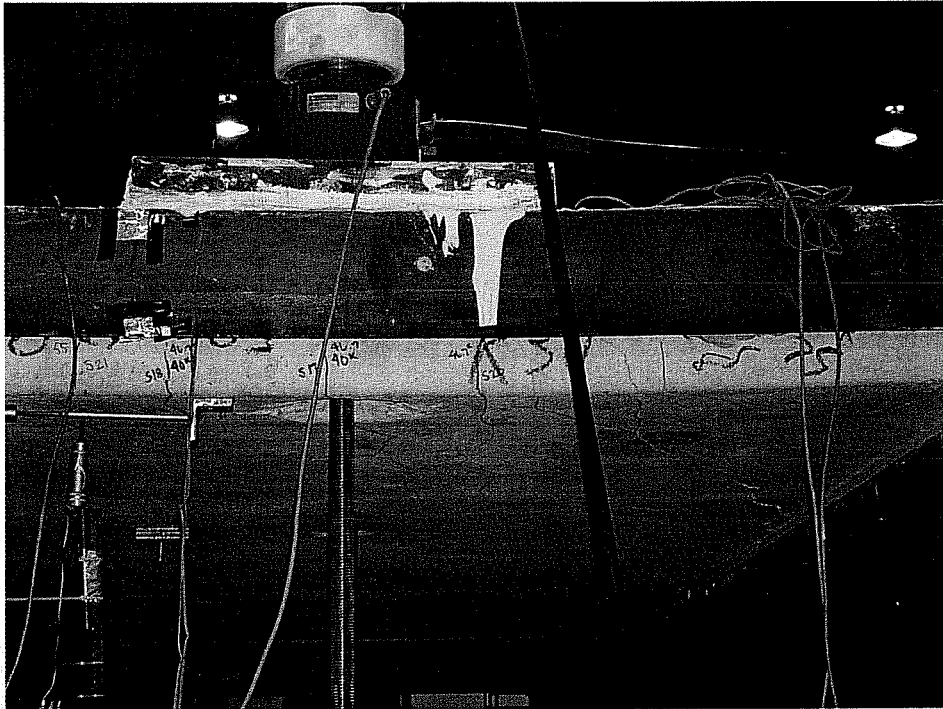
Figure 5.43 East exterior 8-ft bay failure at side of slab, facing south

5.6   6 IN. TOP REINFORCEMENT SPACING, POSITIVE-MOMENT REGION (TEST AREA 3)

5.6.1   Summary of Response

The 6 in. top reinforcement spacing test area was loaded to design and overload levels with the AASHTO tandem load configuration placed to maximize positive moments in the edge detail.

First flexural cracking was visible at 2.2 x HS-25 on the bottom face of the panel, in addition to the widening of the cracks due to shrinkage effects on the top surface of the slab. Top cracks formed over the ends of the panels over the girders and propagated parallel to the girder. Major change in stiffness occurred at approximately 3.4 x HS-25. Even though the first visible cracks (shrinkage

161

effects) were at loads less than the design loads, flexural cracking did not occur until loads higher than design loads. All cracking on the bottom face of the panel was contained within the panels being loaded. Based on the load deflection and load deformation responses, the test area performed well at service load levels. At approximately 3.5 x HS-25, elliptical cracks began to form around the load plates, and the bottom face of the panel exhibited significant cracking that resembled a yield line pattern. However, at 4.3 x HS-25 a punching shear failure initiated at the edge load point in the interior bay.

The relative midspan edge deflection at failure was 0.84 in. in the west exterior 10-ft bay. None of the measured reinforcing bars reached yield strain. The maximum recorded strain was 67% of yield strain (1480 µε), measured at failure at the sixth reinforcing bar from the slab edge on the west face of the girder.

5.6.2   Detailed Description of Response

5.6.2.1   Loading

The 10-ft girder spacing bay constructed with 6-in. top reinforcement spacing was loaded by two 10- by 20-in. steel plates, placed midspan in the west exterior bay (Figure 5.44). During the serviceability test, the slab was loaded to 1.75 x HS-25, 27.3 kips per load point. After the serviceability test, Test Area 3 was loaded to failure after Test Areas 1, 4, and 6 were tested to failure. First visible flexural cracking did not occur until 35 kips per load point, 2.2 x HS-25. At 68 kips per load point, approximately 4.3 x HS-25, a punching shear failure occurred at the edge load point.

162
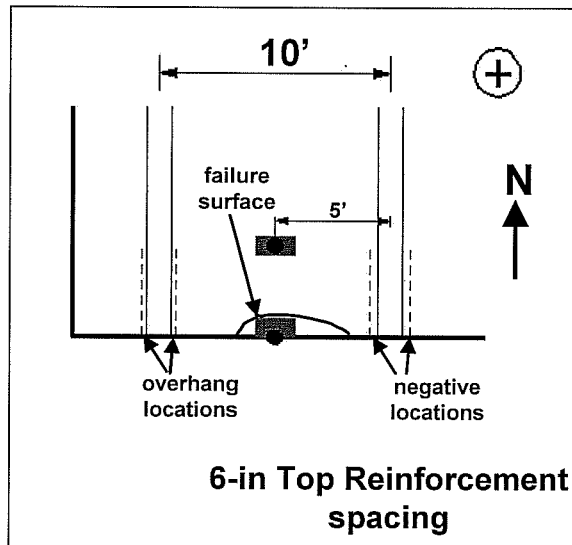
Figure 5.44 6 in. top reinforcement spacing, positive-moment region (Test Area 3)

5.6.2.2 Load-Deflection Behavior

A complete record of the measured load deflection response is shown in Figure 5.45. The load-deflection envelope for the edge deflection in the west exterior bays is also shown in Figure 5.45. At the west exterior bay, the load deflection response for the edge deflection and the deflection measured 4 ft from the slab edge have virtually the same slope to about 1.75 x HS-25. At the low service level loads, the deflections were small relative to the girder spacing, so the load-deflection behavior was essentially linear and elastic at this range. The deflection measured at 4 ft from the slab edge is essentially linear up to 3.4 x HS-25. The maximum measured edge deflection was essentially twice the maximum measured deflection 4 ft from the slab edge at failure loads in the 10-ft bay. Table 5.5 shows the measured deflections at various load steps for this test area.

Table 5.5 Meausred deflections (inches), Test Area 3

	HS-20	HS-25	1.75 HS-25	2.2 HS-25, first flexural cracking	3 HS-25	3.4 HS-25, developed cracking	4.3 HS-25, Failure
10-ft bay, edge	0.043	0.055	0.1	0.18	0.28	0.39	0.84
10-ft bay, 4 ft from edge	0.058	0.068	0.089	0.11	0.14	0.21	0.48

5.6.2.2.1 Load-Deflection Envelope

The load deflection envelope indicates four changes in slab stiffness in the west exterior (10-ft) bay during all tests in the area. The first change in stiffness, occurs in 1.75 x HS-25 just prior to the first observed flexural cracking at 2.2 x HS-25. The first change in stiffness was most likely due to the change in stiffness due to the previous failure tests. The second change in stiffness occurred at 3.4 x HS-25. At approximately, 4.0 x HS-25, the stiffness reduced to nearly zero as failure progressed. At 4.3 x HS-25, the edge region failed in punching shear of the edge load point.

In tests maximizing negative moment, first cracking did not coincide with an observed change in stiffness in the load-deflection response. The overall slab stiffness decreased after the formation of multiple cracks. For the tests maximizing positive moment, initial cracking in the slab did cause a very slight change in stiffness. As defined earlier, developed cracking is identified as the load stage at which the first significant change in the load-deflection response stiffness can be identified. Thus, developed cracking occurred at the same load as fist cracking in the positive moment test regions. Because the "cracks at developed cracking" are identical to the "cracks at first flexural cracking".

164

For the positive moment, the term "major change in stiffness" is used to describe the load at which the second change in stiffness can be identified in the load-deflection response. The second change coincided with the initiation of multiple cracks and subsequent decrease in slab stiffness, so the "cracks at major change in stiffness" will be discussed for test regions where positive moment was maximized. Details on the locations and sizes of the cracks are given in Section 5.6.2.5.
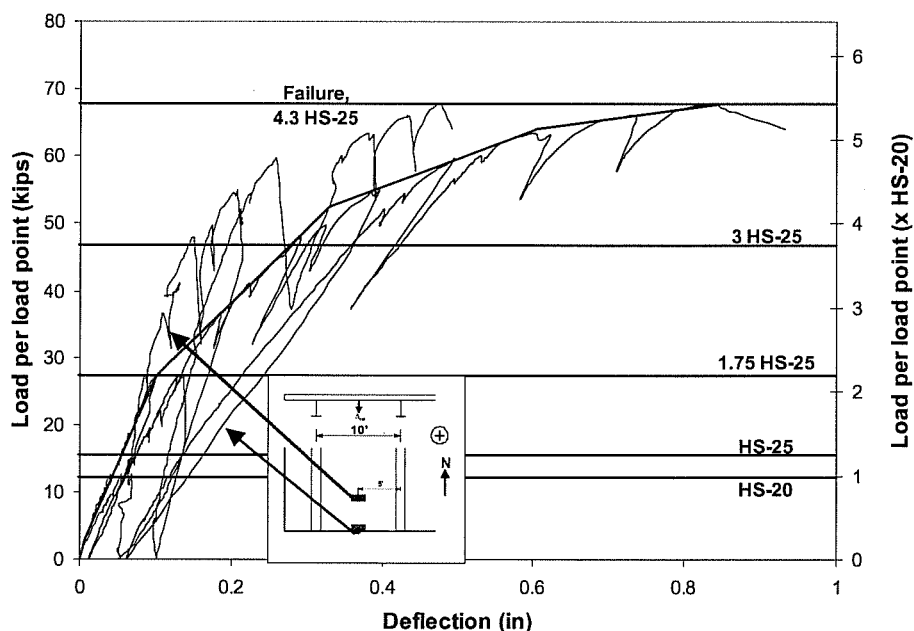
Figure 5.45 Relative midspan deflections and edge deflection envelope, 6-in. top reinforcement spacing, positive-moment region

5.6.2.3 Load-Strain Response

Figure 5.46 shows strain measurements recorded on both faces of the girder and the midspan of the 10-ft bay. At serviceability load levels, strains were small, and maximum strains measured were essentially the same on either side of the girder.

165

At HS-20 and HS-25 load levels measured strains at the girder locations were less than 15% of yield strain (290 με). Maximum strains measured at approximately 1.75 x HS-25 were 20% of yield strain (440 με) on the east face and 21% of yield strain (470 με) on the west face of the west-interior girder. At 3 x HS-25, the load-strain response was no longer linear at any gauge location. Maximum strains measured at approximately 3 x HS-25 were 32% of yield strain (700 με) on the east face and 37% of yield strain (810 με) on the west face of the girder between the load points. None of the measured reinforcing bars reached yield strain. The maximum strain, 67 % of yield strain (1480 με), was recorded on the west face of the girder at the gauge on the sixth reinforcing bar from the slab edge. Maximum strain levels on the east face of the girder were 51% (1130 με) of yield strain. At midspan, the average strain on the bottom surface of the panel was estimated to be about 5690 με over a 9 in. gage length (Figure 5.47).
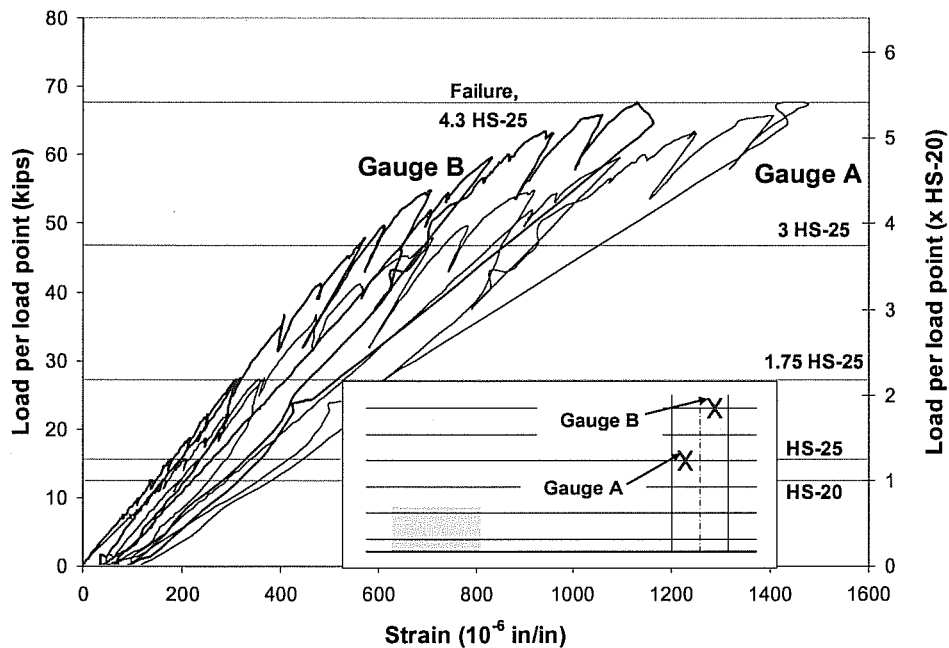
Figure 5.46 Load-strain response, 6 in. top reinforcement spacing, positive - moment region

166
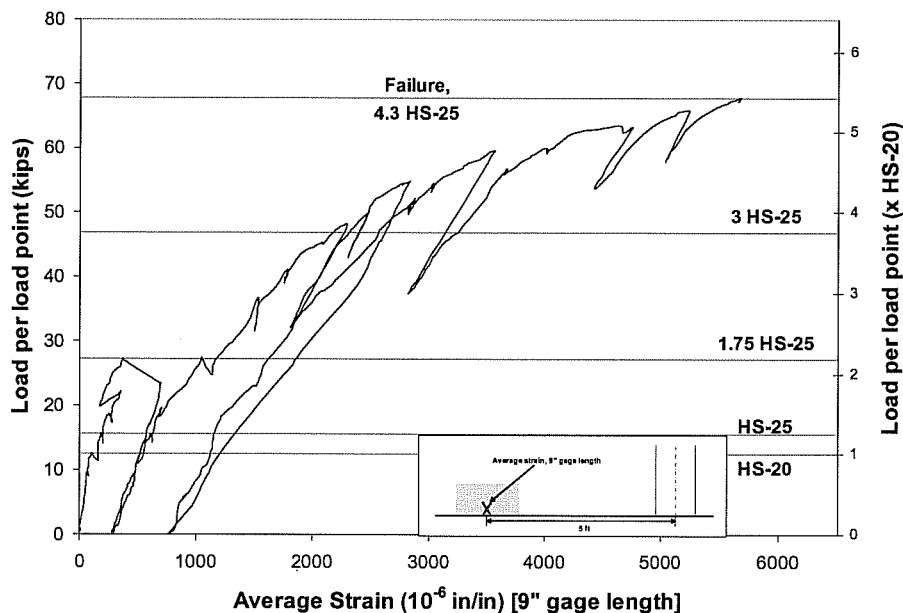
Figure 5.47 Load-average strain response, 6 in. top reinforcement spacing,

positive-moment region, midspan, exterior 10-ft bay, bottom face of the panel

5.6.2.4 Strain Profiles

A primary objective was to evaluate the performance of slabs at HS-20 and HS-25 loads. While the strain profiles show strains increasing with increasing load, strains at both HS-20 and HS-25 were relatively small, never exceeding 15% of yield strain (290 μɛ).

Strain profiles from either face of the girder in the 6 in. top reinforcement spacing, positive moment test section are shown in Figure 5.48 (a) and (b). In this test area, the largest strains occurred on the west face of the girder. The increase in strain from HS-20 to HS-25 is relatively small, where neither strain exceeds 15% of yield strain (290 μɛ). At loads HS-20, HS-25 and 3 x HS-25, the strain distribution is essentially uniform through the edge region.

167
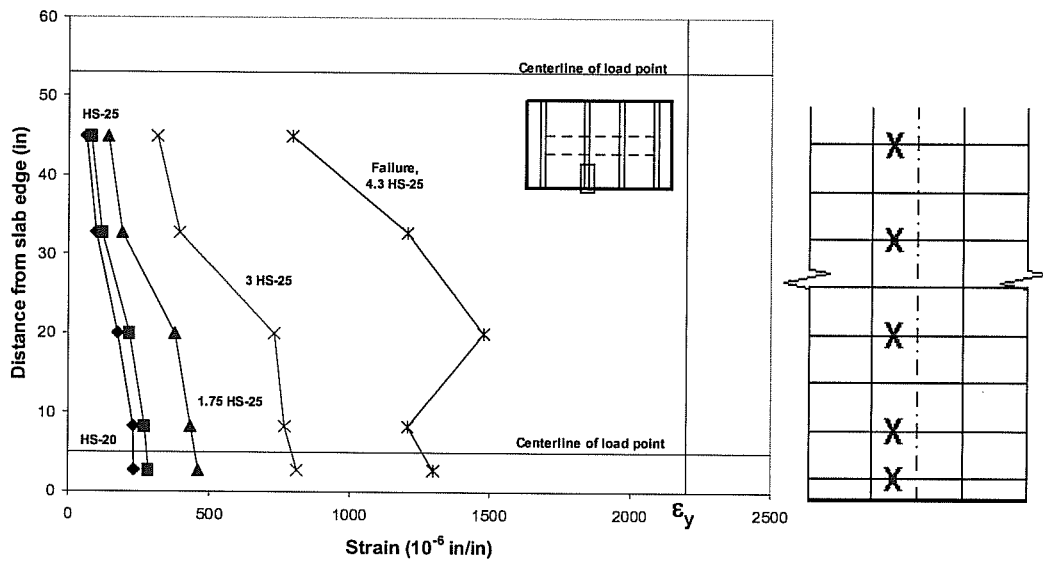
(a) west face of girder, top mat
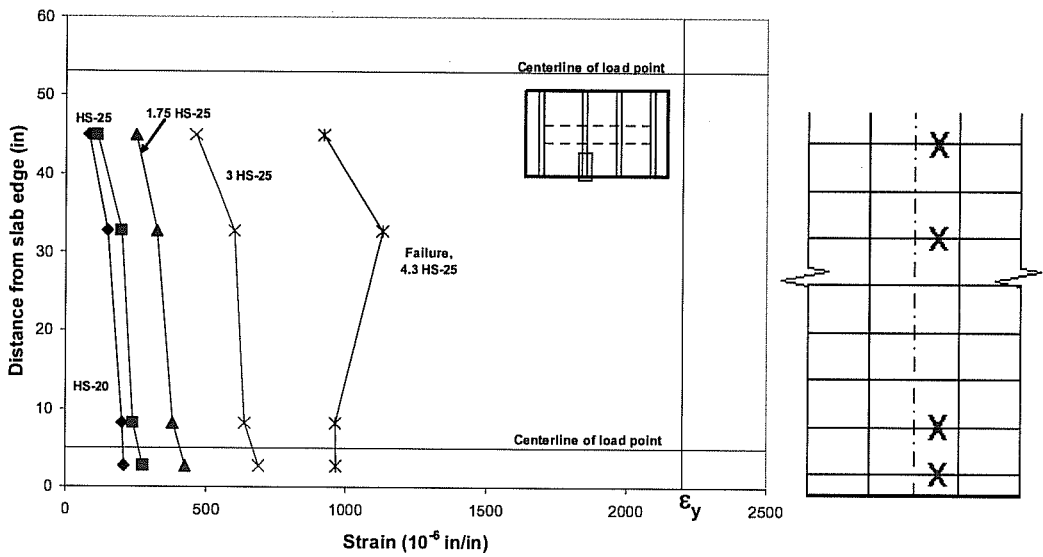
(b) east face of girder, top mat

Figure 5.48 Strain profile, 6 in. top reinforcement spacing, positive-moment region: (a) west face of girder, top map; (b) east face of girder, top mat

168

5.6.2.5 Crack Maps

In Figure 5.49, Figure 5.50, and Figure 5.51, crack maps of the top, side and bottom of the test section are drawn illustrating cracks at 2.2 x HS-25 (first visible flexural cracking), 3.5 x HS-25 (load step after major change in stiffness), and 4.2 x HS-25 (load step before failure).

The crack map at 2.2 x HS-25 shows the size and shape of the initial flexural cracks occurring in the slab. In this test section, the first flexural cracks in the slab occurred on the bottom face of the panel at midspan of the west exterior 10-ft bay, in addition to increased cracks width of the shrinkage cracks on the top surface of the slab. The largest crack width on the bottom face of the panel was 0.003 in. 2.2 x HS-25. A crack formed over the centerline of the west overhang girder on top of the slab. This crack had a width of 0.005 in. The largest crack width on top and side of the slab were 0.013 in. and 0.01 in.

The crack map at 3.5 x HS-25, 55 kips per load point, shows cracks that were observed at the load step after the major change in stiffness after initial flexural cracking. At 3.5 x HS-25, on the top side of the slab, two cracks were visible over the west-interior girder. These cracks began perpendicular to the slab edge (parallel to the girder) and then began to bend towards the loading plates. The largest measured crack width on the top side of the slab at this load step was 0.015 in. On the bottom face of the panels, the existing cracks running parallel to the girder extended much further at this load step than any previous load step. At 3.5 x HS-25, the largest measured crack width on the bottom face of the panels was 0.018 in.

The crack map at 4.2 x HS-25 shows crack formed during testing and just after failure. At 4.3 x HS-25, a shear crack formed around the edge point in the west exterior 10-ft bay. In addition to the shear cracks, some delamination occurred near the east-interior girder and midspan at the interface between the

panel and CIP concrete topping. A shear crack developed on the side surface of the slab just prior to reaching 3.8 x HS-25 near the west-interior girder. The crack passed through both CIP concrete topping and the panel. The largest measured crack width on the side of the slab was 0.03 in., a shear crack near the west-interior girder on the exterior 10-ft bay. The slippage between the panel and the CIP concrete topping near the west-interior girder was measured at 0.01 in. and 0.25 in. at 4.2 x HS-25 and failure, respectively. The measured slippage at the interface at midspan was 0.015 in. at 4.2 x HS-25. Visible on the top of the slab were cracks that circled around the loading plates in both bays at 4.2 x HS-25, indicating a punching shear failure. These cracks circling the loading plates and a few flexural cracks along the length of the girder widened during the final loading stages. The largest measured crack width before failure was 0.007 in. at one of the cracks circling the edge loading plate in the 10-ft bay. As seen from underneath the slab at failure, a series of flexural cracks formed parallel to the girders in the 10-ft bay, fanning out past the load points, indicating a yield line pattern. Flexural cracks formed on the bottom face of the panels in the bay could be seen on the side of the slab. At 4.2 x HS-25, the widest crack visible from the bottom of the slab in the interior bay was 0.04 in. at a crack running parallel to the girder at midspan. All cracking was contained within the panel being loaded; cracks did not propagate into the adjacent panels.
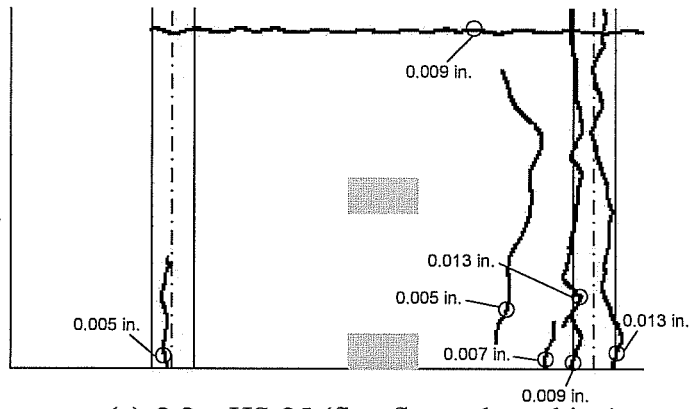
(a) 2.2 x HS-25 (first flexural cracking)
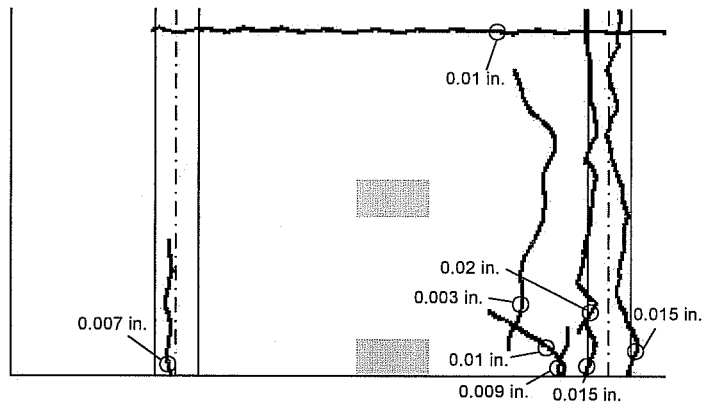
(b) 3.5 x HS-25 (developed cracking)
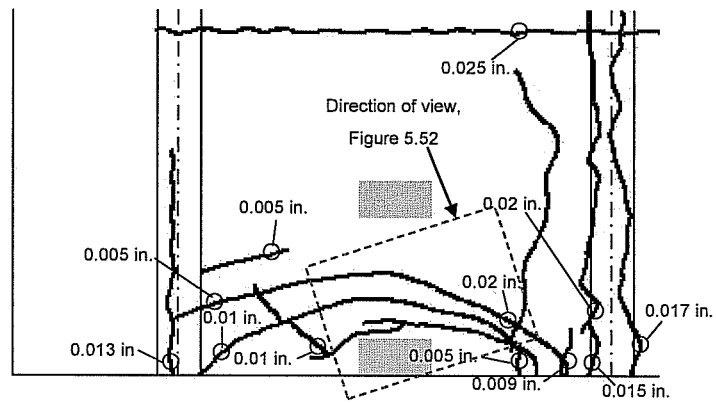
(c) 4.2 x HS-25 (failure)

Figure 5.49 Crack map, 6 in. top reinforcement spacing, positive-moment region, top view of slab
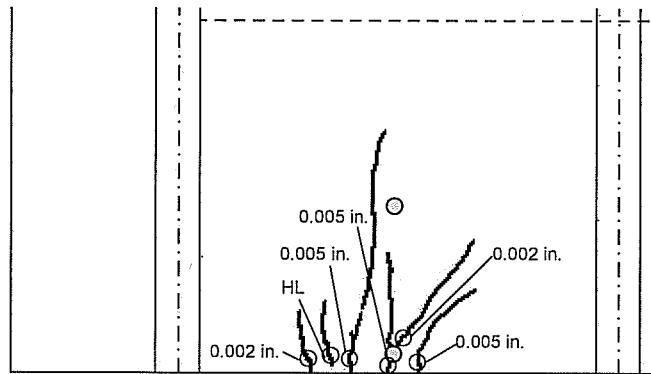
171

(a) 2.2 x HS-25 (first flexural cracking)
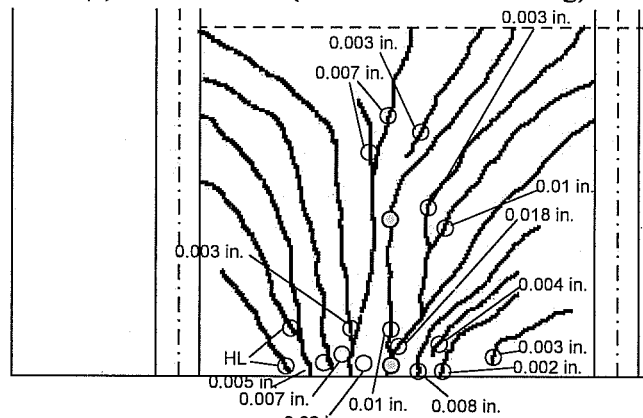
(b) 3.5 x HS-25 (developed cracking)
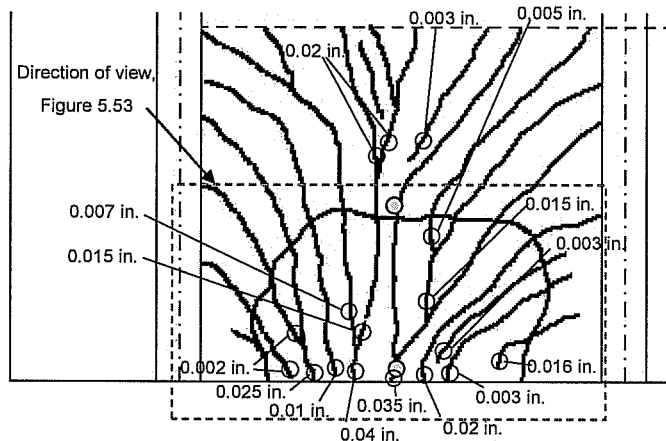
(c) 4.2 x HS-25 (failure)

Figure 5.50 Crack map, 6 in. top reinforcement spacing, positive moment

region; bottom view of slab

172

(a) 2.2 x HS-25 (first flexural cracking)

(b) 3.5 x HS-25 (developed cracking)

(c) 4.2 x HS-25 (failure)
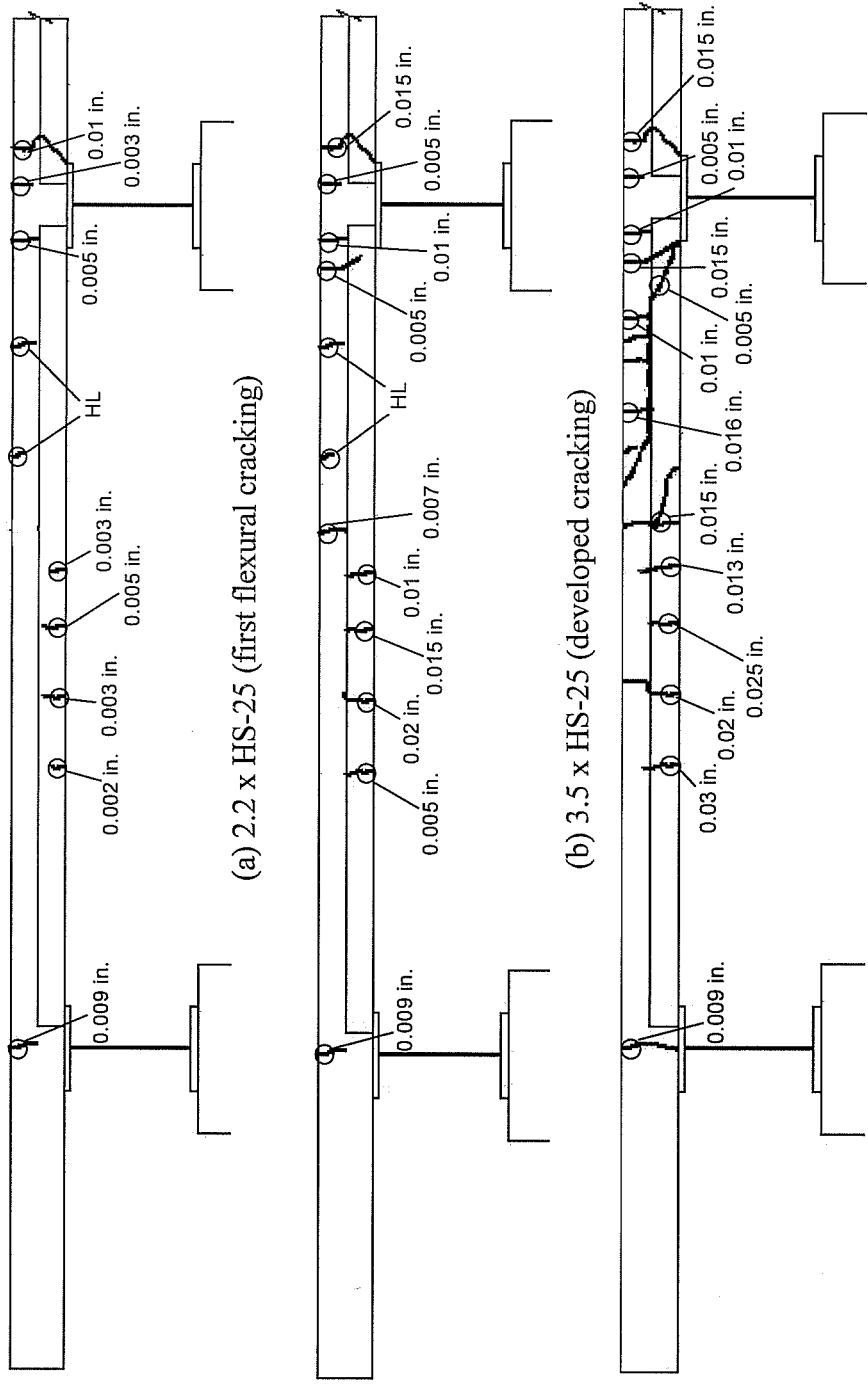
Figure 5.51 Crack map, 6 in. top reinforcement spacing, positive-moment region, side view of slab

173

5.6.2.6 *Appearance after Failure*

At 4.3 x HS-25, a punching shear failure occurred at the edge load point in the 10-ft bay. Pictures were taken of the failure surface (Figure 5.52, Figure 5.53, Figure 5.54). Cracks wrapping semi-circularly around the edge load point formed around 3.5 x HS-25 and existing flexural cracks opened on the top surface up to and at failure. From the side of the slab, shear cracks extend from the CIP topping to the bottom of the panel, with the crack running along the interface near the west-interior girder. The side surface indicated some delamination (Figure 5.54 b) occurring between the panel and the CIP concrete topping at high loads and failure. Some separation was seen around 3.8 x HS-25. The failure surface is easily visible from beneath the slab.
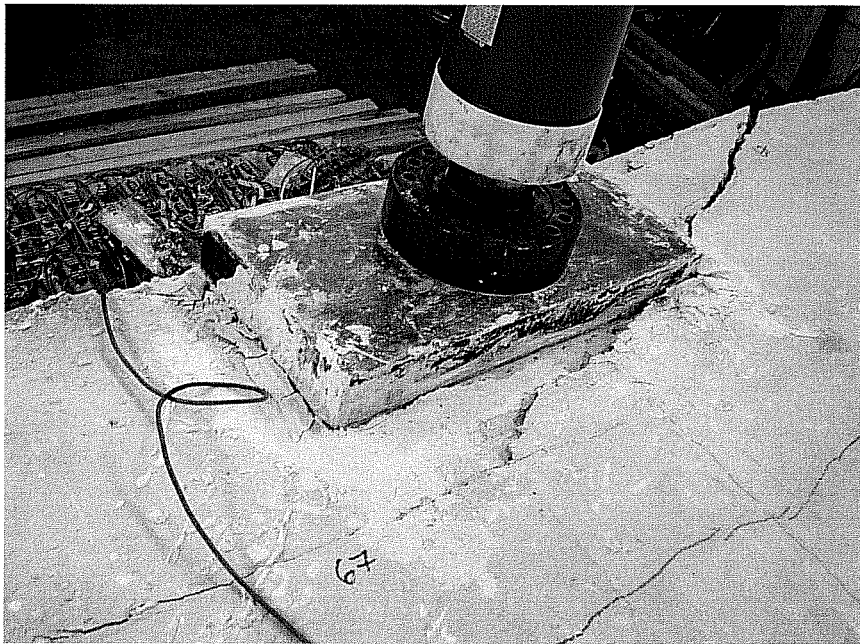
Figure 5.52 West exterior 10-ft bay failure at top of slab, facing southwest
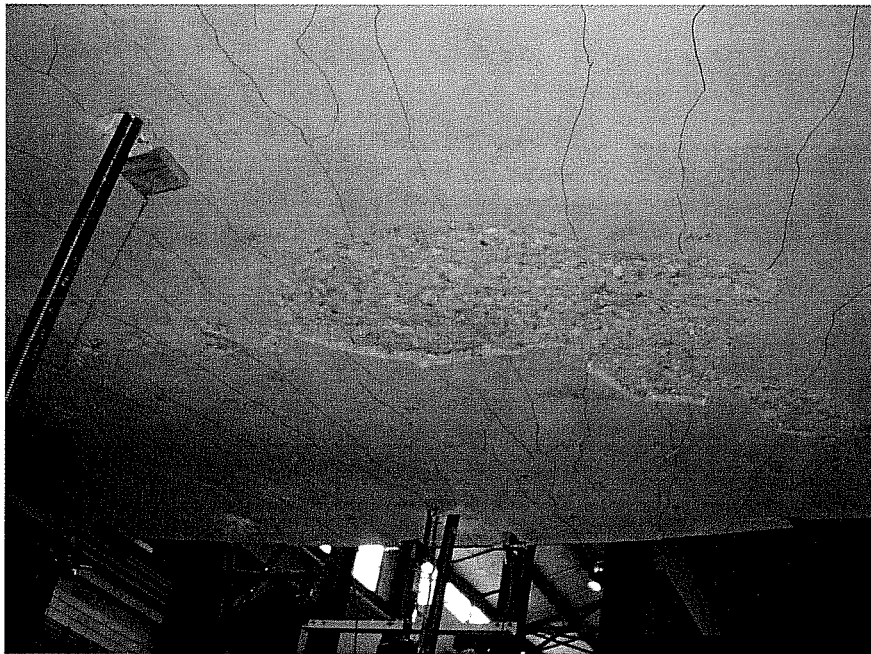
Figure 5.53 West exterior 10-ft bay failure surface at bottom of slab, facing south

175

(a) Facing north

(b) Close up of delamination, facing north

Figure 5.54 West exterior 10-ft bay failure surface at side of slab: (a) facing north; (b) close up of delamination between panel and CIP concrete topping

176

5.7 SEJ, 6 IN. TOP REINFORCEMENT SPACING, POSITIVE MOMENT REGION (TEST AREA 4)

5.7.1 Summary of Response

The SEJ, 6 in. top reinforcement spacing test area was loaded to design and overload levels with the AASHTO tandem load configuration placed to maximize positive moments in the edge detail.

First flexural cracking was visible at 1.75 x HS-25 on the bottom face of the panel, in addition to the widening of the cracks due to shrinkage effects on the top surface of the slab. Top cracks formed over the ends of the panels over the girders and propagated parallel to the girder. Major change in stiffness occurred at approximately 3.4 x HS-25. Even though the first visible cracks (shrinkage effects) were at loads less than the design loads, flexural cracking did not occur until loads higher than design loads. Cracking on the bottom face of the panel resembled a yield line pattern. All cracking on the bottom face of the panel was contained within the panels being loaded. Based on the load deflection and load deformation responses, the test area performed well at service load levels. At approximately 3.5 x HS-25, elliptical cracks began to form around the load plates, and the bottom face of the panel exhibited significant cracking that resembled a yield line pattern. However, at 5.4 x HS-25 a punching shear failure initiated at the edge load point in the interior bay.

The relative midspan edge deflection at failure was 1.01 in. in the west exterior 10-ft bay. None of the measured reinforcing bars reached yield strain. The maximum recorded strain was 67% of yield strain (1480 $\mu\varepsilon$), measured at failure at the fourth reinforcing bar from the slab edge on the west face of the girder. The maximum recorded strain at the face of the SEJ was 1280 $\mu\varepsilon$ at the west face of the girder.

177

5.7.2 Detailed Description of Response

5.7.2.1 Loading

The 10-ft girder spacing bay constructed with SEJ embedded in the CIP topping and 6-in. top reinforcement spacing was loaded by two 10- by 20-in. steel plates, placed midspan in the west exterior bay (Figure 5.55). During the serviceability test, the slab was loaded to 1.75 x HS-25, 27.3 kips per load point. Test Area 3 was loaded to failure after Test Area 6 was tested to failure. First visible flexural cracking did not occur until 1.75 x HS-25. At 85 kips per load point, approximately 5.4 x HS-25, a punching shear failure occurred at the edge load point.
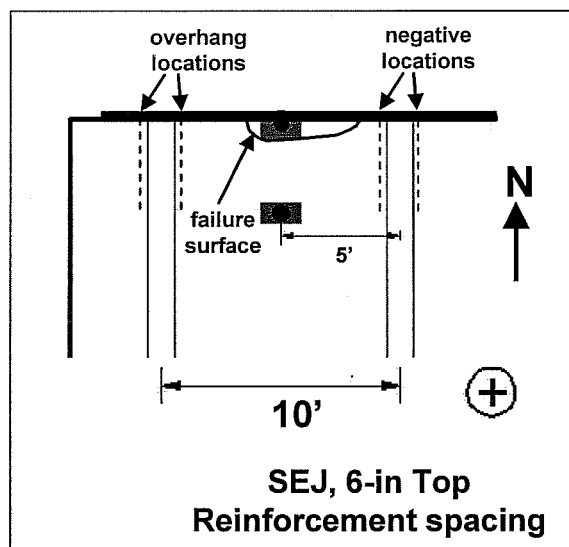
Figure 5.55 SEJ, 6 in. top reinforcement spacing, positive-moment region (Test Area 4)

5.7.2.2 Load-Deflection Behavior

A complete record of the measured load deflection response is shown in Figure 5.56. The load-deflection envelope for the edge deflections in the west

178

exterior bay is also shown in Figure 5.56. At the west exterior bay, the load deflection response for the deflection measured 4 ft from the slab edge has a larger slope than the edge deflection. The deflection measured at 4 ft from the slab edge is essentially linear up to 3.4 x HS-25. At the low service level loads, the deflections were small relative to the girder spacing, so the load-deflection behavior was essentially linear and elastic at this range. The maximum measured edge deflection was essentially twice the maximum measured deflection 4 ft from the slab edge at failure loads in the 10-ft bay. Table 5.6 shows the measured deflections at various load steps for this test area.

Table 5.6 Meausred deflections (inches), Test Area 4

	HS-20	HS-25	1.75 HS-25, first flexural cracking	3 HS-25	3.4 HS-25, developed cracking	5.4 HS-25, Failure
Exterior 10' bay, edge	0.039	0.049	0.1	0.25	0.32	1.01
Exterior 10' bay, 4 ft from edge	0.014	0.025	0.058	0.13	0.17	0.64

5.7.2.2.1 Load-Deflection Envelope

The load deflection envelope indicate four changes in slab stiffness in the west exterior (10-ft) bay during all tests in the area. The first change in stiffness, occurs at 1.75 x HS-25 when the first flexural cracking is observed. The major change in stiffness occurred at 3.4 x HS-25. At approximately, 4.3 x HS-25, the stiffness reduced to nearly zero as failure progressed. At 5.4 x HS-25, the edge region failed in punching shear of the edge load point. Details on the locations and sizes of the cracks are given in Section 5.7.2.5.
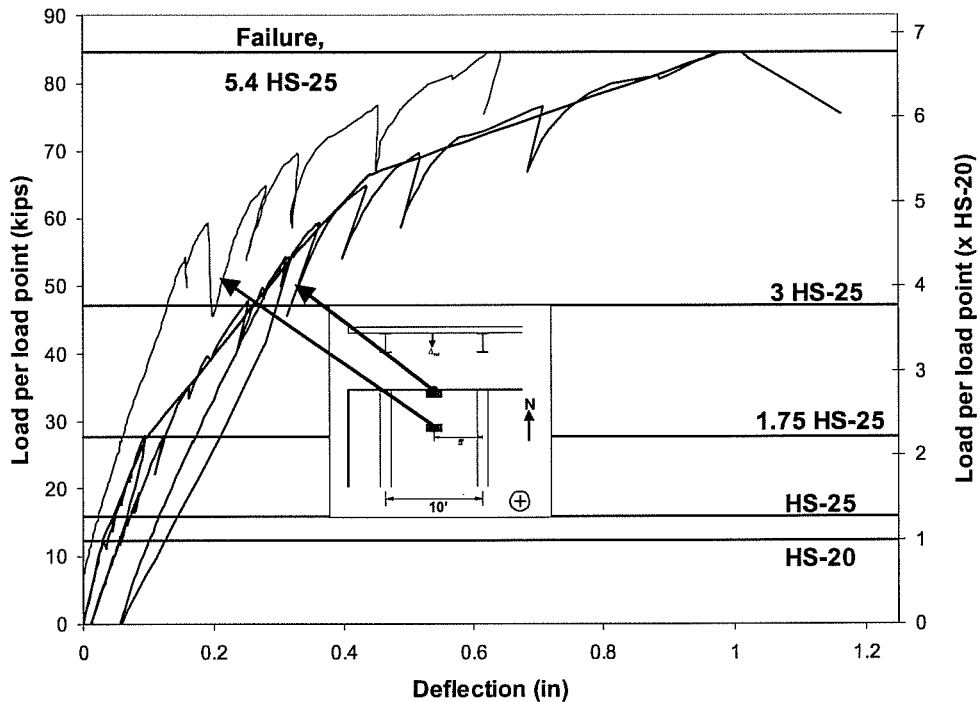
Figure 5.56 Relative midspan deflections and edge deflection envelope, SEJ, 6-in. top reinforcement spacing, positive-moment region

5.7.2.3 Load-Strain Response

Figure 5.57 shows strain measurements recorded on both faces of the girder and the midspan of the 10-ft bay. At serviceability load levels, strains were small, and maximum strains measured were essentially the same on either side of the girder.

At HS-20 and HS-25 load levels measured strains at the girder locations were less than 6% of yield strain (120 $\mu\varepsilon$). The strain at the face of the SEJ did not exceed 100 $\mu\varepsilon$ on either face of the girder at HS-20 and HS-25 load levels. Maximum strains measured at approximately 1.75 x HS-25 were 12% of yield strain (260 $\mu\varepsilon$) on the east face and 8% of yield strain (180 $\mu\varepsilon$) on the west face of the west-interior girder. The strain at the face of the SEJ did not exceed 200 $\mu\varepsilon$

180

on either face of the girder at 1.75 x HS-25. At 3 x HS-25, the load-strain response was no longer linear at any gauge location. Maximum strains measured at 3 x HS-25 were 22% of yield strain (500 με) on the east face and 18% of yield strain (410 με) on the west face of the girder between the load points. The maximum strain measured at the face of the SEJ was 370 με. None of the measured reinforcing bars reached yield strain. The maximum recorded strain, 67% of yield strain (1480 με), was recorded on the west face of the girder at the gauge on the fourth reinforcing bar from the slab edge. Maximum strain levels on the east face of the girder were 61% (1340 με) of yield strain at the fourth reinforcing bar from the slab edge. Maximum measured strain on the SEJ was 1280 με at the west face of the girder. At midspan, the average strain on the bottom surface of the panel in the exterior 10-ft bay was estimated to be about 7010 με over a 9 in. gage length (Figure 5.58).
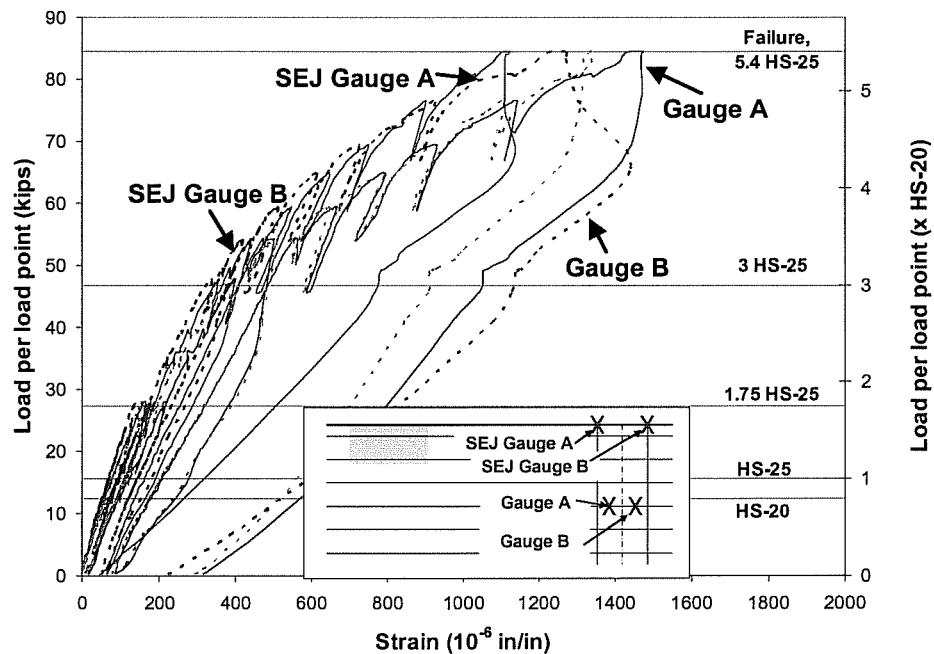
Figure 5.57 Load-strain response, SEJ, 6 in. top reinforcement spacing, positive-moment region
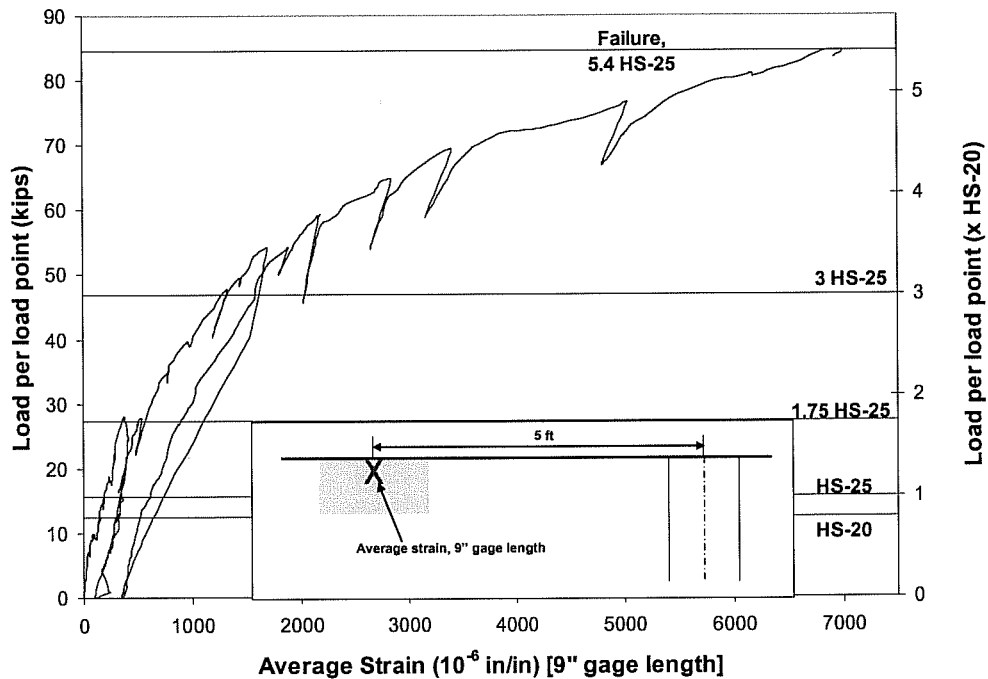
Figure 5.58 Load-average strain response, SEJ, 6 in. top reinforcement spacing, exterior 10-ft bay, midspan, bottom face of the panel

5.7.2.4 Strain Profiles

While the strain profiles show strains on the SEJ and reinforcing bars increasing with increasing load, strains at both HS-20 and HS-25 were relatively small, never exceeding 6% of yield strain (120 $\mu\epsilon$). Strain profiles from either face of the girder in the SEJ, 6 in. top reinforcement spacing, positive moment test section are shown in Figure 5.59 (a) and (b). In this test area, the largest strains occurred on the east face of the girder. The increase in strain from HS-20 to HS-25 is relatively small, where neither strain exceeds 6% of yield strain (120 $\mu\epsilon$). At loads HS-20 through 3 x HS-25, the strain distribution is essentially uniform through the edge region. The strain measured at face of SEJ is significant throughout loading.

182
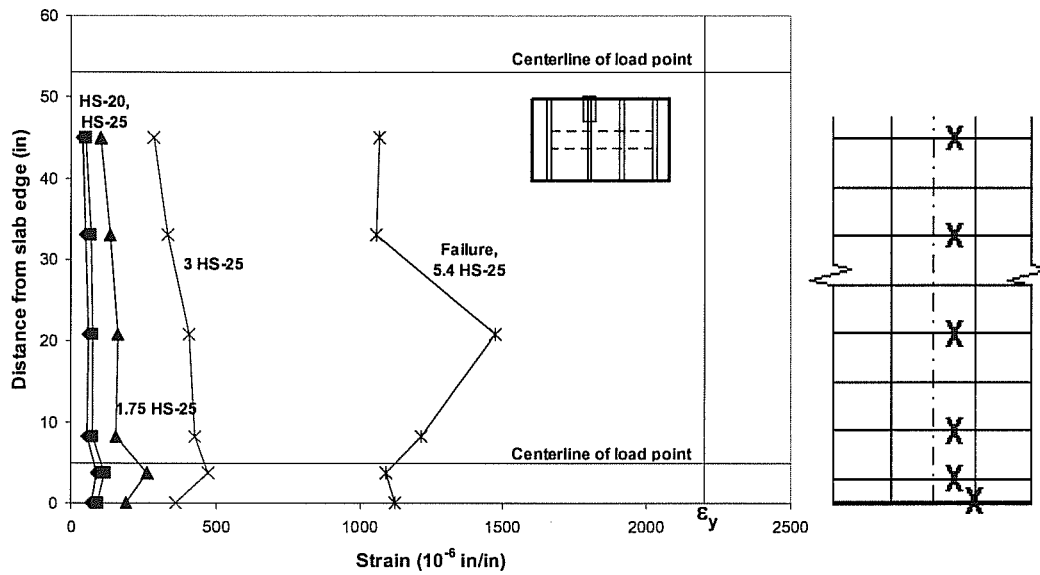
(a) east face of girder, top mat
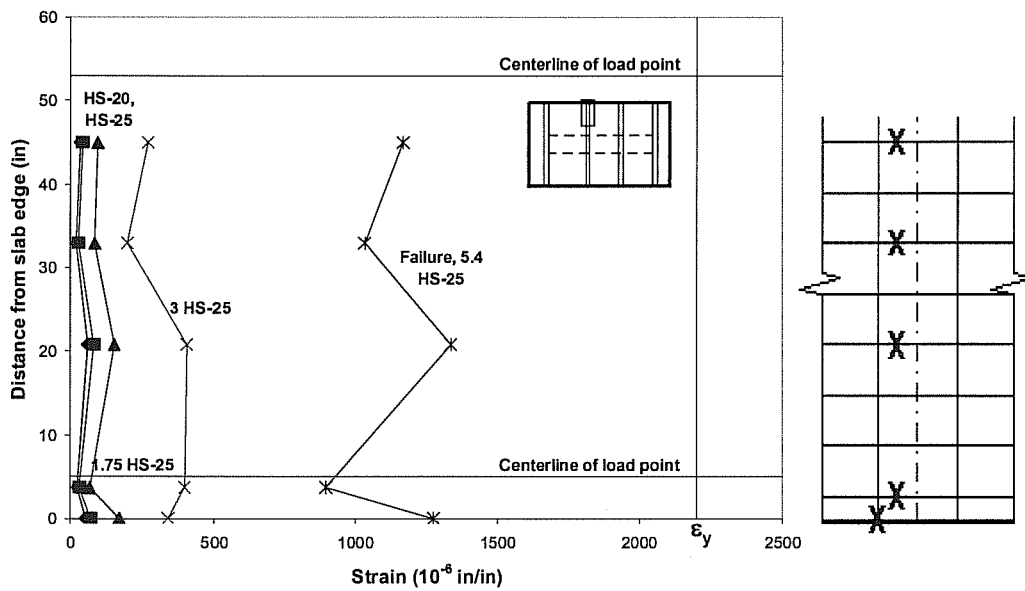
(b) west face of girder, top mat

Figure 5.59 Strain profiles, SEJ, 6 in. top reinforcement spacing, positive-moment region: (a) east face of girder, top mat; (b) west face of girder, top mat

5.7.2.5 Crack Maps

In Figure 5.60, Figure 5.61, and Figure 5.62, crack maps of the top, side and bottom of the test section are drawn illustrating cracks at 1.75 x HS-25 (first visible flexural cracking), 3.5 x HS-25 (load step after major change in stiffness), and 4.8 x HS-25 (load step before failure).

The crack map at 1.75 x HS-25 shows the size and shape of the initial flexural cracks occurring in the slab. In this test section, the first flexural cracks in the slab occurred on the bottom face of the panel at midspan of the west exterior 10-ft bay, in addition to increased crack widths of the shrinkage cracks. The largest crack width on the bottom face of the panel was 0.002 in. at 1.75 x HS-25. The largest crack width on top and side of the slab were 0.007 in. and 0.002 in.

The crack map at 3.5 x HS-25, 55 kips per load point, shows cracks that were observed at the load step after the major change in stiffness. At 3.5 x HS-25, on the top side of the slab, three flexural cracks were visible over the west-interior girder. These cracks began perpendicular to the slab edge (parallel to the girder) and then began to bend towards the loading plates. The largest measured crack width on the top side of the slab at this load step was 0.013 in. On the bottom face of the panels, the existing cracks running parallel to the girder extended much further at this load step than any previous load step. At 3.5 x HS-25, the largest measured crack width on the bottom face of the panels was 0.007 in.

The crack map at 4.8 x HS-25 shows crack formed during testing and just after failure. At failure, a large shear crack formed around the edge load point in the west exterior 10-ft bay. A shear crack developed on the side surface of the slab just prior to reaching 4.5 x HS-25 near the interior-west girder. The crack passed through both CIP concrete topping and the panel, with separation

184

occurring along the interface. The largest measured crack width on the side of the slab was 0.016 in., a shear crack near the west-interior girder on the west exterior 10-ft bay. Visible on the top of the slab were cracks that circled around the loading plates in both bays at 4.2 x HS-25, indicating a punching shear failure. These cracks circling the loading plates and a few flexural cracks along the length of the girder widened during the final loading stages. The largest measured crack width before failure was 0.025 in. at one of the cracks circling the edge loading plate in the west exterior 10-ft bay. As seen from underneath the slab at failure, a series of flexural cracks formed parallel to the girders in the west-exterior 10-ft bay, fanning out past the load points, indicating a yield line pattern. A large section of the panel spalled off near the west-interior girder at failure (Figure 5.65 c). Flexural cracks formed on the bottom face of the panels in both bays could be seen on the side of the slab. Several flexural cracks also formed beneath the location of the loading point 4 ft from the edge of the slab. All cracking was contained within the panel being loaded; cracks did not propagate into the adjacent panels.
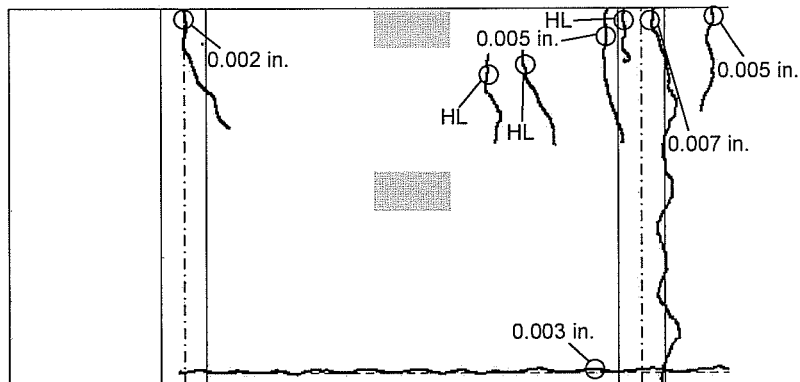
(a) 2.2 x HS-25 (first flexural cracking)
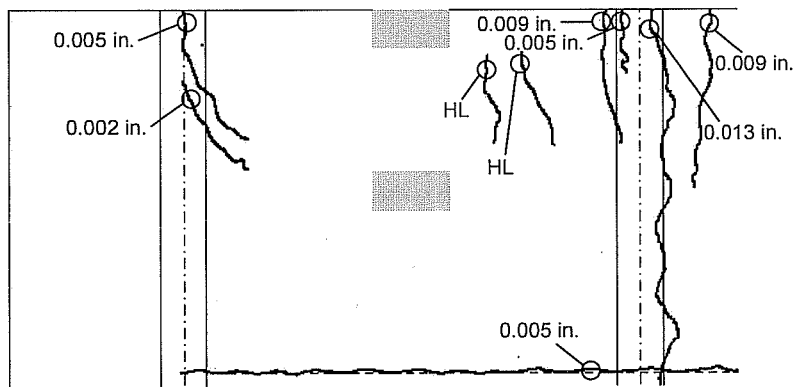
(b) 3.5 x HS-25 (developed cracking)
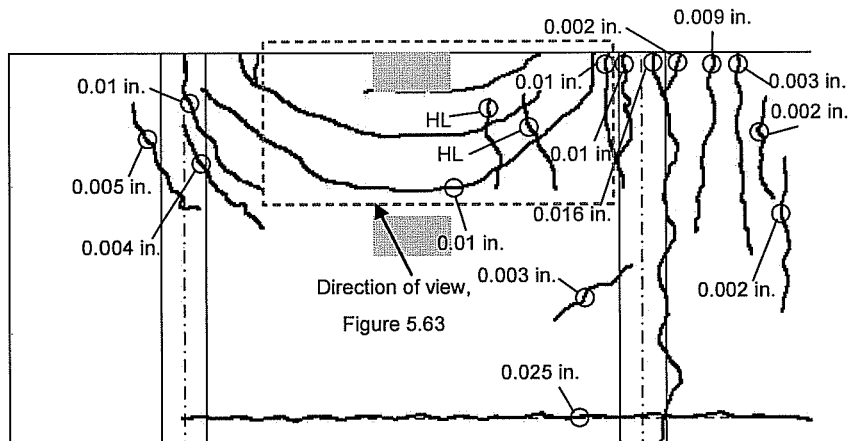
(c) 4.8 x HS-25 (failure)

Figure 5.60 Crack map, SEJ, 6 in. top reinforcement spacing, positive-moment region, top view of slab
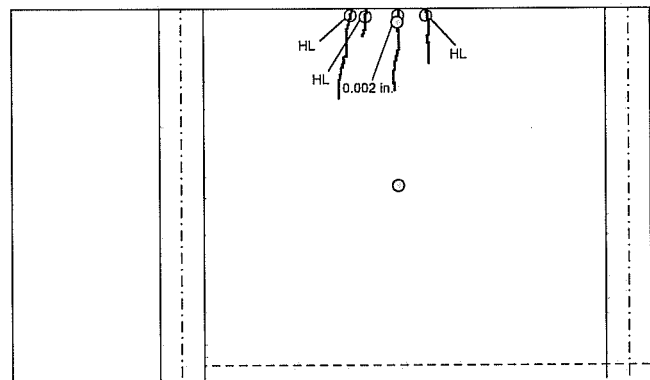
(e) 2.2 x HS-25 (first flexural cracking)
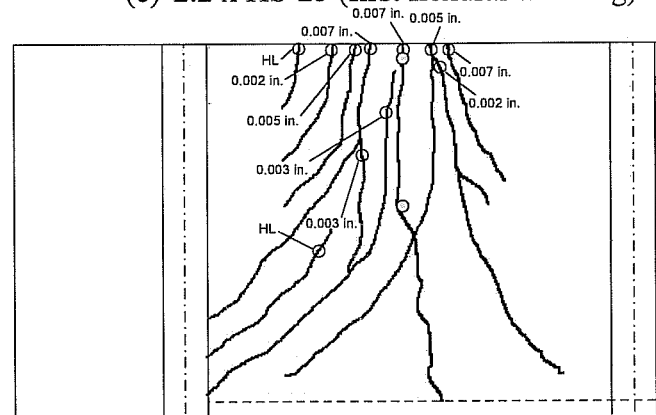
(b) 3.5 x HS-25 (developed cracking)
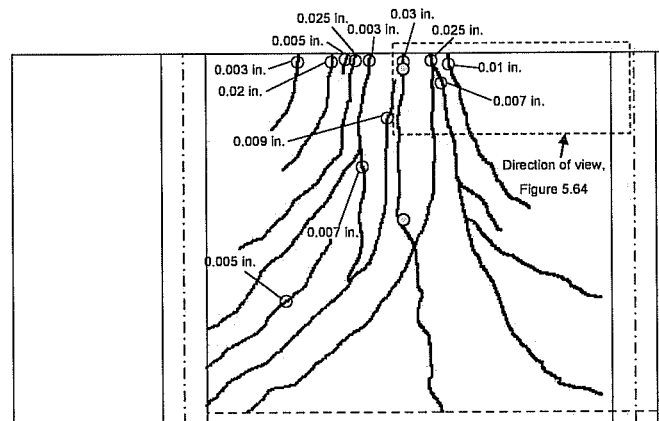
(c) 4.8 x HS-25 (failure)

Figure 5.61 Crack map, SEJ, 6 in. top reinforcement spacing, positive-moment region, bottom view of slab
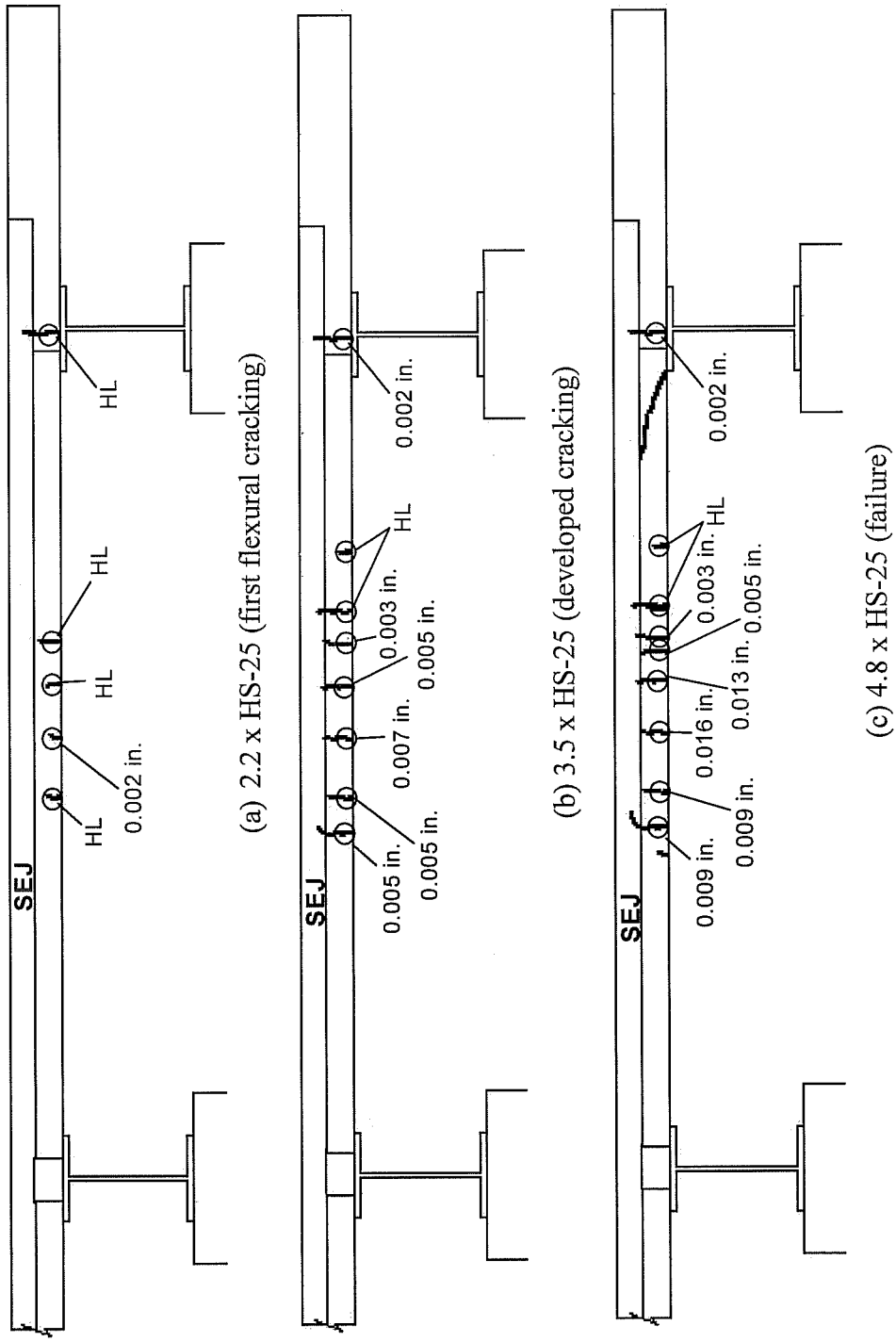
187

Figure 5.62 Crack map, SEJ, 6 in. top reinforcement spacing, positive-moment region, side view of slab

(a) 2.2 x HS-25 (first flexural cracking)

(b) 3.5 x HS-25 (developed cracking)

(c) 4.8 x HS-25 (failure)

5.7.2.6 Appearance after Failure

At 5.4 x HS-25, a punching shear failure occurred at the edge tire in the west exterior 10 ft bay. Pictures were taken of the failure surface (Figure 5.63, Figure 5.64, Figure 5.65). Cracks wrapping semi-circularly around the edge load point formed around 3.5 x HS-25 and existing flexural cracks opened on the top surface up to and at failure. A yield line pattern began to develop on the bottom surface of the panel, and cracking was confined to the panel section being loaded. From the side of the slab, shear cracks extend from the CIP topping behind the SEJ to the bottom of the panel, with the crack running along the interface near the west-interior bay. The side surface indicated some delamination (Figure 5.65 b) occurring between the panel and the CIP concrete topping at high loads and failure. Some separation was seen around 5.0 x HS-25. The failure surface is easily visible from beneath the slab. A large section up to the prestressing strand level near the west interior girder spalled off at failure.

Figure 5.63 West exterior 10-ft bay failure at top of slab, facing northwest

Figure 5.64 West exterior 10-ft bay failure at bottom of slab, facing northwest
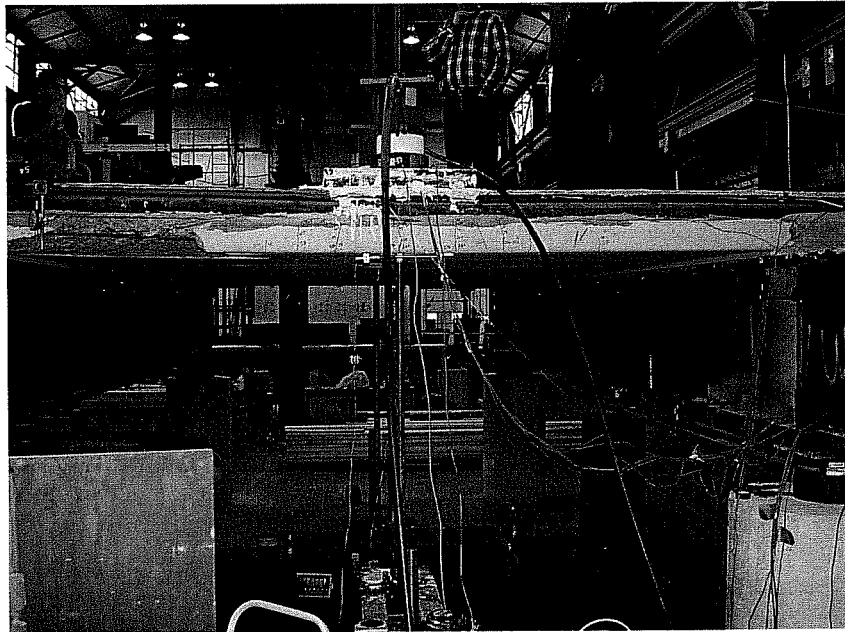
(a) facing south

(b) close up of spalled section

Figure 5.65 West exterior 10-ft bay failure at side of slab: (a) facing south; (b) close up of spalled section; (c) close up of delamination

191
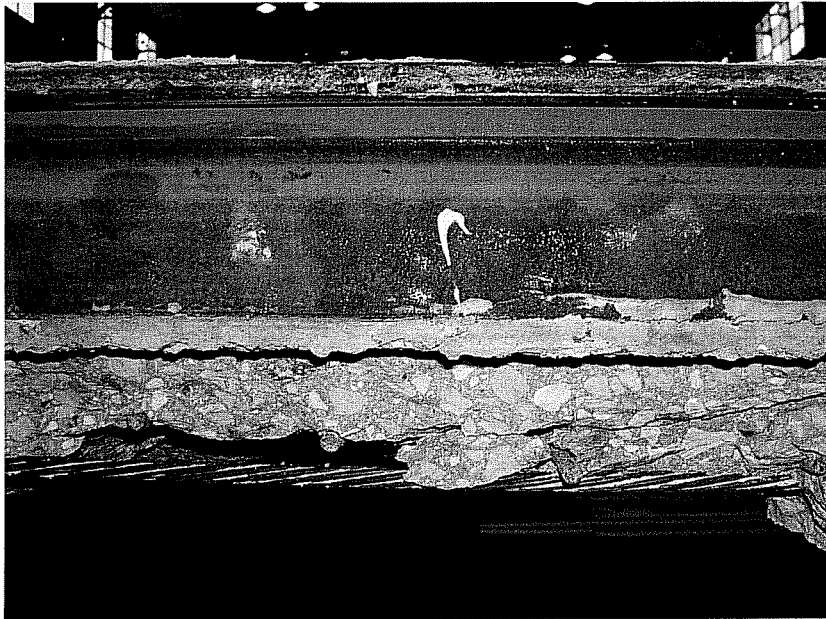
(c) close up of delamination

Figure 5.65 cont'd West exterior 10-ft bay failure at side of slab: (a) facing

south; (b) close up of spalled section; (c) close up of delamination

5.8 DISCUSSION AND COMPARISON OF EXPANSION JOINT EDGE TEST RESULTS

Figure 5.66 shows deflection envelopes for the six test areas on the PC panel specimen. Overall, the tests maximizing negative moments behaved similarly, and the test maximizing positive moments behaved similarly. In the negative-moment failure tests, reserve strength was higher, stiffness was greater, and deflections were smaller than in the positive-moment tests. All test areas exhibited first flexural cracking above design loads. The test areas with the AJ and SEJ rails exhibited a higher stiffness, lower tensile strains, and smaller deflection, than the test areas without AJ and SEJ rails.

192
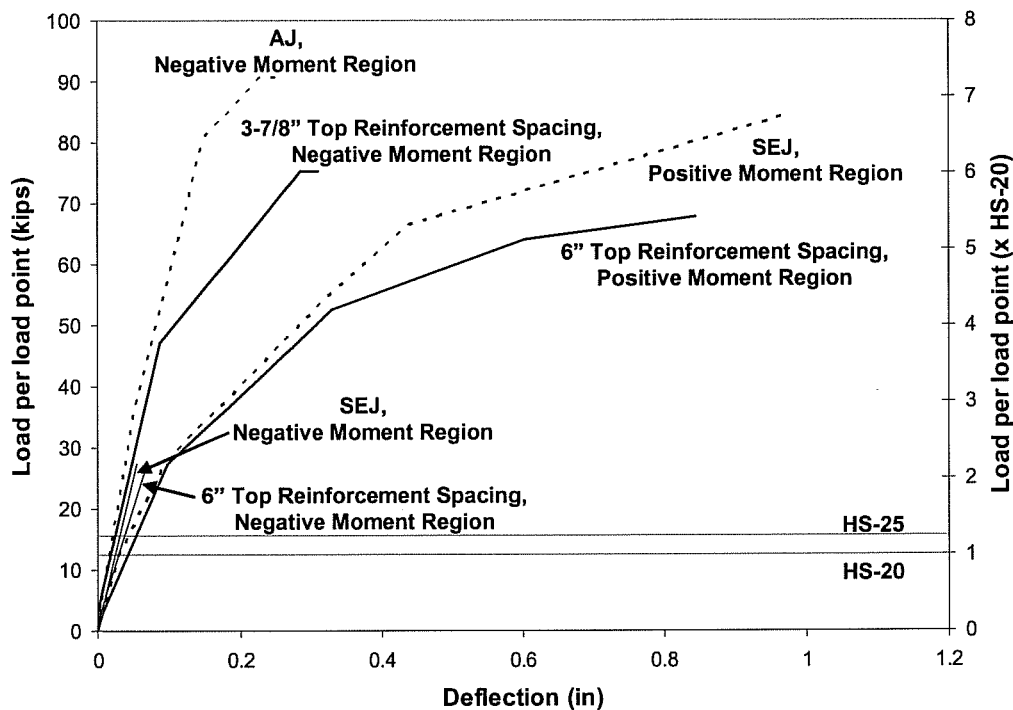
Figure 5.66 Deflection envelopes, all expansion joint edge tests

5.8.1 Negative-Moment Tests

Results from tests maximizing negative moments are summarized in Tables 5.7 through 5.10. Overall, the four negative moment test areas behaved similarly under AASHTO design loads. Deflections at the HS-20 load level were larger in the test areas without AJ and SEJ, and were extremely small (less than 1/4000 for all tests) compared to the girder spacing. Tensile strains at HS-20 were negligible, all under 10% of yield strain, and tensile strains at HS-25 did not exceed 15% in any test areas. Before failure, only one edge (Test Area 1, 3-7/8 in. top reinforcement spacing) observed yielding of the reinforcement. For all test areas, flexural cracking was first observed above the design loads. As shown in the following tables, the crack widths were larger at service load levels for the test

area with 6 in. top reinforcement spacing. The test area with a smaller top reinforcement spacing, 3-7/8 in., provided better control of crack widths at service load levels.

Table 5.7 Summary of 3-7/8 in. top reinforcement spacing, negative-moment region (Test Area 1)

| | 3-7/8 in. top reinforcement spacing, negative-moment region Test Area 1 | | | | |
| | Deflections | | | Maximum strains (% of steel yield strain) | Maximum crack width, negative moment region (in.) |
Load Step	Maximum relative deflection (in)	Flexural Cracked (Yes/No)	Clear span to relative deflection ratio		
HS-20	0.021	No	4570	6	0.007
HS-25	0.026	No	3700	7	0.007
1.75 HS-25	0.04	Yes	2400	9	0.009
3 HS-25	0.09	Yes	1070	30	0.013
Failure	0.37	Yes	160	300	0.02

Table 5.8 Summary of 6 in. top reinforcement spacing, negative-moment region (Test Area 2)

| | 6 in. top reinforcement spacing, negative-moment region Test Area 2 | | | | |
| | Deflections | | | Maximum strains (% of steel yield strain) | Maximum crack width, negative moment region (in.) |
Load Step	Maximum relative deflection (in)	Flexural Cracked (Yes/No)	Clear span to relative deflection ratio		
HS-20	0.028	No	4290	15	0.005
HS-25	0.039	No	3080	20	0.007
1.75 HS-25	0.071	Yes	1690	40	0.013

Table 5.9 Summary of SEJ, 6 in. top reinforcement spacing, negative-moment region (Test Area 5)

Load Step	SEJ, negative-moment region Test Area 5				
	Deflections			Maximum strains (% of steel yield strain)	Maximum crack width, negative moment region (in.)
	Maximum relative deflection (in)	Flexural Cracked (Yes/No)	Clear span to relative deflection ratio		
HS-20	0.026	No	4620	7	0.007
HS-25	0.033	No	3640	10	0.007
1.75 HS-25	0.056	Yes	2150	17	0.009

Table 5.10 Summary of AJ, 6 in. top reinforcement region, negative-moment region (Test Area 6)

Load Step	AJ, negative-moment region Test Area 6				
	Deflections			Maximum strains (% of steel yield strain)	Maximum crack width, negative moment region (in.)
	Maximum relative deflection (in)	Flexural Cracked (Yes/No)	Clear span to relative deflection ratio		
HS-20	0.017	No	5650	4	0.004
HS-25	0.021	No	4570	8	0.005
1.75 HS-25	0.038	No	2530	21	0.009
3 HS-25	0.075	Yes	1280	30	0.01
Failure	0.24	Yes	400	63	0.013

Figure 5.67 shows the locations of major cracks at failure in both of the two failure test areas for maximizing negative moment. For the 8-ft girder spacing, 3-7/8 in. top reinforcement spacing (Test Area 1), a punching shear failure initiated at the edge load plate of the interior bay. The failure surface formed at the edge load plate and then propagated toward the interior plate.

195

Test Area 6, AJ

loading plate where punching shear
failure initiated

—— failure surface, top view of slab

—— failure surface, bottom view of slab
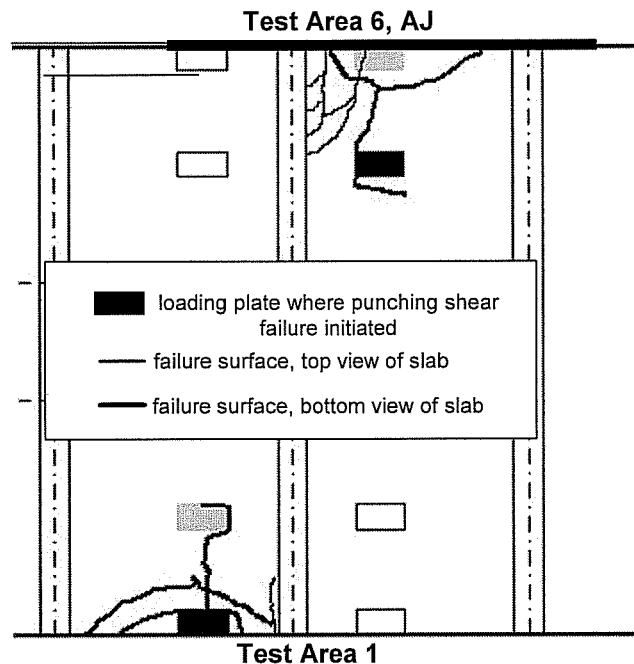
Test Area 1

Figure 5.67 Locations of punching shear failures, negative-moment tests

At the 8-ft girder spacing, AJ and 6 in. top reinforcement spacing (Test Area 6), punching shear failure initiated at the interior load plate of the exterior bay. The failure surface formed around the interior load plate, 4 ft from the AJ, and propagated toward the edge load plate. This failure surface indicates the presence of the AJ has an effect on the punching shear capacity of an edge plate location.

In the areas where negative moment was maximized, failure mechanisms were similar. Punching shear failure occurred on the side of the load points closest to a girder. In Test Area 6, punching shear failure began at the location away for the AJ. There was a 20% difference between the failure loads for Test Areas 1 and 6.

Punching shear capacities can be calculated using design provisions detailed in the ACI-318 code. Design provisions and predictions of capacity for all tests on this specimen are discussed in Sections 5.8.3 and 5.8.4.

196

5.8.2 Positive-Moment Tests

Table 5.11 and Table 5.12 summarize the results obtained from the tests maximizing positive moment. The SEJ edge detail had a slightly higher stiffness than the edge detail (6 in. top reinforcement spacing) without the SEJ rail, as seen in Figure 5.66. Deflections at the HS-20 load levels were almost 1.5 times larger in Test Area 3 than Test Area 4 (SEJ). However, both deflections were relatively small compared to the girder spacing (1/2000 for Test Area 3 and 1/3000 for Test Area 4). Tensile strains at HS-20 and HS-25 were small, less than 10% for both test areas. Strains were approximately 2.5 times higher in Test Area 3 compared to Test Area 4 at design load levels, where the SEJ contributed to the capacity of the edge region. None of the test areas experienced yielding of the reinforcing. For both test areas, flexural cracking was first observed around 1.75 x HS-25. In both tests, first flexural cracking caused a very small change in slab stiffness. The major change in stiffness coincided with multiple cracks forming and widening, and did not occur until approximately 3.5 x HS-25. The cracks were few and wider in Test Area 3, and the cracks were more frequent, smaller and narrower in Test Area 4.

Table 5.11 Summary of 6 in. top reinforcement spacing, positive-moment region (Test Area 3)

	6 in. top reinforcement spacing, positive-moment region Test Area 3				
	Deflections			Maximum strains (% of steel yield strain)	Maximum crack width, positive moment region (in.)
Load Step	Maximum relative deflection (in)	Flexural Cracked (Yes/No)	Clear span to relative deflection ratio		
HS-20	0.058	No	2070	8	N/A
HS-25	0.068	No	1770	15	N/A
1.75 HS-25	0.10	Yes	1200	16	0.003
3 HS-25	0.28	Yes	430	37	0.01
Failure	0.84	Yes	150	67	0.025

Table 5.12 Summary of SEJ, 6 in. top reinforcement spacing, positive-moment region (Test Area 4)

| Load Step | SEJ, positive-moment region Test Area 4 | | | | |
| | Deflections | | | Maximum strains (% of steel yield strain) | Maximum crack width, positive moment region (in.) |
	Maximum relative deflection (in)	Flexural Cracked (Yes/No)	Clear span to relative deflection ratio		
HS-20	0.039	No	3080	3	N/A
HS-25	0.049	No	2450	6	N/A
1.75 HS-25	0.10	Yes	1200	12	0.002
3 HS-25	0.25	Yes	480	22	0.007
Failure	1.01	Yes	120	67	0.03

Figure 5.68 shows the locations of major cracks at failure in both of the test areas where positive moment was maximized. Both test areas failed in punching shear, at loads close to that predicted by the corresponding provisions of ACI 318-02.

Test Area 4, SEJ

loading plate where punching shear failure occurred

loading plate

—— failure surface, top view of slab

—— failure surface, bottom view of slab

Test Area 3
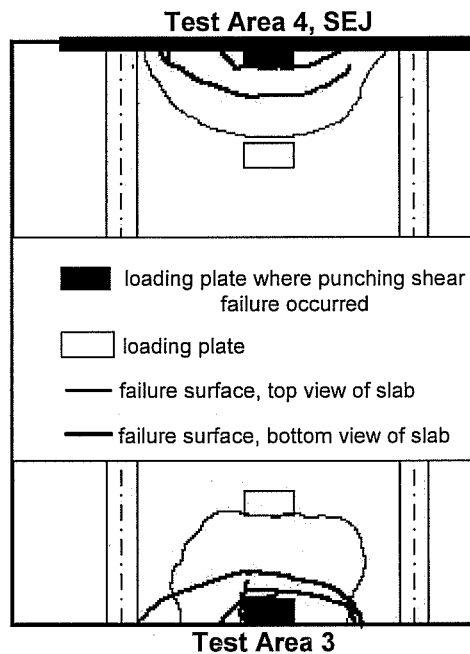
Figure 5.68 Locations of punching shear failures, positive-moment region

The SEJ edge region had a higher capacity than the edge region without the SEJ rail. The 25 % difference in capacities is mostly likely due to the contribution of the SEJ rail. Each edge region had a similar failure surface around the edge load plate. Both test areas showed some signs of delamination, although the delamination was greater in Test Area 3 than Test Area 4 (SEJ). A section of the panel spalled off in both test areas near the interior girder at failure in both test areas.

5.8.3 Observed Punching-Shear Capacity of Bridge Slab Compared to Calculated Nominal Capacity by AASHTO and ACI Provisions

Nominal punching shear capacity is calculated using Section 5.13.3.6 of the AASHTO LRFD Bridge Design Code, repeated in Equation 5.1

$$v_c = \min\left\{ 4\sqrt{f_c'}; \left(\frac{1}{2} + \frac{1}{B}\right) 4\sqrt{f_c'} \right\}$$

Equation 5.1

199

These equations are the same as those proposed by ACI 318-02 in Section 11.12 for a uniform shear distribution (Equation 5.2). ACI 318-02 has one additional equation, and requires that punching shear capacity be computed as the minimum of the terms in Equation 5.2:

$$v_c = \min\left\{ 4\sqrt{f_c'} \; ; \left(\frac{\alpha_s}{(b_o/d)} + 2 \right)\sqrt{f_c'} \; ; \left(\frac{1}{2} + \frac{1}{B} \right)4\sqrt{f_c'} \right\} \qquad \textbf{\textit{Equation 5.2}}$$

where f_c' is the specified concrete compressive strength; b_o is the length of the critical perimeter; d is the effective depth of the slab, α_s is the 40 for interior loading cases and 30 for edge loading cases; and B is the ratio of the length of the longest side of the loaded area to the shorter side. Based on these parameters, the nominal punching-shear capacity of the slab is:

$$V_c = v_c b_o d \qquad \textbf{\textit{Equation 5.3}}$$

ACI 318-02 and the AASHTO LRFD Bridge Specification provisions require the critical perimeter to be calculated at a distance d/2 from the edge of the loading point. For loading at the edge of a slab, the minimum critical, shown in Figure 5.69, includes three sides of the loading plate. (Ryan 2003 and Griffith 2003)
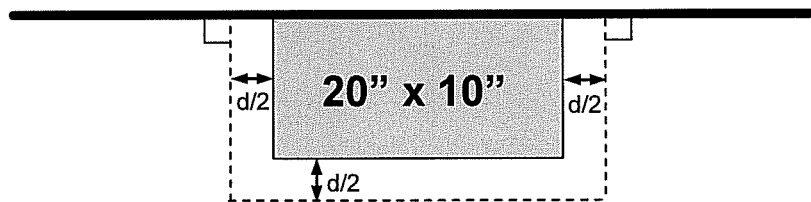
Figure 5.69 Critical perimeter used to determine punching-shear capacity with uniform stress distribution on the perimemter of the critical section

The observed punching-shear capacities from the PC panel specimen failure tests are compared with the nominal capacity by ACI 318-02 provisions

(Equation 5.2 and Equation 5.3), assuming a uniform shear distribution on the perimeter of the critical section in Table 5.13. Similar to TxDOT design procedures, the contribution of the AJ and SEJ were not included in the nominal capacities computed by ACI 318-02 provisions. The concrete compressive strength was adjusted to account for the CIP topping and the PC panels. For the some of the tests on the PC panel specimen, the assumption of uniform stress distributions result in unsafe predictions of punching-shear capacity. The punching capacity of the bridge slab, loaded with an AASHTO load configuration, is only about 80% to 90% of that predicted by ACI 318-02 and AASHTO LRFD provisions, assuming a uniform shear stress distribution.

Table 5.13 Calculated and experimental punching shear capacities

Calculated Punching Shear Capacity, V_{ACI}			
Uniform Shear Stress Distribution		Eccentric Shear Model	
84 kips		52 kips	
Edge Detail	Girder Spacing (ft)	Section (Negative or Positive)	Experimental Punching Shear Capacity (kips)
3-7/8 in. TS	8 ft	Negative	75
6 in. TS	10 ft	Positive	68
AJ	8 ft	Negative	85
SEJ	10 ft	Positive	91

The shape of the critical section assumed in the previous analysis for punching shear did not adequately predict the shape of the failure surface for the edge loading configuration in the PC panel specimen. Figure 5.70 shows the shape of a typical failure surface, as observed from the top of the slab. In the observed failure surfaces, the critical perimeter is longer than that used in the previous calculations. For the failure surface shown in Figure 5.70, the centroidal axis of the critical perimeter does not coincide with the centroidal axis of the

loaded area, resulting in unbalanced moments. ACI 318-02 uses an eccentric shear model to account for this, assuming that a portion of the unbalanced moment is transferred through an eccentricity of shear around the loaded area. A conservative of ultimate strength might be attained by varying the shape of the critical perimeter and applying the eccentric shear model, as seen in Table 5.13. Currently AAHSTO LRFD Bridge Design Specifications do not include an eccentric shear model. (Griffith 2003).

observed shape
of failure surface
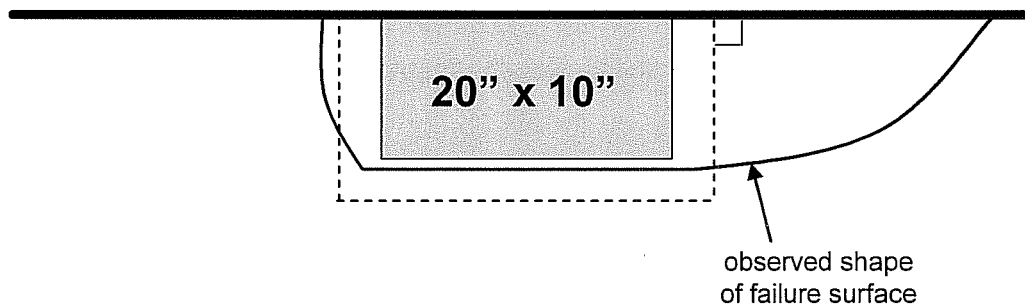
Figure 5.70 Comparison of critical section based on ACI 318-02 and typical failure surface

5.9 PUNCHING SHEAR TESTS

In addition to the expansion joint edge tests, two additional punching shear tests were conducted, one at a location over the panel butt joint and one in an interior location on a panel. The additional punching shear tests were completed to obtain a better understanding of the behavior of the composite section of PC panel and CIP concrete topping.

Since the behavior and ultimate capacity were the primary goal of these tests, strain gauges and linear potentiometers to estimate the strain in the PC panel were not attached to these test areas. Only two linear potentiometers were used to measure the vertical deflection of the PC panel. One linear potentiometer was

placed one foot on either side of the panel butt joint on the joint punching shear test. This set up was repeated at the interior punching shear test.

The punching shear ultimate capacity of the two tests was calculated using ACI and AASHTO guidelines prior to testing. The calculated capacities exceeded 120 kips per load point, which is the ultimate capacity of the loading rods and loading frame. Therefore, punching shear capacity could not be reached in either test.

5.9.1 Joint Punching Shear Test

5.9.1.1 Summary of Response

The joint punching shear area was loaded to 120 kips over the joint between two adjacent panels. First cracking was visible at 55 kips, 3.5 x HS-25, on the bottom face of the panels, in addition to the widening of the cracks formed during Test Area 1. At 100 kips, 6.4 x HS-25, significant cracking and degradation occurred. At 118 kips, the load deflection response indicates a slight change in stiffness. All cracking on the bottom face of the panel was contained within the panels being loaded. The cracks on the bottom face of the panel do not indicate that the joint has an effect on the cracking pattern. Most of the cracks that reach the joint on one panel have a nearly identical crack on the adjacent panel.

Based on the load deflection and load deformation responses, the test area performed well at HS-20 and HS-25. The maximum measured deflection at 120 kips on either side of the joint was 0.17 in. However, the test area did not reach its ultimate capacity before 120 kips. Therefore the ultimate capacity is expected to highly exceed the design load levels.

203

5.9.1.2 Detailed Description of Response

5.9.1.2.1 Loading

As mentioned in Section 5.9, the joint punching shear test was tested where the load plate was seated over the joint between to panels. The test area was loaded after all the expansion joint edge and overhang tests were completed. The area was first loaded up to 100 kips (6.4 x HS-25) and then unloaded. The load cell was then removed, and the area was then loaded to approximately 120 kips (7.7 x HS-25) as measured by the pressure transducer.
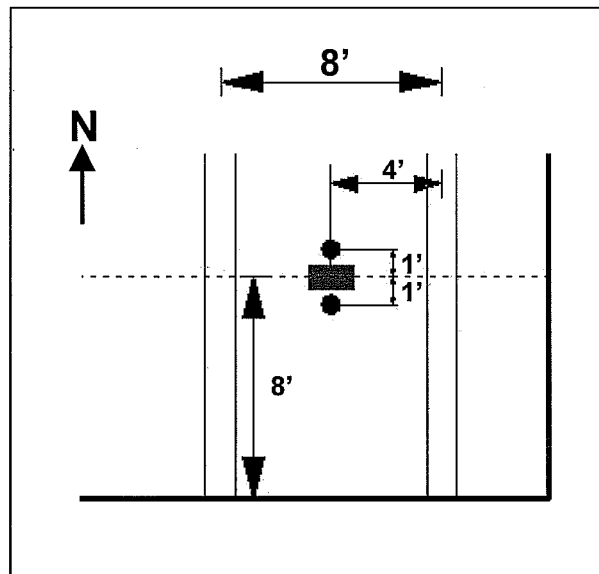
Figure 5.71 Joint punching shear test

5.9.1.2.2 Load-Deflection Response and Envelope

A load-deflection response and envelope is shown in Figure 5.72. The load-deflection response is linear elastic up to approximately 118 kips (7.6 x HS-25). The two linear potentiometers on either side of the joint measured essentially the same deflection and slope throughout the test. The maximum measured

204

deflection at HS-20 and HS-25 was 0.0038 in. and 0.0044 in. The maximum
measured deflection at 120 kips was 0.17 in.
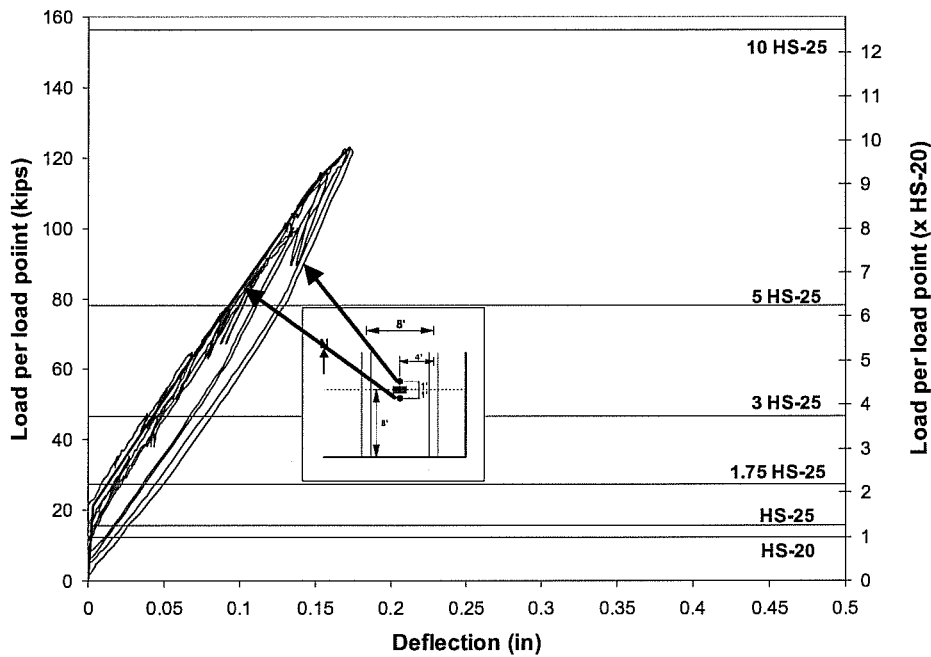
Figure 5.72 Load-deflection envelope, joint punching shear test

5.9.1.2.3 Crack Maps

Similar to the expansion joint edge tests, the locations, widths and lengths
of cracks were photographed, measured and used to produce crack maps that
would convey the pattern and extent of cracking at multiple load levels. The
crack maps for 55 kips (first cracking) and 120 kips (maximum load) are shown in
Figure 5.73.

At 55 kips, the first cracks developed on the bottom surface of the panels
under the loading point and existing cracks from Expansion Joint Edge Test Area
1 began to widen. The two new cracks lined up with each other on either side of

the joint under the load point. These cracks were barely visible, and the existing crack from Test Area 1 had a crack width of 0.002 in.

At 100 kips, several new cracks formed and existing cracks elongated and widened, indicative of a change in stiffness. All cracks began parallel to the girders and then began to bend towards the girders after a certain distance. The largest crack width on the bottom surface of the panel was 0.005 in. At 120 kips, three new cracks developed similar to the previous cracks, where they began parallel to the girder and then bend towards the girders. The largest crack width at 120 kips was 0.007 in. at the crack under the load point near the joint. As seen in Figure 5.73, the cracks on the bottom face of the panel do not indicate that the joint has an effect on the cracking pattern. Most of the cracks that reach the joint on one panel have a nearly identical crack on the adjacent panel.
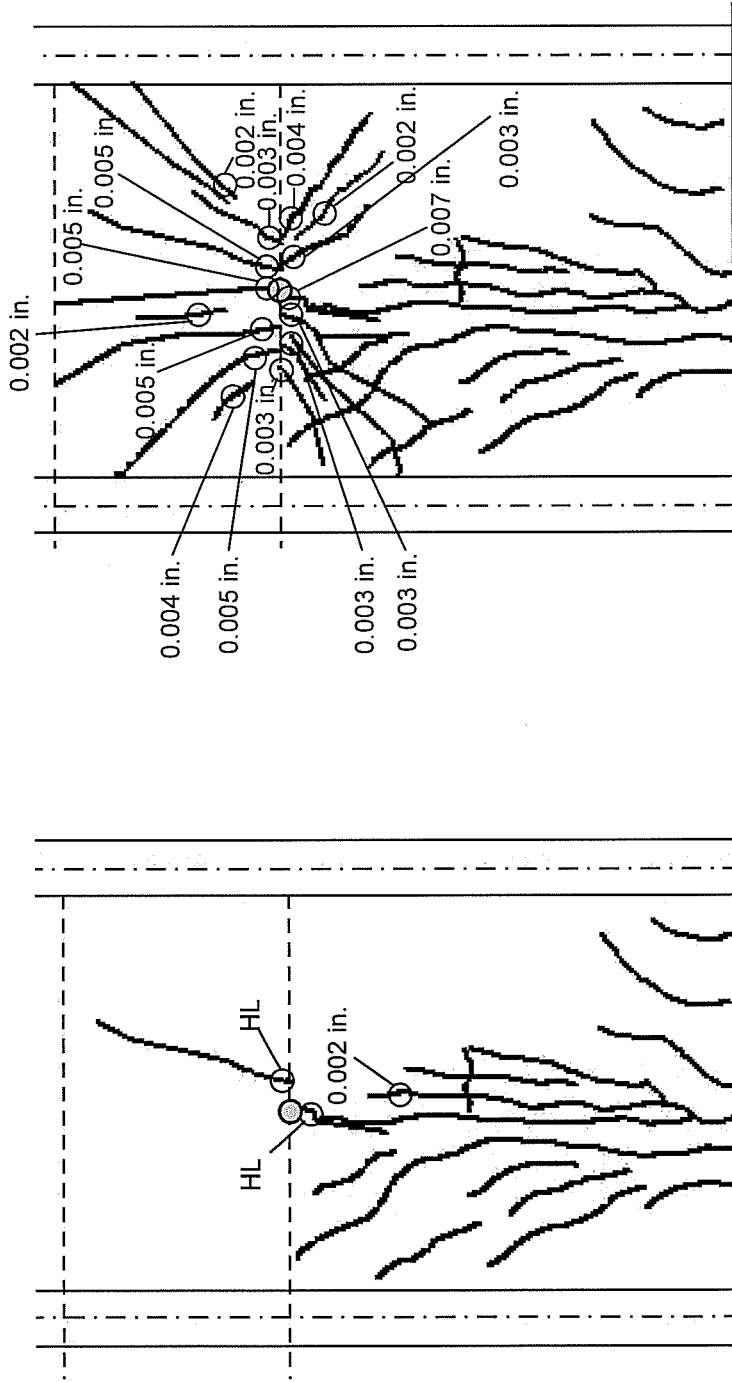
(a) 55 kips (first cracking)

(b) 120 kips (maximum load)

Figure 5.73 Crack map, joint punching shear test, bottom view of slab

207

5.9.2 Interior Punching Shear Test

5.9.2.1 Summary of Response

The interior punching shear area was loaded to 145 kips at in interior location of a panel. First cracking was visible at 37 kips, 2.4 x HS-25, on the bottom face of the panels, in addition to the widening of the cracks formed during Test Areas 5 and 6. At 100 kips, 6.4 x HS-25, significant cracking and degradation occurred. At 120 kips, the load deflection response indicates a slight change in stiffness. All cracking on the bottom face of the panel was contained within the panel being loaded. Most cracks began under the load point and then fanned towards the girders and the edges of the panels.

Based on the load deflection and load deformation responses, the test area performed well at HS-20 and HS-25. The maximum measured deflection at 120 kips and 145 kips was 0.17 in. and 0.25 in. However, the test area did not reach its ultimate capacity before 145 kips. Therefore the ultimate capacity will highly exceed the design load.

5.9.2.2 Detailed Description of Response

5.9.2.2.1 Loading

The interior punching shear test was tested at an interior location of the PC panel. The interior load point in the interior bay for Test Area 6 was chosen since there little damage occurred in that area during Test Area 6. The test area was loaded after the joint punching shear test was completed. The area was first loaded up to 100 kips (6.4 x HS-25) and then unloaded. The load cell was then removed, and the area was then loaded to approximately 120 kips (7.7 x HS-25) as measured by the pressure transducer. At 120 kips, the test area began to show

208

signs of failure. The test area was then loaded further to approximately 145 kips, but did not reach failure.
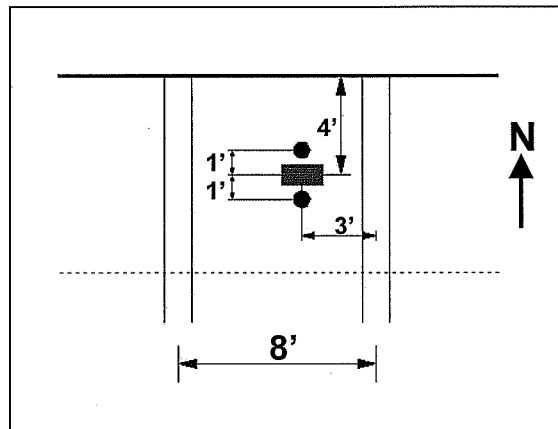
Figure 5.74 Interior punching shear test

5.9.2.3 Load-Deflection Response and Envelope

A load-deflection response and envelope is shown in Figure 5.75. The load-deflection response indicates a linear elastic response up to approximately 120 kips (7.7 x HS-25). The two linear potentiometers measured essentially the same deflection and slope throughout the test. The maximum measured deflection at HS-20 and HS-25 was 0.016 in. and 0.017 in. The maximum measured deflection at 120 kips and 145 kips was 0.17 in. and 0.25 in., respectively.
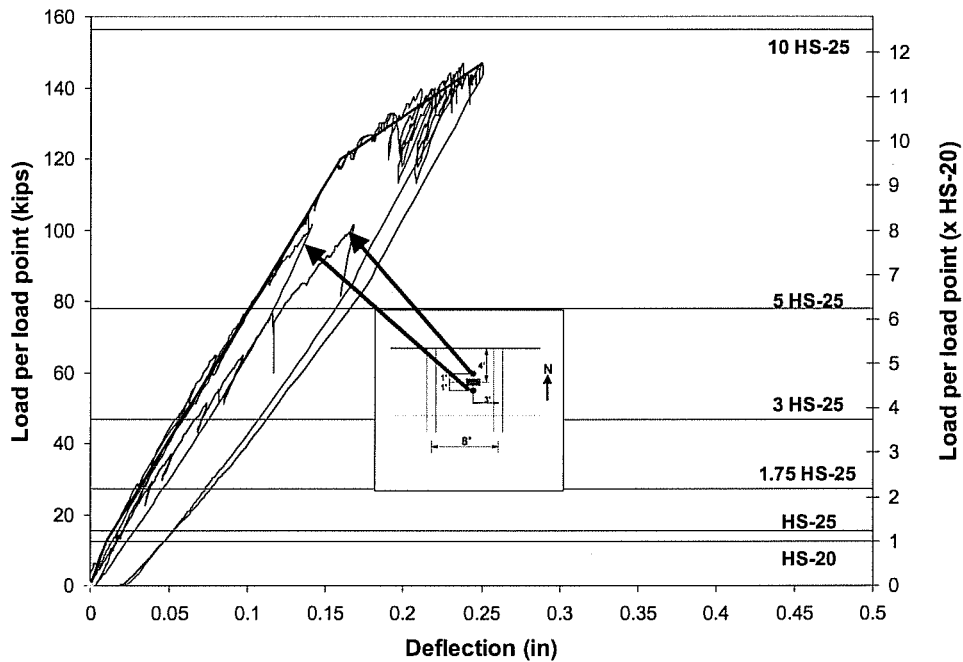
Figure 5.75 Load-deflection envelope, interior punching shear test

5.9.2.4 Crack Maps

Figure 5.76 shows the crack maps for 37 kips (first cracking) and 140 kips (load step prior maximum load).

At 37 kips, the first cracks developed on the bottom surface of the panels and existing cracks from Test Areas 5 and 6 began to widen. The three new cracks formed under the load point that fanned out towards the girders and the edge of the panel. The largest crack width of the new cracks was 0.002 in. In addition to these new cracks, previous cracks from Expansion Joint Edge Test Areas 5 and 6 began to widen, maximum width of 0.004 in.

At 100 kips, several new cracks formed and existing cracks elongated and widened, indicative of a change in stiffness. All cracks began near the underside of the load point and then fanned out towards the girders and the edges of the panels. The largest crack width on the bottom surface of the panel was 0.009 in.

210

As mentioned in Section 5.9.2, at 120 kips, the test area began to show signs of impending failure, so the test area was loaded to 145 kips. Even though failure did not occur at 145 kips, a large crack running diagonally from the load to the corner of the panel formed measuring a width of 0.02 in. Similar to all tests, all cracking was contained within the panel being loaded and did not propagate into adjacent panels.
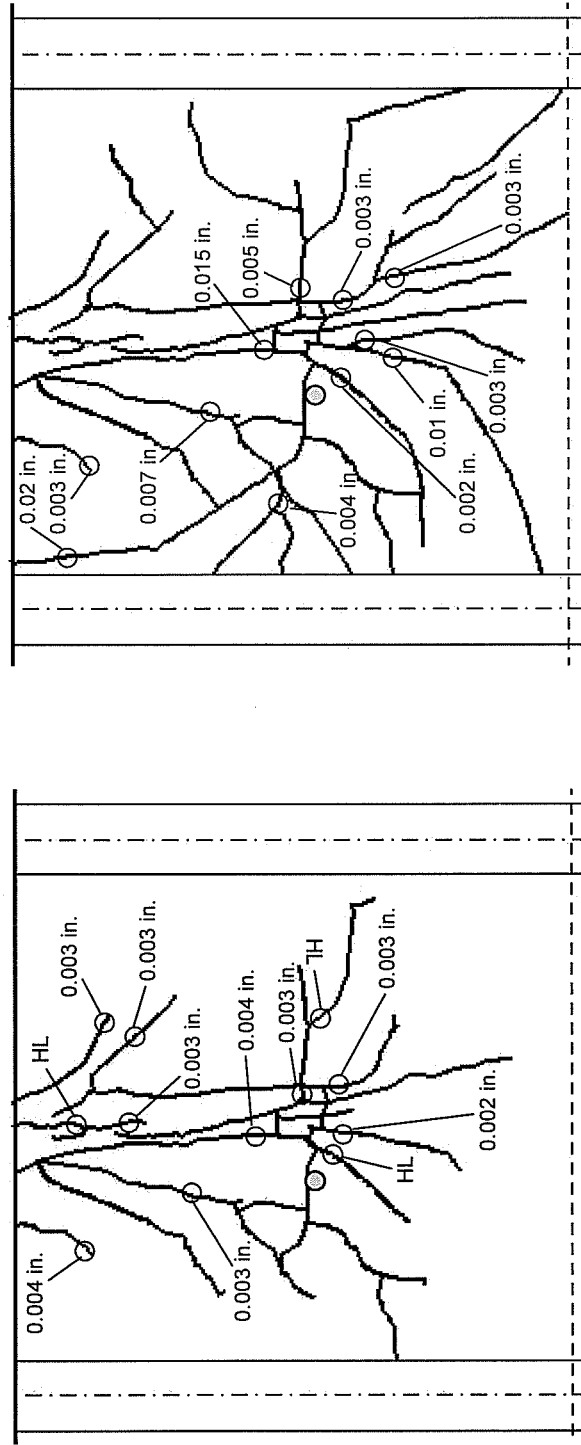
(a) 37 kips (first cracking)

(b) 140 kips (load step prior to maximum load)

Figure 5.76 Crack map, interior punching shear test, bottom view of slab

212

5.10 DISCUSSION AND COMPARISON OF PUNCHING SHEAR TEST RESULTS

Figure 5.77 shows the deflection envelopes for the two punching shear test areas. The joint punching shear test area had a higher stiffness than the interior punching shear test area. This decrease in stiffness in the interior punching shear test area may have been due to the previous testing done in the area from Test Areas 5 and 6. At 120 kips, the two test areas had nearly the same measured deflection, approximately 0.17 in. Each test area had deflections less than 0.05 in. at HS-20 and HS-25 load levels. For both test areas, cracking was first observed past the design load level. Cracking was first observed in the interior punching shear test area at a lower load than the joint punching shear test area.
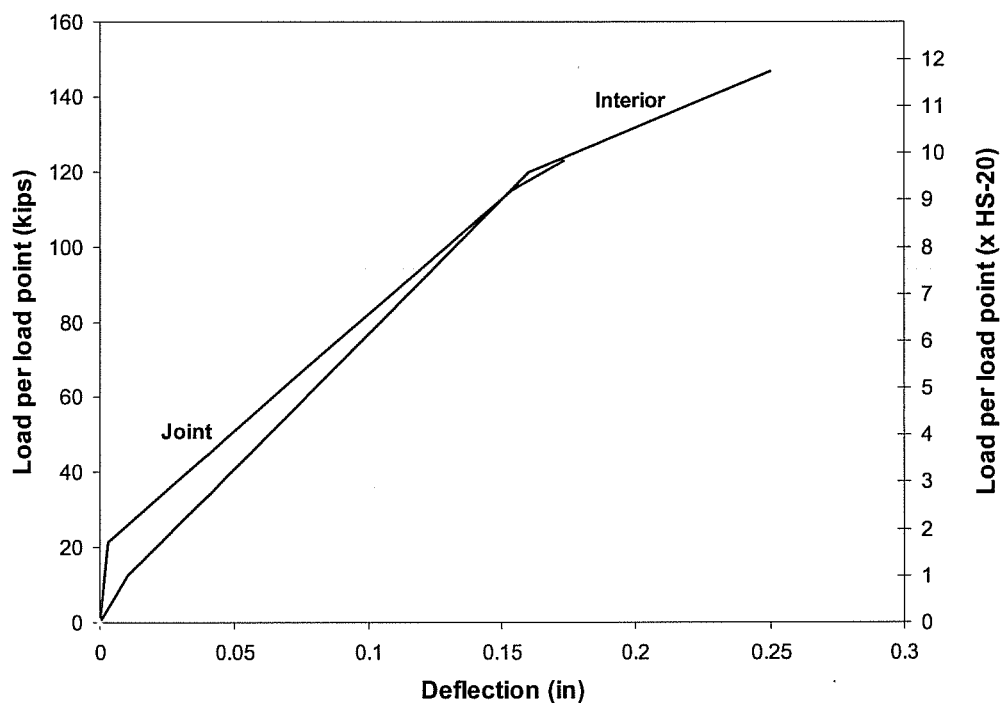
Figure 5.77 Deflection envelopes, punching shear tests

Table 5.14 Summary of interior and joint punching shear tests

Load Step	Joint Punching Shear Test			Interior Punching Shear Test		
	Maximum deflection (in)	Cracked (Yes/No)	Clear span to relative deflection ratio	Maximum deflection (in)	Cracked (Yes/No)	Clear span to relative deflection ratio
HS-20	0.0038	No	25260	0.011	No	8730
HS-25	0.0044	No	21820	0.017	No	5650
1.75 HS-25	0.021	No	4570	0.032	No	3000
3 HS-25	0.051	No	1880	0.058	Yes	1660
5 HS-25	0.10	Yes	960	0.10	Yes	960
6.4 HS-25	0.14	Yes	690	0.13	Yes	740
7.7 HS-25	0.17	Yes	570	0.17	Yes	570

Cracking on the bottom surface of the panels indicated an impending punching shear failure. The cracks began under the load point and then bend towards the girders and the edges of the panels. The joint between adjacent panels did not affect the cracking patterns. Crack widths were similar at higher loads. At 120 kips, the maximum crack width for joint punching shear test was 0.007 in., and the maximum crack width for the interior punching shear test was 0.01 in.

The load deflection and cracking indicates that the composite section in both the joint and interior panel locations performed well at HS-20 and HS-25. Failure did not occur at either test area during loading to the maximum load allowed by the test set-up (145 kips). Failure would be expected to well exceed the design loads.

5.10.1 Observed Punching-Shear Capacity of Bridge Slab Compared to Calculated Nominal Capacity by AASHTO and ACI Provisions

As discussed in Section 5.8.3, the punching shear capacities were calculated using Equation 5.2 and Equation 5.3. The concrete compressive strength, f_c', was assumed to be 4550 psi, an average of the compressive strengths

of the CIP topping and the PC panels. Since the two tests are at locations in the interior of the slab, the critical perimeter include all four sides of the load plate. The effective depth assumed to be the distance to the prestressing strands. The predicted punching shear capacity for these two test areas was 135 kips. The maximum applied load was approximately 145 kips, and neither test area failed. The calculated AASHTO and ACI punching shear capacity is conservative for interior locations.

5.11 SUMMARY

Details of the six test areas on the PC panel specimen were as follows:

- Test Area 1 – 3-7/8 in. top reinforcement spacing, negative-moment region, failure
- Test Area 2 – 6 in. top reinforcement spacing, negative-moment region, serviceability
- Test Area 3 - 6 in. top reinforcement spacing, positive-moment region, failure
- Test Area 4 – SEJ, 6 in. top reinforcement spacing, positive-moment region, failure
- Test Area 5 – SEJ, 6 in. top reinforcement spacing, negative-moment region, serviceability
- Test Area 6 – AJ, 6 in. top reinforcement spacing, negative-moment region, failure

Each was loaded with the AASHTO design tandem load configuration. Deflections, reinforcing bar strains, and crack development and propagation are discussed for each section.

215

Overall, the edge regions with and without AJ and SEJ rails performed well at HS-20 and HS-25 load levels. At these loads, reinforcing bar strains did not exceed 15% of yield strain, flexural cracking was minimal, and deflections were small relative to girder spacing (between 1/2000 and 1/3000). Each test area had stresses due to shrinkage and thermal effects that resulted in cracks developing at loads lower than design levels. All test areas did not develop flexural cracking until at least 1.75 x HS-25.

Negative moment loading produced punching shear failures at around 5 x HS-25, and positive moment at around 4.5 x HS-25. All test areas failed in punching shear at the edge load plate, with the exception of the AJ, negative-moment region, which initiated at the interior load plate.

In the test areas with 3-7/8 in. top reinforcement spacing and the AJ and SEJ rails, the cracks were narrower and more numerous than cracks formed in the 6 in. top reinforcement spacing edge region. The edge regions with and without expansion rails had essentially identical load-deflection responses. Tensile strains in the top flexural reinforcement were significantly lower in the edge regions containing the expansion joint rails. Tensile strains did not exceed yield, except for the 3-7/8 in. top reinforcement spacing edge region. Based on measured strains, the SEJ and AJ rails contributed to the capacity of the edge region. In both negative- and positive-moment regions tested to failure, the edge regions containing the expansion joint rails had a higher ultimate capacity.

CHAPTER 6

Test Results – Overhang Tests

6.1 INTRODUCTION

A total of four overhang tests were conducted on the PC panel specimen to study the performance of representative TxDOT details for overhangs. Overhang reinforcement was detailed according to TxDOT standards for PC panel bridge decks, with and without armor and sealed expansion joint rails (AJ/SEJ). In this chapter, results from the overhang tests are presented and discussed.

6.1.1 Overhang Test Areas

For the PC panel specimen, four overhang tests were performed (Figure 6.1):

- 3-7/8 in. top reinforcement spacing (Overhang Test Area 1)
- 6 in. top reinforcement spacing (Overhang Test Area 2)
- Armor expansion joint (AJ) (Overhang Test Area 3)
- Sealed expansion joint (SEJ) (Overhang Test Area 4).

Overhang Test 3

SEJ   SEJ

Overhang Test 4

AJ   AJ

2 ft.

Overhang Test 2

6 in. top reinforcement
spacing

Overhang Test 1

3-7/8 in. top
reinforcement spacing
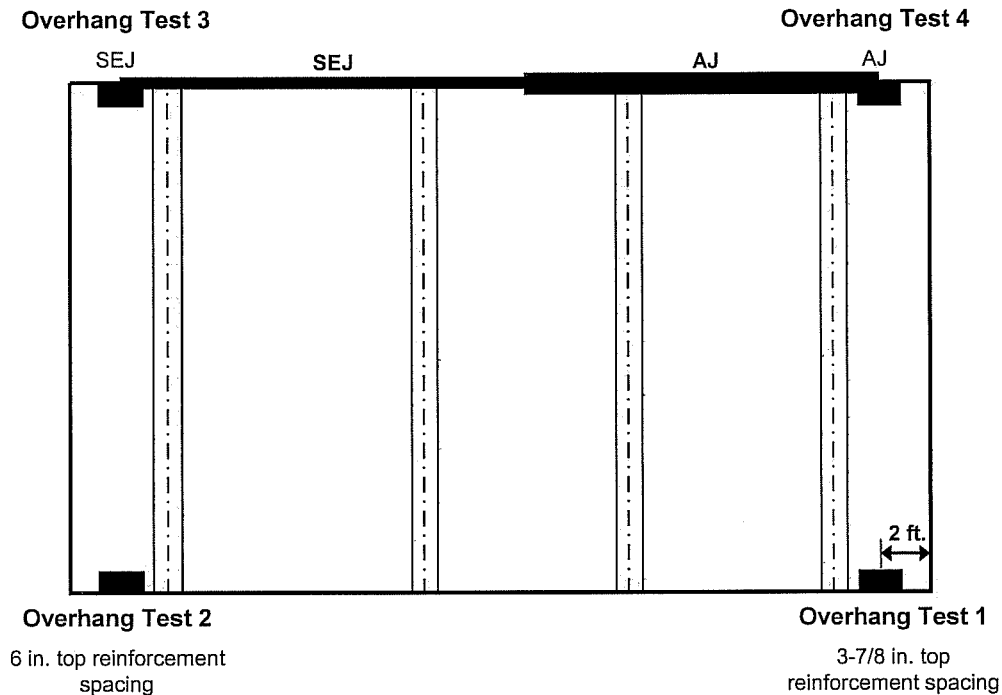
Figure 6.1 Overhang test locations

Overhang Test 1 included 12 flexural reinforcing bars placed 2.3 in. from the top of the slab and spaced 3-7/8 in. on center. Overhang Tests 2, 3 and 4 had 8 flexural reinforcing bars spaced 6 in. on center. Overhang Tests 3 and 4 included either the AJ or SEJ rails, where the rails extended into the overhang, 24 in. from the slab end. All top flexural reinforcement was continuous into the overhangs, parallel to the slab edge. Additional 4 ft long No.4 bars were coupled with each top flexural reinforcing bar in the overhang. In TxDOT details for bridge decks with PC panels, all overhangs are cast-in-place and have a minimum depth of 8 in. The change to full-depth CIP overhangs from the composite panel section required bottom reinforcement to be placed prior to casting (Figure 6.2).

218
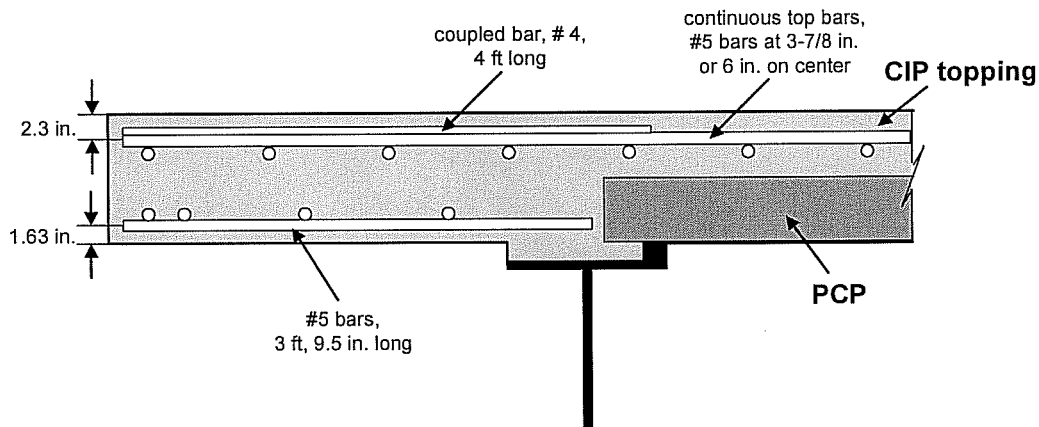
Figure 6.2 Example of overhang reinforcement

Strain gauges placed on either face of the girder on the top flexural reinforcement mat were monitored during testing. Because of the loading imposed on the structure prior to loading the overhangs, it was difficult to determine residual strains or the phenomenon that caused them. In general, such strains were estimated to be less than 15% of yield. No residual strains were included in strains reported for overhang tests. All deflections presented in this chapter are tip deflections, measured at the corner of the slab with linear potentiometers. The initial stiffness of the load-deflection plots may have been greater than the stiffness recorded during testing. Because the expansion joint edge regions had been tested before the overhangs, the slab at the overhang girder was severely cracked near the overhang test sections and in the neighboring edge regions. Due to this previous cracking, a discussion of first flexural cracking is less relevant in a discussion of overhang test results than in the expansion joint edge region results and is omitted from this chapter. Figure 6.3 is an example of the graphic used to illustrate the loading plate, linear potentiometer and strain gauge locations in a test area.

219
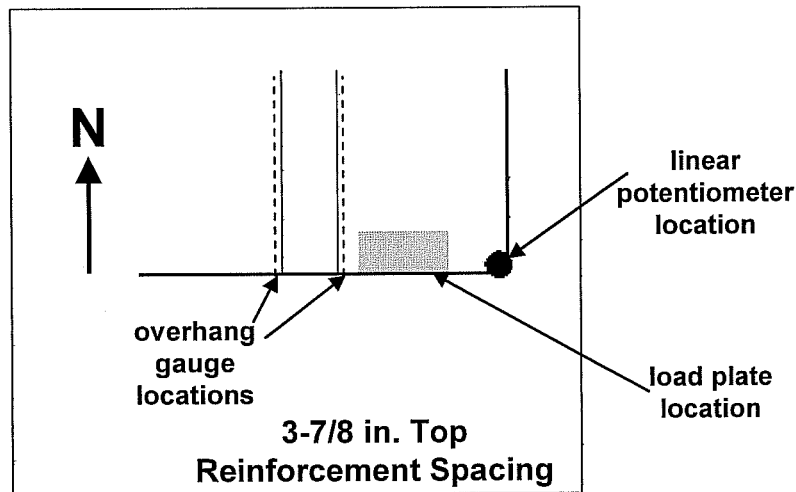
Figure 6.3 Sample overhang test area

6.1.2 Overhang Length

As discussed in Section 3.4.7, the overhang length was extended to 45.5 in. so that the loading plate footprint would lie outside the girder support and 24 in. from the slab end. The overhang geometry was based on the nominal width of the guardrail and dimension of the contact area of the tires.

6.1.3 AASHTO Loads on Overhangs (Griffith 2003)

Two configuration of AASHTO design loads were considered for this project: the AASHTO truck with a single axle; and the AASHTO truck with two tandem axles. These two loading configurations are discussed in more detail in Section 3.2.3. Using either of these configurations, only a single load plate placed on the overhang is considered. Because the single-axle load produces higher stresses on the overhang, it is the basis for the HS-20 load level used on the overhang. Throughout Chapter 6, the load reported as HS-20 is 16 kips per load

point. This is a change from Chapter 5, where HS-20 loads were 12.5 kips per load plate, based on the tandem-axle loading configuration. (Griffith 2003)

6.2   3-7/8 IN. TOP REINFORCEMENT SPACING, OVERHANG TEST AREA 1

6.2.1   Summary of Response

Overhang Test Area 1 failed in one-way shear at 3.6 x HS-25 (72 kips). Cracks on the top surface of the slab formed parallel to the face of the girder at the slab edge (expansion joint) and then bent towards the end of the slab. Cracks on the bottom surface formed perpendicular to the cracks on top of the slab. Reinforcing bars near the slab edge reached yield strains around 3.2 x HS-25 (64 kips). The tip deflection at HS-20 was 0.08 in. and at HS-25 was 0.10 in. The maximum tip deflection at failure was 0.97 in. Crack patterns indicate that torsion played an important role in the failure of the overhang.

6.2.2   Detailed Description of Response

6.2.2.1   Loading

A sketch of Overhang Test Area 1 is shown in Figure 6.4. Strain gauges on either face of the girder were monitored during testing. Deflections were measured at the corner of the overhang. Overhang Test Area 1 with 3-7/8 in. top reinforcement spacing was loaded until it failed in one-way shear along the girder at 3.6 x HS-20, or 72 kips.

Figure 6.4 Overhang Test Area 1, 3-7/8 in. top reinforcement spacing

6.2.2.2 Load-Deflection Behavior

The load deflection behavior at the corner of the overhang is shown in Figure 6.5. The tip deflection was 0.08 in. at HS-20 and 0.10 in. at HS-25. At 1.75 x HS-25 and 3 x HS-25, the deflections were 0.22 in. and 0.63 in., respectively. The largest deflection measured before failure was about 1.0 in.
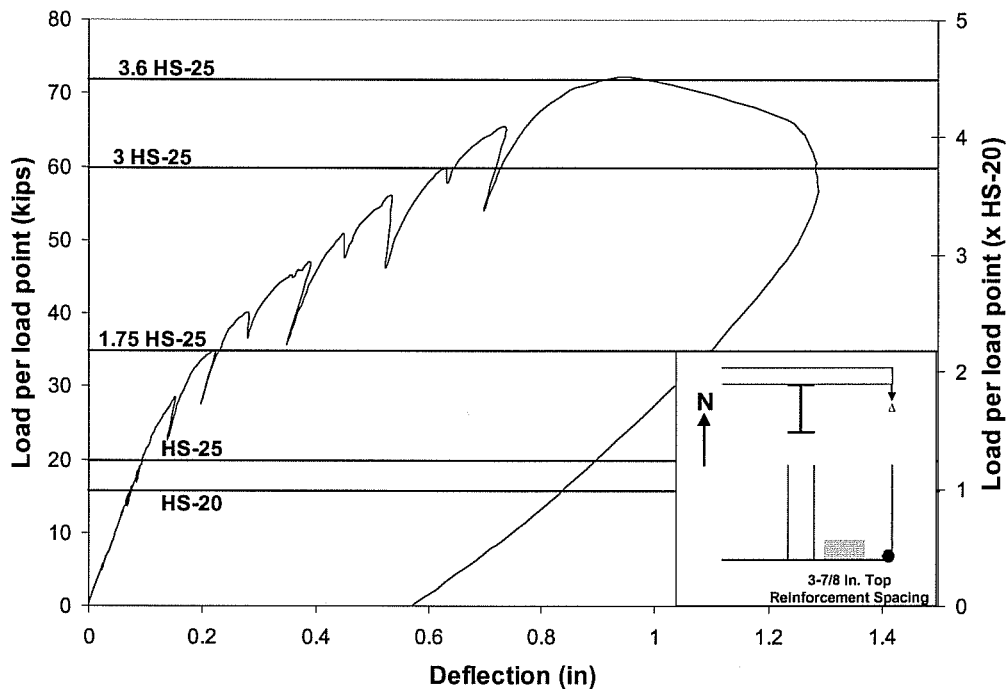
Figure 6.5 Tip deflection, Overhang Test 1, 3-7/8 in. top reinforcement spacing

6.2.2.3 Steel Strains

Tensile strain measured at the faces of the east-exterior girder is plotted against load in Figure 6.6. Strain profiles are shown in Figure 6.7. As mentioned in Section 6.1.1, residual strains were not included in strains reported in this overhang.

Because the load was located on the east overhang, strains on the east face are discussed first. At HS-20 and HS-25, strains were very small, less than 6% of yield strain (135 με). At 1.75 x HS-25, the strain on the overhang side of the girder increased 31% of yield strain (690 με) and at 3 x HS-25, the strain was about 97% of yield strain (2140 με). At the interior face of the girder, the strains at 1.75 x HS-25 and 3 x HS-25 were somewhat less than those on the overhang face of the girder. At approximately 3.2 x HS-25 reinforcing bars near the slab

edge on the overhang face of the girder reached yield strain. The maximum strain on the overhang face of the girder was 1.3 ε_y (2770 $\mu\varepsilon$).
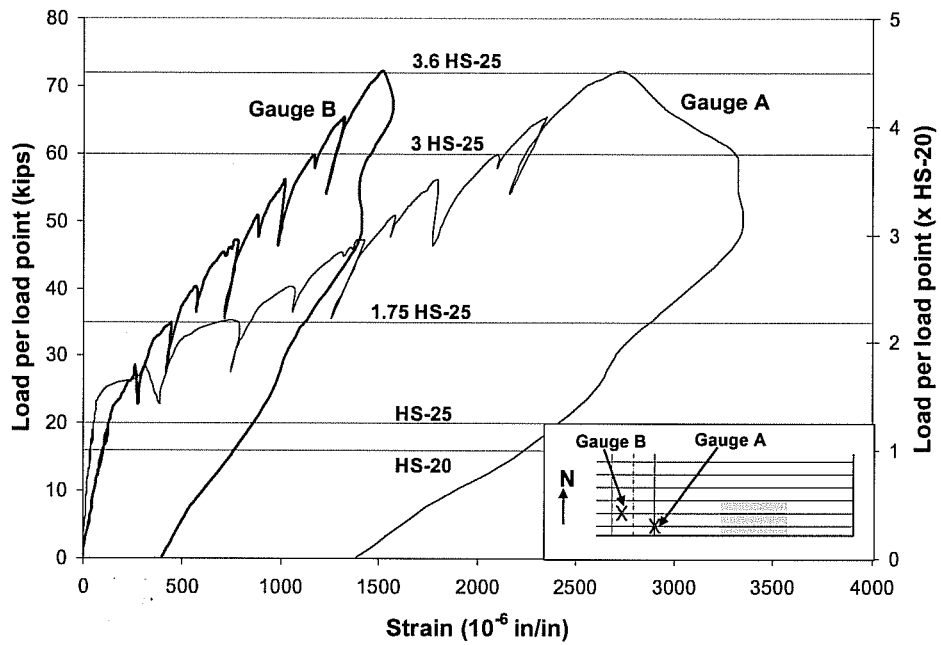
Figure 6.6 Load-strain response, Overhang Test Area 1, 3-7/8 in. top reinforcement spacing
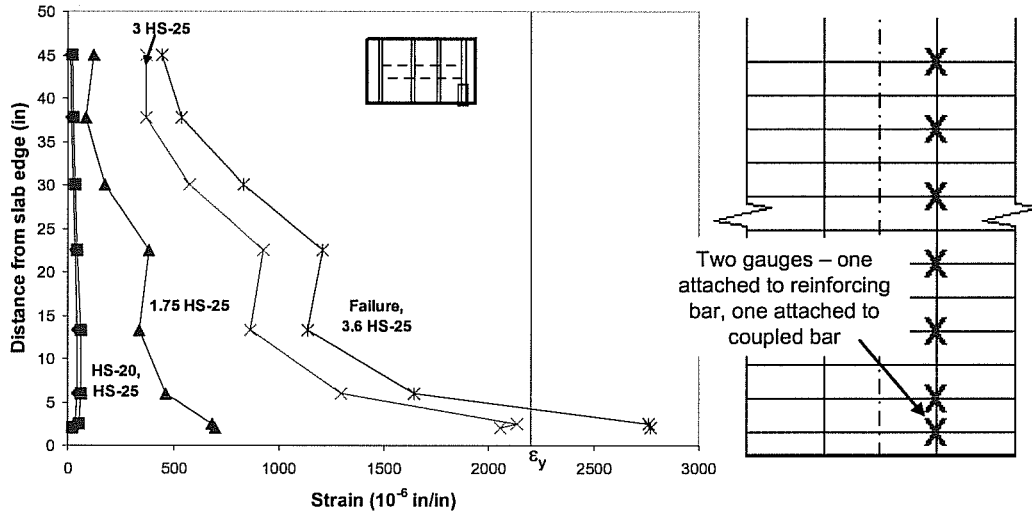
(a) east face of girder, top mat
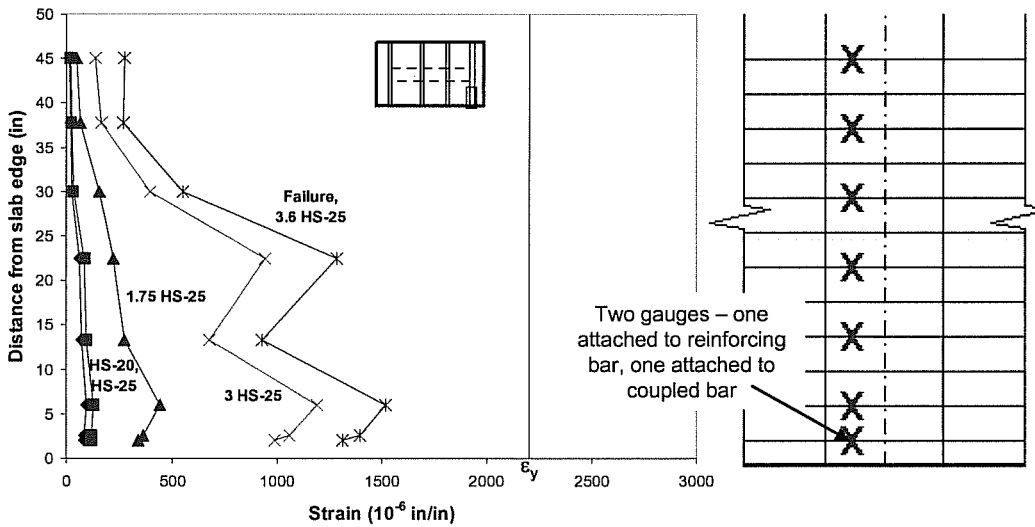
(b) west face of girder, top mat

Figure 6.7 Strain profiles, Overhang Test Area 1: (a) east face of girder, top mat; (b) west face of girder, top mat

225

6.2.2.4 Crack Maps and Appearance after Failure

As discussed in Section 6.1.1, first cracking is less relevant in the overhangs than the expansion joint edge tests, since the overhangs were tested after the expansion joint edge tests were completed. First cracking and cracking patterns are discussed, but only the crack maps at failure are presented here.

Figure 6.8 (a), (b) and (c) show three views of Overhang Test Area 1 at failure load levels. At HS-20, cracks present from previous testing began to widen, and four new cracks formed over the east-overhang girder. As load increased, cracks formed on top of the slab parallel to the girder and then bent towards the end of the slab. Three torsional cracks formed on the bottom face of the slab, perpendicular to the cracks visible on the top surface of the slab. Both flexural, torsional, and shear-induced cracking is evident in the cracking patterns visible after failure.

Figure 6.9, Figure 6.10, and Figure 6.11 show Overhang Test Area 1 (3-7/8 in. top reinforcement spacing) at failure. The failure surface can be seen on the side and bottom surface of the slab. At failure, a shear crack, originating from the bottom of the slab, propagated to the corner of the load plate at the top of the slab (Figure 6.10). This crack originated at the face of the girder, and extended from the edge parallel along the face of the girder on the bottom surface of the slab.

The overhang failed in one-way shear at the section beneath the west side of the load plate (the side of the load plate closest to the girder). The failure was most visible on the side surface of the slab. Only a short length (16 in.) of the failure surface parallel to the face of the girder was visible on the bottom surface of the slab.

**Direction of view,
Figure 6.11**

0.005 in.

HL

0.007 in.

Failure
Surface

(b) bottom view

0.03 in.

0.025 in.

0.007 in.

0.005 in.

0.007 in.

(c) side view

Direction of view, Figure 6.9

0.004 in.

0.01 in.

0.016 in.

0.002 in.

0.004 in.

0.007 in.

0.005 in.

0.04 in.

0.016 in.
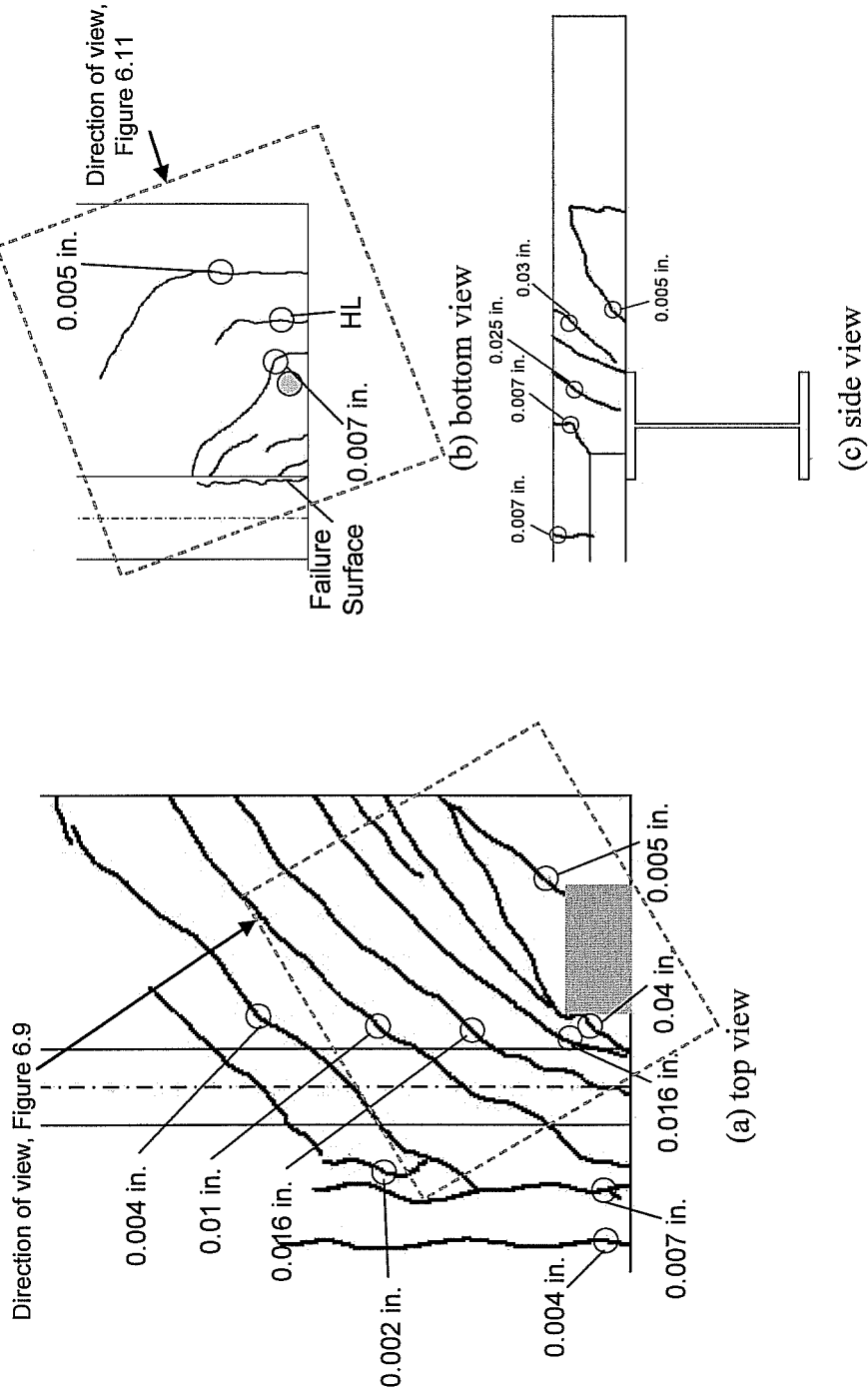
(a) top view

Figure 6.8 Crack map at failure, Overhang Test Area 1, 3-7/8 in. top reinforcement spacing: (a) top view; (b) bottom view; (c) side view, facing north

227
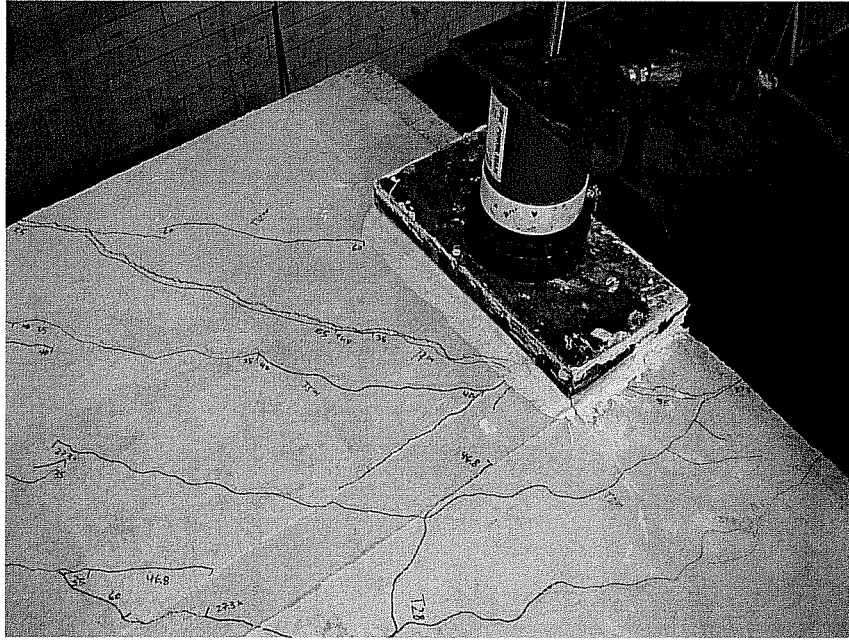
Figure 6.9 Failure of Overhang Test Area 1, top view, facing southeast
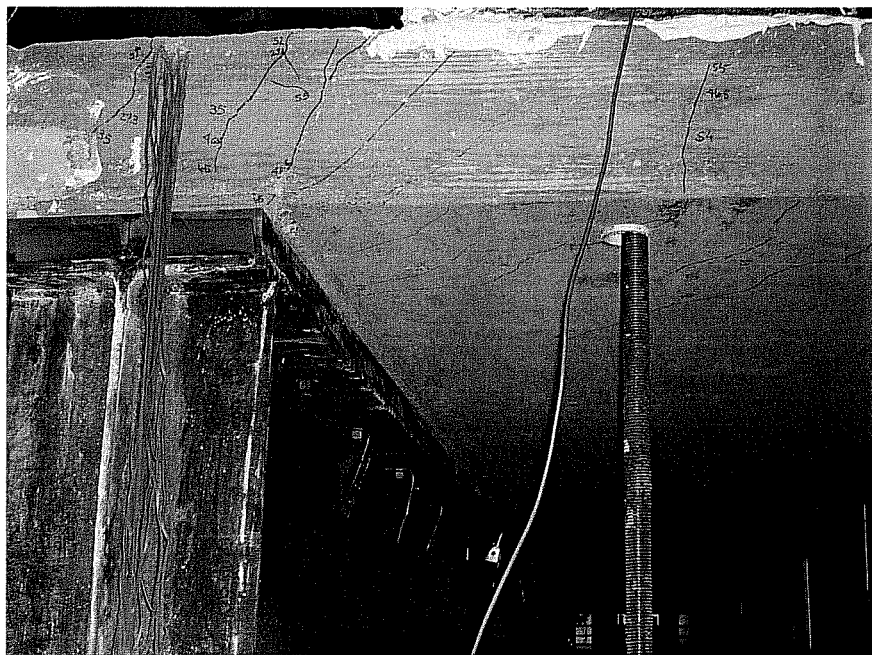
Figure 6.10 Failure of Overhang Test Area 1, side view, facing north
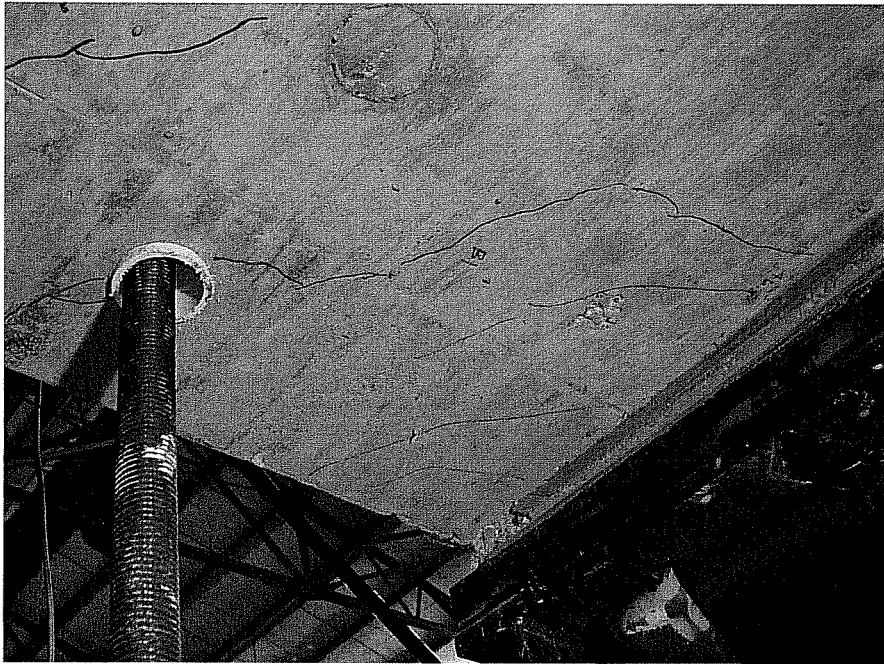
Figure 6.11 Failure of Overhang Test Area 1, bottom view, facing southwest

6.3 6 IN. TOP REINFORCEMENT SPACING, OVERHANG TEST AREA 2

6.3.1 Summary of Response

Overhang Test Area 2 failed in one-way shear at 3 x HS-25 (60 kips). Cracks on the top surface of the slab formed parallel to the face of the girder and then bent towards the end of the slab. Cracks on the bottom surface formed perpendicular to the cracks on top of the slab. The tip deflection at HS-20 was 0.14 in. and at HS-25 was 0.16 in. The maximum tip deflection at failure was 1.19 in. Crack patterns indicate that torsion played an important role in the failure mechanism of the overhang.

229

6.3.2 Detailed Description of Response

6.3.2.1 Loading

A sketch of Overhang Test Area 2 is shown in Figure 6.12. Strain gauges on either face of the girder were monitored during testing. Deflections were measured at the corner of the overhang. Overhang Test Area 2 with 6 in. top reinforcement spacing was loaded until it failed in one-way shear along the girder at 3 x HS-20, or 60 kips.
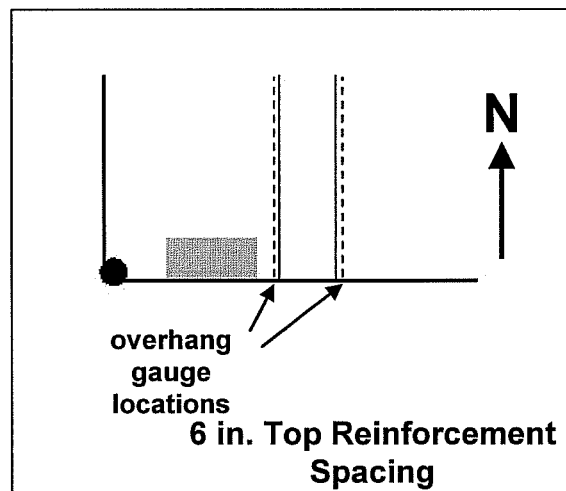
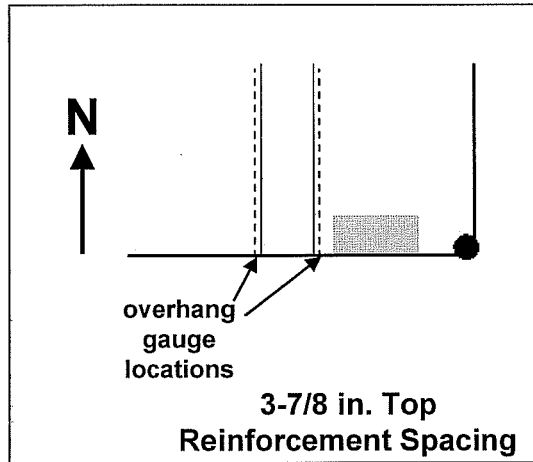*Figure 6.12 Overhang Test Area 2, 6 in. top reinforcement spacing*

6.3.2.2 Load-Deflection Behavior

The load deflection behavior at the corner of the overhang is shown in Figure 6.13. The tip deflection was 0.08 in. at HS-20 and 0.10 in. at HS-25. At 1.75 x HS-25 and 3 x HS-25, the deflections were 0.22 in. and 0.63 in., respectively. The largest deflection measured before failure was 0.97 in.
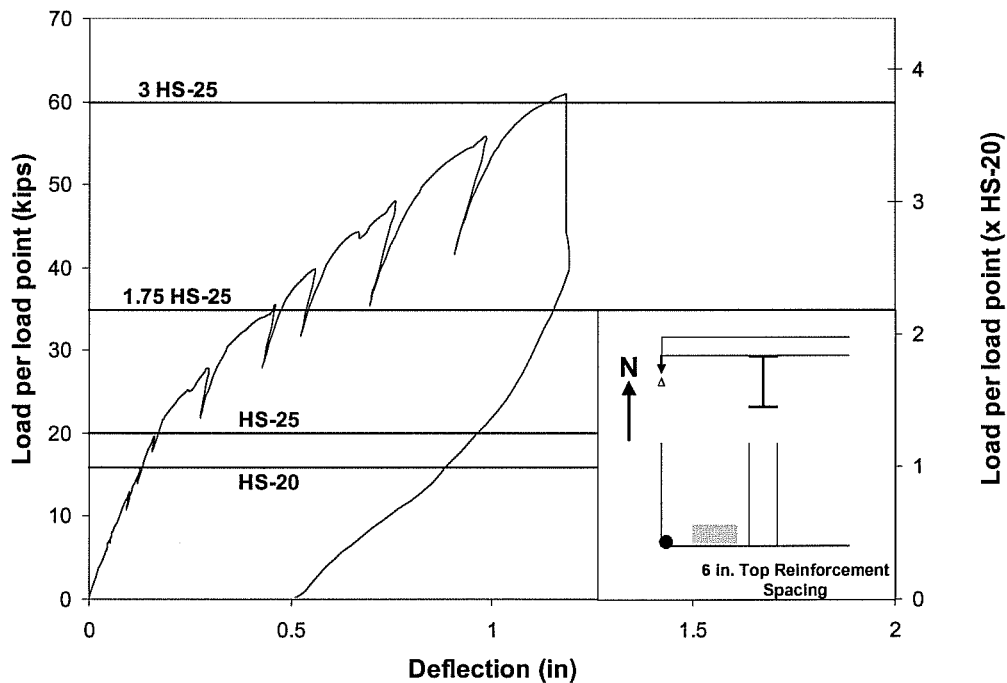
Figure 6.13 Tip deflection, Overhang Test Area 2, 6 in. top reinforcement spacing

6.3.2.3 Steel Strains

Figure 6.14 shows tensile strains measured at the faces of the west-exterior girder. Strain profiles are shown in Figure 6.15 a and b.

At HS-20 and HS-25, the maximum strains were less than 13% of yield strain (290 $\mu\varepsilon$). The strains measured at design loads were roughly double those measured in Overhang Test Area 1; however, the steel spacing was increased from 3-7/8 in. to 6 in. At 1.75 x HS-25, the strain on the overhang face of the girder increased to 71% of yield strain (1570 $\mu\varepsilon$) and reached yield at 2.3 x HS-25 (47 kips). Only the bar nearest the edge reached yield. At the interior face of the girder strains reached 79% of yield strain (1740 $\mu\varepsilon$).
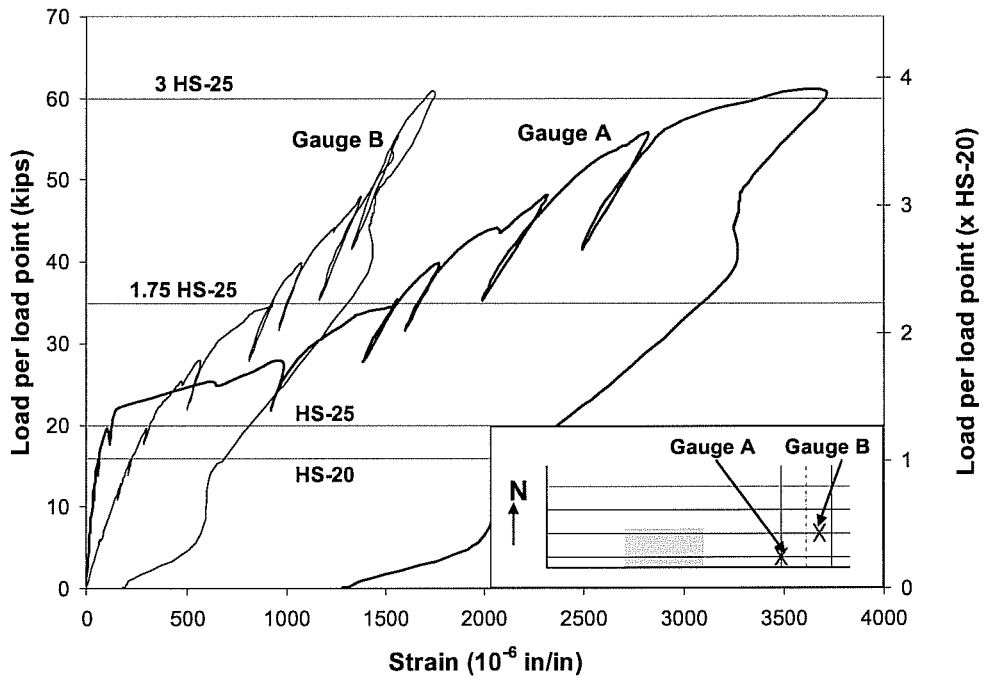
Figure 6.14 Load-strain response, Overhang Test Area 2, 6 in. top reinforcement spacing
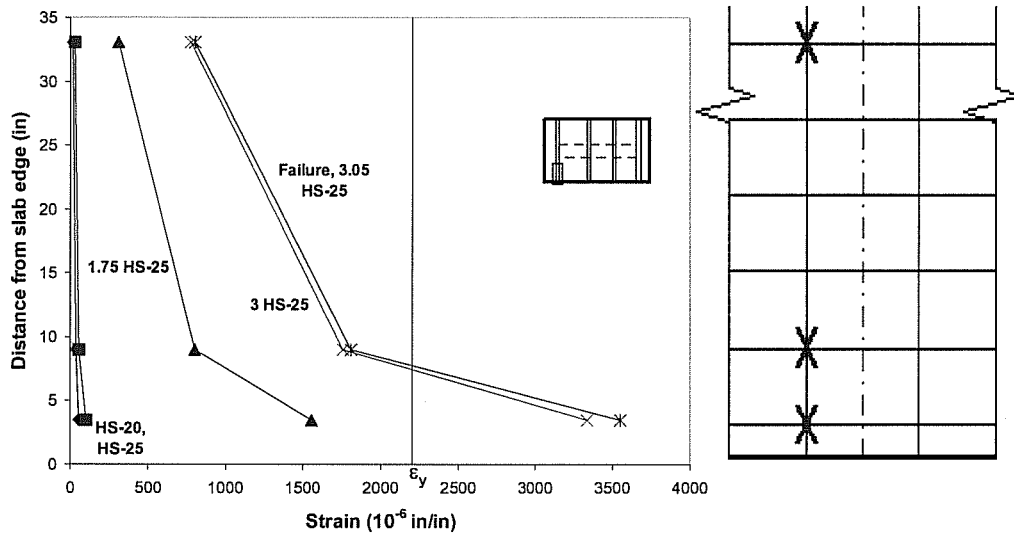
(a) west face of girder, top mat
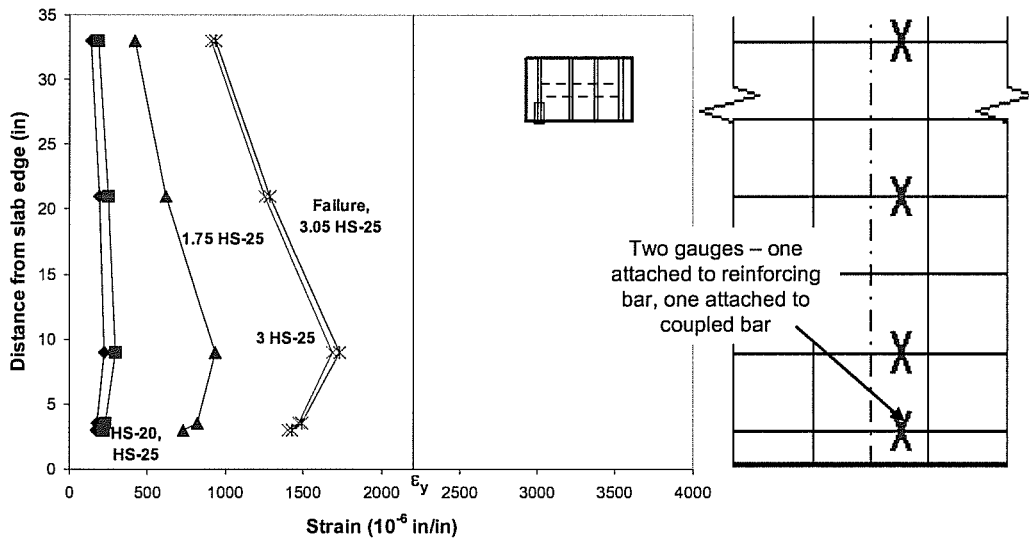
(b) east face of girder, top mat

Figure 6.15 Strain profiles, Overhang Test Area 2, 6 in. top reinforcement

spacing: (a) west face of girder, top mat; (b) east face of girder

233

6.3.2.4 Crack Maps and Appearance after Failure

Figure 6.16 (a), (b) and (c) show three views of Overhang Test Area 2 at failure load levels. At HS-25, cracks formed in previous testing began to widen, and one new crack formed over the west-overhang supporting girder. As load increased, cracks formed on top of the slab parallel to the girder and then bent towards the end of the slab. Four torsional cracks formed on the bottom face of the slab, perpendicular to the cracks visible on the top surface of the slab. Both flexural, torsional, and shear-induced cracking is evident in the cracking patterns visible after failure.

Figure 6.17 and Figure 6.18 show Overhang Test Area 2 (6 in. top reinforcement spacing) at failure. The failure surface can be seen clearly only on the side surface of the slab. At failure, a shear crack, originating from the bottom of the slab, propagated to the corner of the load plate at the top of the slab (Figure 6.18). This crack originated at the face of the girder and ran parallel along the face of the girder on the bottom surface of the slab.
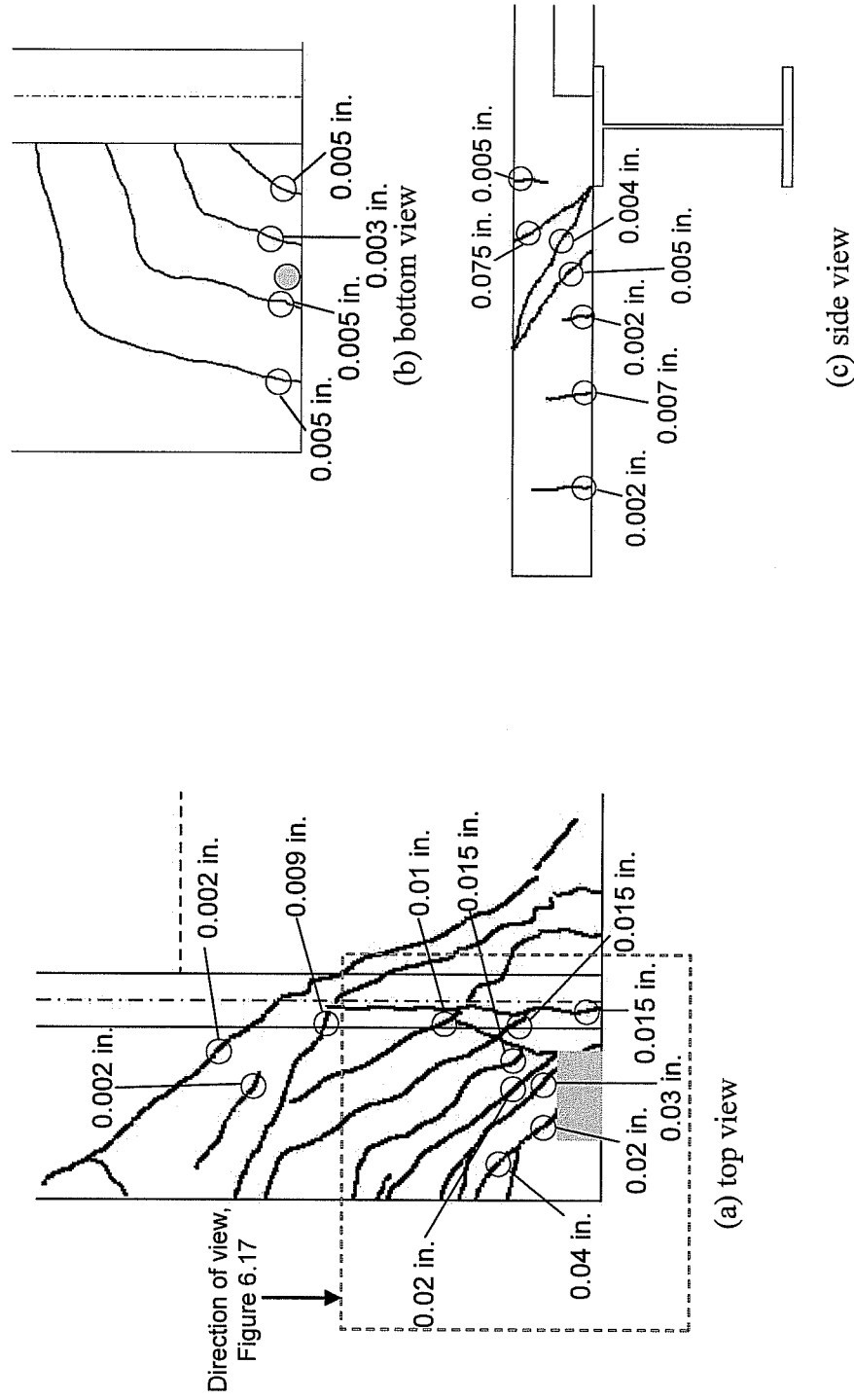
Figure 6.16 Crack map at failure, Overhang Test Area 2, 6 in. top reinforcement spacing: (a) top view; (b) bottom view; (c) side view, facing north

235
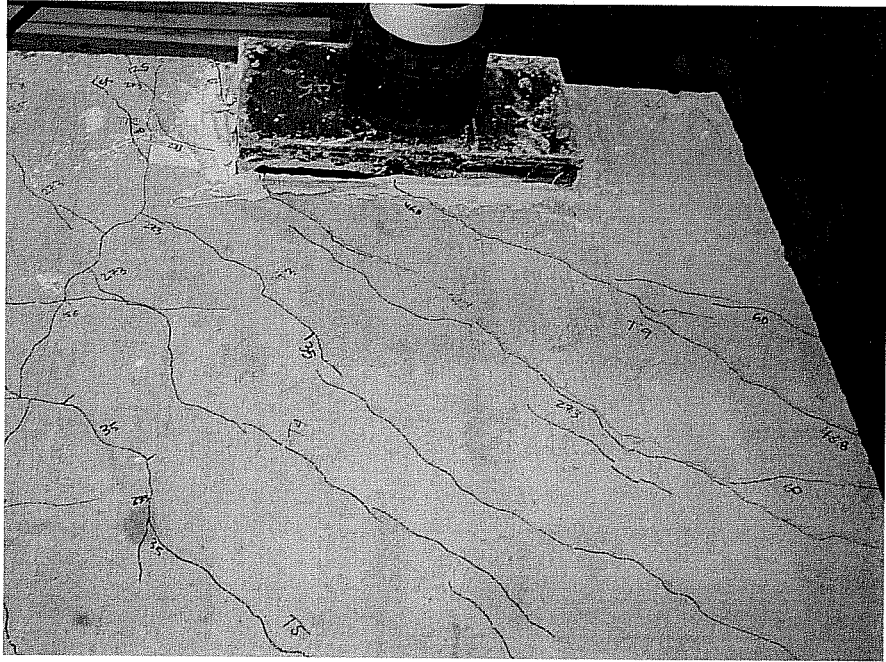
Figure 6.17 Failure of Overhang Test Area 2, top view, facing south
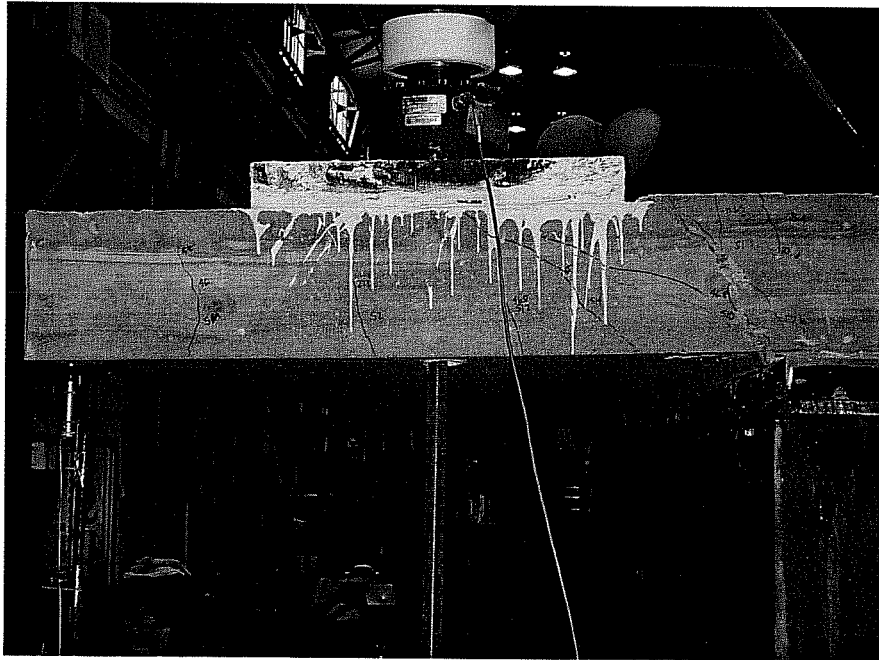
Figure 6.18 Failure of Overhang Test Area 2, side view, facing north

236

6.4 SEALED EXPANSION JOINT (SEJ) RAIL AND 6 IN. TOP REINFORCEMENT SPACING, OVERHANG TEST AREA 3

6.4.1 Summary of Response

Overhang Test Area 3 failed in one-way shear at 4.1 x HS-25 (82 kips). Cracks on the top surface of the slab formed parallel to the face of the girder and then bent towards the end of the slab. Cracks on the bottom surface formed perpendicular to the cracks on top of the slab. Reinforcement near the slab edge reached yield strain around 3.6 x HS-25 (72 kips). The tip deflection at HS-20 was 0.09 in. and at HS-25 was 0.11 in. The maximum tip deflection at failure was 1.34 in. Crack patterns indicate that torsion played an important role in the failure mechanism.

6.4.2 Detailed Description of Response

6.4.2.1 Loading

A sketch of Overhang Test Area 3 is shown in Figure 6.19. The sealed expansion joint extended to 24 in. (typical of TxDOT standards) from the slab end. Strain gauges on either face of the girder were monitored during testing. Deflections were measured at the corner of the overhang. Overhang Test Area 3 with the SEJ and 6 in. top reinforcement spacing was loaded until it failed in one-way shear along the girder at 4.1 x HS-20, or 82 kips.
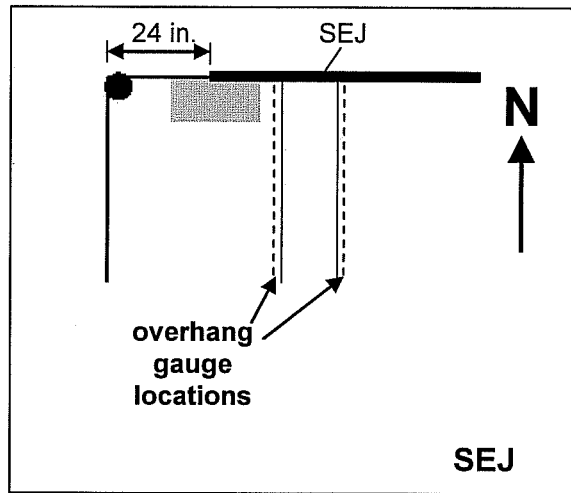
Figure 6.19 Overhang Test Area 3, SEJ and 6 in. top reinforcement spacing

6.4.2.2 Load-Deflection Behavior

The load deflection behavior at the corner of the overhang is shown in Figure 6.20. The tip deflection was 0.09 in. at HS-20 and 0.11 in. at HS-25. At 1.75 x HS-25 and 3 x HS-25, the deflections were 0.22 in. and 0.69 in., respectively. The largest deflection measured before failure was 1.34 in.
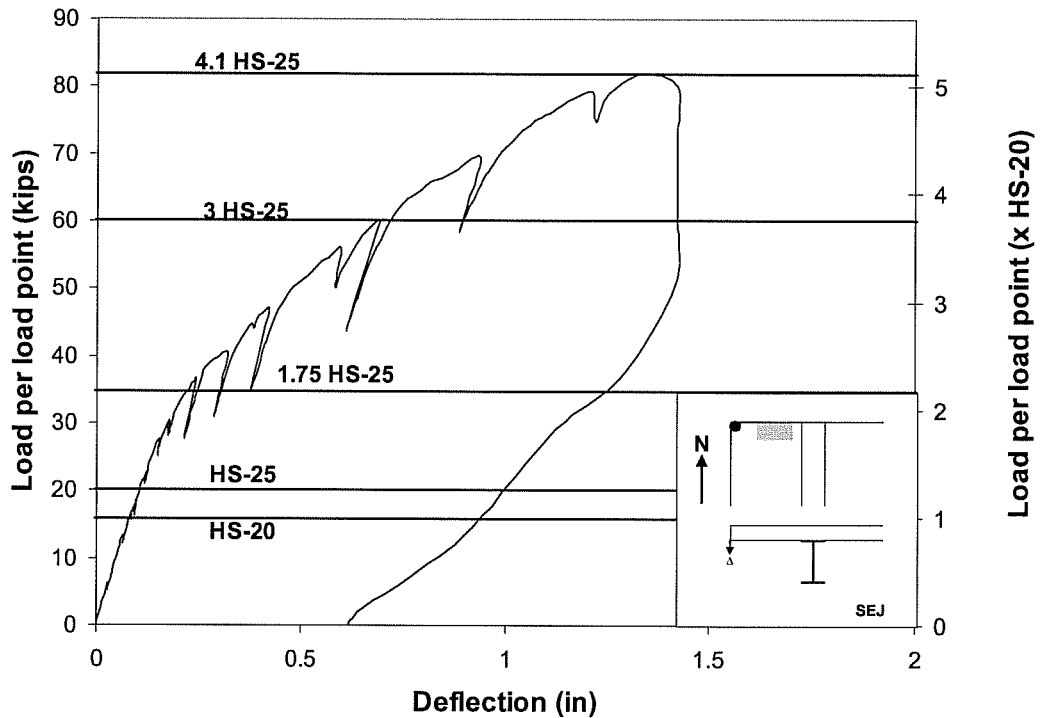
Figure 6.20 Tip deflection, Overhang Test Area 3, SEJ and 6 in. top reinforcement spacing

6.4.2.3   Steel Strains

In Figure 6.21, tensile strains measured at the gauges on either face of the west-exterior girder are shown. Strain profiles are shown in Figure 6.22.

At HS-20 and HS-25, the maximum reinforcement and SEJ strains were less than 6% of yield strain (140 $\mu\varepsilon$). Reinforcement reached yield strain around 3.6 x HS-25 (72 kips). The largest strain measured on the overhang face of the girder at failure was 1.3 ε_y (2800 $\mu\varepsilon$) in the reinforcement and 2800 $\mu\varepsilon$ on the SEJ. The strains measured on the SEJ on the interior face of the girder were negligible. Such low strains were not expected, and it is possible that the gauge

239

on the SEJ was not working properly. However, the transfer of forces from the concrete to the SEJ is a complex process and beyond the scope of this study.
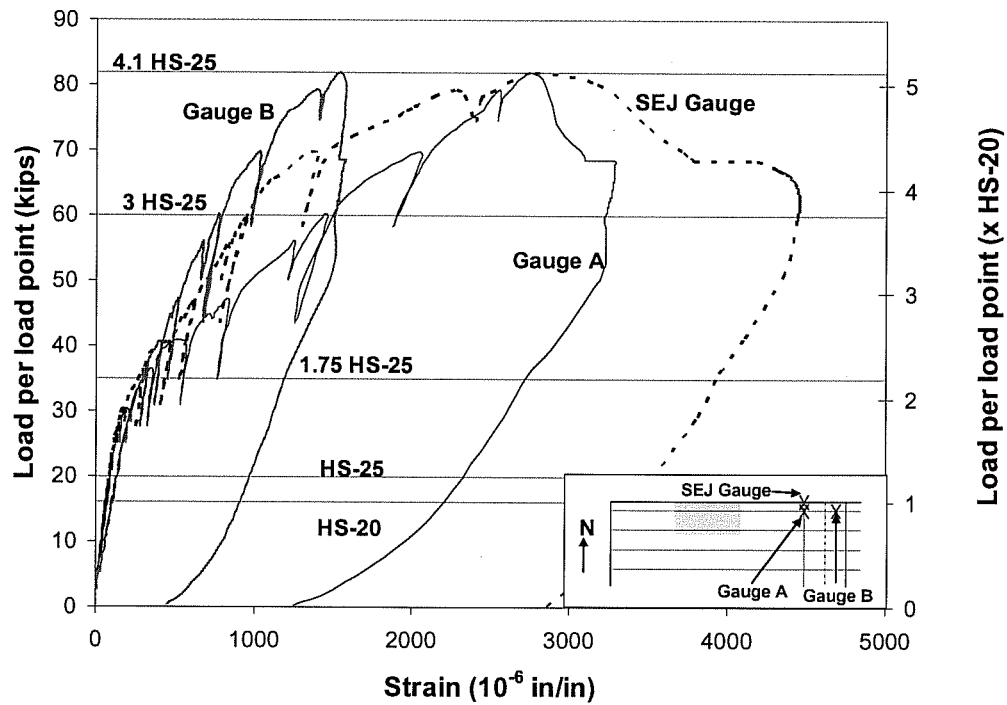
Figure 6.21 Load-strain response, Overhang Test Area 3, SEJ and 6 in. top reinforcement spacing
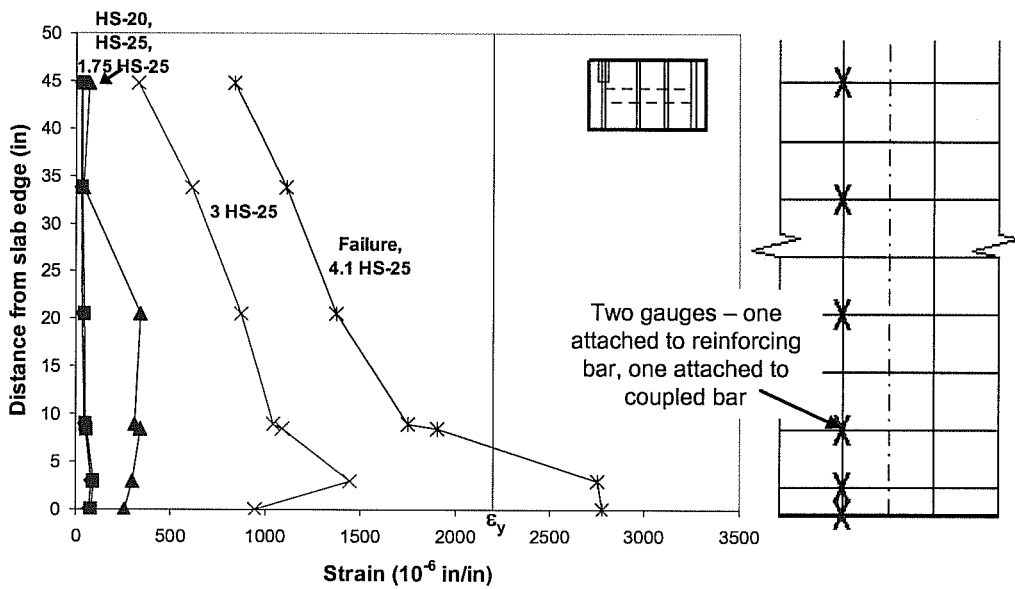
(a) west face of girder
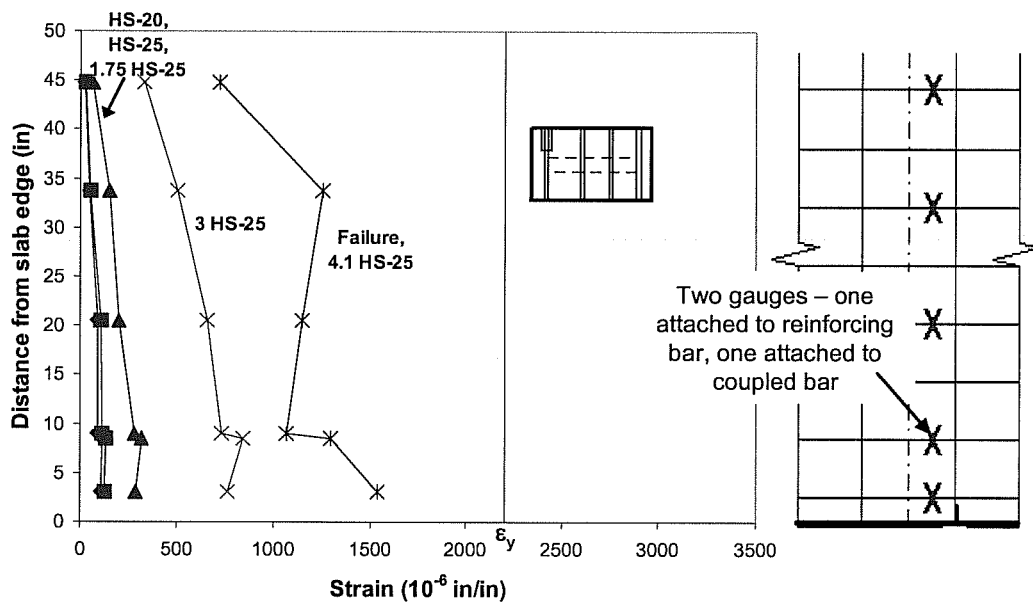
(b) east face of girder, top mat

Figure 6.22 Strain profiles, Overhang Test Area 3: (a) west face of girder, top mat; (b) east face of girder, top mat

6.4.2.4 Crack Maps and Appearance after Failure

Figure 6.23 (a), (b) and (c) show three views of Overhang Test Area 3 at failure load levels. At 1.75 x HS-25, cracks formed in previous testing began to widen, and four additional cracks formed over the west-overhang girder. As load increased, cracks formed on top of the slab parallel to the girder and then bent towards the end of the slab. Five torsional cracks formed on the bottom face of the slab, perpendicular to the cracks visible on the top surface of the slab. Both flexural, torsional, and shear-induced cracking is evident in the cracking patterns visible after failure.

Figure 6.24, Figure 6.25, and Figure 6.26 show Overhang Test Area 3 (SEJ and 6 in. top reinforcement spacing) at failure. The failure surface can be seen clearly only on the side surface of the slab. At failure, a shear crack, originating from the bottom of the slab, propagated to the center of the load plate at the top of the slab (Figure 6.26). This crack originated at the face of the girder and cracked along the bottom edge of the SEJ rail. On the bottom surface of the slab, the failure surface ran parallel along the face of the girder for approximately 22 in. The shear crack was not visible on the top surface of the slab even though an existing crack opened wide at failure.
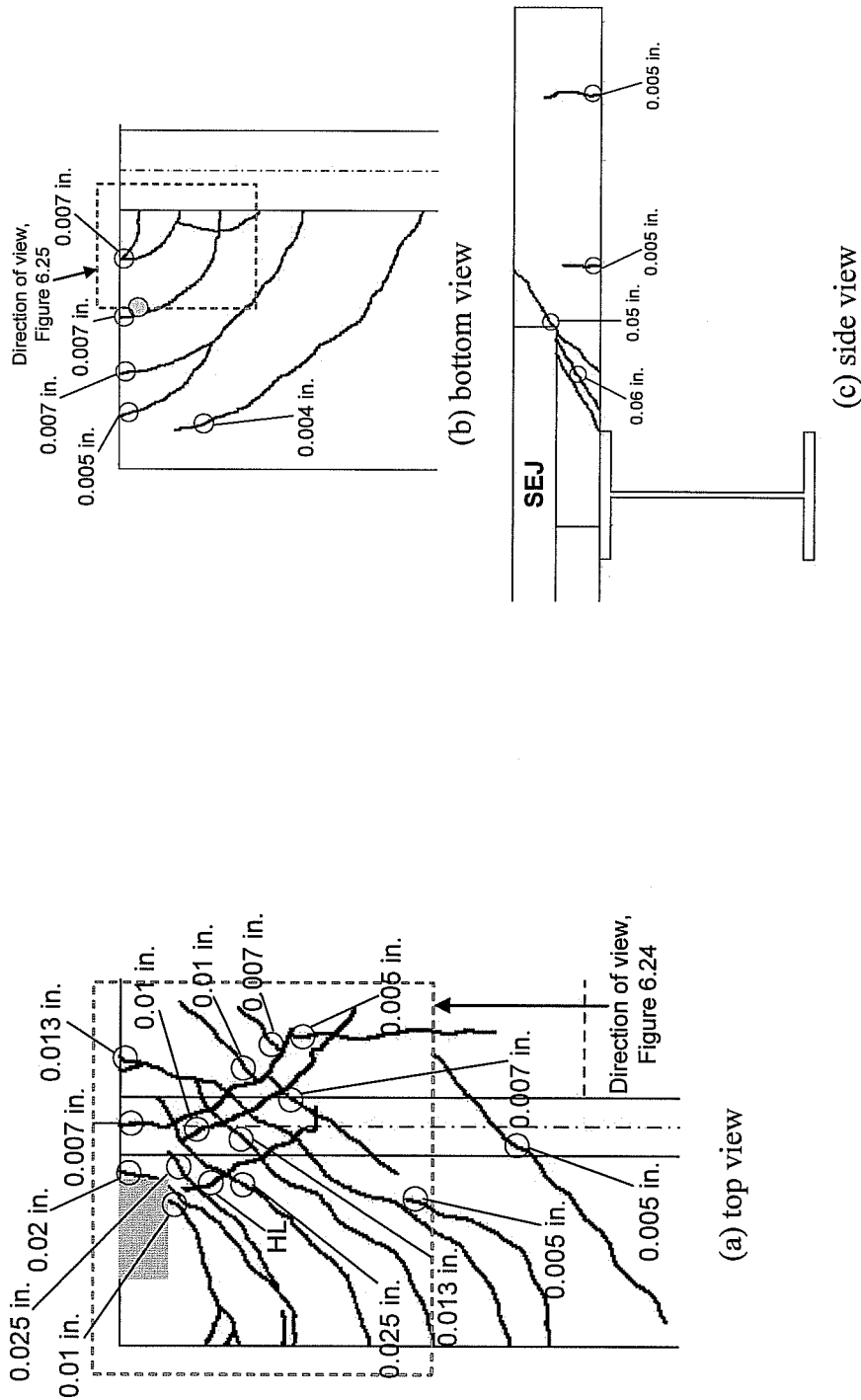
Figure 6.23 Crack map at failure, Overhang Test Area 3, SEJ: (a) top view; (b) bottom view; (c) side view, facing south

243
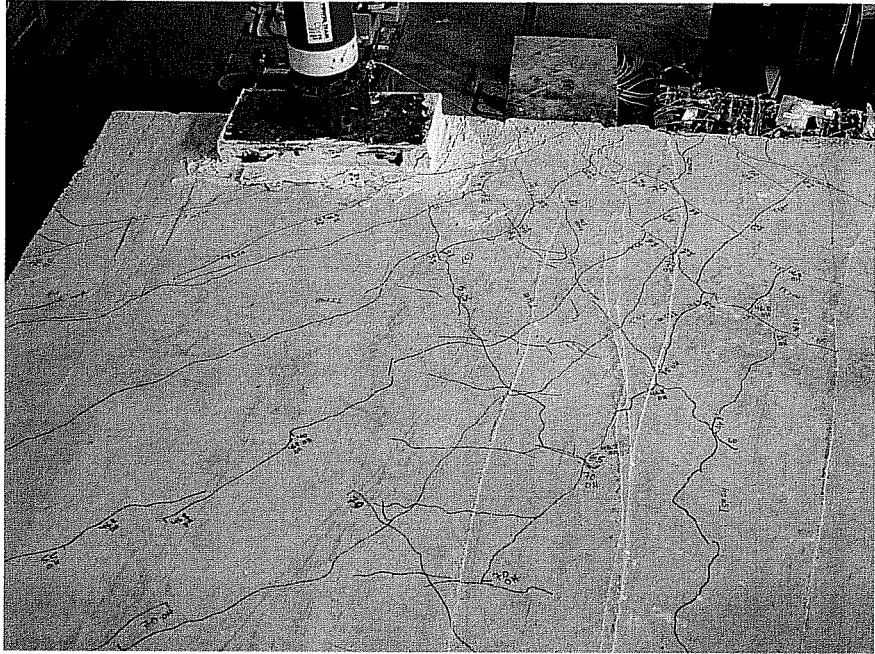
Figure 6.24 Failure of Overhang Test Area 3, top view, facing north

Figure 6.25 Failure of Overhang Test Area 3, bottom view, facing southwest
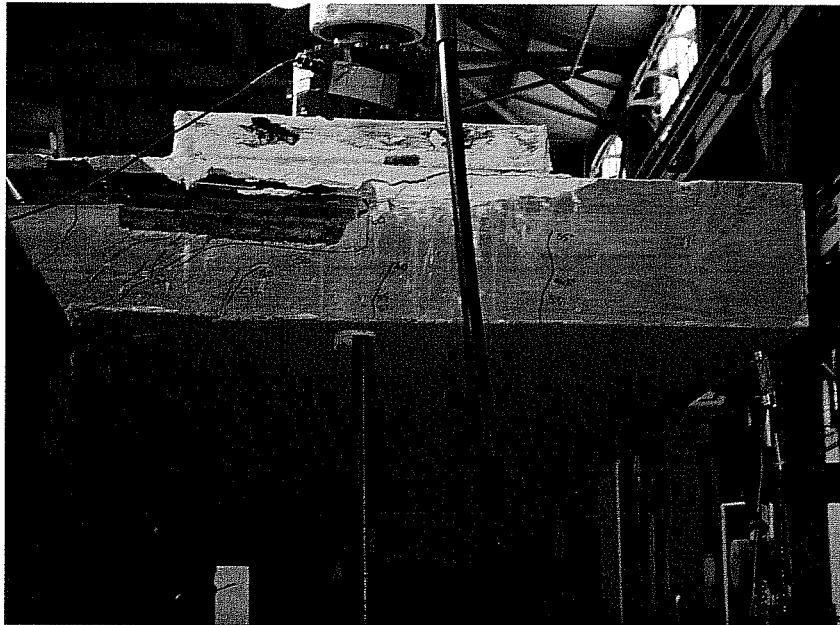
(a)   side view, facing south
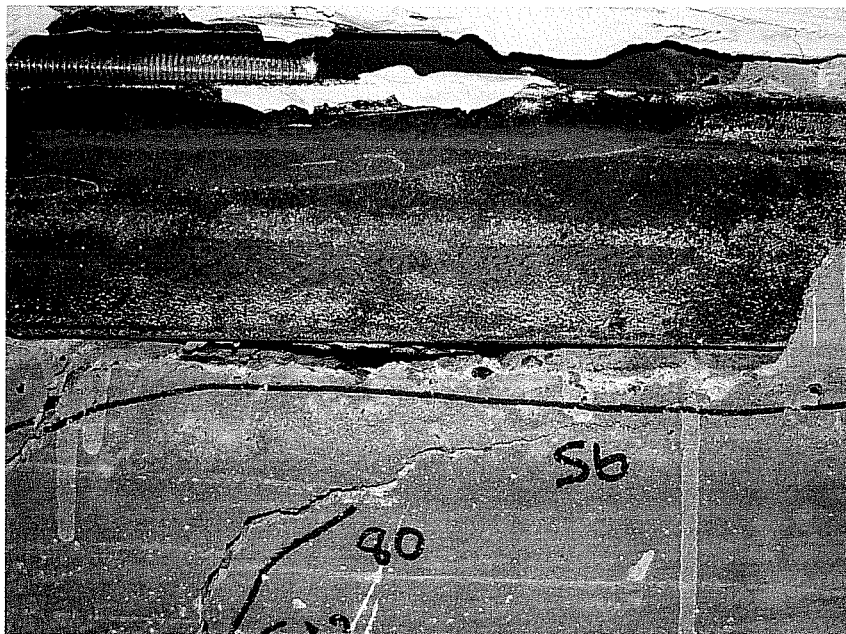
(b) close up of SEJ at failure

Figure 6.26 Failure of Overhang Test Area 3, side view: (a) side view, facing south; (b) close up of SEJ

6.5 ARMOR JOINT (AJ) RAIL AND 6 IN. TOP REINFORCEMENT SPACING, OVERHANG TEST AREA 4

6.5.1 Summary of Response

Overhang Test Area 4 failed in one-way shear at 4.3 x HS-25 (85 kips). Cracks on the top surface of the slab formed parallel to the face of the girder and then bent towards the end of the slab. Cracks on the bottom surface formed perpendicular to the cracks on top of the slab. None of the measured flexural reinforcement reached yield strain before failure. The tip deflection at HS-20 was 0.09 in. and at HS-25 was 0.10 in. The maximum tip deflection at failure was 1.07 in. Crack patterns indicate that torsion played an important role in the failure mechanism.

6.5.2 Detailed Description of Response

6.5.2.1 Loading

A sketch of Overhang Test Area 4 is shown in Figure 6.27. Similar to the SEJ rail, the armor joint (AJ) rail extended to 24 in. from slab end. Strain gauges on either face of the girder were monitored during testing. Deflections were measured at the corner of the overhang. Overhang Test Area 4 with the AJ and 6 in. top reinforcement spacing was loaded until it failed in one-way shear along the girder at 4.3 x HS-20, or 85 kips.
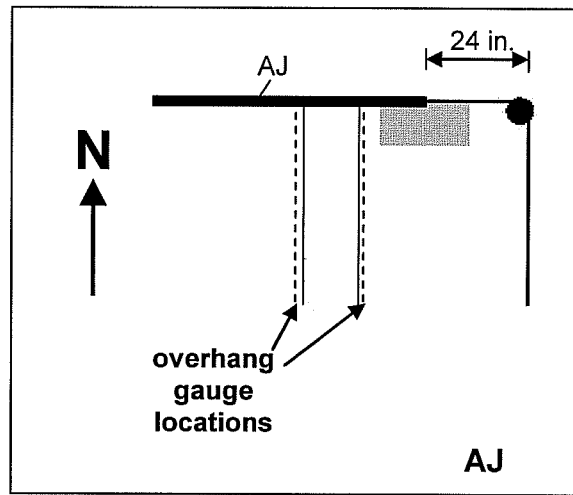
Figure 6.27 Overhang Test Area 4, AJ and 6 in. top reinforcement spacing

6.5.2.2 Load-Deflection Behavior

The load deflection behavior at the corner of the overhang is shown in Figure 6.28. The tip deflection was 0.09 in. at HS-20 and 0.10 in. at HS-25. At 1.75 x HS-25 and 3 x HS-25, the deflections were 0.18 in. and 0.46 in., respectively. The largest deflection measured before failure was 1.07 in.
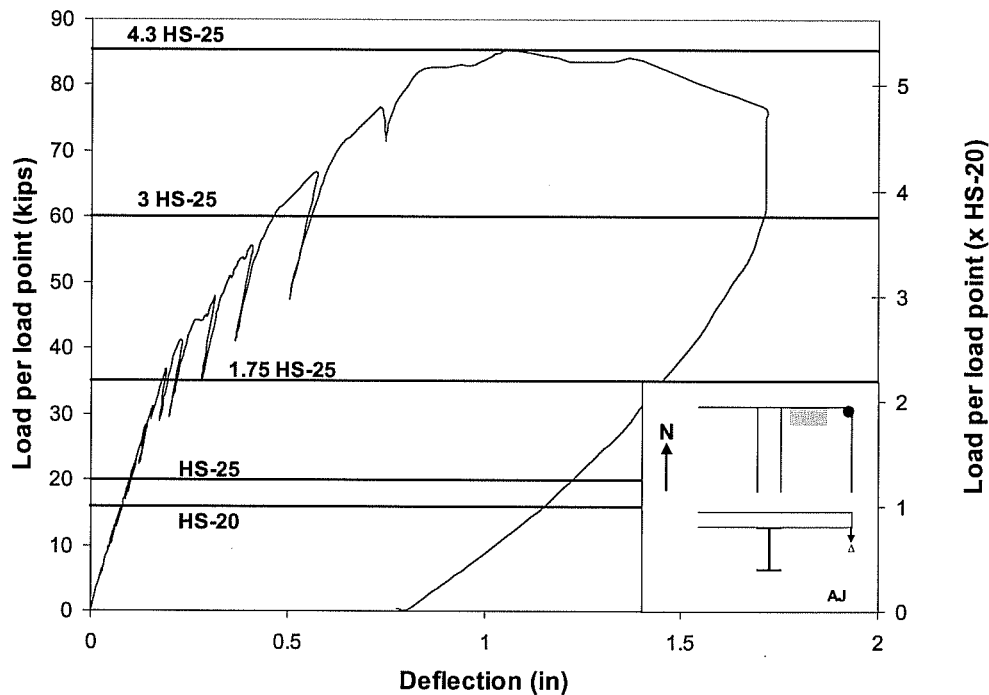
Figure 6.28 Tip deflection, Overhang Test Area 4, AJ and 6 in. top reinforcement spacing

6.5.2.3 Steel Strains

In Figure 6.29, load versus tensile strains are shown. Strain profiles are shown in Figure 6.30. At HS-20 and HS-25, the maximum strains were less than 5% of yield strain (120 $\mu\varepsilon$). The largest strain measured on the overhang face of the girder at failure was 66% of yield strain (1460 $\mu\varepsilon$) on the reinforcement and 1520 $\mu\varepsilon$ on the AJ. On the interior face of the girder, all the strains were slightly less than on the overhang face of the girder. All measured strains were less than yield up to failure.
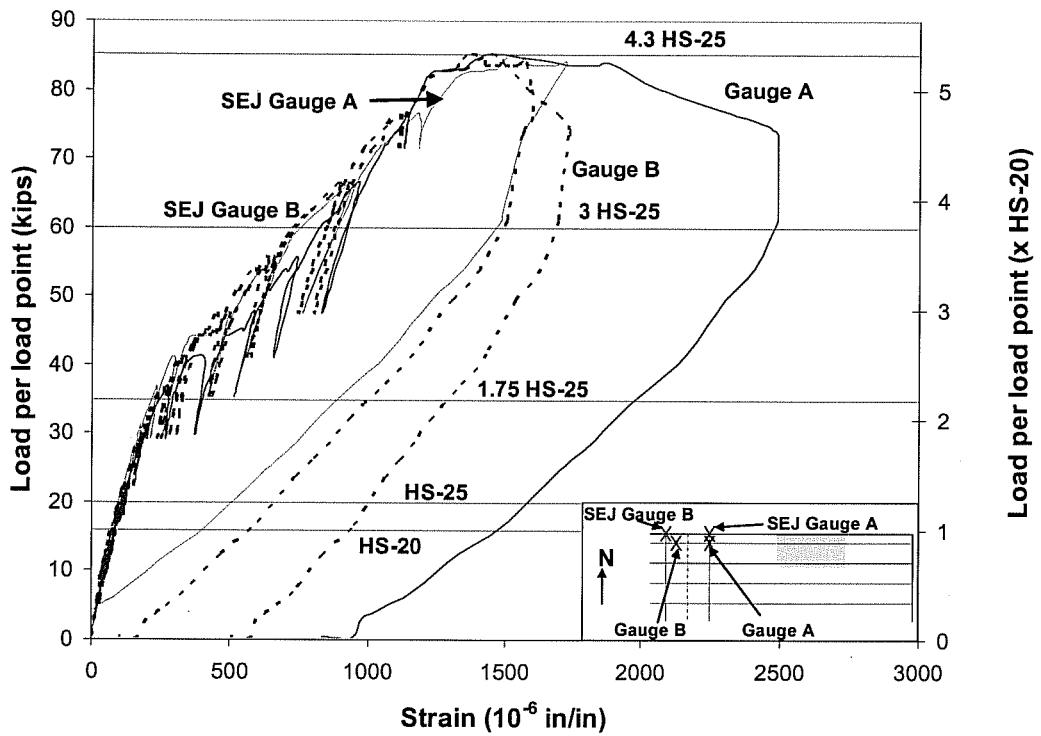
Figure 6.29 Load-strain response, Overhang Test Area 4, AJ and 6 in. top reinforcement spacing
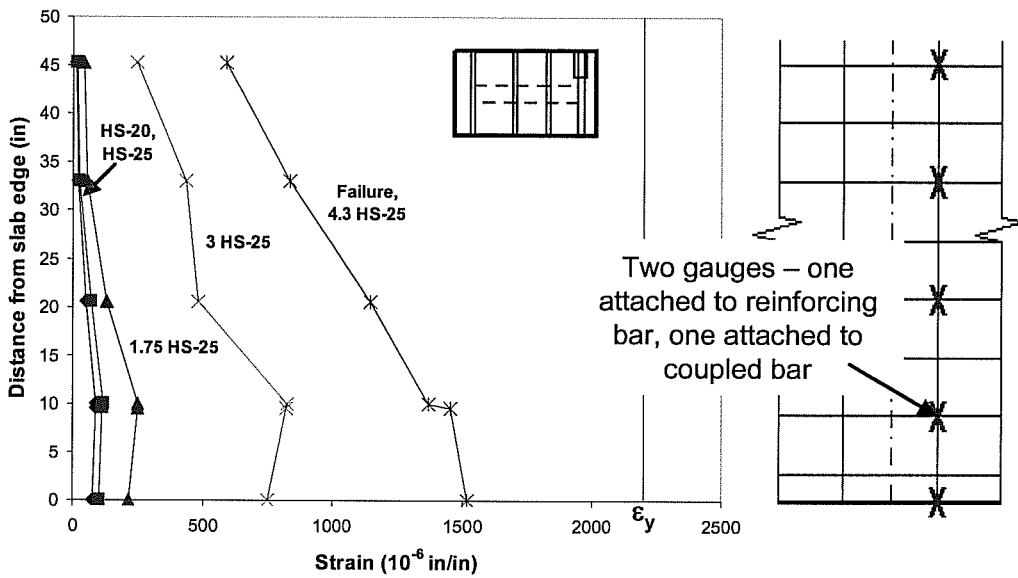
(a) east face of girder, top mat
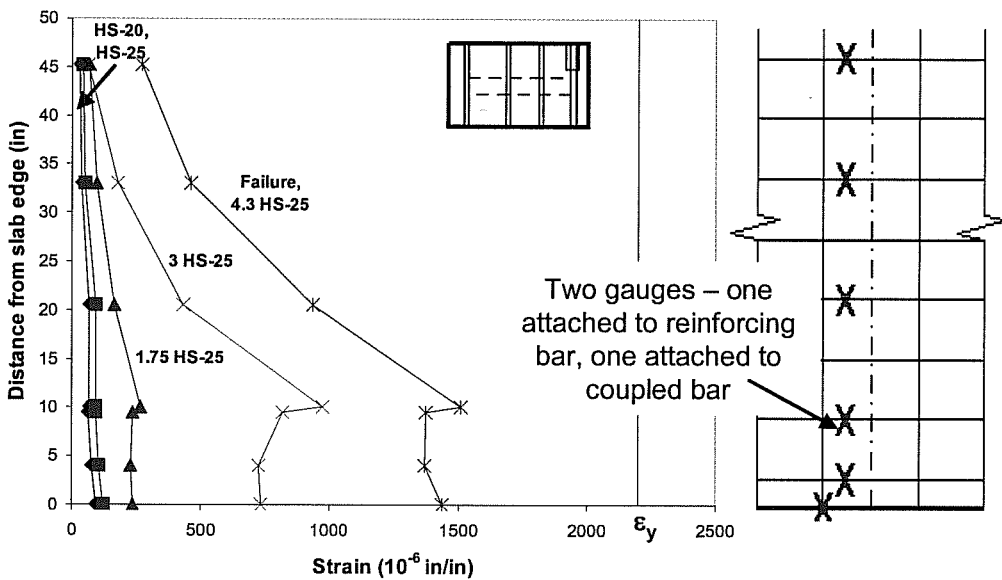
(b) west face of girder, top mat

Figure 6.30 Strain profiles, Overhang Test Area 4: (a) east face of girder, top mat; (b) west face of girder, top mat

250

6.5.2.4 Crack Maps and Appearance after Failure

Figure 6.31 (a), (b) and (c) show three views of Overhang Test Area 4 at failure load levels. At 1.14 x HS-25, cracks formed in previous testing began to widen, and four additional cracks formed over the west-overhang girder. As load increased, cracks formed on top of the slab parallel to the girder and then bent towards the end of the slab. Three torsional cracks formed on the bottom face of the slab, perpendicular to the cracks visible on the top surface of the slab. Both flexural, torsional, and shear-induced cracking is evident in the cracking patterns visible after failure.

Figure 6.32 and Figure 6.33 show Overhang Test Area 4 (AJ and 6 in. top reinforcement spacing) at failure. The one-way shear failure surface can be most clearly seen on the side of the slab. However, some of the failure surface on the side of the slab is hidden by the AJ plate. At failure, a shear crack, originating from the bottom of the slab, propagated to the east side of the load plate at the top of the slab (Figure 6.33). This crack originated at the face of the girder and progressed directly beneath the AJ rail. On the bottom surface of the slab, the failure surface ran parallel along the face of the girder for approximately 31 in. The shear crack was not visible on the top surface of the slab even though existing cracks opened wide at failure.
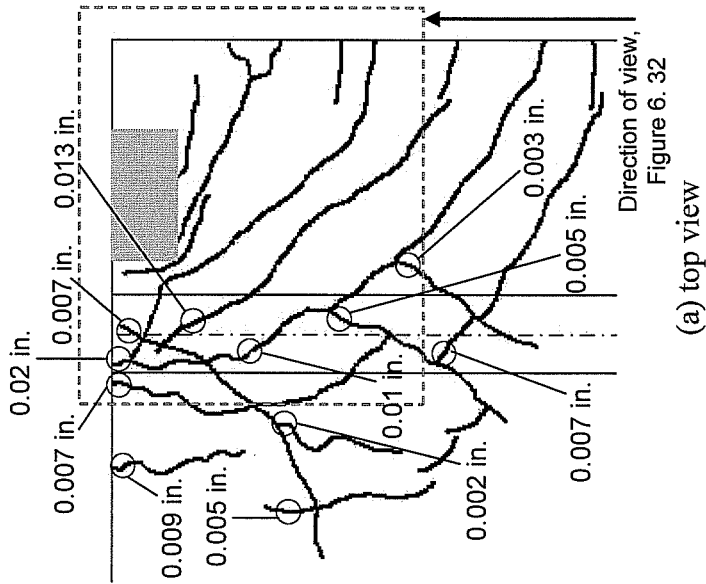
(a) top view
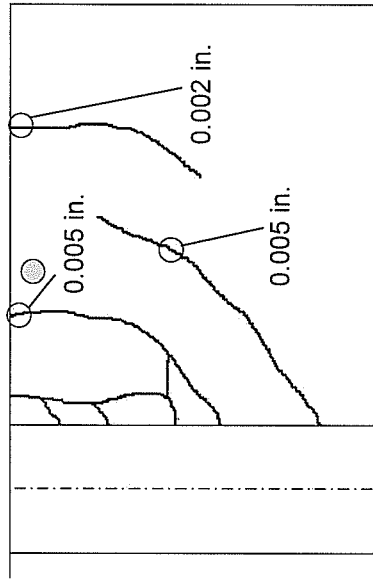
(b) bottom view
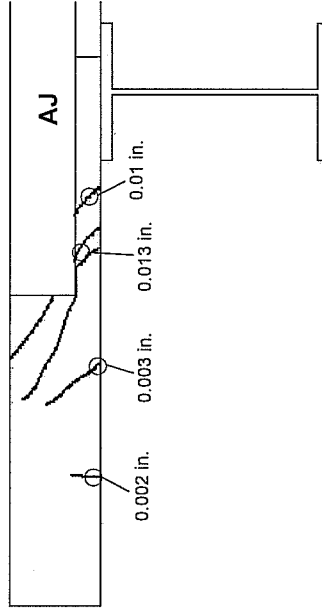
(c) side view

Figure 6.31 Crack map at failure, Overhang Test Area 4, AJ: (a) top view; (b) bottom view; (c) side view, facing south

252
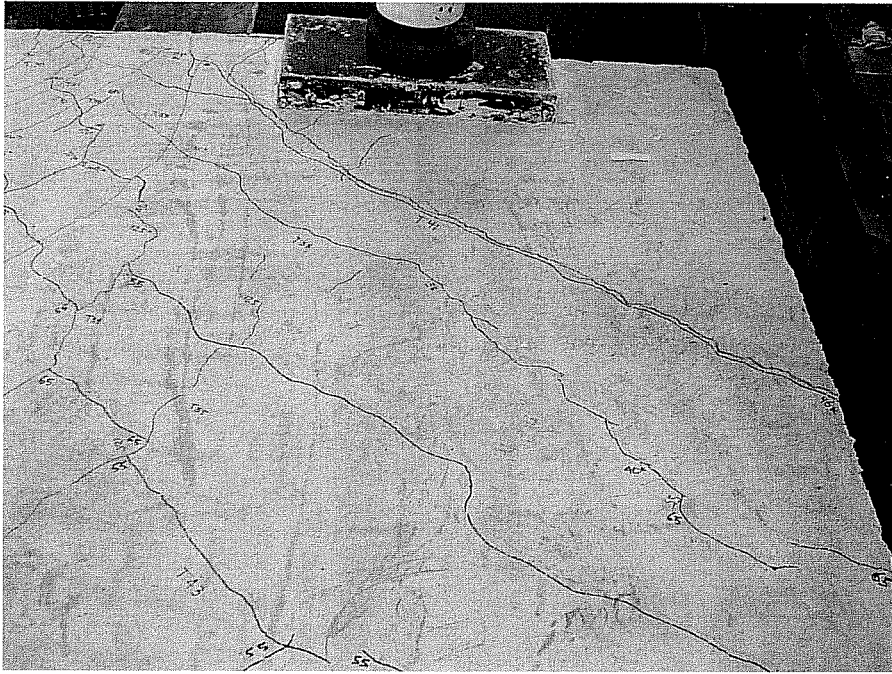
Figure 6.32 Failure of Overhang Test Area 4, top view, facing north
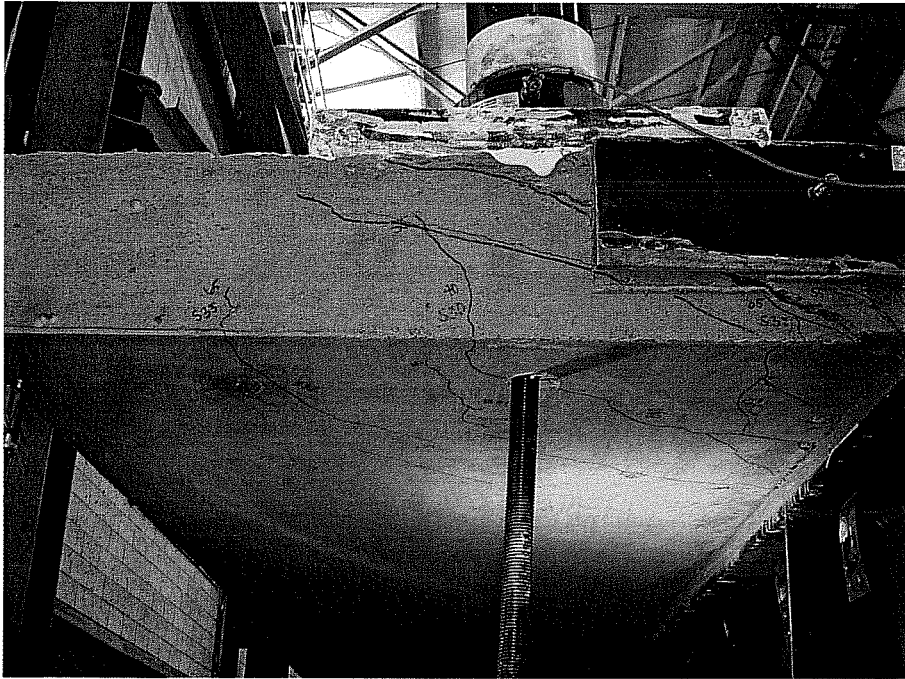
Figure 6.33 Failure of Overhang Test Area 4, side view, facing south

253

6.6 DISCUSSION AND COMPARISON OF OVERHANG TEST RESULTS

Results from the overhang tests are summarized in Table 6.1. All the overhang test areas failed in one-way shear near the girder between 3.0 x HS-25 and 4.3 x HS-25.

Table 6.1 Summary of results from overhang tests

|	Failure load (kips)	Failure Mechanism	Strain (% of yield strain)			Tip Deflection (in)		
			at HS-20	at HS-25	at failure	at HS-20	at HS-25	at failure
3-7/8 in. top reinforcement spacing (OH Test 1)	72, (3.6 x HS-25)	one-way shear	4.6	6.0	130	0.08	0.10	0.97
6 in. top reinforcement spacing (OH Test 2)	61, (3.0 x HS-25)	one-way shear	11	13	160	0.14	0.16	1.19
SEJ & 6 in. top reinforcement spacing (OH Test 3)	82, (4.1 x HS-25)	one-way shear	5.3	6.2	125	0.09	0.11	1.34
AJ & 6 in. top reinforcement spacing (OH Test 4)	85, (4.3 x HS-25)	one-way shear	4.0	5.3	66	0.09	0.10	1.07

All overhangs behaved similarly with cracks forming parallel to the girder and then bending towards the end of the slab. As in the expansion joint edge tests, the cracks in the 3-7/8 in. top reinforcement spacing test area were more closely spaced and narrower than the cracks measured in the 6 in. top reinforcement spacing test area. The cracks were narrower and more closely spaced in the two test areas with the AJ and SEJ rails than the two areas without the rails. Cracks formed at design load levels in the test areas without expansion rails, and for test areas with expansion rails, cracking was first visible at loads beyond the design load levels. Load-deflection and load-deformation responses for all tests were similar at design load levels.

Overall the behavior of the overhang area depended on the top reinforcement spacing and the presence of an expansion rail. The test areas with expansion rails behaved similarly and had only a 4% difference in the failure loads. The tip deflections were nearly identical up to failure, where the depth of the rail (4 in. vs. 6 in.) made a difference in the tip deflection near and at failure.

The two test areas without an expansion rail had capacities approximately 28% less than the two test areas with an expansion rail. The tip deflection was 1.2 times larger in the 6 in. top reinforcement spacing test area than the 3-7/8 in. top reinforcement test area. There was a 15% difference between the failure loads of the two reinforcement spacing test areas. The 6 in. top reinforcement spacing test area was the only region that measured yielding of any reinforcement.

6.7 SUMMARY

Based on the test results, all overhangs performed well at design load levels. The spacing of the top reinforcement and the presence of expansion rails influenced the load-deflection and load-deformation behavior. The test areas with the expansion rails had a higher capacity and had narrower crack widths. The test area with the smaller reinforcement spacing exhibited smaller deflections. The ultimate capacities of all the test areas ranged from 3.0 x HS-25 (6 in. top reinforcement spacing) to 4.3 x HS-25 (AJ and 6 in. top reinforcement spacing).

CHAPTER 7

Comparisons of Responses, CIP Edges and PC Panel Specimen

7.1 INTRODUCTION

Test data gathered from specimen with no skew and IBTS and USTE cast-in-place (CIP) edges and the PC panel specimen permit comparison of the response of the slab edges with and without the use of stay-in-place panels in the edge region. In this chapter, failure modes, capacities, and service-load level behavior are compared for the two specimens, and trends evident from those comparisons are discussed. Failure tests maximizing positive moments and tests maximizing negative moments are addressed separately. Following the comparisons of the test results, the applicability of the test results to slab-edge design is discussed.

7.2 COMPARISON OF NEGATIVE MOMENT LOADING TESTS

In both specimens, negative moments were maximized over a girder between the two 8-ft bays. Load deflection plots for all tests are shown in Figure 7.1 a and b. The edge regions on the PC panel have a slightly lower stiffness than the IBTS and UTSE edge details (Figure 7.1). Relative edge deflections measured at HS-20 and HS-25 load levels were extremely small compared to the girder spacing (less than 1/3000).
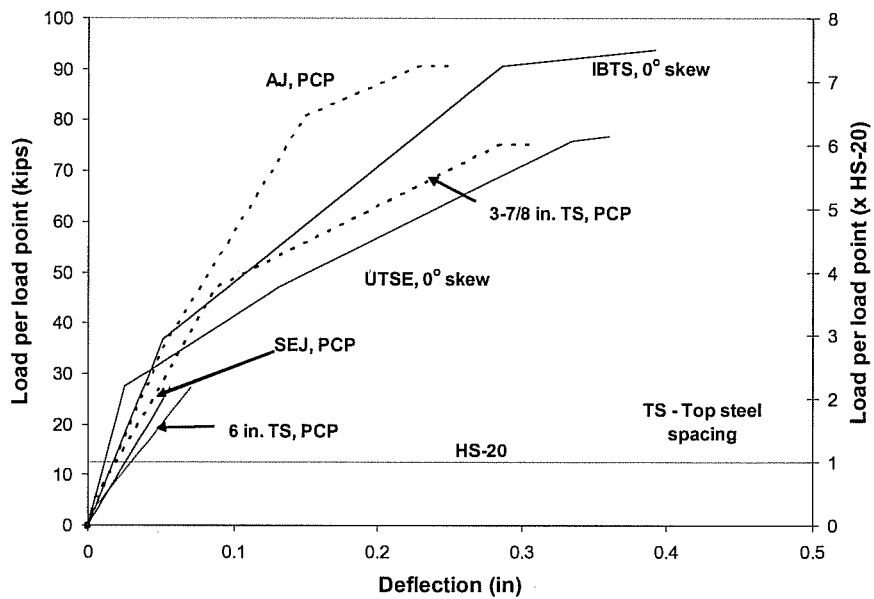
(a) loading to failure*
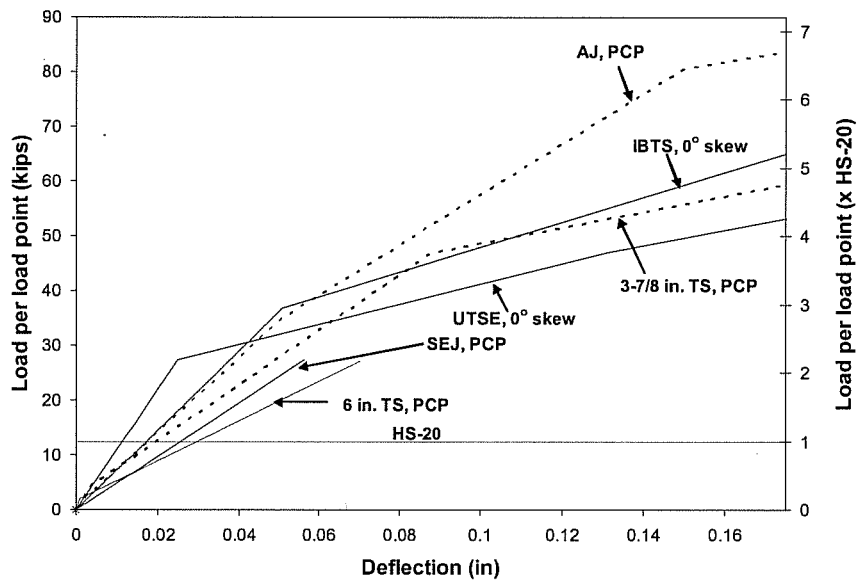
(b) slab initial stiffness*

* IBTS detail – 10 in. slab thickness; all other details – 8 in. slab thickness

Figure 7.1 Deflection envelopes for tests maximizing negative-moment: (a) up to failure; (b) slab initial stiffness

257

For all tests with negative moment loading, the first observed flexural cracks were short: bottom cracks were less than 2 ft long. Lengths of the top cracks are difficult to compare because the flexural cracking for PC panel specimen was influenced by shrinkage cracks in the topping slab that widened as load increased. In all tests with negative moment loading, cracks were first observed at load levels of at least 1.8 x HS-20 (Figure 7.2 a).

For all the edge regions loaded to maximize negative moment, the first observed flexural cracking in the test area did not coincide with a change in stiffness. The first major change in slab stiffness occurred at higher load levels, coinciding with the initiation of several new cracks and propagation and widening of existing cracks. The load at which the first change in stiffness was observed, developed cracking (Chapter 5), was significantly higher for the edge region with the AJ rail than any other edge regions taken to failure. The two edge regions on the PC panel specimen both developed significant cracking at higher loads than the IBTS (10 in.) and UTSE (8 in.) edge details. For most of the test areas, there were fewer and narrower flexural cracks on the top of the slab than on the bottom surface of the slab. Developed cracking occurred at load levels of at least 2.2 x HS-20 (27.5 kips) or higher (Figure 7.2 b).

All test areas failed in punching shear at load levels well above the HS-20 and HS-25 design load levels (Figure 7.2 c). Failure loads for the edge regions with the IBTS (10 in.) detail and the AJ rail (8 in. with PC panel) were around 7.2 x HS-20 (90 kips), and the failure loads for the UTSE (8 in.) detail and PC panel edge detail without the AJ rail (8 in.) were at least 6 x HS-20 (75 kips).

(a) First flexural cracking loads

(b) Developed cracking loads
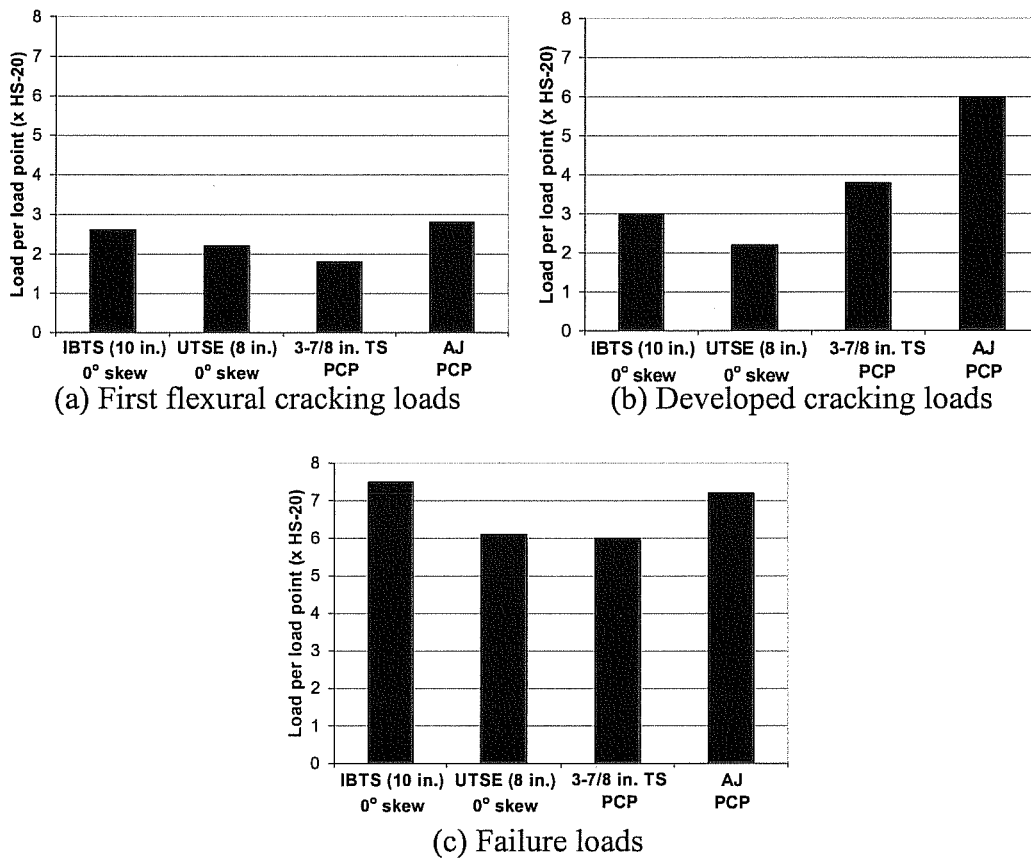
(c) Failure loads

Figure 7.2 Comparison of behavior of negative-moment failure test regions: (a) first flexural cracking loads; (b) developed cracking loads; (c) failure loads

In all tests areas, the strains were measured over the girders only. However, the gauges were not in the same location so direct comparisons cannot be made. For the CIP edges with no skew, strain gauges were placed over the centerline of the girder. Gauges were placed over the ends of the panels, inside the girder edge, in the PC panel specimen. Strains measured in all test areas where negative moment was maximized were extremely small at HS-20 and HS-24 load levels (less than 15% of yield strain). In the IBTS (10 in.) edge detail and the PC panel without an expansion rail (8 in.), while yield strain was not recorded on any instrumented reinforcing bar up to 4.5 x HS-25, some reinforcing bars did

259

reach yield strain at some locations before failure. In test regions with the UTSE (8 in.) and AJ rail (8 in.), the largest measured strain in the flexural reinforcement before failure was 88% and 63% of yield strain. Summaries of strains at various overload levels are shown for the PC panel specimen in Section 5.8.1 of this thesis, and for the no skew specimen in Section 5.6 of Ryan (2003).

7.3 COMPARISON OF POSITIVE MOMENT LOADING TESTS

In both specimens, positive moment was maximized at midspan in the 10-ft bay. All tests maximizing positive moments showed nearly identical initial slab edge stiffnesses, deflections at HS-20 and HS-25 load levels, and ultimate deflections (Figure 7.3 a and b). For all test areas maximizing positive moment, relative edge deflections measured at HS-20 and HS-2 load levels were small compared to the girder spacing (less than 1/1700).
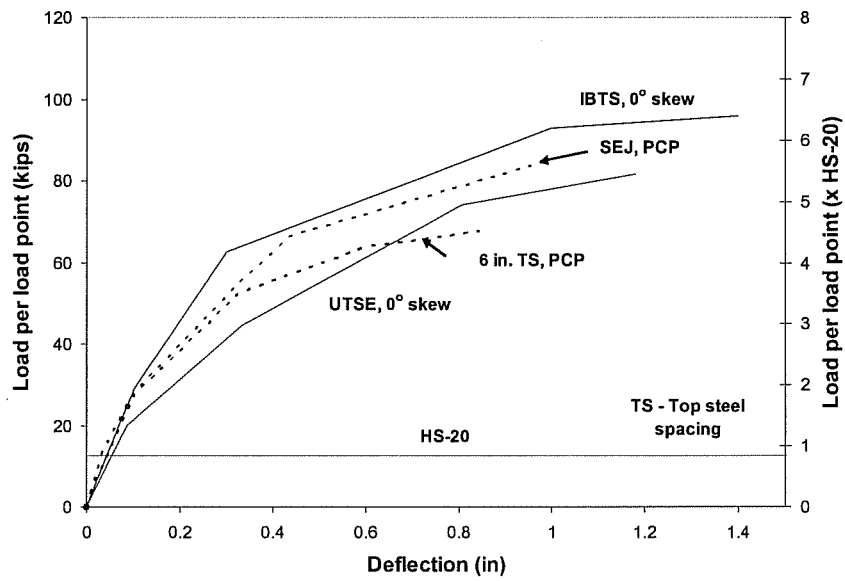
(a) loading to failure*
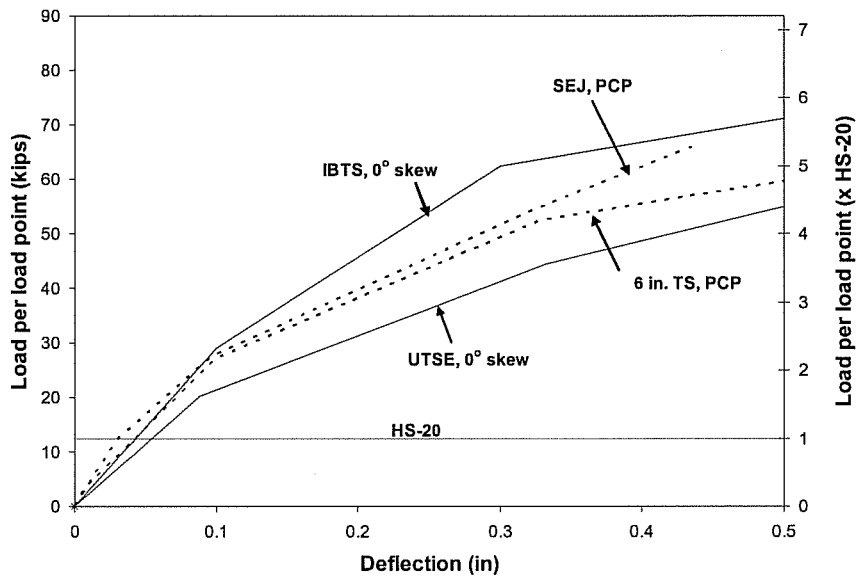
(b) slab initial stiffness*

* IBTS detail – 10 in. slab thickness; all other details – 8 in. slab thickness

Figure 7.3 Deflection envelopes for tests with positive moment loading: (a) up to failure; (b) slab initial stiffness

261

The load levels at the first observation of cracking closely coincided with a small change in stiffness in the load-edge deflection response. Generally, a few, narrow cracks were observed on the bottom of the slab at load levels between 1.3 x HS-20 (16 kips) and 2.8 x HS-20 (35 kips) (Figure 7.4 a). The first flexural cracking only changed the slab stiffness slightly. A larger change in slab stiffness was evident by extensive crack formation and widening that occurred around 2.0 x HS-20 (25 kips) for the 0° skew specimen positive moment test areas and 4.5 x HS-20 (56 kips) for the PC panel specimen positive moment test areas (Figure 7.4 b). Based on the crack patterns observed in the test areas just before failure, there were fewer cracks that formed on the top of the slab than on the bottom of the slab and the crack widths were smaller.

Failure loads for the 0° skew test areas were around 7.0 x HS-20 (88 kips) and around 6.0 x HS-20 (75 kips) for the PC panel specimen test areas (Figure 7.4 c). All test areas failed in punching shear. The test areas on the PC panel specimen showed signs of a developing yield line pattern on the bottom surface of the panel, before the area failed in punching shear.

(a) First flexural cracking loads

(b) Developed cracking loads
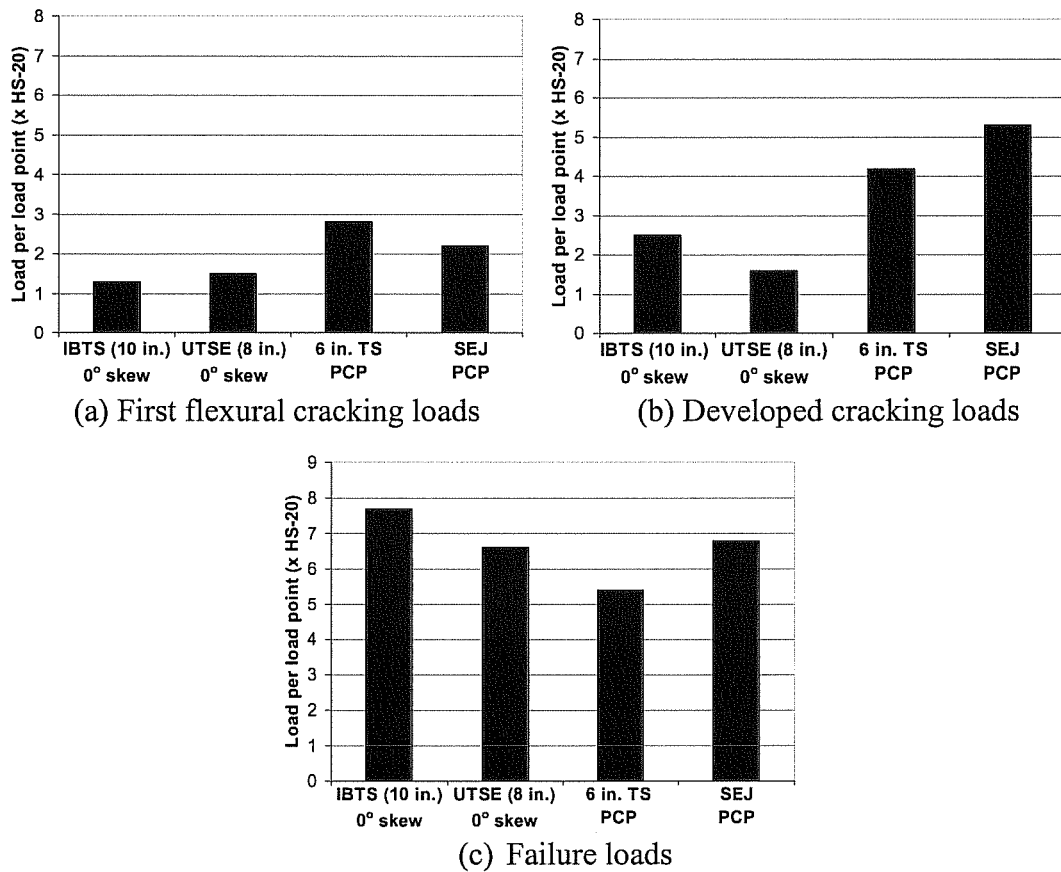
(c) Failure loads

Figure 7.4 Comparison of behavior of positive-moment test regions: (a) first cracking loads; (b) developed cracking loads; (c) failure loads

Similar to the negative moment test areas, strains were measured over the centerline of the girder in the 0° skew specimen and over the ends of the panel over the girder in the PC panel specimen. In all test areas where positive moment was maximized, strains measured in the flexural reinforcement were extremely small at HS-20 and HS-25 load levels (less than 15% of the yield strain). In the IBTS edge detail test area, yield strain was not recorded on any instrumented reinforcing bar until 5.8 x HS-25 (92 kips). No reinforcement in the other test areas reached yield strain during testing to failure. The maximum measured strain for the UTSE edge detail was 80% of yield strain. Strain levels reached 67% of

yield strain in the PC panel specimen with and without expansion rails. Summaries of strains at overloads are shown in Section 5.8.2 for the PC panel specimen and Section 5.6 of Ryan (2003) for the $0°$ skew specimen.

7.4 COMPARISON OF RESPONSES OF IBTS, UTSE AND PCP EDGE DETAILS

The primary objective of this study was to understand the behavior of the IBTS edge detail at expansion joints, as well as investigate the alternate edge details including the UTSE edge detail and details using stay-in-place PC panels. Overall the PC panel edge details with and without expansion rails performed well under service load levels. All PC panel edge regions exhibited no flexural cracking until reaching loads higher than HS-20 and HS-25. For the PC panel edge regions, failure load levels were around 5.4 x HS-20 (68 kips) and as high as 7.2 x HS-20 (90 kips, AJ rail).

All edge details failed in punching shear. According to the punching-shear provisions of the AASHTO LRFD and ACI 318-02, shear capacity is proportional to the distance from the extreme compressive fiber to the centroid of the tensile reinforcement. This distance in the IBTS detail is 2 in. greater than the corresponding distances in the UTSE and PC panel edge details. Based on this punching-shear model and identical punching shear failure surfaces, the capacity of the IBTS section should be higher than either the UTSE or the PC panel edge details. The test results support this hypothesis, as punching shear capacity of UTSE edge details and PC panel edge detail in similarly configured test areas are less than the punching shear capacity of the IBTS edge detail. However, the edge details in the PC panel specimen with the expansion rails had higher punching shear capacities than the UTSE edge detail for similarly configured test areas.

In addition to the section depth, the flexural reinforcement ratio of a section may influence the punching-shear capacity (CEB-FIP 6.4-18). The

264

flexural reinforcement ratio of the UTSE detail was higher than the IBTS. The flexural reinforcement ratio of the PC panel edge detail with the expansion rails are difficult to quantify, but were significant enough that the punching shear capacity of the edge regions were higher than those of the UTSE edge detail. The expansion rails may serve as shear reinforcement as well, which would increase the punching shear capacity of the edge region. Also, the prestressing strands of the PC panel edge regions increased the punching-shear capacity when compared to the typical 8 in. CIP section (UTSE). Although tests results reflect the influence of flexural reinforcement ratio, the tests were too limited to allow for study of the relationship between the ratio and punching-shear capacity. However, test results showed that all edge details have reserve strengths greatly exceeding AASHTO design load levels.

At design load levels of HS-20 and HS-25, the tensile strains were essentially the same in the IBTS, UTSE and PC panel edge details. After the test sections cracked, the UTSE and PC panel edge details had smaller strain levels than the IBTS edge detail. Only the IBTS edge detail and the PC panel detail with 3-7/8 in. top reinforcement spacing reached yield strain in any of the measured reinforcing bars. Neither the UTSE edge detail nor the PC panel details with the expansion rails reached yielding in the instrumented reinforcing bars.

The UTSE edge detail had an increased number of cracks with narrower crack widths than the IBTS edge detail. The PC panel edge details had an increase number of cracks, but wider, cracks than the IBTS edge detail. The PC panel edge details had essentially the same crack pattern as the UTSE edge detail, but the crack widths were larger.

7.5 DESIGN GUIDELINES FOR SLAB EDGES AT EXPANSION JOINTS

AASHTO design provisions require bridge slab to be designed for both service (stresses, deformations and crack widths) and strength (strength and stability) limit states. One of the objectives of this study was to provide guidance for designing deck slabs using the IBTS or alternate edge details. In particular, the effect of a hypothetical increase from HS-20 and HS-25 design load levels on each detail, and the inclusion of PC panels in the edge detail was examined.

When designing a typical TxDOT bridge deck, the behavior of edge details at serviceability load levels and failure load levels is important when designing the edge detail. In this section, the change in overall performance of the IBTS, UTSE, and PC panel edge details under the hypothetical increase in design load levels and the inclusion of PC panels in the edge detail are discussed. In addition, the effects on the AJ and SEJ expansion rails on cracking loads, deflections, reinforcing bar stress levels, and failure loads are addressed.

Similar to Chapter 5, tests are referred to by the moment being maximized, positive moment in the 10-ft bay and negative moment in the 8-ft bay. In previous phases of this project, it was determined that the designer should not expect increased slab capacity or improved behavior for loads applied to girder spacings less than 8 ft.

7.5.1 Crack Formation

In discussion of crack formation, behaviors at first flexural cracking and the developed cracking where there is a marked change in stiffness will be discussed. Even though, the specimens were examined carefully for first cracking, it was difficult to establish exact cracking loads. Test areas were loaded in 5-kip steps, and cracks could have developed at loads up to 5 kips lower than those reported here. For the PC panel specimen, first flexural cracking was

defined as the formation of new cracks, as well as widening of cracks due to shrinkage and thermal effects. Additionally, variations in material properties of concrete produce variations in observed cracking loads in otherwise identical specimens.

First cracking loads are reported in Table 7.1 below. Based on these results, slab edges with the IBTS, UTSE or PC panel detail can be expected to remain uncracked under HS-20 and HS-25 design loads for slabs with and without panels and slabs constructed with 8-ft girder spacings. For the specimens tested with 10-ft girder spacings, first cracking loads are reduced, except for the PC panel edge details with the different top reinforcement spacings, the 6 in. top reinforcement edge detail had higher cracking load then the 3-7/8 in. top reinforcement spacing edge detail. Even though most of the first cracking loads were lower in the 10-ft girder spacings than the 8-ft girder spacings, the loads still remained above HS-20. The lower first cracking loads in the 8-ft girder spacings may be attributed to the significant positive moments imposed due to applied loads in order to maximize negative moment in the 8-ft girder spacings.

Table 7.1 First cracking loads, IBTS, UTSE and PC panel edge details

Edge Detail	Slab Thickness (in)	Girder Spacing (ft)	Section (Negative or Positive)	First Cracking Load x HS-20
IBTS	10	8	Negative	2.6
IBTS	10	10	Positive	1.3
UTSE	8	8	Negative	2.2
UTSE	8	10	Positive	1.5
3-7/8 in. TS	8 with PCP	8	Negative	1.8
6 in. TS	8 with PCP	10	Positive	2.8
AJ	8 with PCP	8	Negative	2.8
SEJ	8 with PCP	10	Positive	2.2

For all tests, first flexural cracking was observed at loads between 1.3 x HS-20 (16 kips) and 2.8 x HS-20 (35 kips). Developed cracking patterns, however, did not form until higher loads. "Developed cracking" was defined as the change in crack formation and overall behavior, mainly stiffness, of the slab edge as load levels are increased. In the 10-ft girder spacings, where positive moment was maximized, first cracking caused a minor reduction in the stiffness of the slab edge. In the 8-ft girder spacings, where negative moment was maximized, first cracking did not produce a noticeable change in stiffness at the slab edge. All tests maintained nearly linear elastic load deformation behavior until the load level labeled "developed cracking" (change in stiffness). "Developed cracking" loads were all greater than 1.5 x HS-20 (19 kips), and shown in Figure 7.1 and Figure 7.3. For tests performed on all the edge details, crack widths at load steps closest to "developed cracking" load levels are shown in Table 7.2 and Table 7.3. These widths were measured from the tests performed, and are intended to serve only as a comparative index of crack severity. PC panel edge details had larger crack widths than the IBTS and UTSE edge details. However, the PC panel edge details exhibited higher developed cracking loads.

Table 7.2 Largest measured crack width for developed crack pattern, 8-ft girder spacing, negative bending

Edge Detail	Largest measured crack width (in.)		
	Top of slab	Bottom of slab	Side of slab
IBTS (10")	0.002	0.004	0.003
UTSE (8")	0.003	0.005	0.004
3-7/8" TS (8" w/PCP)	0.013	0.007	0.005
AJ (8" w/PCP)	0.013	0.005	0.005

Table 7.3 Largest measured crack width for developed crack pattern, 10-ft girder spacing, positive bending

Edge Detail	Largest measured crack width (in.)		
	Top of slab	*Bottom of slab*	*Side of slab*
IBTS (10")	N/A	0.005	0.005
UTSE (8")	HL	0.002	0.002
6" TS (8" with PCP)	0.02	0.02	0.02
SEJ (8" with PCP)	0.013	0.007	0.007

7.5.2 Reinforcement Strain

Maximum tensile strains measured at HS-20, HS-25, and overload levels are given for the 0° skew specimen in Ryan (2003) in Section 5.6 and for the PC panel specimen, in Section 5.8.1 and Section 5.8.2 of this thesis. For the edge details tested, the tensile strains did not exceed 10% of yield strain at HS-25 load level. For all tests, the strain levels at both HS-20 and HS-25 load levels were insignificant, and the increase in strains between HS-20 and HS-25 load levels was slight. Instrumented reinforcement reached yield strains in the IBTS edge regions, both negative and positive moment regions, and the PC panel edge region with 3-7/8 in. top reinforcement spacing, negative moment region. In the other PC panel edge regions and the UTSE edge regions, the measured reinforcement did not reach yield strain. Strains measured on the expansion rails indicated the rail contributed to the distribution of stresses throughout the edge regions. Strains measured on the reinforcing bars in the edge regions with an expansion rail were smaller compared to reinforcing bar strains in regions without an expansion rail. The maximum tensile strain measured in every test section before failure is summarized in Table 7.4. Strains were measured over the centerline of the girder in the 0° skew specimen, which may not be the maximum strains occurring in the flexural reinforcement in the slab edge (most likely the faces of the girders).

269

These strains are included in this chapter, to provide an indication of maximum measured strain in 0° skew test areas.

Table 7.4 Maximum measured tensile strain at failure, all edge details

Edge Region	Slab Thickness (in)	Girder Spacing (ft)	Section (Negative or Positive)	Largest tensile strains (multiples of yield strain)
IBTS	10	8	Negative	1.1*
IBTS	10	10	Positive	1.2*
UTSE	8	8	Negative	0.88*
UTSE	8	10	Positive	0.74*
3-7/8 in. TS	8 with PCP	8	Negative	3.0
6 in. TS	9 with PCP	10	Positive	0.67
AJ	10 with PCP	8	Negative	0.63
SEJ	11 with PCP	10	Positive	0.67

* Strain measurement made at centerline of girder and may not be the maximum strain

7.5.3 Slab Edge Deflection

Lists of relative edge deflections measured at midspan at HS-20, HS-25, and overload load levels are given for the 0° skew specimen in Ryan (2003) and for the PC panel specimen in Section 5.8.1 and 5.8.2 of this thesis. The hypothetical increase from the HS-20 to HS-25 load level had an insignificant effect on the relative slab edge deflection measured in all test areas. In the 8-ft girder spacings, negative moment region, maximum edge deflections were small relative to the girder spacing (1/3000). The UTSE edge detail had smaller deflection in the 8-ft girder spacing than the IBTS and PC panel edge details. For positive bending tests, 10-ft girder spacing, the IBTS edge detail and the PC panel edge detail with the SEJ rail had smaller edge deflections than the UTSE edge detail and other PC panel edge details. The maximum service-deflection allowed by AASHTO LRFD provisions (AASHTO 2.5.2.6.2) is 1/800. For negative bending tests performed in the 8-ft girder spacings, slab edge deflections reached

this level at loads ranging between 3.5 x HS-25 (55 kips) to 4.5 x HS-25 (70 kips). For the 10-ft girder spacings, positive moment region, slab edge deflections reached this deflection at loads about 2.0 x HS-25 (31 kips) to 2.9 x HS-25 (45 kips).

The use of panels did not effect the maximum edge deflections at design load levels. At load levels below the developed cracking loads, slab edge deflection remained small. The use of the AJ and SEJ rails did reduce the maximum edge deflections at failure compared to the PC panel edge details without the expansion rails. The larger top reinforcement spacing (6 in.) resulted in a larger maximum edge deflection than the edge detail with 3-7/8 in. top reinforcement spacing.

7.5.4 Predictions of Slab Edge Capacity

All slab test areas failed in punching shear. The AASHTO LRFD provisions (AASHTO 5.13.3.6.3) can be used to predict the punching shear capacity of slab edges and the beam shear capacity of the IBTS and UTSE edge regions. Additionally, flexural capacity can be predicted using yield-line analysis and the strip method. The punching shear capacity and flexural capacity for the PC panel edge details are more complicated due to the composite section. The complete interaction between the precast concrete panels and the cast-in-place concrete topping is unknown and difficult to quantify. In addition to the flexural resistance and shear resistance of the composite section, testing done on the AJ and SEJ rails is not sufficient enough to quantify their contribution to the punching shear and flexural capacity of the slab edge.

7.5.4.1 Punching-Shear Capacity

Using Equations 5.2, 5.3 and 5.4, punching-shear capacity of IBTS, UTSE, and PC panel edge details were calculated assuming a uniform distribution

of shear stress. For the observed failure capacities of all sections tested, these predictions were unconservative. The nominal punching-shear capacities calculated for the IBTS, UTSE and PC panel edge detail were 1.0 to 1.25 times the observed capacities.

For both specimens, the ACI 318-02 eccentric-shear model (ACI 11.12.6.3) conservatively predicts the punching shear capacities measured from the tests performed on slab edges with the IBTS, UTSE and PC panel edge details. The eccentric shear model is not included in the AASHTO LRFD. As mentioned in Section 7.5.4, punching shear strength of the PC panel edge regions is difficult to estimate correctly because of the prestressing strands and the composite section.

7.5.4.2 Flexural Capacity

Both the upper bound method, yield-line analysis, and the lower bound method, Hillerborg strip method, can be used to predict the flexural capacities of the IBTS, UTSE, and PC panel edge details. Flexural capacity, however, not expected to be a primary concern, since all edge details tested failed in punching shear.

7.5.4.2.1 Yield Line Analysis

There are many reasons why a yield-line analysis is not ideal for predicting failure loads for bridge slab edges with the details included in this study. First, yield-line analysis predicts the capacity of slabs at the formation of a collapse mechanism. All of the tested edge details failed in punching shear, not flexure. Neither the IBTS nor UTSE edge details formed a collapse mechanism. However in the PC panel edge details tested in positive bending, cracking patterns resembling a yield-line pattern did develop, but the test areas eventually failed in punching shear. The yield-line method could be used to verify that a flexural

272

failure will not occur before a punching shear failure mechanism occurs. Second, the boundary conditions are difficult to define for a yield-line analysis at the edge detail. Solutions may be misleading if the boundary conditions chosen do not describe the loading configuration being analyzed. For these bridge slab edges, the boundary conditions along the girders are neither fully fixed nor simply supported. Third, yield-line analysis is an upper bound method, and if the chosen yield-line pattern is not the critical pattern, the prediction could well exceed the failure load predicted by the critical pattern. Determining the critical pattern requires optimization of many variables, which is a time consuming process that may or may not result in the critical pattern. Fourth, when considering the PC panel edge details, the flexural resistances used in the yield-line analyses may not be very accurate, since the flexural resistances are calculated by assuming a monolithic section of the panel and the cast-in-place concrete topping.

To illustrate the weaknesses of applying the yield-line analysis to predicting the capacities of configurations of slabs tested in this study, the results of applying the analysis to simple examples applicable to this study are presented. A sample yield-line pattern is shown in Figure 7.5. For the 0° skew specimen, the yield line pattern shown in Figure 7.5 resulted in a collapse load of 105 kips per load point in the 8-ft girder spacing and 95 kips per load point in the 10-ft girder spacing. The same yield line pattern was applied to the PC panel specimen properties, excluding the expansion joint rails, and the resulting collapse load for the 8-ft girder spacing was 95 kips per load point and for the 10-ft girder spacing, 69 kips per load point. The yield-line analyses predicted collapse loads near the observed failure loads of the punching shear mechanism. None of the edge details, excluding the PC panel edge details tested in positive bending, had crack patterns resembling a complete flexural yield line pattern.
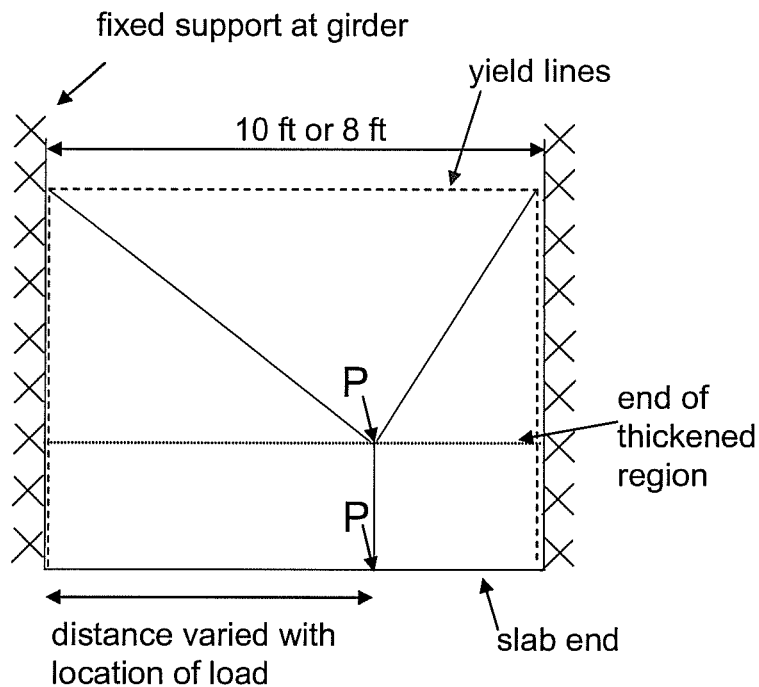
Figure 7.5 Yield-line mechanism, 0° skew slab edge (Griffith 2003)

7.5.4.2.2 Hillerborg Strip Method

The Hillerborg Strip Method is a lower bound method which should result in conservative capacity predictions. Designers can use the method by determining the distribution of moments in the slab, and then distribute the reinforcement accordingly. When slabs are designed using the strip method, the reinforcement is placed according to a distribution of forces that will result in small crack widths and deflections. If the assumed distribution of forces is incorrect, flexural resistance may be adequate, but crack widths and deflection may become large.

For bridge slabs designed with the IBTS and UTSE edge details, the distribution of forces in the slab edge can be difficult to determine due to the combination of bending, shear and torsion. Additional complexities from the

274

discontinuities in the slab from the panels make determining the distribution of forces in the PC panel edge more difficult. However, designers can assume all forces to be distributed in a single strip the width of the slab edge detail. This assumption may result in excessive flexural capacity and preclude a punching shear failure mechanism. Serviceability issues regarding crack widths and deflections will be minimized.

7.6 SUMMARY

Comparisons have been made between the cast-in-place details, IBTS and UTSE, and the PC panel edge details. The PC panel edge details performed well, if not better, at design loads. At design loads, the deflections were small compared to the girder spacing for all the details (less than 1/1700). Overall, the PC panel edge details had similar load-deflection responses to the cast-in-place details. Almost all PC panel edge details had higher first flexural cracking loads and developed cracking loads than the CIP details, IBTS and UTSE. design load levels. The cracking patterns in the PC panel edge detail test areas were similar to the UTSE detail, but crack widths were larger. Only one test area for the PC panel edge detail reached yield strain. Overall, the strains measured in the PC panel edge details were similar to strains measured in the UTSE detail. The PC panel edge details all failed in punching shear around load levels similar to the UTSE detail, since the details have the same concrete thickness. All details reached failure at loads well above design load levels.

CHAPTER 8

Summary, Conclusions, and Recommendations

8.1 SUMMARY

The Texas Department of Transportation (TxDOT) currently uses the "IBTS" standard detail for bridge slab edges at expansion joints. The detail provides additional transverse stiffness without using diaphragms by increasing the slab thickness by 2 in. Typical bridge deck construction uses stay-in-place precast prestressed (PC) panels in the interior of the bridge deck and a concrete topping slab, and at the slab edges, formwork is needed for the full depth cast-in-place IBTS edge detail.

The primary objective of this research study was to evaluate the behavior and capacity of the IBTS and an alternate 8 in. (Uniform Thickness Slab Edge) detail at expansion joints, especially on skewed edges of bridge slabs. In previous phases of the study, two full-scale specimens, 0° and 45° skews, were constructed to test the effect of skew on the two details. The test results showed that at design load levels skew had no significant effect on the behavior of the two details. All test areas failed in shear, predominantly punching shear. The UTSE detail failed at slightly lower load levels than the IBTS detail due to a 2 in. difference in section depth. However, both details had ultimate capacities at loads well above the design load levels.

Another objective of this research study was to develop alternate details and investigate construction issues of those alternate details. Since the UTSE performed satisfactorily at design and ultimate load levels, an alternate detail using the stay-in-place PC panels in the edge regions was developed and tested.

276

Use of the PC panels in the edge region is attractive since it would eliminate special formwork construction and reduce safety concerns associated with such formwork construction at heights. Another full-scale specimen with no skew was built since panels cannot be easily incorporated into for a skewed edge. Construction in a continuous precasting bed would be difficult. In addition to the behavior and capacity of an edge detail with PC panels, the effects of armor (AJ) and sealed expansion joint (SEJ) rails on slab edges at design and ultimate loads were investigated. PC panels at slab edges complicate the installation of the AJ and SEJ rails, which are usually installed in the full-depth cast-in-place IBTS detail. Modifications were made to the AJ and SEJ rails, either raising or bending the stud anchors, in order for the rails to be anchored in the topping slab over the PC panels.

The specimen with PC panels was tested using load configurations similar to the other two specimens. For all specimens, negative moments and positive moments were maximized in 8-ft and 10-ft bays, respectively. Additional overhang tests were conducted on the four overhang corners of the third specimen.

8.2 CONCLUSIONS

Based on the results of the tests performed on the slab edges of the PC panel deck, the following conclusions can be drawn about the general behavior of the slab edges with PC panels:

- Service-level behavior:
  - An increase in applied loads from HS-20 to HS-25 load levels resulted in a nearly proportional increase in midspan deflection and strain in reinforcement.

- At both HS-20 and HS-25 load levels, tensile strains in the flexural reinforcement and the deflection-to-girder-spacing ratio were both extremely small (less the 10% of yield strain and 1/1700 respectively).
- Tensile strains from restrained shrinkage and applied loads, caused cracking at very low load levels; however, flexural cracking did not occur until load levels beyond HS-25.
- Crack widths were larger for the 6 in. top reinforcement spacing at negative moment regions. The 3-7/8 in. top reinforcement spacing provided better control of crack widths at the same load levels.
- After first cracking, extensive propagation of cracks occurred at load levels at or above 4.0 x HS-20.
- Initial slab edge stiffness was higher for the edge details with expansion rails.
- Failure-level behavior:
  - Edge details with PC panels loaded with AASHTO design load configurations failed in punching shear at loads ranging from 5.4 to 7.0 times HS-20 (68 to 90 kips).
- Effects of Expansion Rails:
  - Midspan edge deflections were smaller in spans with expansion joint rails.
  - Failure loads were 20 to 25% higher for the PC panel edge detail with an AJ or SEJ compared with an edge detail without expansion joint.
- Comparison of IBTS, UTSE and PC panel edge details:

o The number of cracks in the PC panel edge detail were similar to the UTSE edge detail, but crack widths were larger.

o The load-deflection response of decks with the three details was nearly identical at HS-20 and HS-25 design load levels.

o Flexural reinforcement at the edge reached strains ranging upward from 70% in all tests. However, the capacity was always controlled by punching shear failures prior to development of yield lines or a flexural failure mechanism.

o All details failed in punching shear at loads greater than 5.4 x HS-20 (68 kips). The punching shear capacity of the UTSE and PC panel edge details were less than that in corresponding IBTS slab edges. The reduced depth of the UTSE and PC panel edge details resulted in a lower capacity.

8.2.1 Behavior of Overhangs

Using the AASHTO LRFD bridge specifications, a 10- by 20-in. loading plate, when placed on a standard 3-ft overhang in accordance with AASHTO design provisions, would be placed at a location over the girder. Since this loading configuration would not be the critical situation, the overhang lengths were increased to 45.5 in. to represent an overhang in a bridge with a horizontal curve of 600 ft. Based on the tests of the overhangs, the following conclusions can be drawn:

• All overhangs failed in one-way shear at loads greater than 3 x HS-25 (61 kips).

279

- The use of different top reinforcement spacing and expansion rails resulted in a 30% difference between the failure loads.

- Cracks in the 3-7/8 in. top reinforcement spacing and the expansion joint rail overhang areas were narrower and more closely spaced than those with a 6 in. top reinforcement spacing overhang area.

8.3 DESIGN RECOMMENDATIONS

The following recommendations are based on the test data gathered for slabs with no skew.

8.3.1 Recommendations for Implementation

- PC panel edge details performed as well as the current IBTS detail and the alternate UTSE (8 in.) detail at design load levels. The PC panel edge detail failed at loads well beyond design load levels (5 to 7 x HS-20). Crack widths were larger in the negative moment region with 6 in. top reinforcement spacing. However, crack widths are better controlled when a smaller top reinforcement spacing, 3-7/8 in., is used in the edge region.

- Bridge slabs designed with the IBTS, UTSE and PC panel edge details performed well at HS-20 and HS-25 design load levels. The 25% increase from HS-20 to HS-25 load levels did not significantly change performance.

- For bridge slabs constructed with expansion rails, results showed that expansion rails contribute significantly to the behavior and capacity of slab edges. However, excluding the contribution from the expansion rails is a conservative approach.

- Punching shear capacity should be checked using the eccentric shear model of ACI 318-02. AASHTO provisions consider only concentric shear conditions.

8.3.2 Recommendations for Further Research

- The adhesion at the interface between panel and the cast-in-place concrete topping was sufficient for the section to act as a unit. The flexural resistance and other properties of the composite section are complex to accurately model, and further investigation is needed to fully understand the properties of the composite section.

- Cracks due to restrained shrinkage are inevitable in bridge decks using PC panels. Although, the shrinkage cracking has no detrimental effect on capacity and performance, further investigation is needed to develop procedures to reduce cracking.

- Although testing indicated the expansion rails contributed significantly to the performance of slab edges, the testing completed in this study is too limited to provide a complete understanding of the transfer of forces from the concrete to the expansion rails, and requires further investigation.

- Previous research on PC panel decking did not evaluate performance of the deck under static and fatigue loading at slab edges. This research study focused on the PC panel decking at slab edges under static loading; therefore, fatigue performance of PC panel system at slab edges needs to be studied.

References

1. American Association of State Highway and Transportation Officials (1998), *AASHTO LRFD Bridge Design Specifications, 2nd Edition.*

2. ACI Committee 318 (2002), "Building Code Requirements for Structural Concrete (ACI 318-02) and Commentary (318R-02)," American Concrete Institute, Farmington Hills, Mich., 319 pp.

3. Abendroth, R. (1995), "Nominal Strength of Composite Prestressed Concrete Bridge Deck Panels," *Journal of Structural Engineering*, Vol. 121, No. 2, Feb., pp. 307-318.

4. Azad, A., Baluch, M., Al-Mandil, M., Sharif, A., and Kareem, K. (1993), "Loss of Punching Capacity of Bridge Deck Slabs from Crack Damage," *ACI Structural Journal*, Vol. 90, No. 1, Jan.-Feb., pp. 37-41.

5. Azad, A., Baluch, M., Abbasi, M., and Kareem, K. (1994), "Punching Capacity of Deck Slabs in Girder-Slab Bridges," *ACI Structural Journal*, Vol. 91, No. 6, Nov.-Dec., pp. 656-661.

6. Batchelor, B. and Hewitt, B. (1976), "Tests of Model Composite Bridge Decks," *ACI Structural Journal*, Vol. 73, No. 6, Jun., pp. 340-343.

7. Batchelor, B., Hewitt, B., Casgoly, P., and Holowka, M. (1978), "Investigation of the Ultimate Strength of Deck Slabs of Composite Steel/Concrete Bridges," *Transportation Research Record*, No. 664, p. 162-170.

8. Bazant, Z. and Cao, Z. (1987), "Size Effect in Punching Shear Failure of Slabs," *ACI Structural Journal*, Vol. 84, No. 1, Jan.-Feb., pp. 44-53.

9. Beal, David B. (1982), "Load Capacity of Concrete Bridge Decks," *Proceedings*, ASCE, No. ST4, Apr., pp. 814-831.

10. Bieschke, L.A. and Klingner, R.E. (1982), "The Effect of Transverse Strand Extensions on the Behavior of Precast Prestressed Panel Bridges," *Research Report 303-1F*, Center for Transportation Research, The University of Texas at Austin, Austin, Texas, Jun., 106 pp.

282

11. Binici, B. (2003), "Punching Shear Strengthening of Reinforced Concrete Slabs using Fiber Reinforced Polymers," Doctoral Dissertation, The University of Texas at Austin, Texas, Dec., 284 pp.

12. Brown, M. D. (2002), "Evaluation of Innovation Materials to Control Restrained Drying Shrinkage Cracking in Concrete Bridge Decks," Master's Thesis, The University of Texas at Austin, Texas, Aug., 124 pp.

13. Buth, E., Furr, H.L., and Jones, H.L. (1972), "Evaluation of a Prestressed Panel, Cast-In-Place Concrete Bridge," Research Report 145-3, Texas Transportation Institute, Texas A&M University, College Station, Texas, Sept., 140 pp.

14. Cao, L., Allen, J., Shing, P., and Woodham, D. (1996), "Behavior of RC Bridge Decks with Flexible Girders," *Journal of Structural Engineering*, Vol. 122, No. 1, Jan., pp. 11-19.

15. Christiansen, K. (1963), "The Effect of Membrane Stresses on the Ultimate Strength of the Interior Panel in a Reinforced Concrete Slab," *The Structural Engineer*, Vol. 41, No. 8, Aug., pp. 261-265.

16. Csagoly, P., Holowka, M., and Dorton, R., (1978), "The True Behavior of Thin Concrete Bridge Slabs," *Transportation Research Record*, No. 664, pp. 171-179.

17. Dolan, V. and Frank, K.H. (1994), "Evaluation of Failure in Bridge Expansion Joint Rails," Research Report 1309-1F, Center for Transportation Research, The University of Texas at Austin, Austin, Texas, Oct., 38 pp.

18. Dorton, R., Holowka, M., and King, J. (1977), "The Conestogo River Bridge-Design and Testing," *Canadian Journal of Civil Engineering*, Vol. 4, No. 1, pp. 18-39.

19. Ebeido, T. and Kennedy, J. (1996), "Punching Strength of Deck Slabs in Skew Composite Bridges," *Journal of Bridge Engineering*, Vol. 1, No. 2, May, pp. 59-65.

20. Fagundo, F.E., Tabatabai, H., Soongswang, K., Richardson, M., and Callis, E.G. (1985), "Precast Panel Composite Bridge Decks," *Concrete International: Design and Construction*, Vol. 7, No. 5, May, pp. 59-65.

21. Fang, I., Worley, J., Burns, N., and Klingner, R. (1990), "Behavior of Isotropic R/C Bridge Decks on Steel Girders," *Journal of Structural Engineering*, Vol. 116, No. 3, Mar., pp. 659-678.

22. Fang, I., Lee, J., and Chen, C. (1994), "Behavior of Partially Restrained Slabs under Concentrated Load," *ACI Structural Journal*, Vol. 91, No. 2, Mar.-Apr., pp. 133-139.

23. Fang, I., Tsui, C., Burns, N., and Klingner, R. (1990), "Fatigue Behavior of Cast-In-Place and Precast Panel Bridge Decks with Isotropic Reinforcement," *PCI Journal*, Vol. 35, No. 3, May-Jun., pp. 28-39.

24. Fenwick, R. and Dickson, A. (1989), "Slabs Subjected to Concentrated Loading," *ACI Structural Journal*, Vol. 86, No. 6. Nov.-Dec., pp. 672-678.

25. Gamble, L., Sozen, M. and Seiss, C. (1962), "Tests of a Modified Reinforced Concrete Two-Way Slab," *Journal of the Structural Division*, ASCE, Vol. 95, No. ST6, June, pp. 1097-1116.

26. Graddy, J., Kim, J., Whitt, J., Burns, N. and Klingner, R. (2002), "Punching-Shear Behavior of Bridge Decks under Fatigue Loading," *ACI Structural Journal*, Vol. 99, No. 3, May-Jun., pp. 257-266.

27. Griffith, E. (2003), "Behavior of Bridge Slab Ends at Expansion Joints," Master's Thesis, The University of Texas at Austin, Dec., 282 pp.

28. Hewitt, B. and Batchelor, B. (1975), "Punching Shear Strength of Restrained Slabs," *Journal of the Structural Division*, ASCE, Vol. 101, No. ST9, Sept., pp. 1837-1850.

29. Jackson, P. (1990), "The Global and Local Behavior of Bridge Deck Slabs," *The Structural Engineer*, Vol. 68, No. 6, Mar., pp. 112-116.

30. Jiang, D. and Shen, J., (1986), "Strength of Concrete Slabs in Punching Shear," *Journal of Structural Engineering*, Vol. 112, No. 12, Dec., pp. 2578-2591.

31. Kluge, R.W. and Sawyer, H.A. (1975), "Interacting Pretensioned Concrete Form Panels for Bridge Decks," *PCI Journal*, Vol. 20, No. 3, May-Jun., pp. 34-61.

284

32. Kuang, J. and Morley, C. (1992), "Punching Shear Behavior of Restrained Reinforced Concrete Slabs," *ACI Structural Journal*, Vol. 89, No. 1, Jan.-Feb., pp. 13-19.

33. Law, S., Ward, H., Shi, G., Chen, R., Waldron, P., and Taylor, C. (1995), "Dynamic Assessment of Bridge Load-Carrying Capacities," *Journal of Structural Engineering*, Vol. 121, No. 3, Mar., pp. 478-495.

34. Miller, R., Aktan, A., and Shahrooz, B. (1994), "Destructive of Decommissioned Concrete Slab Bride," *Journal of Structural Engineering*, Vol. 120, No. 7, Jul., pp. 2176-2197.

35. Moehle, J., Kreger, M., and Leon, R. (1988), "Background to Recommendations for Design of Reinforced Concrete Slab-Column Connections," *ACI Structural Journal*, Vol. 85, No. 6, pp. 636-644.

36. Ockleston, A.J. (1955), "Load Tests on a Three Story Reinforced Concrete Building in Johannesburg," *The Structural Engineer*, Oct., pp. 304-322.

37. Ockleston, A.J. (1958), "Arching Action in Reinforced Concrete Slabs," *The Structural Engineer*, Jun., pp. 197-201.

38. Park, R. and Gamble, L. (2000), *Reinforced Concrete Slabs*, John Wiley and Sons, New York.

39. Petrou, M. and Perdikaris, P. (1996), "Punching Shear Failure in Concrete Decks as Snap-Through Instability," *Journal of Structural Engineering*, Vol. 122, No. 9, Sept., pp. 998-1005.

40. Petrou, M., Perdikaris, P., and Duan, M. (1996), "Static Behavior of Noncomposite Concrete Bridge Decks under Concentrated Loads," *Journal of Bridge Engineering*, Vol. 1, No. 4, Nov., pp. 143-154.

41. Ryan, J. (2003), "Zero-skew Bridge Deck Behavior at Expansion Joints," Master's Thesis, The University of Texas at Austin, Texas, Aug., 319 pp.

42. Wood, R.H. (1961), *Plastic and Elastic Design of Slabs and Plates*, Ronald Press So., New York.

43. Youn, S. and Chang, S. (1998), "Behavior of Composite Bridge Decks Subjected to Static and Fatigue Loading," *ACI Structural Journal*, Vol. 95, No. 3, May-Jun., pp. 249-258.

Vita

Christin Jennifer Coselli, the daughter of Ralph and Deborah Coselli, was born in Houston, Texas on June 22, 1980. She grew up in Houston, Texas, where she completed high school in 1998. In 1998, she entered The University of Texas at Austin, where she received a Bachelor of Science degree in civil engineering in 2002. In August, 2002, she entered The Graduate School at The University of Texas at Austin.

Permanent Address: 18230 Spruce Creek

Houston, Texas 77084

This thesis was typed by the author.